Thesis submitted for the degree of
Doctor of Philosophy
at the University of Leicester

by

Ercüment Türkoğlu BSc (ITU Istanbul)
Department of Engineering
University of Leicester

April 2007

Velilerime ve kardeşime, sevgimle ve şükranlarım

Abstract

The thesis is concerned with the application of robust controller synthesis and analysis tools to a rotary-wing aircraft: the *Bell 205* teetering-rotor helicopter.

The $\mathcal{H}_\infty$ loop-shaping approach is central to the work and two main issues concerned with its application will be considered. Firstly, the construction of diagonal (structured) and non-diagonal (unstructured) weighting functions will be considered. Secondly, the analysis of the implications of different weighting function structures in the controller implementation.

A two stage cross-comparative analysis of a series of 1 Dof (Degree of Freedom) and 2 Dof controllers synthesized with both diagonal and non-diagonal weights using the $\mathcal{H}_\infty$ loop-shaping technique will be presented for square and non-square multi input multi output, unstable, non-minimum phase and ill-conditioned models of the helicopter.

Handling qualities of each control law augmented system will be assessed quantitatively and qualitatively. A quantitative analysis, in view of the specifications in ADS-33E, will be given based on a combination of flight data from in-flight tested controllers and, desk-top simulations run on a fully augmented 12 Dof nonlinear helicopter model provided by *QinetiQ*, UK. A qualitative analysis will be given based on the pilot comments compiled (in view of the Cooper-Harper handling qualities rating scale) from the evaluated in-flight control laws.

Acknowledgements

First and foremost I would like to express my sincere gratitude to my supervisor, Professor Ian Postlethwaite, for his guidance over the past few years in the course of the research and for being a priceless source of support while writing this thesis. This thesis would not start and, certainly, would not have reached this successful end at the University of Leicester, without his very patience and understanding. I am also deeply thankful to him for offering me the opportunity to be part of a challenging, but exciting and rewarding in several ways Helicopter project. It has been my privilege to be his student. I would also like to thank my co-supervisor, Dr. Declan Bates, for his insightful comments in the initial phase of my research work.

The members of the 'Helicopter Group', Dr. Matthew Turner and Dr. Emmanuel Prempain, who warmly welcomed me in the group, provided several coding templates and have been collaborative and supportive, deserve truly special thanks. Particularly Dr. Turner who, at very short notice, would be willing to take pen and paper and the time it takes to explain diligently and rigorously any project-associated or other technical issues. I am also thankful to him for introducing me to the power of typesetting system LaTeX. Similarly, I would also like to thank sincerely Dr. Guido Herrmann for his timely and friendly advices, and his readiness to share his knowledge at short notice.

I cannot forget to mention, and to thank, Dr. George Papageorgiou for the willingness he showed in sharing (through a couple of e-mails) his experience on the non-diagonal weights in the very initial phases of my research. His comments were valued very much.

On the professional side: the flight trials on the *Bell 205* helicopter could not have been conducted without the help of Bill Gubbels and Kris Ellis, and the test pilots Robert Erdos and Stephan Carignan from the NRC IAR Flight Research Laboratory in Ottawa. All their help and efforts were very much appreciated. Special thanks also go to Simon Howell and Andy McCallum from *QinetiQ*, Bedford for supplying the nonlinear *Bell 205* helicopter model and the technical support in the initial phases of the project.

Student life after my third year was not easy without a constant and stable income, particularly when my financial balance was 'hovering' around the absolute zero, and with debts at very high 'altitudes'. It was at these times that, first and foremost, my family -my parents and my brother- and also Dr. Cuma Yarim, have generously assisted me financially- to the best of their efforts, and available resources. This assistance was instrumental in ensuring the continuity of my presence in the UK for the writing-up of this thesis. I am ineffably grateful to them.

The times I spent in the Control Systems Research group will remain associated with pleasant memories; the friendly and multiculturally spiced atmosphere in the daily coffee breaks will be missed greatly.

Conversations I had with Prathyush Menon on a very broad spectrum of (technical, but more non-technical) topics from life were very pleasant and enriching. His friendship, indeed deserves a special mention.

In addition to all friends and colleagues mentioned so far, I would certainly not like to forget to thank some present members, in particular: Dr. Xing-Gang Yan, Dr. Liqun Yao, Dr. Sajjad Fekriasl, Dr. Kannan Natesan, Halim Alwi, Abhishek Kumar and Paul Roberts; along with some past members: Irina Stefanescu, Dr. Nai One Lai, Dr. Sarah Blaney, Dr. Edwin Tan, Dr. Turhan Özen, Dr. Roderick Hebden and Dr. Khalid Khan either for their support or for the company.

The moral support, throughout the research, from some of my very close relatives in Bulgaria has always been very special.

The scientific scrutiny to which the thesis was subjected by the examiners has strengthened the content of the thesis, and improved the style of presentation. Their constructive comments and recommendations were extremely useful and thus, were very much appreciated.

I would like to take the opportunity to acknowledge gratefully the UK Engineering and Physical Sciences Research Council (EPSRC) for financially supporting three years of my PhD research project.

Finally, but above all, and on a more personal note, I am deeply indebted to my parents and my brother, and sincerely thankful to Dr. Eleni Tzima, for their constant love, moral and mental support, confidence in me, encouragement and guidance, which I always endeared in my heart and thoughts, over the time leading up to and during the development of this work. Without their unwavering support, the completion of this thesis would not have been possible. I hope that I have given them happiness in return.

Ercüment Türkoğlu
Leicester
United Kingdom

Notation and Symbols

$\mathbb{R}$	field of real numbers
$\mathbb{C}$	field of complex numbers
$\mathbb{F}$	field of either real or complex numbers
$\sigma_i(A)$	i-th singular value of A
$\overline{\sigma}(A)$	the largest singular value of A
$\underline{\sigma}(A)$	the smallest singular value of A
$\kappa(A)$	condition number
$\eta(A)$	the number of right-half plane poles
$A^{\sim}$	shorthand for $A^T(-s)$
prefix $\mathcal{R}$	real rational, e.g. $\mathcal{RH}_\infty$, $\mathcal{RH}_2$
A^T	transpose of matrix A
A^{-1}	inverse of matrix A
A^*	complex conjugate transpose of matrix A
$det(A)$	determinant of A
$A^{\sim}$(s)	shorthand of A^T(-s)
λ(A)	eigenvalue of A
ρ(A)	spectral radius
R(A)	range space of A
N(A)	null space of A
χ_-(A)	stable invariant subspace of A
Ric(A)	the stabilising solution of an ARE
η(A)	number of right-half plane poles
θ_0	collective pitch input to the main rotor actuators
$\dot{\theta}_0$	main rotor collective actuator rate
θ_{1c}	main rotor lateral cyclic actuator
$\dot{\theta}_{1c}$	main rotor lateral cyclic actuator rate
θ_{1s}	main rotor longitudinal cyclic actuator
$\dot{\theta}_{1s}$	main rotor longitudinal cyclic actuator rate
θ_{0tr}	tail rotor collective actuator (pitch) input
$\dot{\theta}_{0tr}$	tail rotor collective actuator (pitch) input rate
β_0	coning angle
$\dot{\beta}_0$	coning rate
β_{1c}	lateral flapping

$\dot{\beta}_{1c}$	lateral flapping rate
β_{1s}	longitudinal flapping
$\dot{\beta}_{1s}$	longitudinal flapping rate
β_d	differential coning
$\dot{\beta}_d$	differential coning rate
u	velocity along X axis
v	velocity along Y axis
w	velocity along Z axis
p	roll rate
q	pitch rate
r	yaw rate
ϕ	roll attitude
θ	pitch attitude
ψ	yaw attitude
$\psi_{heading}$	heading angle
λ_{1o}	rotor uniform inflow
λ_{1c}	first harmonic component- cosine inflow
λ_{1s}	first harmonic component- sine inflow
Q_e	engine torque
$\dot{Q}_e$	engine torque rate
τ_p	phase delay
$\omega_{BWphase}$	phase limited bandwidth
ω_{BWgain}	gain limited bandwidth
ω_c	crossover frequency
ω_n	undamped natural frequency
ζ	damping ratio
$\mathcal{L}_2$ (-∞,∞)	time domain square integrable functions
$\mathcal{L}_2$ ($j\mathbb{R}$)	square integrable functions on $\mathbb{C}_o$ including at ∞
$\mathcal{H}_2$	subspace of $\mathcal{L}_2$ ($j\mathbb{R}$) with functions analytic in Re(s)>0
$\mathcal{L}_\infty$ ($j\mathbb{R}$)	functions bounded on Re(s)=0 including at ∞
$\mathcal{H}_\infty$	the set of $\mathcal{L}_\infty$ ($j\mathbb{R}$) functions analytic in Re(s)>0
$\mathcal{F}_l(\bullet,\bullet)$	lower LFT
$\mathcal{F}_u(\bullet,\bullet)$	upper LFT
ϵ	stability margin

$b_{(G,K)}$	stability margin
ρ	scaling factor
$\rho(A)$	spectral radius of A
$\lambda(A)$	eigenvalue of A
μ	structured singular value
wno(G)	winding number
$\bigcap$	intersection
$\bigcup$	union
$\subset$	subset
$\in$	belong to
$\subseteq$	subset equal

List of Acronyms

ACAH	Attitude Command Attitude Hold
ADS	Aeronautical Design Standard
AFCS	Automatic Flight Control System
ARE	Algebraic Riccati Equation
CRHP	Closed Right Half Plane
Dof	Degree-of-freedom
EA	Eigenstructure Assignment
FbW	Fly by Wire
FCS	Flight Control System
GCARE	Generalised Control Algebraic Riccati Equation
GFARE	Generalised Filter Algebraic Riccati Equation
HQ	Handling Qualities
HQR	Handling Qualities Requirements
inf	(infimum) the greatest lower bound
lcf	left coprime factorisation
LFT	Linear Fractional Transformation
LHP	Left Half Plane
LLFT	Lower Linear Fractional Transformation
LMI	Linear Matrix Inequalities
LSDP	Loop Shaping Design Procedure
LTI	Linear Time Invariant
LTR	Linear Transfer Recovery
LQG	Linear Quadratic Gaussian
MIMO	Multi Input Multi Output
ORHP	Open Right Half Plane
RCAH	Rate Command and Attitude Hold
RC	Rate Command
rcf	right coprime factorisation
RHP	Right Half Plane
RMS	Root Mean Square
SISO	Single Input Single Output
sup	(supremum) the least upper bound
SVD	Singular Value Decomposition

TRC	Translational Rate Command
UCE	Usable Queue Environment
ULFT	Upper Linear Fractional Transformation

Contents

List of Figures

List of Tables

Chapter 1

Introduction

1.1 From modern to advanced control of helicopters: recent historical perspective

Piloting of rotary-wing aircraft can be extremely demanding due to their inherent instabilities in some flight regimes, and their highly complex asymmetric aeromechanical structures. The requirements to satisfy stringent flying handling qualities embodied in Aeronautical Design Standard [Ano00], which impose constraints on the allowable interaxis cross-coupling as well as on the frequency domain and time domain responses of the helicopter, make the task of flying even more challenging. It is therefore important that, in order to meet these requirements and to reduce a pilot's workload, the rotary-wing aircraft has high bandwidths in controlled channels[1] and high-authority flight control system/s.

Since the early 1970's, various methods from the continuously evolving modern control theory have found application in the design of flight control laws for rotary-wing aircraft. A pioneering study into the area of flight control system design was given in [HJBJ73], where a hover hold controller was designed for a helicopter model in which was embedded a simple model of rotor dynamics. Studies on the effect of inclusion of the rotor dynamics concluded that an increase in the bandwidth of the system could lead to instability of the rotor flap regressive mode, therefore this increment must be continuously monitored.

In the following years, the requirements introduced by interchannel cross-coupling, robustness to uncertainties and maintaining high performance throughout the flight

[1]Achieving higher bandwidths is possible only through augmenting the rotorcraft with a flight control system.

envelope engendered considerable research interest into the application of modern and multivariable robust control law design methods. Research was carried out mainly in North America and Europe, and conducted chiefly under the auspices and support of major defence research industry contractors like: *NASA, DLR, DERA* and *QinetiQ*.

Design methods that draw attention ranged from Eigenstructure Assignment (**EA**) to **LQG/LTR**, from advanced robust control techniques ($\mathcal{H}_2$, $\mathcal{H}_\infty$) to adaptive and non-linear control methods [Pie95]. Not surprisingly, therefore, a significant amount of research has been documented on presenting and discussing the relative merits and drawbacks of different control law applications to models and real rotary-wing aircraft systems [MGS90], [WCG94], [RR97], [PPT+05]. Depending on the type of model used, these analyses can be grouped into two classes: *linear* and *nonlinear*. Eigenstructure Assignment, **LQG/LTR**, the structured singular value (μ) and *Riccati* based ($\mathcal{H}_2$, $\mathcal{H}_\infty$) methods fall into the first category and sliding mode techniques into the second. For example [IC94] [2] presents a comparative analysis of three MIMO controller design methods namely: Eigenstructure Assignment coupled with **LTR**, **LQG** coupled with **LTR** and $\mathcal{H}_\infty$. Eigenstructure Assignment, which, due to its structure exhibits sensitivity to small perturbations, relies on the designer to assign properly the eigenvalues and eigenvectors in order to meet the desired closed loop robustness and performance objectives. This is difficult in application to multivariable and unstable systems like helicopters. The application of Eigenstructure Assignment to the design of an ACAH response type controller for the *Lynx* helicopter in forward flight was demonstrated in [HMS90] [3]. Some other applications of Eigenstructure Assignment to helicopter control were also reported in [GLP89] and [SAP90] [4]. Alternative methods for multivariable helicopter control like Linear Quadratic Gaussian were reported in [Gri93], which presented a design and evaluation of **LQG** control on a linear model configured with the *Westland Lynx* helicopter characteristics. However, **LQG**, as discussed in Chapter 3, often results in a controller providing optimal nominal performance but (as in Eigenstructure Assignment) with potentially fragile robustness characteristics.

In the infancy years of the applications of **LQ** based methods to rotary-wing aircraft, encouraging results were reported in [BMG94] with a successfully flight tested full-state feedback **LQR** designed Translational Rate Command system (TRC). Stable **LQR** controllers were reported for hover control- but these were with duration of 40 sec

[2] Evaluated through linear and nonlinear desk-top simulations.
[3] Evaluated through linear and nonlinear desk-top simulations.
[4] Evaluated through linear and nonlinear desk-top simulations.

and thus prevented rigorous conclusions to be drawn with regards to suitability of this technique to MTEs demanding higher bandwidths of the rotorcraft. Some concerns and difficulties in implementing high bandwidth systems using time-domain methods such as **LQG** were, instead, reported and addressed in [TCM+99].

The fragility in robustness properties of Eigenstructure Assignment and Linear Quadratic Gaussian based methodologies for (in-)flight control law design for rotary-wing aircrafts, combined with increased system complexity and demanding manoeuvrability performance requirements have rendered these control laws inadequate in the control of advanced helicopters; the need of more advanced, inherently multivariable and amenable to optimisation control techniques have emerged. $\mathcal{H}_\infty$ robust optimal control could readily accommodated these characteristics.

The design and flight testing of Flight Control Systems (FCS) for fixed-wing aircraft using $\mathcal{H}_\infty$ methods is well advanced compared to developments of the method's use in rotary-wing aircraft flight control design. Interest in utilizing the well celebrated robustness and performance properties of Hardy space (in particular $\mathcal{H}_\infty$) control methods in the design of helicopters control laws dates back to the research reported in [Tom87]. The research presented in [Tom87] sets a milestone in accommodating the $\mathcal{H}_\infty$ "*mixed*" sensitivity (S/KS) controller design problem in the helicopter context. A few years later the pioneering work of Postlethwaite and collaborators in investigating the feasibility of, $\mathcal{H}_\infty$ centred, advanced multivariable robust control techniques in rotary-wing flight control system design was taken further in [YPP89] and [YP90]. This work was based on a two block $\mathcal{H}_\infty$ mixed sensitivity approach (S/KS) for a generic 6 Dof Helisim helicopter model configured with *Westland Lynx* helicopter characteristics. Designs were verified with successful on-the-ground piloted simulations.

Over the past decade this helicopter model (while accommodating various improvements along the way) has served as a platform for further research. A control law derived using an alternative 2 Dof control architecture was described in [WP96], for the large motion simulator configuration of a *Lynx* at the research facilities of *DERA* (now *QinetiQ*), Bedford (UK), and significantly improved handling qualities ratings (HQR) were reported. The same rotorcraft model provided a platform for the design, flight simulation and handling qualities evaluation of an LPV gain-scheduled flight control system reported in [PKS+99]. A design of $\mathcal{H}_\infty$ gain-scheduled controllers for the same helicopter, based on a decoupling two degree-of-freedom structure, was considered in [PP00][5]. Reference [TWA01] [6] describes the design of an $\mathcal{H}_\infty$ controller in a limited authority configuration and gives an account of its ground-based implementation on *Westland Lynx MK7* helicopter.

Other controller types from Hardy space (like $\mathcal{H}_2$) have also found application in rotorcraft FCS designs; a flight-test of an $\mathcal{H}_2$ optimal control law which was based on ACAH type response controller was reported in [BMG94]. To our knowledge, from the accessible literature available in the public domain, this was the first control law (from the family of Hardy space optimal control theory) flight-tested on a helicopter. The flight-tested $\mathcal{H}_2$ control law was unstable, mainly due to significant deficiencies in the 8 state Heffley based model [HJLVW79] of the *Bell 205* helicopter.

Motivated by the fact that mapping realistically many design objectives into a single norm cost function brings compromises, [TP01] presented a critical assessment of the use of mixed ($\mathcal{H}_2$ - $\mathcal{H}_\infty$) norm control in the design of robust controllers for the *Bell 205* operating in a steady hover flight regime. In this synergistic approach, the $\mathcal{H}_2$ norm was optimized, as a model-following performance measure, subject to an upper bound on the $\mathcal{H}_\infty$ norm. The application of this mixed norm approach was based on a frequency domain approximated model augmented with a standard 6 Dof linear model of the *Bell 205* helicopter.

Techniques from nonlinear control theory, although not widely accepted (yet), have also found application platform (with)in helicopter control law designs. An important nonlinear technique which has been studied for rotorcraft control system design is sliding mode control with application to *Bell 205* helicopter model as in [Pie95]; more studies using nonlinear control were reported in [ABDL03], and [IMS03]. It is just to assert that for feasibility, for practicality (in implementation) and most importantly, for safety reasons linear controllers have dominated the FCS designs for rotary-wing aircraft industry over the past decade.

Starting in the early 1990's there has been almost a decade of collaborative research which has paved the way to successful and innovative research between the Control and Instrumentation Group at the University of Leicester, the Defence Evaluation and Research Agency (*DERA*)- *QinetiQ*, Bedford (UK) and the IAR (Institute for Aerospace Research) at the National Research Council (NRC), Ottawa (Canada). The research platform was initially focused on the establishment of the required infrastructure that

[5] Evaluated through linear and nonlinear desk-top simulations.

[6] Evaluated on ground-based-simulators.

would enable the full potential of the $\mathcal{H}_\infty$ theory to be realized. Experience gained through extensive desk-top simulations and on ground-based flight simulators, of different helicopter models [WP96], confirmed the feasibility of the $\mathcal{H}_\infty$ method for rotary-wing control law design and provided sufficient confidence to proceed to applying the multivariable technique to a real helicopter plant- the NRC *Bell 205* helicopter. This helicopter has served as a useful platform for the application of various techniques within $\mathcal{H}_\infty$ optimal control and enhancement of in-flight handling qualities. Research has been conducted simultaneously along three interconnected avenues: enhancing the fidelity of the rotorcraft dynamic model, the application of various advanced $\mathcal{H}_\infty$ robust control techniques and the study of their effect (as well as impact) on advancing the handling and flying qualities of the *Bell 205* helicopter. This culminated in the first ever $\mathcal{H}_\infty$ loop-shaping controller, reported in scientific literature, to be flight-tested on board of the NRC *Bell 205* helicopter [PSW+99].

In the same paper, because of the low order model used, and in the absence of some high frequency dynamics (mainly, rotor uniform inflow and first harmonic components- sine and cosine inflow) the achieved bandwidths were somewhat low. Despite this, the system proved stable and flyable. The robustness in stability can be associated with the properties of the $\mathcal{H}_\infty$ method. An increase in the controller bandwidth of roll channel, and significant enhancement of the pilot's handling qualities were reported with in [SWP+01], which also employed an observer based 2 Dof controller architecture obtained with 1 step design. Further improvements in handling and flying qualities became possible after acquiring an updated 9 Dof (*QinetiQ*) nonlinear model of the *Bell 205* helicopter [SH98]. In all reported (flight-tested) control laws, cross couplings continued to dominate in the response type characteristics. It was clear that the fidelity of the mathematical representative model of the aeromechanical structure of the helicopter had to be improved if better (performance) results were to be obtained.

More designs (with or without *"mixed rates"*) and flight-tests have been presented in [WTS+99a] and [WTG00] which provide an account on the flight testing of a decoupled longitudinal and lateral $\mathcal{H}_\infty$ *"mixed"* sensitivity controllers for a 9 Dof mathematical model of the *Bell 205*. The designs have been complemented with both qualitative and quantitative assessment prior to flight testing.

In February 2001 the research (project) on flight control law designs for the *Bell 205* has gained significant momentum. The existing 9 Dof model (that has served as a base for numerous designs) was upgraded to 12 Dof. The work included in this thesis represents the most recent description of the research carried out on enhancing the in-flight handling and flying qualities of the helicopter by using $\mathcal{H}_\infty$ loop-shaping procedure for controller designs on the *Bell 205* helicopter.

And in the attempt to present the research work completed by the author since 2001 toward fulfilment of the objective, this thesis considers $\mathcal{H}_\infty$ robust control as a tool for designing flight control laws for *Bell 205* fly-by-wire teetering rotor helicopter, and the construction of non/diagonal weighting functions as manipulative elements of this tool as a means for attaining desired (robustness and performance) characteristics of the control laws. Particular emphasis is given to controller designs with the $\mathcal{H}_\infty$ loop-shaping technique; comparative analyses conducted on the frequency and time domains are presented of four flight-tested control laws. Weighting functions with diagonal and non-diagonal structures are used in the synthesis of controllers, and their direct impact on attaining desired closed loop characteristics is studied in detail together with their advantages and disadvantages in practical applications. Flight control laws' response characteristics and handling qualities are assessed quantitatively using ADS 33E standards and flight-test data. Pilot comments on several flight-tested multi-axis mission task element manoeuvres are presented in view of the Cooper-Harper handling qualities rating scale and comprise qualitative assessment of the rotorcraft handling qualities.

1.2 Structure of the Thesis

The thesis consists of six chapters and an appendix, the contents of which are outlined below:

Chapter 2: Preliminaries in matrix analysis and linear algebra This chapter provides a motivational presentation of some fundamental concepts, terms, facts and tools of Matrix Algebra, Linear Control Theory and Functional Analysis many of which implicitly or explicitly underlie the material presented in this thesis. The topics are relevant to controller design and analysis studies of *Linear, Time-invariant* and *Finite dimensional* systems operating in the continuous time.

Chapter 3: Feedback control: Robust $\mathcal{H}_\infty$ control perspective This chapter initially presents some fundamental principles of feedback control and outlines the linear operators which are accepted as robustness and performance indicators in linear control systems. The $\mathcal{H}_\infty$ optimal control problem is introduced as a machinery for synthesis of robust, linear, multivariable controllers, and analysis of robustness of closed loop systems; the latter is addressed by using Small gain theorem. As an integral part of the $\mathcal{H}_\infty$ robust controller design framework, four types of uncertainties are presented together with sufficient conditions for a controller-plant interconnected system to satisfy in order to ensure robustness in the presence of any one from those (stable) perturbations. The motivating reasons behind the selection of normalized *coprime* factor uncertainty representation as the tool for obtaining robustness characteristics of the $\mathcal{H}_\infty$ loop-shaping controller are also discussed.

Chapter 4: Advance control via $\mathcal{H}_\infty$ loop-shaping This chapter is central to the work in this thesis, and aims to provide sufficient background on a linear, multivariable design procedure- $\mathcal{H}_\infty$ loop-shaping. Open loop shaping is of paramount importance to the success of the method and two types of weighting functions -diagonal and non-diagonal- are presented as essential tools for the purpose (of shaping of the singular values). Two algorithms for the construction of non-diagonal weights are outlined, however a step-by-step emphasis of use is given only on one of them. Two different $\mathcal{H}_\infty$ loop-shaping controller architectures with practical significance are presented and issues concerning different aspects of control law design: model reduction, positioning and real implementation are reviewed.

Chapter 5: Flight control law design for Bell 205 This chapter presents detailed studies of the design and frequency domain analysis of four $\mathcal{H}_\infty$ loop-shaping control laws, which are all real flight-tested on a multi-purpose variable stability *Bell 205* helicopter. Detailed exposition on both diagonal and non-diagonal weight construction is given within each control law design presentation. An extended version of the non-diagonal weight construction algorithm in Chapter 4 is developed and used to allow for the construction of non-diagonal weighting function for systems with more outputs than inputs. Comprehensive cross-comparative analysis of the control laws' performance and robustness characteristics is carried out in the frequency domain using interpretations of appropriate closed loop operators.

Chapter 6: Simulations, Flight-tests and Analyses This chapter presents comparative evaluations of the four $\mathcal{H}_\infty$ loop-shaping control laws designed in Chapter 5. Time histories of responses of the linear and nonlinear models of the helicopter to various input demands are presented as a partial indicator of the fitness of each control law before flight testing. Handling qualities of each control law augmented system are assessed quantitatively and qualitatively. For quantitative assessment: bandwidth and phase delay parameters are derived from flight data of manually induced frequency sweep manoeuvres, and linear models of the dynamics of each principal axis are used in conjunction with ADS-33E standard specifications. Pilot comments on the characteristics of each control law in several flight-tested multi-axis mission task element manoeuvres are presented in view of the Cooper-Harper handling qualities rating scale and comprise qualitative assessment of the rotorcraft handling qualities. The relative merit of each of the four controllers is discussed in detail in the course of the cross comperative analysis of flight-tested control laws.

Chapter 7: Concluding remarks This chapter, in its first part, summarises the main contributions of the thesis to the area of flight control law design for an unstable helicopter- in general, and to the understanding of practical feasibility of complex weighting functions in their use in complex engineering systems. In its second part, possible directions for continuing research in the area of rotorcraft flight control law design are outlined.

Appendix: Appendix A This appendix presents a compilation of definitions, terms and parameters used in the pre and post-flight quantitative and qualitative handling qualities evaluation of the designed and flight-tested control systems presented in this research.

1.3 Contributions

The main contributions of this thesis to the field of rotary-wing (helicopter) flight control law synthesis and analysis by utilizing the advanced multivariable $\mathcal{H}_\infty$ robust control theory can be summarised as follows:

- The design of all the $\mathcal{H}_\infty$ loop-shaping controllers presented in this thesis was based on a laterally and longitudinally coupled nonlinear model of the *Bell 205* helicopter plant.

- The thesis presents the best performing, coupled, 1 Dof $\mathcal{H}_\infty$ loop-shaping control law to have been flight-tested to date on the 12 Dof nonlinear mathematical model of the *Bell 205* helicopter; the model was exclusively made available by *QinetiQ* for this project only. It builds up on the previous (9 Dof) model of the helicopter with the addition of some elements representing high frequency dynamic characteristics of the helicopter. Without these elements, the achievement of *Level 1* flying qualities has not been possible [SWP+01].

- While the construction of diagonal weighting functions and their application to a wide range of engineering systems has reached a mature phase, the construction of non-diagonal (full block or unstructured) weighting functions has been a subject of study only in recent years [PGH97], [PG97], [Lan01] and [PG02]. The thesis contributes to this direction of research by presenting studies on the impact of the structure of the weighting functions on attaining the desirable design qualities and by presenting comprehensive comparative analyses of 1 Dof controllers synthesised on the augmented plant, with diagonal and non-diagonal weights.

- Applications of non-diagonal weight construction algorithms have so far been reported only for square system plants (where the number of inputs were equal to the number of outputs). In this thesis an existing design procedure for the construction of non-diagonal weights [PG97], [Pap02] has been extended using algebraic manipulations described in Chapter 2 (subsection 2.1.2) to allow for the construction of non-diagonal weighting functions for system plants with a non-square (rectangular) structure.

- It is known that the non-square structure of the system plant, i.e.

$$dim(R(\mathbf{G})) \oplus dim(N(\mathbf{G}^*)) \neq dim(R(\mathbf{G}^*)) \oplus dim(N(\mathbf{G})) \tag{1.1}$$

  imposes certain limitations on the achievable performance of the system [SBG97], [Che00] and [CCM02]. The presentation herein, to the best of the author's knowledge, constitutes the first reporting of a real application of non-diagonal weights to the shaping of the singular values of a non-square helicopter system plant.

- The work describes the first ever reported non-diagonal weight synthesised coupled, 1 Dof $\mathcal{H}_\infty$ loop-shaping controller that has been flight-tested by a pilot on a real helicopter. The challenges faced in the course of the non-diagonal weight design for such a high order plant have been carefully addressed and recommendations outlined.

- The set of $\mathcal{H}_\infty$ loop-shaping controllers presented in this thesis, along with those in [PPTT02], [PPT+02] and in [PPT+05], has not made use of the "*mixed*" [7] rate technique. This is in contrast to most of the previous control law designs reported on the *Bell 205* helicopter, prior to 2001. This indicated that $\mathcal{H}_\infty$ loop-shaping controllers that deliver to the expectations of the pilots and facilitate *Level 1* flying qualities in-flight can be synthesised without the inclusion of p_{mix} and q_{mix}.

- The distinct advantages of implementing the $\mathcal{H}_\infty$ loop-shaping controller based on an exact plant observer plus state feedback are well documented in [PGH97], [PG99], [Hyd95] and [SP96]. The controllers presented in this thesis are not based on the exact plant observer plus state feedback. They employ only state feedback of selected state variables (namely attitudes and rates) and yet they delivered highly rated (by the pilots) in-flight performance characteristics. Previously designed[8] and flight-tested $\mathcal{H}_\infty$ loop-shaping controllers [PSW+99], [SWP+01] on the same helicopter used observer-based configurations in the implementation phase.

- The current work reports on the first ever design of longitudinally and laterally coupled, 1 Dof $\mathcal{H}_\infty$ loop-shaping controller which attained, in flight tests, *Level 1* Handling Quality ratings for several high precision and demanding manoeuvres (such as *Pirouette, Turn to Target* and *Precision Hover*) on the *Bell 205* helicopter. These results have not previously been disseminated in written form to the scientific community. It is important to emphasise that, they were rated by the pilots higher than any coupled 1 Dof $\mathcal{H}_\infty$ loop-shaping control laws previously reported in scientific literature, including those (developed for the *Bell 205* and) presented in [PSW+99], [SWP+01], [PPTT02], [PPT+02] and [PPT+05]; where the last three sets of control laws used, for synthesis purposes, a nonlinear helicopter model of *Bell 205* which is identical to the one in this research.

- Comprehensive analyses of the (performance and robustness) response characteristics of a series of (square and non-square) 1 Dof and 2 Dof controller architectures were carried out:

[7] The "*mixed*" rates are p_{mix} and q_{mix}. When used for feedback they develop open loop predictor derived signals at frequencies above flexible mast rocking mode of the helicopter- in the frequency range 11.5 rad/sec and 14 rad/sec- and have been frequently used to alleviate some undesirable transient response characteristics and improve performance characteristics, such as: overshoot and small damping coefficient (ζ).

[8] The designs were based on the 9 Dof *Bell 205* nonlinear helicopter model.

a) In the time domain, using both linearised and nonlinear (Simulink) flight aero-mechanic models of the helicopter.

b) In the frequency domain, using singular value sensitivity operators and different notions of stability measures (e.g. stability margin- ϵ, ν-gap metric).

- The thesis presents a preliminary investigation into the effect of inclusion of extra measurements (namely, the Roll (p) and Pitch (q) rates) on the robustness and performance properties of 1 Dof $\mathcal{H}_\infty$ loop-shaping control law.

- The handling qualities toolbox [How90]- based on a previous version of the ADS 33 standard- was updated to reflect the most-up-to-date ADS-33E [Ano00] standard properties. Quantitative handling qualities evaluations of the flight-tested control laws were then based on the updated version of the toolbox. This update has facilitated better quantitative predictions to be made on the Handling Qualities.

Chapter 2

Preliminaries

The purpose of this chapter is to acquaint the reader with some of the most useful and fundamental concepts, key topics, terms, facts and tools of Linear Algebra (more specifically Matrix Algebra), Linear Control Theory and Functional Analysis- many of which implicitly or explicitly underlie the material covered in this thesis. The topics are relevant to controller design and analysis studies of *Linear, Time-invariant* and *Finite dimensional* systems operating in continuous time. The exposition will be rather motivational without any proofs and thus without exhaustive treatment of the topics. Wherever possible and appropriate, connections between mathematical terminology and Control Engineering will be established.

For more detailed treatment of the topics, the interested reader is encouraged to consult with [GVL96], [HJ85], [Mey00] on Matrix Analysis; [You88] , [NS00] on Functional Analysis and Operator Theory, and [SP96], [GL95], [ZDG96] on Linear Control Theory as well as the exhaustive list of references therein.

2.1 Matrix Algebra

2.1.1 Eigenvalues and Eigenvectors

Definition 2.1 *[GVL96]*

Let $\mathbf{A}$ *be a square matrix such that* $\mathbf{A} \in \mathbb{C}^{n \times n}$. *The eigenvalues of a matrix A are the* n *roots of its characteristic polynomial* $p(\lambda)$ =$det(\lambda I - A)$. *The set of all eigenvalues of a matrix A is the spectrum of A and is denoted by* $\rho(A)$=$\{\lambda_1, \lambda_2, \ldots, \lambda_n\} \subseteq \mathbb{C}$.

If $\lambda \in \rho(A)$, *then the nonzero vectors* $x \in \mathbb{C}^n$ *that satisfy:*

$$Ax = \lambda x$$

are the right eigenvectors of A for λ. Similarly the left eigenvectors of A for λ are determined from:

$$x^* A = \lambda x^*.$$

Roughly speaking eigenvalues and eigenvectors are useful mainly for two reasons; one algorithmic, the other physical. Mathematically, eigenvalue analysis can simplify solutions of certain problems by reducing a coupled system to a collection of scalar problems; whereas from a physical point of view, insight can be gained into the behavior of systems governed by linear equations. The study of resonance (of instruments and structures) and of a system's stability over large time scales is particularly eased by investigating the locations of the eigenvalues on the complex plane.

The relationship between a matrix and its eigenvalues is not very straightforward to elaborate, however *Gerschgorin's* theorem [Ger31] states that eigenvalues of matrix A lie in the collection of circles- called *Gerschgorin circles* centred at the diagonal elements a_{ii} of the matrix A:

$$\|z - a_{ii}\| \leq r_i, \quad \textit{where} \tag{2.1}$$
$$r_i = \sum_{i \neq j=1}^{n} \|a_{ij}\| \quad \textit{for} \quad i = 1, 2, \ldots, n. \tag{2.2}$$

Note that the radii of these circles depend on the magnitudes of the off-diagonal entries. It was the belief that control objectives for the overall multivariable plant can be posed as objectives on the eigenvalue loci (also called characteristic loci), so that the generalized Nyquist stability criterion assessment of the stability can be conducted via consideration of eigenvalues. These ideas form the basis of Nyquist array design methodologies [PM79]. However, studies supported with numerous applications have shown that eigenvalue "*phase*" and "*gain*" margins imply very little about stability robustness for the overall system, e.g. [Mac82], [SP96].

Eigenvalues of a multivariable plant are not suitable and reliable indicators of robust stability. Additionally, as they cannot always account for loop interactions they may be misleading indicators of performance as well. For example, consider transfer function matrix $\mathbf{G} \in \mathbb{C}^{2\times 2}$:

$$\mathbf{G}(s) = \begin{bmatrix} 1 & \Gamma(s) \\ 0 & 1 \end{bmatrix} \tag{2.3}$$

The off diagonal term $\mathbf{G}_{12}$(s) may cause significant inter-loop coupling between the second input and the first output. However, this interaction cannot be captured by the eigenvalues of **G**(s) since they are independent of the off-diagonal term $\Gamma(s)$.

It becomes obvious that, although eigenvalues of an open loop plant can be used to assess the stability of the nominal closed loop systems and thus are of paramount importance in studying structural characteristics and stability analysis of some type of systems they fall short in capturing the interactions between the different inputs and outputs of a MIMO system. Hence, in most cases where cross-coupling is strong they will fail to be useful indicators of robust stability and performance of the closed loop.

As pointed out in [SP96] the eigenvalues measure the gain for special cases when the inputs and outputs are in the same direction of the eigenvector. Additionally, being applicable only to square systems (and even then lacking rigour), not satisfying the triangular and multiplicative inequalities (common in robustness analysis) provides further drawbacks.

It was in the late 1960's when robust stability for MIMO systems and methods of achieving it emerged as a key problem in feedback control systems. This however could not be successfully addressed by considering the eigenvalues of the plant (represented by a transfer function matrix). To cope with this and provide a unified means for performance analysis for a multivariable system, a "*new*" quantitative measure had to be introduced. This is the matrix norm $\| \bullet \|_\infty$. While there are many norms, in this thesis, we will extensively make use of the induced 2-norm, the so called $\mathcal{H}_\infty$ norm, denoted by $\| \bullet \|_\infty$.

2.1.2 Singular Value Decomposition

The orthogonal decomposition theorem [Mey00] used as a tool to decompose $\mathbb{R}^n$ with rectangular matrices produces the *URV* factorization [Mey00]. This factorization which is usually not a similarity transformation specialises to become the *Singular Value Decomposition- SVD*.

As one of the basic but fundamental tools of modern numerical analysis and numerical linear algebra, the SVD in its long history has evolved to become one of the most important decompositions, being used in statistics and relatively recently, in image processing [BT94] and systems and control theory- particularly in the area of linear systems [SP96], [ZDG96]. [KL80] provides a succinct yet detailed survey of the history, numerical details and some applications in above mentioned areas.

The *Singular Value Decomposition* (*SVD*) was first established for $\mathbb{R}^{m\times m}$ real square matrices by Beltrami and Jordan in the 1870's [Bel73], [Mac33] [p.78].

A few decades later (in 1913) the computations were extended by [Aut02] to encompass complex, square matrices $\mathbb{C}^{n\times n}$. Extensions to general and non-square (rectangular) matrices were derived by [EY36] in 1936. The work has also paved the way to the *Autonne-Eckart-Young* theorem [EY39].

We will not pursue many of the details here, but we shall define the SVD and state some of its attractive properties and leave the reader to refer to a combination of sources listed above for a more thorough treatment.

The *Singular Value Decomposition* is a numerical algorithm that makes it possible to decompose a matrix in any shape G into two unitary (orthogonal) matrices and one diagonal matrix.

Theorem 2.1 *For each matrix $G \in \mathbb{R}^{m\times n}$ of rank r, there are orthogonal matrices ($U^T = U^{-1}$) with $U \in \mathbb{R}^{m\times m}$ and ($V^T = V^{-1}$) with $V \in \mathbb{R}^{n\times n}$, and a diagonal matrix $\Sigma_{r\times r} = diag(\sigma_1, \sigma_2, ..., \sigma_r) \in \mathbb{R}^{r\times r}$ such that*

$$G = U \begin{bmatrix} \Sigma & 0 \\ 0 & 0 \end{bmatrix}_{m\times n} V^T$$

with

$\bar{\sigma} = \sigma_1 \geq \sigma_2 \geq , ..., \geq \sigma_r = \underline{\sigma} > 0$ *and* $\sigma_{r+1}, \ldots, \sigma_n = 0$.

When $r \leq p = min(m,n)$, G is said to have $p - r$ additional zero singular values.

The fundamental result stated for the real case continues to hold for the complex matrices when $(\star)^T$ is replaced with $(\star)^*$, and orthogonal matrices are replaced by unitary matrices ($U^* = U^{-1}$ and $V^* = V^{-1}$).

The symbols $\sigma_1, \sigma_2, ..., \sigma_r$ together with $\sigma_{r+1}, ..., \sigma_n = 0$ are named the *singular values* of G, ordered on the diagonal of Σ with descending values, and they are positive square roots of the eigenvalues of G^TG,$[G^*G]$, namely $\sqrt{\lambda_i(G^TG)}$ or $\sqrt{\lambda_i(G^*G)}$. The columns of orthogonal (unitary) matrix $U = [u_1, u_2, ...u_m]$ are the *left singular vectors* of G (and the orthonormal eigenvectors of GG^T, GG^*). Similarly the columns of orthogonal (unitary) matrix $V = [v_1, v_2, ..., v_n]$ are the *right singular vectors* of G (and also comprise the orthonormal eigenvectors of G^TG, G^*G). The choice of G^TG, $[G^*G]$ rather than GG^T, $[GG^*]$ is unimportant since the non-zero singular values of G, G^T and G^* are the same. U (V) can be partitioned as $U = [U_1|U_2]$, ($V = [V_1|V_2]$) where $U_1 = [u_1, u_2, ..., u_r]$, ($V_1 = [v_1, v_2, ..., v_r]$) and $U_2 = [u_{r+1}, ..., u_m]$, ($V_2 = [v_{r+1}, ..., v_n]$). From geometric, numerical and control engineer perspectives only the non-zero singular values are of interest. The number of non-zero singular values defines the *rank* of G, such that $r = rank(G)$, since the *Singular Value Decomposition* provides a full-rank factorization of G.

At this point it is worth mentioning that the number of zero singular values of G need not agree with the number of zero eigenvalues of G^*G (or GG^*) [Mey00].

The distinction of non-zero singular values ($\sigma \neq 0$) from zero (or near zero) singular values ($\sigma \approx 0$) in the presence of rounding error is a non-trivial task and can be computationally expensive. Computation of the singular values from the eigenvalues of GG^T (GG^*) or G^TG (G^*G) may result in a loss of information and an erroneous conclusion about the *rank* of G, therefore an alternative approach must be used.

A practical algorithm for computing the *SVD* is available based on an implementation of the *QR* iteration that is cleverly applied to G^TG without ever explicitly computing G^TG- [GR70] based on [GK65].

The following Lemma establishes the condition on the orthonormal set of eigenvectors for G^*G (or GG^*) that can be used as right hand or left hand singular vectors of matrix G.

Lemma 2.1 *The columns v_i of any unitary ($(\star)^* = (\star)^{-1}$) matrix V that diagonalizes G^*G (or GG^*) as in*

$$V^*G^*GV = \begin{bmatrix} \Sigma^2 & 0 \\ 0 & 0 \end{bmatrix}_{n \times n},$$

can serve as right-hand singular vectors for non-singular matrix G. Note that if G is non-singular then the zero diagonal block does not exist.

In conjunction with *Lemma* 2.1, we have

Lemma 2.2 *The corresponding left-hand singular vectors u_i are constrained by the relationships*

$$Gv_i = \sigma_i u_i,$$
$$i = 1, 2, ..., r \Rightarrow u_i = \frac{Gv_i}{\sigma i} = \frac{Gv_i}{||Gv_i||_2},$$

and satisfy

$$u_i^* G = 0, i = 1, 2, ..., m \Rightarrow span[u_{r+1}, u_{r+2}, ..., u_m] = N(G^*).$$

The construction of left and right singular vector matrices will be discussed later in the chapter.

The proof of the existence of the singular value decomposition is not constructive, since it presupposes we have on hand a vector that generates the norm of G. For a proof, the reader is referred to sources such as [Ste73], [Ste98], [GVL96].

The SVD is a computationally attractive matrix factorization mainly for two reasons:

- it can be computed with a numerically stable algorithm - directly from G
- the singular value problem is always perfectly well conditioned.

Additionally, the singular value decomposition (SVD) is acknowledged as the most reliable method of numerically determining the rank of a matrix [GW76], however at the expense of computational complexity- which constitutes a minor but nevertheless important pitfall when compared to, for example, QR factorization.

The singular value matrix Σ (of a matrix $G \in \mathbb{R}^{m \times n}$) is either a *"tall"* matrix if $m > n$ with a trailing zero block of order $(m - n) \times n$ at the bottom of Σ; or a "fat" matrix $m < n$ with trailing zero block of order $m \times n - m$ on the right of the matrix Σ. The columns of $[U_1]$ and $[U_2]$, $[V_1]$ and $[V_2]$ where $U = [U_1|U_2]$ and $V = [V_1|V_2]$ form the orthonormal basis for four fundamental subspaces of G discussed later.

For a given a transfer function matrix evaluated at frequency ω rad/sec the number of columns denote the number of inputs, whereas the number of rows denote the

number of outputs of the system. It is usual (as we will see in our helicopter plant configuration) for the numbers of rows and columns to be different, that is to say, the numbers of inputs and outputs may be different, $m \neq n$. In the most encountered case in practical applications when the system has more controlled outputs than inputs, without a loss of generality, the size of U can be reduced to n and an alternative $U_p \subset U$ can be set:
$U_p = [u_1, u_2, ..., u_p]$. This leads to decomposition often referred as *Singular Value Factorization* $G = U_p \Sigma V^*$. Singular vectors corresponding to single distinct singular values are unique up to a factor of modulus one. This property will play an important role in the construction of non-diagonal weighting functions in Chapter 5.

In the construction of pre-filters (weighting functions) for non-square systems ($row \neq column$) the block of trailing zeros (if necessary) can be left out. If correspondingly the last $m - n$ columns of U (for $m > n$) and $n - m$ rows of V (for $m < n$) are left out then the new matrices are given the same name U, Σ, V^*. Σ is square and either U or V will consist of part of a unitary matrix then called subunitary matrix ($U_p \subset U, V_p \subset V$). It can be shown that the singular values σ_i are unique whereas the singular vectors u_i,v_i are not. Assume that the singular value σ_i is distinct from the other singular values then the corresponding left u_i and right v_i singular vectors are uniquely defined up to same scalar factor -with unit magnitude- of the form $\exp^{j\theta}$ and $\|e^{j\theta}\| = 1$, a so called *all pass* factor. There exists $e^{j\theta} \in \mathbb{C}$ s.t. $u_i' = u_i e^{j\theta}$ and $v_i' = v_i e^{j\theta}$ are another pair of left and right singular vectors. Hence $u_i v_i^*$ and $v_i^* u_i$ are uniquely defined.

The singular value decomposition is one of the many matrix decompositions that are essentially "*unique*" [Ste98]. Therefore, any unitary reduction to diagonal form must exhibit the same singular values on the diagonal. Repeated singular values are a source of nonuniqueness.

Singular values of a general matrix have appealing analogies with the eigenvalues of *Hermitian* matrices. If a matrix G is hermitian, then the singular values of G are just the absolute values of the eigenvalues of G. A square matrix G is called *Hermitian* if it is self-adjoint, i. e. $G = G^*$.

From a geometric perspective, the SVD is a mapping of a unit sphere onto an ellipsoid. That is, if one takes a unit sphere in n -dimensional space, and multiplies each vector in it by an $m \times n$ matrix G, one gets an ellipsoid in m -dimensional space. The singular values $\Sigma_{r \times r} = diag(\sigma_1, \sigma_2, ..., \sigma_r)$ give the lengths of the principal axes of the ellipsoid. Geometrically, $\sigma_1 = \|G\|_2$ and $\sigma_r = \frac{1}{\|G^{-1}\|_2}$ correspond to the longest and shortest principal axes on this ellipsoid. From an input/output point of view $v_1(v_n)$ is the *highest (lowest) gain input direction*, while $u_1(u_m)$ is the *highest (lowest) gain observation direction.*

If the matrix G is singular, in some way this will be reflected in the shape of the ellipsoid. In fact, the ratio of the largest singular value ($\sigma_1 = \overline{\sigma}$) of a matrix to the smallest singular value ($\sigma_r = \underline{\sigma}$) gives a condition number of the matrix, which determines, for example, the accuracy of numerical matrix inverses. In this sense, singular values can provide an explicit picture of the level of distortion that can occur under transformation by a given matrix G. The degree of distortion of a unit sphere under this transformation can be measured by $\kappa_2 = \frac{\sigma_1}{\sigma_r}$ (also referred to as the two norm condition number), which corresponds to the ratio of the largest ($\overline{\sigma}$) to the smallest ($\underline{\sigma}$) singular value where:

$$\max_{\|x\|_2=1} \|Ax\|_2 = \|A\|_2 = \|U\Sigma V^T\|_2 = \|\Sigma\|_2 = \sigma_1 = \bar{\sigma}$$

and

$$\min_{\|x\|_2=1} \|Ax\|_2 = \frac{1}{\|A^{-1}\|_2} = \frac{1}{\|V\Sigma^{-1}U^T\|_2} = \frac{1}{\|\Sigma^{-1}\|_2} = \sigma_r = \underline{\sigma}$$

Therefore the 2-norm condition number of G is $\kappa = \kappa_2 = \frac{\|A\|_2}{\|A^{-1}\|_2}$. Although different norms result in condition numbers with different values, the order of magnitude is more or less the same as κ, which provides the same qualitative information about the distortion.

The number κ is also called a *magnification factor* that dictates how much the relative change in G is magnified. If κ is small relative to 1 (i.e if G is well conditioned) then a small relative change (or error) in G cannot produce a large relative change (or error) in the inverse G^{-1}. However if κ is large (that is, if G is ill-conditioned), then a small relative change (or error) in G is highly likely (but not necessarily) to result in a large relative change (or error) in the inverse G^{-1}. The degree of ill-conditioning is, therefore, gauged by the condition number κ. Therefore we can say that the sensitivity of a non-singular matrix to a relative change (or error) in itself represents its conditioning.

The largest singular value $\bar{\sigma} = \sigma_1$ of a matrix corresponds to the 2-norm of the same matrix $\sigma_1 = \|G\|_2$.

2.1.3 Spaces

A vector space is a fundamental setting for matrix theory. A vector space $\mathcal{V}$ over a field $\mathcal{F}$ ($\mathbb{R}$,$\mathbb{C}$) is a set $\mathcal{V}$ of objects (called vectors) which is closed under a binary operation ("*addition*") which is associative and commutative and has an identity ("0") and additive inverse in the set. The set is also closed under an operation of left multiplication of the vectors by elements of the scalar field $\mathcal{F}$ with some known properties [Mey00].

A vector space involves four things:

- a non-empty set $\mathcal{V}$ of objects- n tuples or a set of matrices
- a scalar field of real numbers $\mathbb{R}$, or a scalar field of complex numbers $\mathbb{C}$
- vector addition- as an operation between elements of $\mathcal{V}$
- scalar multiplication- as an operation between elements of $\mathcal{V}$ and $\mathcal{F}$

2.1.3.1 Subspaces

A subspace U of a vector space $\mathcal{V}$ is a subset of $\mathcal{V}$ that is, by itself, a vector space over the same scalar field. Usually a subspace of a vector space $\mathcal{V}$ is defined by some relation that identifies particular elements of $\mathcal{V}$ in such a way that the resulting set is closed under addition in $\mathcal{V}$.

Definition 2.2 *Let S be a non-empty subset of a vector space $\mathcal{V}$ over $\mathcal{F}$ ($S \subseteq \mathcal{V}$), then S is said to be **subspace** of $\mathcal{V}$ if and only if:*

- $x,y \in S \Longrightarrow x+y \in S$
- $x \in S \Longrightarrow \alpha x \in S$

for all $\alpha \in \mathcal{F}$

Subspaces are related to linear functions; which follow in the next subsection.

2.1.3.2 Fundamental Subspaces

Given an m-by-n matrix A , there are two important subspaces associated with this matrix:

$$Range(A) \doteq R(A) \equiv Image(A) \equiv Im(A)$$

and

$$Null(A) \doteq N(A) \equiv Kernel(A) \equiv Ker(A)$$

Every matrix[1] $A \in \mathbb{R}^{m\times n}$ generates a subspace of $\mathbb{R}^m$ by means of the range of the linear function f(x)=Ax. Similarly, the transpose of $A \in \mathbb{R}^{m\times n}$ defines a subspace of $\mathbb{R}^n$ by means of the range of f(y)=A^Ty. $R(A)$ is nothing more than a subspace spanned by all the linear combination of the columns of matrix A, hence often called the **column space** of A. Likewise, $R(A^T)$ is the set of all possible combinations of the rows of matrix A, hence called the **row space.** These two *"range spaces"* are two of the four fundamental subspaces associated with a given matrix operator. A more formal exposition follows:

Definition 2.3 *The **range of a matrix** $A \in \mathbb{R}^{m\times n}$ is defined to be the subspace $R(A)$ of $\mathbb{R}^m$ that is generated by the range of $f(x)$=Ax, i.e.*

$$R(A) = \{Ax|x \in \mathbb{R}^n\} \subseteq \mathbb{R}^m.$$

*Similarly, the **range** of A^T is the subspace of $\mathbb{R}^n$ defined by*

$$R(A^T) = \{A^Ty|y \in \mathbb{R}^m\} \subseteq \mathbb{R}^n.$$

The other two fundamental subspaces associated with each matrix $A \in \mathbb{R}^{m\times n}$ are the **nullspace** (also named as **kernel**) of A and the **left-hand null space** of A.

Definition 2.4 *Given a matrix $A \in \mathbb{R}^{m\times n}$ the set of all solutions to the homogeneous system Ax=0 is called the **null space** of A denoted by $N(A)$ where:*

$$N(A) = \{x \in \mathbb{R}^n|Ax = 0\}.$$

The set

$$N(A^T) = \{y \in \mathbb{R}^m|A^Ty = 0\}$$

[1]Without loss of generality these definitions also hold for complex matrices.

*is called the **left-hand null space** of A. In other words $N(A^T)$ is the set of all solutions to the left-hand homogeneous system $y^T A = 0^T$.*

2.1.4 Construction of Unitary Matrices

Consider a matrix $A \in \mathbb{C}^{m\times n}$. It is known that over the complex field the unitary matrices correspond to the orthogonal matrices, in particular, $U \in \mathbb{C}^{n\times n}$ is unitary if $U^*U = UU^* = I_n$. Unitary matrices preserve norms, including the 2-norm. And while the SVD of a complex matrix involves unitary matrices it also reveals a great deal of information about the structure of a matrix. Some useful properties of SVD are collected in the following *Lemma.*

Lemma 2.3 ([ZDG96]) *Let* $A \in \mathbb{C}^{m\times n}$ *and*

$\sigma_1, \sigma_2, \ldots, \sigma_r > \sigma_{r+1} = \ldots = \sigma_n = 0, r \leq min\{m, n\}$.

Then

1. $rank(A) = r;$
2. *a)*$R(A) = range(A) = span\{u_1, u_2, \ldots, u_r\};$
   b) $N(A^*) = null(A^*) = span\{u_{r+1}, u_{r+2}, \ldots, u_m\};$
3. *a)* $R(A^*) = range(A^*) = span\{v_1, v_2, \ldots, v_r\};$
   b) $N(A) = null(A) = span\{v_{r+1}, v_{r+2}, \ldots, v_n\};$
4. $A \in \mathbb{F}^{m\times n}$ *has a dyadic expansion* : $A = \sum_{i=1}^{r} \sigma_i u_i v_i^* = U_r \Sigma_r V_r^*$.

The dyadic expansion characterizes the dependance of the gain to the system input direction. This directionality property is a distinct characteristic of MIMO systems.

Starting with V to build U,

• the first r left-hand (u_i) singular vectors for A are uniquely determined by the first r right-hand (v_i) singular vectors, while the last $m - r$ can be any orthonormal basis for $N(A^*)$.

Starting with U to build V,

• taking the columns of a unitary matrix U that diagonalizes AA^* as left-hand (u_i) singular vectors for A, right-hand (v_i) singular vectors can be built following *Lemma 1.1*.

The construction of U from V and vice versa, guarantees U (or V) to be unitary, as shown below:

Partition U and V as,

$$U = [u_1 \ldots u_r | u_{r+1} \ldots u_m] = [U_1 | U_2]$$

and

$$V = [v_1 \ldots v_r | v_{r+1} \ldots v_n] = [V_1 | V_2]$$

The matrix V is unitary to start with (V_1 and V_2 each contain orthonormal columns), but additionally,

$$R(V_1) = R(V_1 \Sigma) = R([V_1 \Sigma][V_1 \Sigma]^*) = R(A^* A) = R(A^*).$$

That is, the columns of V_1 comprise the orthonormal basis for the row space of A. Therefore the input direction is in the row space, $R(A^*)$, of matrix A and

$$R(V_2) = R(A^*)^{\perp} = N(A).$$

In U, both U_1 and U_2 contain orthonormal columns.

$$\begin{aligned} R(U_1) &= R(AV_1\Sigma^{-1}) = R(AV_1) = R(AV_1\Sigma) \\ &= R([AV_1\Sigma][AV_1\Sigma]^*) = R(AA^*AA^*) \\ &= R(AA^*) = R(A) = N(A^*)^{\perp} = R(U_2)^{\perp}. \end{aligned}$$

where the columns of U_1 form an orthonormal basis for the column space of A, and the output direction is in the column space, $R(A)$, of A.

The singular value decomposition can be regarded as a particularly nice way of choosing orthonormal bases which *span* right and left singular subspaces in $\mathbb{R}^n, \mathbb{C}^n$ and $\mathbb{R}^m, \mathbb{C}^m$ so that the gains of A along the basis vector directions can be characterized by some minimax conditions.

A thorough evaluation from a system's point of view of these minimax conditions is given in [MSJ79].

2.1.5 Signals

The set of equivalence classes of signals (signals that can occur in an engineering system, but also those signals that cannot conceivably occur in any engineering system) can be defined as:

$$\mathcal{S} = \{f : \mathbb{R} \to \mathbb{R}^n\}$$

where f is a *Lebesgue* measurable function that maps real numbers from $\mathbb{R} \to \mathbb{R}^n$.

For convenience we will define two subspaces:

$$\mathcal{S}_+ = \{f \in \mathcal{S} : f(t) = 0 \;\text{ for all }\; t < 0\} \tag{2.4}$$

and

$$\mathcal{S}_- = \{f \in \mathcal{S} : f(t) = 0 \;\text{ for all }\; t > 0\} \tag{2.5}$$

2.1.5.1 The size of signals

The size of a signal $f \in \mathcal{S}$ can be measured by a 2-norm (widely named as the *Euclidean* norm, $\|f\|_2 = \sqrt{f'f}$) and is defined over either a finite or infinite time interval.

In order to address stability issues, the behaviour (dynamics/history) of signals over infinite time intervals must be taken into account. Thus only this set of signals will present any interest here. The infinite-time-horizon *Lebesgue* 2 space is the time domain space of signals or vectors of signals that are all square integrable and *Lebesgue* measurable functions and have finite 2-norm defined by:

$$\mathcal{L}_2(-\infty, \infty) \doteq \{f \in \mathcal{S} : \|f\|_2 < \infty\} \tag{2.6}$$

where

$$\|f\|_2 = \left\{ \int_{-\infty}^{\infty} \|f(t)\|_2^2 dt \right\}^{\frac{1}{2}} = (\langle f, f \rangle)^{\frac{1}{2}}$$

Related to these we can partition the $\mathcal{L}_2\ (-\infty, \infty)$ *Banach* space and define the subspaces $\mathcal{L}_2\ [0, \infty) = \mathcal{S}_+ \cap \mathcal{L}_2(-\infty, \infty)$ and $\mathcal{L}_2\ (-\infty, 0] = \mathcal{S}_- \cap \mathcal{L}_2(-\infty, \infty)$.

$\mathcal{L}_2\ (-\infty, 0]$ denotes the space of signals defined for negative time and zero for positive time, and $\mathcal{L}_2\ [0, +\infty)$ denotes the space of signals defined for positive time and zero for negative time. Then it follows that $\mathcal{L}_2\ (-\infty, +\infty)$=$\mathcal{L}_2\ (-\infty, 0] \cup \mathcal{L}_2[0, +\infty)$.

The infinite-time-horizon *Lebesgue* space is also a *Hilbert Space* with *inner product* defined by:

$$\langle f, g \rangle = \int_{-\infty}^{\infty} f'(t) g(t) dt \tag{2.7}$$

where g' denotes the transpose of g; $f(t), g(t) \in \mathbb{R}$ and if $f \in \mathcal{L}_2[0, \infty)$, and $g \in \mathcal{L}_2(-\infty, 0]$ then $\langle f, g \rangle = 0$, which implies that signals f and g are orthogonal, and $\mathcal{L}_2(-\infty, 0]$ and $\mathcal{L}_2[0, \infty)$ are orthogonal subspaces of $\mathcal{L}_2\ (-\infty, \infty)$.

All these spaces are *Hilbert spaces* with inner product integral taken over appropriate time span (interval). Any inner product satisfies the *Cauchy-Bunyakovskii-Schwarz* inequality: $|\langle f, g \rangle| \leq \|f\|_2 \|g\|_2$.

2.1.5.2 Signals in the frequency domain

Since all the synthesis and most of the analysis of controllers presented in this thesis is going to be performed in the frequency domain, it is appropriate to introduce briefly the relevant terminology that we will make use of throughout the work.
A signal in the frequency domain is a measurable function $f(j\omega)$ which satisfies the property $(f(j\omega))^* = f^T(-j\omega)$ where ω is the real frequency variable in radians per second [rad/sec]. Given the transfer function model $\mathbf{G}(s)$ and by replacing s with $j\omega$, we get $\mathbf{G}(j\omega)$ which gives the frequency response of the transfer function model $\mathbf{G}(s)$. There are many advantages of conducting analysis using the frequency response of a system. It provides insight into the benefits of feedback and a first hand view on the necessary trade-offs of feedback control. It is fundamental to understanding the response of a multivariable system in terms of its *Singular Value Decomposition*, and it

offers a clear physical interpretation of how a system responds to persistent sinusoidal inputs of the form $u(t) = u_o e^{j\omega t}$ where ω is a varying frequency, and u_o is a constant vector. For a stable system, the output $y(t)$ is given by $y(t) = \mathbf{G}(j\omega)u_o e^{j\omega t}$ in phasor notation.

The 2-norm in the frequency domain is defined by

$$\|f\|_2 = \left\{\frac{1}{2\pi}\int_{-\infty}^{\infty} f^*(j\omega)f(j\omega)d\omega\right\}^{\frac{1}{2}} \tag{2.8}$$

where the factor $\frac{1}{2\pi}$ is introduced to create consistency with the 2-norm of the corresponding impulse response [SP96].

The frequency domain *Lebesgue* 2-space ($\mathcal{L}_2$) consist of signals or vectors of signals with bounded energy:

$$\mathcal{L}_2 = \{f : \|f\|_2 < \infty\}, \tag{2.9}$$

and as the infinite-time-horizon *Lebesgue* space, it is also a *Hilbert space* under the inner product

$$\langle f|f\rangle = \frac{1}{2\pi}\int_{-\infty}^{\infty} f^*(j\omega)f(j\omega)d\omega \tag{2.10}$$

with

$$f(j\omega) = \begin{bmatrix} f_1(j\omega) & f_2(j\omega) & f_3(j\omega) & f_4(j\omega) & \dots & f_n(j\omega) \end{bmatrix}^T \in \mathbb{C}^n$$

and thus $f \in \mathbb{C}$.

Remark 2.1 *Fourier transform is a Hilbert space isomorphism between $\mathcal{L}_2(-\infty,\infty)$ and $\mathcal{L}_2$, that is, $\mathcal{L}_2(-\infty,\infty)$ and $\mathcal{L}_2$ are isomorphic. This property preserves the inner product and the second norm, which explains why the same symbol for the norm and the inner product in time and frequency domain has been used.*

For matrix valued functions evaluated at $s = j\omega$ the $\mathcal{L}_2$ norm is:

$$\|G(s)\|_2 = \left\{\frac{1}{2\pi}\int_{-\infty}^{\infty} Trace[G^*(j\omega)G(j\omega)]\right\}^{\frac{1}{2}} d\omega = \sqrt{\langle G|G\rangle}. \tag{2.11}$$

All real rational strictly proper (see section 2.2) transfer matrices with no poles on the imaginary axis form a (non-closed) subspace of $\mathcal{L}_2$ $(j\mathbb{R})$ denoted by $\mathcal{RL}_2 = \mathcal{R} \cup \mathcal{L}_2$. Where $\mathcal{R}$ denotes the set of real rational matrix valued transfer functions (of s). These can be thought of as representative of both finite dimensional and physically realizable systems.

2.1.6 The space $\mathcal{H}_2$

The $\mathcal{H}_2$ Hardy space (named after the British Mathematician Godfrey H. Hardy) is a space of $\mathcal{L}_2$ functions of a complex variable $(s = j\omega)$ that are analytic in the $\Re(s) > 0$ ($\Re(s) = \{s : Re(s) > 0\}$, the open-right-half-plane) and have finite norm:

$$\mathcal{H}_2 = \{f : f(s) \text{ is analytic in } \Re(s) \text{ and } \|f\|_2 < \infty\} \tag{2.12}$$

where

$$\|f\|_2 = \left\{\frac{1}{2\pi}\int_{-\infty}^{\infty} f^*(j\omega)f(j\omega)\right\}^{\frac{1}{2}} d\omega.$$

For matrix valued functions, $\mathcal{H}_2$ is a (closed) subspace of $\mathcal{L}_2$ $(j\mathbb{R})$ with matrix functions analytic in $\Re(s) > 0$. Then the corresponding norm is defined as

$$\|G(s)\|_2^2 = \frac{1}{2\pi}\int_{-\infty}^{\infty} Trace[G^*(j\omega)G(j\omega)]d\omega. \tag{2.13}$$

The norm $\mathcal{H}_2$ can be computed just as it can for $\mathcal{L}_2$. The real rational subspace of $\mathcal{H}_2$ denoted by $\mathcal{R} \cup \mathcal{H}_2 = \mathcal{RH}_2$ consists of all strictly proper, real-rational and stable transfer function matrices.

Hereafter attention will be devoted only on transfer functions and operators.

2.1.6.1 Least upper bounds and greatest lower bounds

Definition 2.5 *([Abb01]) A set $A \subseteq \mathbb{R}$ is* bounded above *if there exists a number $b \in \mathbb{R}$ such that $a \leq b$ for all $a \in A$. The number b is called an upper bound for A. Similarly, the set A is bounded below if there exists a lower bound $l \in a$ for every $a \in A$.*

Definition 2.6 *A real number s is the least upper bound for a set $A \subseteq \mathbb{R}$ if it meets the following two criteria: (i) s is an upper bound for A;*
(ii) if b is any upper bound for A, then $s \leq b$.

The least upper bound is also frequently called the ***supremum*** *or as we will denote it in Control Theory context for short* ***sup****.*

Every set can have only one least upper bound.

2.1.6.2 Maximum modulus principle

The *maximum Modulus Theorem* provides a well known property of analytic functions. This will serve as a tool to make generalizations to the $\mathcal{H}_\infty$ norm by mapping $\Re(s) > 0$ to the imaginary axis.

Theorem 2.2 *[ZDG96] [p.97]*

Let f(s) be a defined, complex valued function continuous on a closed-bounded set S and analytic on the interior of S, then the maximum of $|f(s)|$ on S is attained on the boundary of S, i.e.,

$$\max_{s \in S} |f(s)| = \max_{s \in \partial S} |f(s)|$$

where ∂S denotes the boundary of S.

The maximum modulus principle roughly speaking says that if a function f (of a complex variable) is analytic in or on the boundary of some domain $\mathcal{D}$, then the maximum moduli (amplitude) occurs on the boundary of this domain. For instance if a system is closed loop stable then the maximum amplitude of this closed loop transfer function over the *RHP* of the complex plane will always occur on the imaginary axis.

2.1.7 The space $\mathcal{L}_\infty$

$\mathcal{L}_\infty$ is a *Banach* space defined as $\mathcal{L}_\infty = \{\mathbf{G} : \|\mathbf{G}\|_\infty < \infty\}$ of all classes of matrix (or scalar) valued functions that are essentially bounded on the imaginary axis $j\mathbb{R}$ with norm:

$$\|\mathbf{G}(s)\|_\infty = ess \sup_{\omega \in \mathbb{R} \cup \infty} \overline{\sigma}(\mathbf{G}(j\omega)) \tag{2.14}$$

$\| \bullet \|_\infty$ is a norm which satisfies the important multiplicative property: $\|\mathbf{GK}\|_\infty \leq \|\mathbf{G}\|_\infty \|\mathbf{K}\|_\infty$ which is a distinctive characteristic of the ∞ norm and leads to a useful design tool for multivariable systems.

Providing that $\mathbf{G}$ is real-rational and has not got any poles on the imaginary axis, that is, it does not contain integrators and its inverse exists, then $\mathbf{G} \in \mathcal{RL}_\infty$. In this case $\bar{\sigma}(\mathbf{G}(j\omega))$ is a continuous function of ω and:

$$\|\mathbf{G}\|_\infty < \gamma \Leftrightarrow \bar{\sigma}(\mathbf{G}(j\omega)) < \gamma \tag{2.15}$$

for all $\omega \in \mathbb{R} \cup \infty$.

Thus, bounds on the infinity norm of $\mathbf{G}$ are equivalent to uniform bounds on $\bar{\sigma}(\mathbf{G}(j\omega))$. This enables the designer to emphasize many constraints and requirements in terms of bounds on the $\mathcal{H}_\infty$ norm of various closed loop transfer functions.

2.1.8 The space $\mathcal{H}_\infty$

A *Hilbert Space* is a complete inner product space with a norm induced by its inner product.

Theorem 2.3 *([Con90])*
A Hilbert space is a vector space $\mathcal{H}$ over either the real field $\mathbb{R}$ or complex field $\mathbb{C}$, together with an inner product $\langle \bullet, \bullet \rangle$ such that relative to the metric $d(x,y) = \|x-y\|$ induced by the norm, $\mathcal{H}$ is a complete metric space.

$\mathcal{H}_\infty$ is a closed subspace of the *Banach* space $\mathcal{L}_\infty$ forming the set of functions of the complex variable s that are analytic for every s in $\Re(s) > 0$ (ORHP) and have finite *supremum*. The $\mathcal{H}_\infty$ norm subspace is defined as:

$$\mathcal{H}_\infty = \{\mathbf{G} : \mathbf{G}(s) \text{ is analytic in } \Re(s) \text{ and } \|\mathbf{G}\|_\infty < \infty\} \tag{2.16}$$

$$\|\mathbf{G}(s)\|_\infty = \sup_{s:\Re(s)>0} \bar{\sigma}(\mathbf{G}(s)) = \sup_{\omega \in \mathbb{R} \cup \infty} \bar{\sigma}(\mathbf{G}(j\omega)). \tag{2.17}$$

The space of all proper, stable, real rational transfer function matrices constitute a rational subspace of $\mathcal{H}_\infty$ denoted by $\mathcal{RH}_\infty$.

If **G** is real and rational then the supremum is attained on the boundary $s = j\omega$ (for possibly infinite ω) to give:

$$\|\mathbf{G}(s)\|_\infty = \sup_{\omega \in \mathbf{R} \cup \infty} \bar{\sigma}(\mathbf{G}(j\omega)). \tag{2.18}$$

For $\mathcal{H}_\infty$ and $\mathcal{L}_\infty$ we have *supremum*, whereas for $\mathcal{RH}_\infty$ (where $\mathcal{R} \cup \mathcal{H}_\infty = \mathcal{RH}_\infty \subset \mathcal{L}_\infty$) and $\mathcal{RL}_\infty$ (where $\mathcal{R} \cup \mathcal{L}_\infty = \mathbb{R}\, \mathcal{L}_\infty \subset \mathcal{L}_\infty$) we have *supremum* replaced by *max* therefore $\|\mathbf{G}(s)\|_\infty$ simplifies to:

$$\|\mathbf{G}(s)\|_\infty = \max_{\omega \in \mathbf{R} \cup \infty} \bar{\sigma}(\mathbf{G}(j\omega)) \tag{2.19}$$

since $\mathcal{H}_\infty \subset \mathcal{L}_\infty$, $\mathcal{RH}_\infty \subset \mathcal{L}_\infty$.

2.2 Systems

It is a well known fact that all systems encountered in nature are intrinsically nonlinear. While there are methods which can successfully be used for controller design and analysis [Isi95], [Kha02] of such systems, here, our attention will be devoted to linear controller design and synthesis strategies which have found considerable appeal from practising control engineers. In particular we will use the power of the $\mathcal{H}_\infty$ norm and notions of classical loop-shaping, culminating in the so called $\mathcal{H}_\infty$ loop-shaping approach [GM89], [MG92]. We apply the techniques to *linear, time-invariant, causal, non-minimum phase* and *unstable* systems. *Linear time-invariant* state-space systems have transfer function matrices that are rational functions of the $\mathcal{L}$aplace transform variable s.

However, in order to acquire a *"near"* realistic picture of the feasibility of the controller, later in Chapter 6, simulations and post-design analysis will be performed on the nonlinear system models.

A system is described as an operator mapping signals from one signal space- the input space, to another signal space- the output space:

$$\mathbf{G} : \mathcal{S}_1 \to \mathcal{S}_2,$$
$$u \to y = \mathbf{G}u$$

where u belongs to the input signal space, $u \in \mathcal{S}_1$, and y to the output signal space $y \in \mathcal{S}_2$.

For example a matrix $\mathbf{G} \in \mathbb{C}^{m \times n}$ represents a linear operator $\mathbf{G} : \mathbb{C}^n \rightarrow \mathbb{C}^m$ taking the input (control) vector $u \in \mathbb{C}^n \doteq \mathcal{S}_1$ into the output (measurement) vector such as $y = \mathbf{G}u \in \mathbb{C}^m \doteq \mathcal{S}_2$. The gain of the operator $\mathbf{G}$ strongly depends on the direction of the input signal vector u.

A *linear* system is one that satisfies:
$\mathbf{G}(\alpha u_1 + \beta u_2) = \alpha \mathbf{G} u_1 + \beta \mathbf{G} u_2$ for all scalars α, β and for all $u_1, u_2 \in \mathcal{S}$.

Systems form a linear space under addition, $(\mathbf{G}_1 + \mathbf{G}_2)u = \mathbf{G}_1 u + \mathbf{G}_2 u$, and multiplication by a scalar, $(\alpha \mathbf{G})u = \alpha(\mathbf{G}u)$.

Let $y(t)$ be the response of a system $\mathbf{G}$ corresponding to an input $u(t)$. If the response of the operator G to a time-shifted input $u(t-T)$ identically maps on to the output resulting in a response $y(t-T)$, the system is called *time-invariant*.

A system is *causal* if, for every T, the output $y(t)$ up to time T depends only on the input $u(t)$ up to time T and the initial condition(s). A system $\mathbf{G}$ is *stable* if $y = \mathbf{G}u \in \mathcal{L}_2\,[0, \infty)$ whenever $u \in \mathcal{L}_2\,[0, \infty)$.

Any linear time-invariant system may be represented as a convolution integral e.g. [GL95]:

$$y(t) = \int_{-\infty}^{\infty} G(t-\tau) u(\tau) d\tau \tag{2.20}$$

We are dealing with systems that are extremely nonlinear in nature, but nearly every nonlinear system can be described by a set of nonlinear (partial/ordinary) differential equations which can be linearized about an equilibrium point or points. This linearization will result in a set of ordinary linear differential equations. Thus, it follows that virtually every system can be mathematically represented by equations in this form, which can also be written as equations in the state-space:

$$\begin{aligned} \dot{x}(t) &= \mathbf{A}x(t) + \mathbf{B}u(t) \\ y(t) &= \mathbf{C}x(t) + \mathbf{D}u(t) \end{aligned} \tag{2.21}$$

These equations are equivalent to the system in (Equation 2.20). $\mathbf{A}$ is a state matrix, $\mathbf{B}$ is a control matrix, $\mathbf{C}$ is the output matrix and $\mathbf{D}$ is the transition matrix; all real and of appropriate dimensions.

Taking the laplace transform $\mathcal{L}[y(t)] = y(s)$ ([Oga02]) of (Equation 2.20) we get $y(s) = \mathbf{G}(s)u(s)$, where $\mathbf{G}(s) = \int_{-\infty}^{\infty} G(t)e^{-st}dt$ is the complex valued *transfer function* matrix of the system, with variable s, and $y(s)$, $u(s)$ are the Laplace transforms of the output, input signals respectively. As we will see later u and y may be real or complex valued functions.

Thus an alternative input-output description corresponding to system in (Equation 2.20), is the *transfer matrix* (sometimes also referred to as *transfer function matrix*). We will make extensive use of this description in this work.

Due to the hypothesis of *finite* dimensionality, the transfer function matrix $\mathbf{G}(s)$ is a matrix whose entries are ratios of polynomials with real coefficients. The transfer function is related to the state-space description in (2.21) as follows:

$$\mathbf{G}(s) = \mathrm{C}(sI - \mathrm{A})^{-1}\mathrm{B} + \mathrm{D}$$

which is also denoted as G(s)$\equiv \left[\begin{array}{c|c} A & B \\ \hline C & D \end{array}\right]$.

Any system that can be described by a transfer function matrix is *linear* and *time-invariant*. Evaluated at sufficiently high frequencies (i.e. $\omega \rightarrow \infty$) practical systems will have $\mathbf{G}(s) = 0$ therefore they will be strictly proper (*D=0*) and hence well-posedness for most practical systems is guaranteed.

However, it is convenient to model high frequency effects by a non-zero D term and hence semi-proper models are frequently used. The above mentioned notions are summarised below:

$$\mathbf{G}(s) \text{ is } \begin{cases} 1, \text{strictly proper} & \text{when} \quad \lim_{s\rightarrow\infty} \mathbf{G}(s) = 0, D = 0, \\ 2, \text{semi proper or bi-proper} & \text{when} \quad \lim_{s\rightarrow\infty} \mathbf{G}(s) \neq 0, D \neq 0 \\ 3, \text{proper} & \text{if} \quad \textit{strictly proper or bi-proper.} \end{cases}$$

where $s = j\omega$ and $(s \rightarrow \infty)$ implies $(\omega \rightarrow \infty)$.

We have seen how the above definitive descriptions of a system are related to functional spaces ($\mathcal{L}_2$, $\mathcal{H}_2$, $\mathcal{L}_\infty$, $\mathcal{H}_\infty$).

If the quadruple of matrices (A, B, C, D) is a non-unique minimal realization of G, a point $q \in \mathbb{C}$ is called a transmission zero, or simply zero of G if there exist complex vectors Ξ^* and Ψ_o^* satisfying the following equality:

$$[\Xi^* \quad \Psi_o^*] \begin{bmatrix} qI - A & -B \\ -C & -D \end{bmatrix} = 0, \tag{2.22}$$

where $\Psi_o^* \Psi_o = 1$.

Then the vector Ψ_o is named as the *output zero* direction associated with q, and $\Psi_o^* \mathbf{G}(q) = 0$ is satisfied.

Transmission zeros verify a similar property with the *input zero* direction, i.e. there exists a complex vector Ψ_i with $\Psi_i^* \Psi_i = 1$ such that $\mathbf{G}(q)\Psi_i = 0$.

Also the location of the zero q defines whether the system is *minimum phase* or not; $\mathbf{G}$ is said to be *non-minimum phase* if it has a zero at $s = q$ with q in the CRHP. If it is not *non-minimum phase* it is *minimum phase.* Similarly the locations of the poles of $\mathbf{G}$ determine its stability and $\mathbf{G}$ is said to be *unstable* if it has a pole at $s = p$ with p in the *CRHP*. The poles p of a transfer function matrix $\mathbf{G}$ are the eigenvalues of the evolution matrix of any minimal realization of $\mathbf{G}$ [SBG97].

We will consider systems as operators on $\mathcal{H}_2$. If $\mathbf{G}$ is a *linear time-invariant* system's transfer function matrix, then $\mathbf{G}$ is said to be stable if and only if $y = \mathbf{G}u \in\mathcal{H}_2$ for every $u\in\mathcal{H}_2$, derived from the fact that $\mathcal{L}_2\ [0,\infty)$ is isomorphic to $\mathcal{H}_2$. That is, a system is stable, if for an input in $\mathcal{H}_2$, the output is also in $\mathcal{H}_2$. Stable systems map bounded energy inputs into bounded energy outputs, whereas an unstable system may have an infinite energy output in response to a bounded energy input. Therefore a stable system has finite energy, and consequently, finite $\mathcal{H}_\infty$ norm. $\mathcal{H}_\infty$ is a space of stable proper, linear time invariant, continuous systems (transfer functions) and the $\mathcal{H}_\infty$ norm represents the maximum energy gain of the system.

2.2.1 Adjoint system

Let $\mathcal{S}_1$ and $\mathcal{S}_2$ be two *Hilbert* spaces ($\mathcal{L}_2$ [0,T],$\mathcal{L}_2$ [0,∞)), together with a bounded linear operator $\mathbf{G}\mathcal{S}_1 \longrightarrow \mathcal{S}_2$. Then there exists a unique linear operator (a transfer function matrix) mapping $\mathcal{L}_2$ to $\mathcal{L}_2$ $\mathbf{G}^* : \mathcal{S}_2 \longrightarrow \mathcal{S}_1$ that has the property

$$\langle \mathbf{G}u, y\rangle_{\mathcal{S}_2} = \langle u, \mathbf{G}^* y\rangle_{\mathcal{S}_1} \tag{2.23}$$

for all $u \in \mathcal{S}_1$ and all $y \in \mathcal{S}_2$. $\mathbf{G}^*$ is called the *adjoint* of $\mathbf{G}$ where $\mathbf{G}^*(s) = \mathbf{G}^T(-s)$, and if the quadruple of matrices (A, B, C, D) is a realization of

$$\mathbf{G} = \left[\begin{array}{c|c} A & B \\ \hline C & D \end{array}\right]$$

then its *adjoint* is

$$\mathbf{G}^T(-s) = \left[\begin{array}{c|c} -A^T & -C^T \\ \hline B^T & D^T \end{array}\right].$$

If $\mathbf{G}(s) \in \mathbb{R}^{m \times n}$ then $\mathbf{G}(-s)^T = \mathbf{G}^*(s)$ denotes complex conjugate transpose. For complex matrices $\mathbf{G}(s) \in \mathbb{C}^{m \times n}$, $[\mathbf{G}(j\omega))]^* = \mathbf{G}^*(j\omega)$.

2.2.2 All pass system

If $\mathcal{S}_1$ and $\mathcal{S}_2$ are signal spaces $\mathcal{L}_2\,[0,T]$ or $\mathcal{L}_2\,(-\infty,\infty)$ with norms denoted by $\|\bullet\|_{\mathcal{S}_1}$ and $\|\bullet\|_{\mathcal{S}_2}$, a system $\mathbf{G} : \mathcal{S}_1 \to \mathcal{S}_2$ is an isometric operator and an all-pass system if the norm of the output is equal to the norm of the input $\|\mathbf{G}u\|_{\mathcal{S}_2} = \|u\|_{\mathcal{S}_1}$, for all $u \in \mathcal{S}_1$. This suggest that an *all-pass* system, unlike other systems such as *low-pass, band-pass* or *high-pass* will leave all input signals with unchanged magnitude, the system acts like a unitary matrix in which ($\mathbf{U}^* = \mathbf{U}^{-1}$). If a system is *inner* $\mathbf{G}^*\mathbf{G} = I$ then it is *all-pass*. Therefore normalized (left/right) *coprime* factor graphs [ZDG96] [p.483]

$$\left\| \begin{bmatrix} M \\ N \end{bmatrix} \right\|_\infty, \quad \|[\widetilde{N} \quad \widetilde{M}]\|_\infty$$

are *all-pass*, with $\|[\widetilde{N} \quad \widetilde{M}]^\sim\|_\infty = \|\,[M \quad N\|_\infty = 1$, and therefore

$$[M \quad N][M^\sim \quad N^\sim]^\sim = I.$$

2.2.3 Size of a System

The infinity norm $\|\bullet\|_\infty$ of a transfer function matrix can be used as a useful measure of size of *linear, time-invariant* systems. It is equally suited to the frequency domain design techniques for multivariable systems. However, in cases where systems are nonlinear and *time-varying*, a generalization of the notion of size is necessary and this is indeed possible by a quantity known as the incremental gain [GL95] [p.90]. Incremental gain as a norm satisfies the sub-additive and sub-multiplicative properties and enjoys the characteristic that it is identical to the (Lipschitz) induced norm and infinity norm for systems that are causal, stable and time-invariant. In our work, however, incremental gain will not play a role.

Finite dimensional, linear time-invariant (in nature) Multi-Input Multi-Output (MIMO) systems and their behaviour can be described or at least approximated by a set of ordinary differential equations with constant real coefficients. Once represented with ordinary differential equations they can also be represented by real-rational transfer function matrices (whose elements are ratios of polynomials in s with real coefficients). For example $\mathbf{G}(s) \in \mathbb{R}^{m \times n}$ is a real rational transfer function with n inputs and m outputs. If G(s) is finite (proper and stable- no poles in the *CRHP*) and $\mathbf{G}(s) \in \mathbb{R}^{m \times n}$ then its "*size*" can be measured by its $\| \bullet \|_\infty$ norm:

$$\|\mathbf{G}(s)\|_\infty = \max_{\omega \in \mathbb{R} \bigcup \infty} \bar{\sigma}(\mathbf{G}(j\omega)).$$

For SISO systems there is only one singular value which is therefore the maximum singular value, and it corresponds to the magnitude of $\mathbf{G}(j\omega)$.

The $\mathcal{H}_\infty$ norm ($\| \bullet \|_\infty$) depending on its domain of use has interpretations in the frequency and time domains. In the frequency domain it depicts how large the frequency response of the system can get, whereas in the time domain it shows the maximum possible **RMS** energy gain over all possible bounded energy inputs.

2.3 Summary

The material presented in this chapter, is regarded as mostly standard in several classical textbooks on Matrix Analysis, Linear Algebra and Linear System Theory. Its analysis here is aimed at facilitating a smooth transition to the more advanced topics in this project work by acquiring the general readership with the tools to handle confidently the content in the remaining parts of this thesis. The next chapter will motivate the use of $\mathcal{H}_\infty$ control and particularly $\mathcal{H}_\infty$ Loop-shaping as a frequency domain method for designing and analysing controllers for Multi Input Multi Output systems.

Chapter 3

Feedback Control: Robust $\mathcal{H}_\infty$ Control Perspective

3.1 Basic tools in Feedback control

This section will introduce the general unity feedback configuration depicted in Figure 3.1 and study some of the most important elements and characteristics of feedback structure.

The fundamental work of Bode [Bod45] and Nyquist [Nyq32] founded a frequency domain approach to feedback control systems design where the objective can be described as: given a rational transfer function representation $\mathbf{G}(s)$ of the dynamics of a dynamical system, design a rational stabilizing compensator $\mathbf{K}(s)$ that will meet certain robustness and performance requirements.

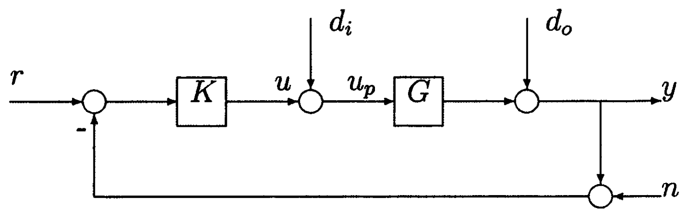

Figure 3.1: General Feedback Configuration

For a given bounded (in $\mathcal{H}_2$ sense) input the output of an open-loop system can be extremely sensitive to uncertainties in the plant description. Moreover in the presence of disturbances acting on the plant the open-loop will do nothing more than transmit them to the output. Both to reduce the sensitivity of the plant to any discrepancies in itself, to modelling uncertainties and to mitigate any (internal/external) disturbances feedback has to be introduced.

Figure 3.1 shows a standard physically realizable feedback configuration of a (SISO or) MIMO-*LTI* plant-controller architecture. Operators G(s) and K(s) are proper rational transfer function matrices with appropriate dimensions which represent the plant and controller respectively. The design problem may be cast as: find a controller K(s) which makes the closed loop system internally stable for all possible plants $\mathbf{G}(s) + \Delta(s)$ while satisfying mathematically described qualitative performance and robustness objectives in the presence of the set of external vector valued signals: reference command r, plant input disturbance d_i, plant output disturbance d_o, and measurement noise n; and each vector signal is assumed to belong to a unit ball in $\mathcal{L}_2$.

An important performance objective is to require the error signal $(e(s) = r(s) - y(s))$[1] to be sufficiently small in the $\mathcal{L}_2$ norm sense.

3.1.1 Well posedness

Definition 3.1 *The feedback interconnection in Figure 3.1 is said to be well posed if all possible closed loop transfer functions formed from the external signals $[r\ n\ d_o\ d_i]^T$ to $[u\ y]^T$ exist (i.e. they are well defined) and are proper.*

Knowing that the transfer functions from $d_o \to u$ and $n \to u$ are the same and differ only by a sign from the transfer function from $r \to u$ it can be shown that *well-posedness* of the feedback system reduces to the existence and properness of the transfer matrix

$$\begin{bmatrix} d_i & d_o \end{bmatrix}^T \to u$$

For internal stability analysis of the plant-controller interconnection, the configuration in Figure 3.1 can be simplified [ZDG96] by regrouping the external *input* signals d_o, n and r into the feedback loop as w_2, and replacing the variable d_i by w_1. *Input* signals of the controller and the plant will be denoted correspondingly as e_2 and e_1. The resulting reduced feedback configuration is depicted on Figure 3.2 and is well-posed if and only if the transfer matrix from

$$\begin{bmatrix} w_1 & w_2 \end{bmatrix}^T \to e_1$$

[1]Although there are other, alternative descriptions for the error [SP96], in this thesis we will make use of the one presented in [Oga02], emphasizing that the sign will have no effect on the structure of the controller and its practicality.

exists and is proper.

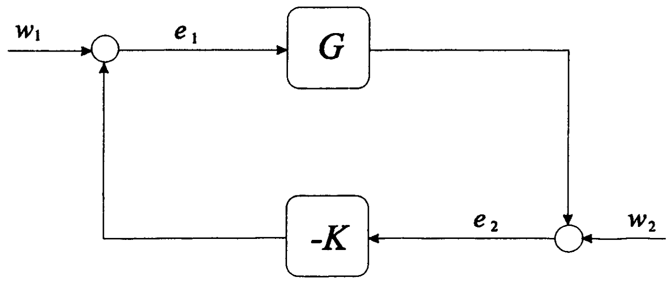

Figure 3.2: Internal stability analysis diagram

Well-posedness of the simplified general feedback configuration of Figure 3.2 can also be described as follows.

Lemma 3.1 *The new feedback system is well posed if and only if* $(I + G(\infty)K(\infty))$ *and* $(I + K(\infty)G(\infty))$ *are invertible, which is equivalent to* $det(I + GK)(s) \neq 0$ *and* $det(I + KG)(s) \neq 0$*, respectively for some* $s \in \mathbb{C}$.

3.1.2 Internal stability

Ensuring stability of a (feedback) system is usually an initial fundamental requirement of the control system design. Although there are a few definitions for internal stability from algebraic and functional analysis view points [DGKF89], [ZDG96] they are all equivalent. We will use the following:

Definition 3.2 *The interconnection in Figure 3.2 is said to be internally stable if and only if the transfer function matrix from*

$$\begin{bmatrix} w_1 \\ w_2 \end{bmatrix} \longrightarrow \begin{bmatrix} e_1 \\ e_2 \end{bmatrix}$$

with the following representation

$$\begin{aligned} \begin{bmatrix} I & K \\ -G & I \end{bmatrix}^{-1} &= \begin{bmatrix} G \\ I \end{bmatrix} (I + KG)^{-1} [-K \;\; I] \\ &= \begin{bmatrix} K \\ I \end{bmatrix} (I + GK)^{-1} [G \;\; I] \end{aligned} \tag{3.1}$$

belongs to $\mathcal{RH}_\infty$. Which requires that all closed loop transfer functions in Figure 3.2 are stable.

Remark 3.1 *Internal stability as a basic requirement for a feedback system is a more stringent stability requirement than the simple input-output stability of the closed loop system, because it also bans right-half-plane pole-zero cancelations between the cascaded systems in the closed loop. Internal stability is a state-space notion [ZDG96] [p.121].*

In the later sections, for brevity of notation, we will drop the dependence of the (open/closed)-loop transfer functions on 's'.

3.1.3 Coprime factorization

A *Coprime* factorization as a mathematical tool plays a cental role in many aspects of control theory as several of the fundamental ideas in $\mathcal{H}_\infty$ optimization, model reduction and robust stabilization have their basis in *coprime* factor theory [Vid85], [GM89], [MGV90]. The notion of the *coprime* factor representation of a given plant **G** or a controller **K** will be extensively used throughout this thesis. The following are some standard results revolving around the *coprime* factorization and important facts on *coprime* factors. Two transfer functions $M(s), N(s) \in \mathcal{RH}_\infty$ are said to be *coprime* over $\mathcal{RH}_\infty$ if there exist two other functions $X(s), Y(s) \in \mathcal{RH}_\infty$ satisfying the equality:

$$XM + YN = 1,$$

which holds if N and M do not have common zeros in the closed right-half-plane or at $s = \infty$. In fact any common *RHP* zeros of N and M would lead to hidden *RHP* pole/zero cancellations in the factorization.

Let **G** be a proper real-rational matrix.

Definition 3.3 *A right-coprime factorization (rcf) of* **G** *is a factorization* $\mathbf{G} = \mathbf{N}\mathbf{M}^{-1}$, *where the matrices* **M** *and* **N**, *both in* $\mathcal{RH}_\infty$, *are right coprime over* $\mathcal{RH}_\infty$ *if they have* <u>*the same number of columns*</u> *and if there exist matrices* X_r *and* Y_r *that satisfy the Bezout (or Aryabhatta's [Wae84]) identity:*

$$\begin{bmatrix} X_r & Y_r \end{bmatrix} \begin{bmatrix} M \\ N \end{bmatrix} = I.$$

Similarly,

Definition 3.4 *A left-coprime factorization has the form* $\mathbf{G} = \widetilde{\mathbf{M}}^{-1}\widetilde{\mathbf{N}}$*, where the two matrices* $\widetilde{\mathbf{M}}$ *and* $\widetilde{\mathbf{N}}$*, both in* $\mathcal{RH}_\infty$ *, are left coprime over* $\mathcal{RH}_\infty$ *if they have the same number of rows and if there exist matrices* X_l *and* Y_l *both in* $\mathcal{RH}_\infty$ *satisfying:*

$$\begin{bmatrix} \widetilde{\mathbf{M}} & \widetilde{\mathbf{N}} \end{bmatrix} \begin{bmatrix} X_l \\ Y_l \end{bmatrix} = I.$$

Every real-rational transfer function matrix representation of a proper plant admits *left* and *right coprime* factorizations:

$$\mathbf{G} = \widetilde{\mathbf{M}}^{-1}\widetilde{\mathbf{N}} = \mathbf{N}\mathbf{M}^{-1}.^2 \tag{3.2}$$

Hereafter where appropriate, *left* and *right coprime* factorizations will be respectively denoted by l.c.f and r.c.f.

An arbitrary large number of lcf or rcf can be generated for given rational transfer functions (Theorem 4.43) [Vid85].

All l.c.f and r.c.f of transfer function matrices are *unique* up to a matrix $W \in \mathcal{RH}_\infty$ such that W is a unit, i.e. $W, W^{-1} \in \mathcal{RH}_\infty$, *Lemma* **A.2.1** [GL95]. For example

$$\begin{bmatrix} N_2 \\ M_2 \end{bmatrix} = \begin{bmatrix} N_1 \\ M_1 \end{bmatrix} W$$

The computation of a *coprime* factorization involves selecting a stabilizing state-feedback (estimate) gain matrix, and a stable observer gain matrix [GL95], [GM89].

A control oriented interpretation of the *right coprime* factorization comes out naturally by changing the control variable by a state feedback [ZDG96] [p.127].

Coprime factorizations can be used to obtain alternative characterizations of conditions for the internal stability of interconnected systems (**G**,**K**) as depicted in Figure 3.1.

A particular and useful type of l.c.f or r.c.f is one in which the factors **N** and **M** are *normalized*.

[2] Both **M** and $\widetilde{\mathbf{M}}$ are square, nonsingular and $0 < \|M^{-1}\|_\infty < \beta, \beta \in \mathbb{R}$.

Definition 3.5 *The ordered pair* $[M \;\; N]'$, *a right coprime factorization of* $\mathbf{G} = NM^{-1}$ *with* $N, M \in \mathcal{RH}_\infty$, *is called a normalized right coprime factorization if* $M^*M + N^*N = I$ *for every* $s \in \mathbb{C}$, *i.e. if* $\begin{bmatrix} M \\ N \end{bmatrix}$ *is inner.*

A *normalized left coprime factorization* can be similarly defined:

Definition 3.6 *The ordered pair* $\begin{bmatrix}\tilde{M} & \tilde{N}\end{bmatrix}$, *a left coprime factorization of* $\mathbf{G} = \tilde{M}^{-1}\tilde{N}$ *with* $\tilde{N}, \tilde{M} \in \mathcal{RH}_\infty$, *is called a normalized left coprime factorization if* $\tilde{M}\tilde{M}^* + \tilde{N}\tilde{N}^* = I$ *for every* $s \in \mathbb{C}$, *i.e. if* $\begin{bmatrix} \tilde{M} & \tilde{N} \end{bmatrix}$ *is co-inner.*

If (square or nonsquare) $\mathbf{N} \in \mathcal{RH}_\infty$ and $\mathbf{N}^*\mathbf{N} = \mathbf{I}$ then $\mathbf{N}$ is called *inner*. Separately, if $\mathbf{N}$ satisfies $\mathbf{N}\mathbf{N}^* = \mathbf{I}$ then $\mathbf{N}$ is called *co-inner*. Inner matrices, due to their norm preserving property, have an important role to play in control systems synthesis.

A state-space construction for the *normalized left* (respectively *right*) *coprime* factorizations can be obtained in terms of the solution to the generalized control (respectively filter) Algebraic Riccati Equations [GM89] and the plant does not need to be strictly proper [Vid88].

It can be shown that *normalized left* and *right coprime* factors can be bounded from above [MG92].

Remark 3.2 *If* $(\tilde{\mathbf{N}}_s, \tilde{\mathbf{M}}_s)$ *is a normalized left coprime factorization of a given shaped plant* $\mathbf{G}_s$ *such that* $\mathbf{G}_s = \tilde{\mathbf{M}}_s^{-1}\tilde{\mathbf{N}}_s$ *then it can be shown that* $\overline{\sigma}(\tilde{\mathbf{N}}_s) \leq 1$ *and* $\overline{\sigma}(\tilde{\mathbf{M}}_s^{-1}) \leq 1$ *for all frequencies* $\omega \in \mathbb{R}$.

It is important to note that *coprime* factorization and stabilization of a given system are closely related. This establishes one of the motivations for using *coprime* factorization in $\mathcal{H}_\infty$ loop-shaping for synthesizing robustly stabilizing controllers. Later in Chapter 4 we will see how the *normalized coprime* factorization is used in the solution of the robust stability problem within an $\mathcal{H}_\infty$ loop-shaping framework. Engineering interpretation of *coprime* factorisation follows from the above two definitions; the factorisation allows an unstable plant $\mathbf{G}$ to be partitioned into two stable subsystems $\mathbf{N}$ and $\mathbf{M}$.

3.1.4 Small gain theorem

The small gain theorem is one of the key theorems in the analysis of robust stability of interconnected systems. With reference to Figure 3.3 it essentially states that if a feedback loop consists of stable systems and the loop-gain is less than unity, then the feedback loop is internally stable.

Theorem 3.1 *([ZDG96] p.218) Suppose $M \in \mathcal{RH}_\infty$ and let $\gamma = \epsilon^{-1} > 0$. Then the interconnected system shown in Figure 3.3 is well posed and internally stable for all $\Delta(s) \in \mathcal{RH}_\infty$ with*

a) $\|\Delta\|_\infty \le \epsilon$ *if and only if* $\|M(s)\|_\infty < 1/\epsilon$;

b) $\|\Delta\|_\infty < \epsilon$ *if and only if* $\|M(s)\|_\infty \le 1/\epsilon$.

The theorem continues to hold even if the subsystems of the interconnection in Figure 3.3 are infinite dimensional systems.

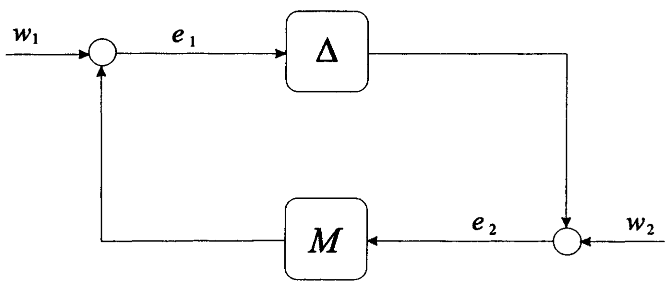

Figure 3.3: Small Gain Interconnection

It is possible that the hypotheses of the small gain theorem will get violated by the system or systems making up the feedback loop. It is possible, however, by introducing loop transformations [ZDG96], [GL95] to extend the range of applicability of the small gain theorem while preserving the stability properties of the feedback system. This will allow the feedback system to be modified and stability of the closed loop system established by applying the small gain theorem.

Among several versions of the small gain theorem the one which is based on the fixed point theorem (also contraction mapping theorem [GL95])uses the incremental gain and it guarantees the existence of solutions to the loop equations and their stability.

3.2 Important relationships in the standard feedback configuration

It is known that with feedback we can achieve a significant reduction of the effects of uncertainty for certain signals of importance at the expense of small increases due to other signals. In order to acquire an insight into the concept of design trade-offs for conflicting objectives we will consider some equalities relating various signals of interest.

Consider the standard feedback configuration depicted in Figure 3.1.

It is convenient to define the *input loop transfer matrix*, $\mathbf{L}_i$, as $\mathbf{L}_i = \mathbf{KG}$ formed by breaking the loop at the input u of the plant. Similarly the *output loop transfer matrix*, $\mathbf{L}_o$, is defined as $\mathbf{L}_o = \mathbf{GK}$ obtained by breaking the loop at the output y of the plant. It must be noted that unlike SISO systems, in MIMO systems $\mathbf{L}_o \neq \mathbf{L}_i$. This clearly holds for other closed loop transfer functions like $\mathbf{S}_{i,o}$ and $\mathbf{T}_{i,o}$ etc.

The transfer function matrix $[d_i \rightarrow u_p]$ relating the disturbance at the plant input d_i and the input to the plant u_p, i.e. $u_p = \mathbf{S}_i d_i$, defines the *input sensitivity* of the system. $\mathbf{S}_i = (I + \mathbf{L}_i)^{-1}$, where $(I + \mathbf{L}_i)$ is called the *input return difference matrix*. Similarly the *output sensitivity* matrix is defined as the transfer function matrix mapping the output disturbance d_o of the plant to the system's output y as in $y = \mathbf{S}_o d_o$ where $\mathbf{S}_o = (I + \mathbf{L}_o)^{-1}$, and $(I + \mathbf{L}_o)^{-1}$ is called the *output return different matrix*.

The complement of the sensitivity $\mathbf{S}$ is denoted by the symbol $\mathbf{T}$ and satisfies $\mathbf{S}+\mathbf{T} = I$. This constitutes an inherent algebraic design limitation in terms of the *input* and *output complementary sensitivity* matrices, namely:

$$\mathbf{T}_i = I - \mathbf{S}_i = \mathbf{L}_i(I + \mathbf{L}_i)^{-1}$$

and

$$\mathbf{T}_o = I - \mathbf{S}_o = (I + \mathbf{L}_o)^{-1}\mathbf{L}_o$$

Typical sensitivity- $\mathbf{S}_{i,o}$ and co-sensitivity- $\mathbf{T}_{i,o}$ plots are shown in Figures 5.6 and 5.8 respectively.

Looking at Figure 3.1 it is straightforward to show that feedback loop variables and external (disturbance) signals are related by the following equalities:

$$y = \mathbf{T}_o(r - n) + \mathbf{S}_o\mathbf{G}d_i + \mathbf{S}_o d_o \tag{3.3}$$

$$r - y = \mathbf{S}_o(r - d_o) + \mathbf{T}_o n - \mathbf{S}_o\mathbf{G}d_i \tag{3.4}$$

$$u = \mathbf{KS}_o(r - n) - \mathbf{KS}_o d_o - \mathbf{T}_i d_i \tag{3.5}$$

$$u_p = \mathbf{KS}_o(r - n) - \mathbf{KS}_o d_o + \mathbf{S}_i d_i \tag{3.6}$$

These relationships hold whether or not the system is stable.

Table 3.1 summarizes the transfer functions in expressions 3.3-3.6.

$\mathbf{T}_{\{out\equiv row, input\equiv col\}}$	d_i	d_o	n	r
y	$\mathbf{S}_o\mathbf{G}$	$\mathbf{S}_o$	$-\mathbf{T}_o$	$\mathbf{T}_o$
u_p	$\mathbf{S}_i$	$\mathbf{KS}_o$	$-\mathbf{KS}_o$	$\mathbf{KS}_o$
e=r-y	$-\mathbf{S}_o\mathbf{G}$	$-\mathbf{S}_o$	$\mathbf{T}_o$	$\mathbf{S}_o$
u	$-\mathbf{T}_i$	$-\mathbf{KS}_o$	$-\mathbf{KS}_o$	$\mathbf{KS}_o$

Table 3.1: Relations between exogenous inputs (ω) and the outputs (z)

Several performance[3] trade-offs inherent in feedback design can be understood using the set of Equations (3.3-3.6) and the well-known multiplication and addition properties of singular values [GL95].

For example, good disturbance rejection at the system's output y against a disturbance d_o at the plant output, from Equation 3.3, requires that the output sensitivity $\mathbf{S}_o$ is small [4].

This leads to

$$\overline{\sigma}(\mathbf{S}_o) = \frac{1}{\underline{\sigma}(I + \mathbf{GK})} \leq \frac{1}{\underline{\sigma}(\mathbf{GK}) - 1} \ll 1 \tag{3.7}$$

Following similar logic, good disturbance rejection at the system's output y against disturbances d_i at the plant input can be achieved, from Equations 3.3 and 3.4, by making $\overline{\sigma}(\mathbf{S}_o\mathbf{G})$ (and $\overline{\sigma}(\mathbf{GS}_i)$[5]) small.

[3]By performance we mean: good reference tracking, good disturbance rejection at the plant input and output, and good input/output decoupling.

[4]The notion of smallness will relate to the size of a transfer function matrix measured by its maximum singular value as a function of frequency, $\overline{\sigma}(\bullet) \ll 1$.

[5]It can easily be shown that $\overline{\sigma}(\mathbf{S}_o\mathbf{G}) = \overline{\sigma}(\mathbf{GS}_i)$.

It follows from Equation 3.6 that the impact of disturbances (d_i) and (d_o) on the plant input u_p can be reduced if

$$\overline{\sigma}(\mathbf{S}_i) = \frac{1}{\underline{\sigma}(I + \mathbf{KG})} \leq \frac{1}{\underline{\sigma}(\mathbf{KG}) - 1} \tag{3.8}$$

is made small (for d_i), and if $\overline{\sigma}(\mathbf{KS}_o)$ is made small for d_o, respectively.

It is important to note that in the above the closed loop transfer functions are required to be small where disturbances d_i and d_o are significant, and this is usually at low frequencies.

3.2.1 Design tradeoffs in feedback systems for conflicting objectives

It has been emphasised that internal stability is of primary importance. However, rarely is it the only motivation for introducing feedback in control. In the case of a stable plant it can be shown that feedback control may even have a detrimental effect on the stability robustness of the system as it actually increases the effects of uncertainty and increases sensitivity in the frequency ranges where uncertainty is large [GL95], [ZDG96]. Secondly, but an equally important motivator for introducing feedback control is the desire to enhance performance in the presence of conflicting objectives dictated both by the plant and by the operating environment over different frequency ranges of interest. Objectives which are typically important in the low frequency range of operation of the system are disturbance attenuation and reference command tracking (and are related to sensitivity reduction). Whereas constraints on the magnitude of the control signal and mitigation of sensor noise are characteristically high frequency objectives.

It is well known that stability and performance requirements impose respectively structural and magnitude constraints on certain closed loop transfer functions. As we will see it is possible that these constraints can also be expressed in terms of the open loop transfer functions.

For SISO plants the differentiation of α with respect to β gives the relative (or percentage) change in α due to a relative (or percentage) change in β. This is denoted by: $S_\beta^\alpha = \frac{\partial\alpha}{\partial\beta}\frac{\beta}{\alpha}$. It is a measure of how sensitive a quantity α is to changes in a quantity β.

Sensitivity is an operator which has an important role to play in the assessment of feedback objectives such as closed loop tracking and disturbance rejection.

Using the singular values as a tool and the closed loop depicted on Figure 3.1 where

G-the modelled plant and K-the controller are both square we will try to summarize the most important design objectives from a performance perspective.

Below are several of the design objectives with corresponding performance criteria.

3.2.1.1 Disturbance rejection

Because systems do not operate in ideal environments they will inevitably become prone to disturbances from various sources e.g. load variations on air frames, adverse weather conditions like heavy rain or wind gusts. As mentioned earlier, attenuation or -if possible- elimination of the effect of these at the plant input and output or some other critical points in the feedback-loop emerges as one of the main requirements for performance. Depending on the application see [SP96], [GL95] the disturbance signal may be filtered through a transfer function matrix $\mathbf{G}_d$.

A few linear algebraic manipulations[6] should convince the reader that good disturbance attenuation will be achieved if $\underline{\sigma}(\mathbf{L}_o) \gg 1$ in $[0, \omega_l)$, i.e. if the loop gain is sufficiently large at low frequencies. Disturbance attenuation is also possible via feed-forward compensation.

$$\frac{1}{\underline{\sigma}(\mathbf{L}_o)+1} \leq \overline{\sigma}(\mathbf{S}_o) \leq \frac{1}{\underline{\sigma}(\mathbf{L}_o)-1}, \quad if \ \underline{\sigma}(\mathbf{L}_o) > 1 \tag{3.9}$$

$$\therefore \overline{\sigma}(\mathbf{S}_o) \ll 1 \Longleftrightarrow \underline{\sigma}(\mathbf{L}_o) \gg 1 \tag{3.10}$$

It follows from the right-hand-side of the inequality in Equation 3.9 that in order to reduce the impact of plant output disturbance d_o on the system's output y, the output sensitivity $\mathbf{S}_o$ must be minimized, such that $||S_o||_\infty < \gamma$, $\gamma \in \mathbb{R}$. Minimization of $||\mathbf{S}_o||_\infty$ is a worst-case optimization, because it amounts to minimising the effect on the output, y, of the worst disturbance d_o (a harmonic disturbance at the frequency where $\mathbf{S}$ has its peak value) when measured with appropriate norm. This ensures that $||y(j\omega)||_2 = \gamma_{dr}||d_o(j\omega)||_2$ [7]. By using feedback this is indeed possible and one of the most effective ways to achieve it, is to make the output loop-gain, L_o, large-Equation 3.10.

[6]Through the use of the singular value inequalities, Equations (3.9 and 3.12) relate $\mathbf{S}_i(\mathbf{S}_o)$ to $\mathbf{L}_i(\mathbf{L}_o)$.

[7]The parameter γ_{dr} is associated with the disturbance rejection problem.

Similarly, from

$$\overline{\sigma}(\mathbf{GS}_i) = \overline{\sigma}(\mathbf{S}_o\mathbf{G}) = \overline{\sigma}((\mathbf{G}^{-1} + \mathbf{K})^{-1}) \approx \overline{\sigma}(\mathbf{K}^{-1}) = \frac{1}{\underline{\sigma}(\mathbf{K})} \quad (3.11)$$

it follows that in order to desensitize the effect of plant internal disturbance d_i at the system's output y, the designer needs to ensure large enough controller gain ($\underline{\sigma}(\mathbf{K}) \gg 1$) at low frequencies $\Omega \in (0, \omega_l]$.

We recall that:

$$\frac{1}{\underline{\sigma}(\mathbf{L}_i) + 1} \leq \overline{\sigma}(\mathbf{S}_i) \leq \frac{1}{\underline{\sigma}(\mathbf{L}_i) - 1}, \ \textit{if} \ \underline{\sigma}(\mathbf{L}_i) > 1 \quad (3.12)$$

$$\therefore \overline{\sigma}(\mathbf{S}_i) \ll 1 \Longleftrightarrow \underline{\sigma}(\mathbf{L}_i) \gg 1 \quad (3.13)$$

In the presence of internal disturbances d_i, their impact onto the plant input signal u_p can be minimized by minimizing the size of the input sensitivity $\mathbf{S}_i$. From the right-hand-side of the inequality of Equation 3.12 it follows that this is attainable if the input loop-gain, $\mathbf{L}_i$, is made large at low frequencies $\Omega \in (0, \omega_l]$, where the need to suppress the disturbances at the plant input or output, or penalize large reference command signals exists.

In summary, the objective of reducing the effect of disturbances acting on the input and output of the plant translates into bounds on the size of the input $||\mathbf{S}_i||_\infty$ and output sensitivity $||\mathbf{S}_o||_\infty$ as well as $||\mathbf{S}_o\mathbf{G}||_\infty$.

3.2.1.2 Command tracking

Design of a system for successful tracking of the command input (or reference signal) r, with a steady-state gain of **1** between that reference command and plant output y formulates yet another performance objective. This objective referred to as the *tracking* or *servo problem* is usually relevant at low frequencies [8] and can be attained by making the transfer function relating r to y, namely the co-sensitivity transfer function $\mathbf{T}_o$ equal to unity matrix. It is practically impossible to bring $\mathbf{T}_o = \mathbf{I}$, therefore a more feasible approach is to consider the minimization of the equivalent transfer function $\mathbf{S}_o$ from reference r to e, where $e = r - y$. In the induced norm sense, this is $||y(j\omega) - r(j\omega)||_2 \leq \gamma_{ct}||r(j\omega)||_2$, where $\gamma_{ct} \in \mathbb{R}$ [9], and preferably $\gamma \ll 1$. The problem

[8] We will denote low frequency range with $(0, \omega_l)$, and correspondingly the high frequency range with (ω_h, ∞).
[9] The parameter γ_{ct} is associated with the command tracking problem.

is similar to reducing the effects of output disturbances as considered earlier. Thus using Equation 3.9, closed loop objectives can be expressed by bounds on the relevant open-loop $\mathbf{L}_o$ transfer function gain, and from Equation 3.10 it follows that $\underline{\sigma}(\mathbf{L}_o) \gg 1$ in the low frequency range $\Omega \in (0, \omega_l)$ derives an equivalent requirement to ensure good *tracking*.

In a design problem all the above mentioned low frequency performance objectives cannot be met simultaneously, since $\mathbf{S} + \mathbf{T} = \mathbf{I}$ constitutes an algebraic constraint and requires trade-offs. That is, some performance objectives will come in conflict with other objectives that are important at high frequencies (ω_h, ∞), namely robustness and sensor noise rejection which we will consider briefly a little later. Therefore, establishing emphasis on any of them as well as defining relevant frequency ranges is left to the designers experience, intuition and knowledge.

3.2.1.3 Noise rejection

It is a well known fact that the successful operation and high performance of a feedback system relies on accurate measurements of the feedback quantities. This process requires sensors which are accurate over the operating bandwidth of that system. However, as the plant operates in an environment which is not noise free this will undoubtedly affect the accuracy of the measurements being read by the sensors. Similar to disturbances the impact of sensor errors can be profoundly detrimental to the performance of a feedback system. It is therefore important that their effect on the system output is reduced as much as possible. This is how in feedback control mitigation of the effect of noises on various points in the loop, but mainly the output, in addition to the objectives listed so far, emerges as an important performance objective with robustness emphasis. The task of reducing the effects of inaccurate sensors is predominantly a high frequency phenomenon and thus arises as a high frequency requirement.

Since the transfer function mapping $n \to y$ is the co-sensitivity transfer function $\mathbf{T}_o$, the requirement for good sensor noise error rejection at the system's output essentially reduces to minimization of $\overline{\sigma}(\mathbf{T}_o)$ in the frequency range where noise reduction is needed. From $\|y(j\omega)\|_2 \geq \gamma_{nr}\|n(j\omega)\|_2$, $\gamma_{nr} \in \mathbb{R}$ [10] this ensures that the energy of the output signal y is least effected by the variations in the magnitude of the sensor noise

[10] The parameter γ_{nr} is associated with the noise rejection problem.

n.

However, from ($\|y\|_2 = (I - \overline{\sigma}(\mathbf{S}_o))\|n\|_2 \ll 1$) it becomes obvious that good disturbance rejection and tracking (i.e $\overline{\sigma}(\mathbf{S}_o) \ll 1$) imply that sensor noise model errors n will get to the system's output (almost) unattenuated. This indicates that for $\overline{\sigma}(\mathbf{S}_o) \ll 1 \Rightarrow \overline{\sigma}(\mathbf{T}_o) \approx 1$ noise attenuation conflicts with objectives requiring high-loop gain $\underline{\sigma}(\mathbf{L}_o) \gg 1$. Therefore it emerges that there must be a frequency separation between low and high frequency control system design objectives.

Remark 3.3 *Frequencies (ω_l, ω_h) that serve as bounds on correspondingly low and high frequency regions are problem dependent, and require information about modelling uncertainties, sensor noise levels and disturbance characteristics of the plant [SBG97].*

Since

$$\overline{\sigma}(\mathbf{T}_o) = \frac{\overline{\sigma}(\mathbf{GK})}{\underline{\sigma}(\mathbf{I}+\mathbf{GK})} \ll 1 \tag{3.14}$$

some simple algebraic manipulation will convince the reader that requirements on

$$\overline{\sigma}(\mathbf{T}_o) \ll 1 \tag{3.15}$$

boil down to requirements on having the open-loop gain low, $\overline{\sigma}(\mathbf{GK}) \ll 1$.

Arbitrary large loop-gains over a large frequency span in the low frequency region will conflict with some robustness requirements in the high frequency region. Large loop-gains $\underline{\sigma}(\mathbf{L}_{i,o}) \gg 1$ in the frequency range stretching far beyond the plant $\mathbf{G}$'s bandwidth may lead to unacceptable control activity possibly resulting in actuator saturation, on which, as a robustness objective, we will devote our attention next.

3.2.1.4 Control effort

So far most of the objectives in control system design have been enhanced by ensuring a high open-loop gain. The closed loop bandwidth, however, cannot be made significantly greater than the open-loop without invoking high controller gain. Any objective requiring high loop gain $\underline{\sigma}(\mathbf{GK}) \gg 1$ beyond the open-loop will demand high gain from the controller. Such high gain can result in excessive activity of the actuators. This is why, it is the action of limiting or reduction of control effort that will ensure that the magnitudes of actuator control signals do not exceed their limits of operation, which may lead to instability. In the cases where actuator saturation is likely, anti-windup techniques successfully applied in actuator saturation prevention can be employed [HTPG04].

Assuming, for convenience, that **G** is *square* and invertible, then whenever $\underline{\sigma}(\mathbf{L}_o) \gg 1$ and thus $\overline{\sigma}(\mathbf{S}_o) \ll 1$ at the frequencies beyond the open-loop bandwidth ($\overline{\sigma}(\mathbf{G}) \ll 1$) the external signals (disturbance and noise) will be amplified at the plant input u_p. Transfer function:

$$(I + \mathbf{KG})^{-1}\mathbf{K} = \mathbf{K}(I + \mathbf{GK})^{-1} \tag{3.16}$$

plays a crucial role in the assessment of the impact of external disturbances on the control signal. It also arises in the analysis of stability robustness of a closed loop system with respect to additive model error- which we will briefly review later in this chapter.

Referring to Figure 3.1 in the presence of external disturbances d_o, good performance at the plant input u_p requires that $\overline{\sigma}(\mathbf{KS}_o) = \overline{\sigma}(\mathbf{S}_i\mathbf{K})$ [11] be made small in the frequency range where d_o is significant. As can be seen from Equation 3.17 one way of achieving that is in the case when the plant's gain is large enough. This, however, constitutes an inherent plant limitation and thus cannot be altered by the controller design. Instead, it requires an alteration in the dynamics of the system.

$$\overline{\sigma}(\mathbf{S}_i\mathbf{K}) = \overline{\sigma}(\mathbf{KS}_o) = \overline{\sigma}((\mathbf{K}^{-1} + \mathbf{G})^{-1}) = \frac{1}{\underline{\sigma}(\mathbf{K}^{-1} + \mathbf{G})} \approx \frac{1}{\underline{\sigma}(\mathbf{G})} \tag{3.17}$$

or

$$\overline{\sigma}(\mathbf{KS}_o) = \overline{\sigma}(\mathbf{K}(I + \mathbf{GK})^{-1}) \leq \frac{\overline{\sigma}(\mathbf{K})}{\underline{\sigma}(I + \mathbf{GK})^{-1}} \leq \frac{\overline{\sigma}(\mathbf{K})}{\underline{\sigma}(\mathbf{GK}) - I} \tag{3.18}$$

where **G** and **K** are invertible. At high frequencies in order to prevent actuator saturation the controller gain $\overline{\sigma}(\mathbf{K})$ should be kept to a "reasonable" size so that the loop-gains are small: $\overline{\sigma}(\mathbf{L}_i) \ll 1$ and $\overline{\sigma}(\mathbf{L}_o) \ll 1$.

Achieving good performance boils down to a set of requirements on $\underline{\sigma}(\mathbf{L}_i) \gg 1$, $\underline{\sigma}(\mathbf{L}_o) \gg 1$ and $\underline{\sigma}(\mathbf{K}) \gg 1$ at low frequencies $(0, \omega_h)$. Whereas achieving good robustness and sensor noise rejection, are high frequency (ω_h, ∞) phenomena requiring that $\overline{\sigma}(\mathbf{L}_i) \ll 1$, $\overline{\sigma}(\mathbf{L}_o) \ll 1$ and $\overline{\sigma}(\mathbf{K}) \leq M$ where $M \in \mathbb{R}$ is not too big[12].

[11] Simple algebraic manipulations can convince the reader in the validity of the equality.

[12] The value of M is problem dependent, but frequency analyses of several flight-tested controllers have shown that controllers satisfying M $\leq$ 4 exhibited good robustness properties.

It can be concluded that low frequency high loop gain objectives such as disturbance attenuation and tracking together with high frequency low loop gain objectives such as sensor noise and control signal activity constitute an important trade-off which the designer should take care of in the design of any feedback control system.

If disturbances and measurement noise are neglected it is possible [Ast00] to obtain a closed loop system with arbitrary high bandwidth. However, in the presence of measurement noise and actuator saturation this is not possible. If care is not taken, measurement noise injected into the system can result in large control signals which will lead to saturation of actuator control signals (see Equation 3.18). This is why measurement noise and actuator saturation are factors that may limit the performance by affecting the stability of a system. Recall the fundamental relationship (mentioned earlier) that relates $\mathbf{S}$ and $\mathbf{T}$ algebraically, $\mathbf{S}+\mathbf{T}=\mathbf{I}$. Which shows that $\mathbf{S}$ and $\mathbf{T}$ cannot be made small simultaneously.

3.3 Modelling and Uncertainty in Multivariable Systems

A fundamental requirement on the performance of any feedback control system is its ability to maintain the stability of the closed loop system- representing the real system which also embeds the uncertain hardware- provided that certain stabilisability and detectability conditions are satisfied. To circumvent degradation in the performance of the synthesized linear controller once it has been implemented on the nonlinear plant discrepancies between the plant and the derived mathematical model must be accounted for. Through appropriate selection of uncertainty model, the perturbed plant will provide a sound base for the synthesis of a controller which will perform in a satisfactory manner on the real system $\mathbf{G}_r$- which is also uncertain.

Amongst the main motivating reasons for using uncertainty is to capture the difference or mismatch between the nominal system model and an uncertain system model- obtained through laws of physics, thermodynamics etc., and to facilitate a realistic closed loop stability analysis. The use of uncertainty to represent the set of possible plants by $\mathbf{G}_\Delta$ is to facilitate approximation of the modelled plant $\mathbf{G}$ to the real -actual plant $\mathbf{G}_r$, which can also be formulated and considered as a model approximation problem with objective $\inf\|\mathbf{G}_r-\mathbf{G}_\Delta\|_\infty$. We assume that the real plant $\mathbf{G}_r$ will fall in the set $\mathbf{G}_\Delta$, i.e $\mathbf{G}_r \subset \mathbf{G}_\Delta$.

A key assumption in representing discrepancies in the model is that the uncertain part of a process can be separately represented from the known part of the process-the nominal plant. Depending on the information available about the uncertainty and their source, the uncertainties can be categorized mainly in three forms: structured, unstructured and parametric. Due to the nature of our problem the focus will be on unstructured uncertainty.

Structured uncertainty, as its name suggests, is uncertainty which has a structure, typically diagonal or diagonally dominant and thus it is transparent in reflecting the sections of a process model from which stems information about the source of the uncertainty. However, sources and locations of uncertainty may not always be known and thus structuring the uncertainty in the complex interconnected systems, although very desirable, is rather uncommon. This is the case in the multi actuator driven nominally unstable helicopter plant which will be a subject of our research. Therefore, it has been assumed that all uncertainties are unstructured. In mathematical modelling of a system, low frequency dynamical behaviour will usually be sufficiently accurately captured by the model, however high frequency behaviour will be represented to a lesser extent. In a process, a very common way of modelling high frequency and usually hard to capture dynamics of a system is via unstructured uncertainty. This type of uncertainty denoted by the same symbol as in structured uncertainty, i.e. Δ(s), where $s \in \mathbb{C}$, presents no, or very scarce, information about its internal structure except that an upper bound on its magnitude as a function of frequency is known: $||\Delta||_\infty < \epsilon \equiv \sup_{\omega \in \mathbb{R} \bigcup \infty} \overline{\sigma}(\Delta(j\omega)) < \epsilon$, for $\forall\, \omega$.

3.3.1 Uncertainty and the role of the weighting function

In the $\mathcal{H}_\infty$ framework, all the uncertainties are represented in the frequency domain as functions of the frequency variable ω rad/sec and thus, they are complex. The size of the uncertainty $\Delta(s)$ by replacing s with $j\omega$ is a function of frequency. Knowing that the size of uncertainty in the plant is a function of frequency, a well established method to specify the importance of uncertainty at different frequency ranges is through transfer function matrices frequently named as weighting functions, denoted by **W**. These frequency dependent weights derive their name from the fact that they can be used on some closed/open-loop transfer functions allowing the $\mathcal{H}_\infty$ design engineer to reflect on the relative importance of their response, or to penalize the magnitude of the disturbance, noise and error signals at frequency ranges of importance.

There are three fundamental approaches to modelling the unstructured uncertainty that can be embedded in to the nominal system **G**, and allow for their successful use in controller synthesis and analysis. These are correspondingly via *additive* and *multiplicative* perturbations of the nominal system **G** or in the form of *additive* perturbations on the *coprime* factors of **G** [DS81], [Vid92], [ZDG96]. All perturbations denoted by the operator $\Delta(s)$ are assumed to have their poles in the $\Re(s) < 0$, that is $\Delta(s) \in \mathcal{RH}_\infty$.

We will devote more attention to the *coprime* factor type of uncertainty representation as it is a core tool of the $\mathcal{H}_\infty$ loop-shaping approach which we shall later make extensive use of in our controller design. We will also underline the motivational reasons for representing unstructured uncertainty in the nominal system as *coprime* factor perturbations rather than in *additive* or *multiplicative* form which we will also present for the sake of completeness. A comparison will further strengthen the choice of our uncertainty.

A more detailed account on representative types of physical uncertainties in the plant can be found in [ZDG96] [p.221 – 228] and [SP96].

The following are some of the forms through which unstructured uncertainty in the model can be represented.

3.3.2 Additive uncertainty

For a given transfer function **G** and unknown but otherwise bounded uncertainty transfer function Δ, with $\|\Delta\|_\infty < \epsilon$, the real plant $\mathbf{G}_r$ can be approximated by

$$\mathbf{G}_{\Delta_A} = \{(\mathbf{G} + \Delta) : \Delta \in \mathcal{RH}_\infty, \|\Delta\|_\infty < \epsilon\} \tag{3.19}$$

where $\mathbf{G}_r \in \mathbf{G}_{\Delta_A}$. This configuration of uncertainty representation in the model is known as *additive* uncertainty, or sometimes named as absolute uncertainty, where the uncertainty is represented by an *additive* perturbation of the nominal plant **G**.

Figure 3.4 shows a schematic of a feedback interconnection of a perturbed plant $\mathbf{G}_{\Delta_A}$ represented by an *additive* perturbation Δ and nominal plant **G** together with a controller **K** which is internally stabilizing the nominal closed loop and perturbed plants. The signals v_1 and v_2 are noise on the compensator output and on the measurements respectively, u is input to the real plant and y is output from the real plant.

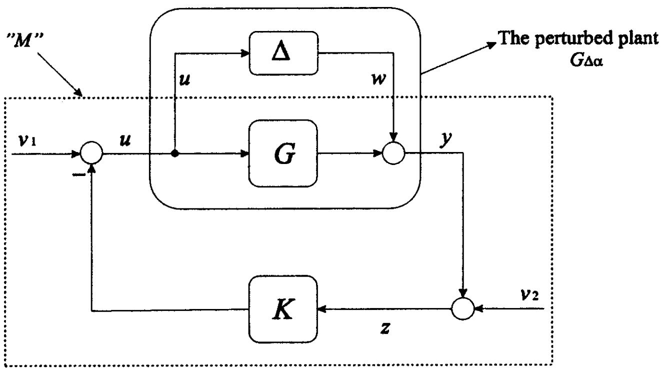

Figure 3.4: Additive Uncertainty Represention

3.3.2.1 Stability robustness analysis under additive uncertainty

In the process of design, it is important to know the smallest size of $||\Delta||_\infty$ that will destabilize the closed loop. In the case when uncertainty in the plant is modelled in the form of an *additive* perturbation i.e. $\mathbf{G}_{\Delta_A} = \mathbf{G} + \Delta$, $||\Delta||_\infty < \epsilon$, where $\epsilon \in \mathbb{R}$, then we can formulate a robust stabilization problem which reduces to finding a stabilizing controller $\mathbf{K}$ for all plants of the form $\mathbf{G} + \Delta$ in which allowable $||\Delta||_\infty$ is maximized. Then, a controller that maximizes $||\Delta||_\infty$ is optimally robust in the sense that it stabilizes the largest ball of plants with centre $\mathbf{G}$, and stability robustness of the closed loop can be assessed using the small gain theorem [Zam63] (see section 3.1.4).

Consider the Figure 3.4, where v_1 and v_2 are both zero, then

$$y = \mathbf{G}z + w$$
$$u = z = \mathbf{K}y$$
$$z = \mathbf{KG}z + \mathbf{K}w$$
$$z = (I - \mathbf{KG})^{-1}\mathbf{K}w$$

Application of the small gain theorem shows that the interconnection $[\mathbf{M}, \Delta]$, where $\mathbf{M} = (I - \mathbf{KG})^{-1}\mathbf{K}$, is stable for all $\Delta \in \mathcal{RH}_\infty$, providing that $||\mathbf{M}||_\infty < \frac{1}{\epsilon}$ and $||\Delta||_\infty||\mathbf{M}||_\infty < 1$. In other words, the reciprocal of the largest singular value of $\mathbf{M}$, $\overline{\sigma}(\mathbf{M})$ serves as a measure of the smallest unstructured perturbation Δ that will result in instability of the feedback system interconnection. Mathematically, at any frequency $s = j\omega \in \overline{\mathbb{C}}_+$ (where $\overline{\mathbb{C}}_+$ is the bounded set of positive complex numbers) this can be written as:

$$\overline{\sigma}(\mathbf{M}(s)) = \frac{1}{\min\{\overline{\sigma}(\Delta) : det(I - \mathbf{M}(s)\Delta) = 0, \Delta - unstructured\}}. \tag{3.20}$$

When Δ is considered structured and complex, the concept leads to a generalization and a new mathematical measure of robustness and performance, the so called structured singular value $\mu_\Delta(\mathbf{M}(s))$ [PD93].

The optimal robustness problem therefore requires a stabilizing controller that minimizes $\|(I - \mathbf{KG})^{-1}\mathbf{K}\|_\infty$.

The stability of both $[\mathbf{G}, \mathbf{K}]$ feedback loop and $[\mathbf{M}, \Delta]$ feedback loop is sufficient to guarantee the stability of the interconnection $[\mathbf{G}_\Delta, \mathbf{K}]$ [Vin00].

Note that for the *additive* type of uncertainty representation, the nominal plant $\mathbf{G}$ and the perturbed plant $\mathbf{G}_{\Delta_A}$ need to share the same number of *RHP* poles, but their location can vary as long as Δ is bounded in infinity norm sense [Vin00]. If η denotes the number of *RHP* poles then, $\eta(\mathbf{G}_{\Delta_A}) = \eta(\mathbf{G})$.

If the nominal plant $\mathbf{G}$ and the perturbed plant $\mathbf{G}_{\Delta_A}$ do not share the same number of *RHP* poles then there will not exist any stable Δ, such that $\mathbf{G}_{\Delta_A} = \mathbf{G} + \Delta$.

In the case of an *additive* uncertainty representation, to guarantee a satisfactory stability result the gain of the compensator should be small; consider $\|\mathbf{K}(I - \mathbf{GK})^{-1}\|_\infty$ as an example.

3.3.3 Multiplicative uncertainty

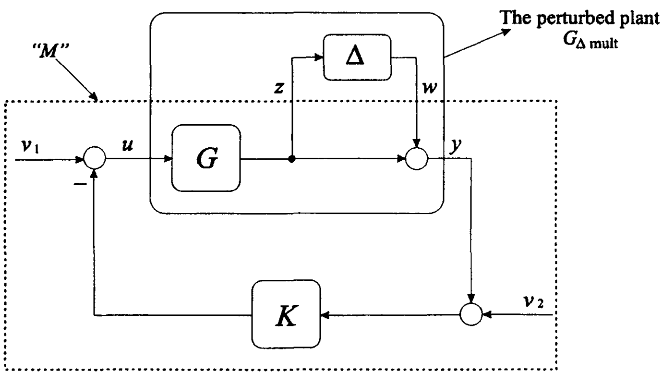

Figure 3.5: Multiplicative Uncertainty

Figure 3.5 depicts a schematic representation of *output multiplicative* uncertainty modelling for a nominal plant G. *Multiplicative* uncertainty, also referred to as relative uncertainty $\Delta_{mult} = \Delta_{add}\mathbf{G}^{-1}$, is a weighted form of *additive* uncertainty and mathematically can be represented as

$$\mathbf{G}_{\Delta_{mult}} = \{(I+\Delta)\mathbf{G} : \Delta \in \mathcal{RH}_\infty, \|\Delta\|_\infty < \epsilon\}, \tag{3.21}$$

where $\mathbf{G}_{\Delta_{mult}}$ forms the perturbed plant and the perturbation Δ is weighted by the plant $\mathbf{G}$.

Depending on the location at which the perturbation is inserted, the *multiplicative* uncertainty can be treated as *input* or *output*. In the case of placing the perturbation at the *output* of the plant as in Figure 3.5 this uncertainty representation becomes useful in characterizing *RHP* zeros, neglected and unmodelled high frequency dynamics of the sensors or plant; whereas the case of locating a perturbation at the *input* of the plant is favourable in characterizing actuator errors.

In practice, uncertainty at high frequency arises mainly due to unmodelled dynamics and parasitic effects in the system. Tolerance against the so-called unstructured *multiplicative* uncertainty at the plant output can therefore be achieved by making the output complementary sensitivity transfer function $\mathbf{T}_o$ small at high frequency [DS81]; see also section 3.2.1. A large amount of multiplicative uncertainty is dealt with by making the loop gain small.

For *multiplicative* uncertainty, as it was for *additive* uncertainty, the requirement that all the systems described by the set $\mathbf{G}_{\Delta_{mult}}$ must have the same number of *RHP* poles as in the nominal system $\mathbf{G}$ continues to hold. From a practical perspective, however, this constraint is unrealistic. It makes it impossible to perturb the number of *RHP* poles by incorporating uncertainty in them. It has been shown in [Glo86] that in the robust stabilization of *additive* perturbations, the largest robustly stabilizable region with a single controller has a nonstabilizable plant on its boundary. The same remark applies to unstructured *multiplicative* perturbations, and the non-linear and time-varying controllers can do no better [KGP87]. Modelling of small uncertainty in the pole locations of a pair of lightly damped resonant poles with *additive* or *multiplicative* perturbation of finite norm is difficult [GSM90].

Therefore both *additive* and *multiplicative* uncertainty in some cases may become inadequate as tools for modelling uncertainty with the purpose for robust control system design. In cases where *additive* and *multiplicative* uncertainty modelling falls short in representing perturbations without any violation of the unstable poles, an alternative mathematical framework can and will be used. Modelling uncertainties via a normalized *coprime* factor framework offers a remedy to the above mentioned drawbacks which are part of *multiplicative* and *additive* uncertainty modelling frameworks.

3.3.4 Inverse multiplicative uncertainty

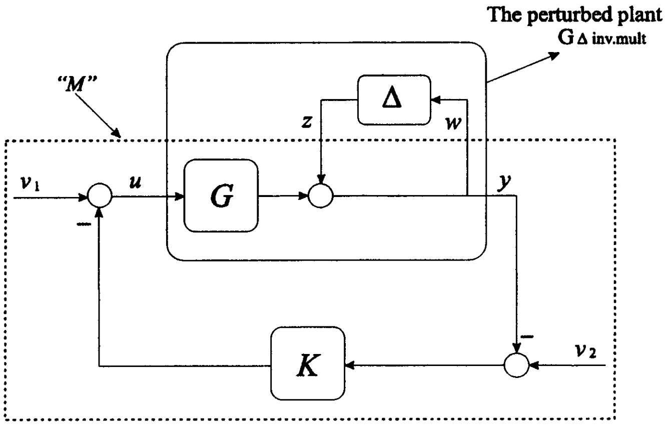

Figure 3.6: Inverse Multiplicative Uncertainty

Figure 3.6 illustrates an *inverse multiplicative* uncertainty representation in the modelled plant, which mathematically can be represented as $\mathbf{G}_{\Delta_{inv.mult}} = (I + \Delta)^{-1}\mathbf{G}$.

This mathematical framework is more useful for representing variations in *RHP* poles, variations in model dynamics such as low frequency errors produced by parameter variations with operating conditions, or system ageing.

Unlike for *additive* and *multiplicative* uncertainties, a large amount of inverse multiplicative uncertainty is the sort of uncertainty that can be dealt with by large feedback gains.

Remark 3.4 *For scalar systems where $g = nm^{-1}$ is a normalized right coprime factorization of g it can be shown that [p.36 [Vin00]] when the plant's gain $|g(j\omega)| \to 0$, $|\delta_n(j\omega)|$ is allowed to be large, whereas $|\delta_m(j\omega)|$ must be small. This corresponds to large amount of multiplicative uncertainty being allowed, simply because the region we can allow $|g(j\omega)|$ to be small is at high frequencies. Therefore making $|g(j\omega)|$ small at the same frequency will ensure that the system is robust to uncertainties that can be captured via multiplicative uncertainty modelling framework.*

Conversely, if $|g(j\omega)| \to \infty$ then $|\delta_m|$ is allowed to be large but $|\delta_n(j\omega)|$ must be small. This corresponds to a large amount of inverse multiplicative uncertainty being allowed but, only a *small amount of multiplicative uncertainty. Making $g(j\omega)$ large is the goal of the designer at low frequency range as this will make the system robust to uncertainty that in nature can be captured via inverse multiplicative uncertainty.*

Remark 3.5 *The differences between multiplicative and inverse multiplicative uncertainties become obvious only when the uncertainty is large. However, irrespective of the size of the uncertainty Δ, the multiplicative uncertainty description set will never include the point at infinity, $s \to \infty$ since $\omega \to \infty$ and $s = j\omega$, which forbids any RHP poles moving from one side of the complex plane to the other. The set of plants described by the inverse multiplicative set, if stabilizable, share precisely the same number of RHP zeros- their location can vary; the number and location of RHP poles can also vary [Vin00]. The set of inverse multiplicative uncertainty will not include the origin point $s = 0$ of the complex plane; this condition bans the movement of any zeros between the half planes of the complex plane.*

Inverse multiplicative and *multiplicative* can be associated with regions of high and low loop gain, or with low $(0, \omega_l)$ and high (ω_h, ∞) frequency regions respectively. Low frequency parametric uncertainty in nature can be modelled mathematically by *inverse multiplicative* uncertainty, whereas high frequency is usually associated with a plant's unmodelled high frequency dynamics and can be mathematically captured by *multiplicative* uncertainty.

Multiplicative and *inverse multiplicative* classes of uncertainties can be unified to form the fundamentals of a unique and symmetric (in geometrical configuration) type of uncertainty representation: normalized *coprime* factor perturbations. This type of uncertainty does not only provide a unified framework for capturing *multiplicative* and its *inverse* classes of uncertainty, but also captures the non trivial dynamic characteristics of the system in the transition crossover region, and it will be discussed next.

3.3.5 Normalized coprime factor uncertain plant description

An alternative to the model error representations of uncertain plants presented so far is the so called normalized *coprime* factor uncertainty description. Geometrically symmetric this approach to model error representation can be readily used to capture a broader class of perturbed systems compared to *additive* and both types of *multiplicative* uncertainty representations. Similar to those uncertainty descriptions it is also based on the use of unstructured, stable, unknown, but otherwise bounded perturbations $\Delta(s)$ on the normalized *coprime* factors of the nominal **G** (or shaped $\mathbf{G}_s$) plant [VK86]. This representational framework of uncertainty forms the basis of $\mathcal{H}_\infty$ loop-shaping design elaborated in [GM89], [MG92].

Coprime factor uncertainty can be regarded as a plausible combination of two types of uncertainties- namely *multiplicative* and *inverse multiplicative* uncertainties. The plant **G** plays the role of an implicit weight and determines the trade-off between them. As a sensible way to manipulate the trade-off between these two uncertainties, the designer can use stable minimum phase as well as unstable weights [Mei95] as a means to weight the nominal plant **G** with the *pre-filter* $\mathbf{W}_1$ and *post-filter* $\mathbf{W}_2$ and to allow the shaped plant to take the form of $\mathbf{G}_{s\Delta_{cf}} = \mathbf{W}_2\mathbf{G}\mathbf{W}_1 = \mathbf{M}_s^{-1}\mathbf{N}_s$ and the perturbed plant:

$$\mathbf{G}_{\Delta_{cf}} = \{(\widetilde{\mathbf{M}} + \Delta_{\widetilde{M}})^{-1}(\widetilde{\mathbf{N}} + \Delta_{\widetilde{N}}) : \; [\Delta_{\widetilde{M}} \;\; \Delta_{\widetilde{N}}] \in \mathcal{RH}_\infty, \;\; \|[\Delta_{\widetilde{M}} \;\; \Delta_{\widetilde{N}}]\|_\infty < \epsilon = \gamma^{-1} \;\}. \tag{3.22}$$

The introduction of *coprime* factor uncertainty perturbations, named also as numerator-denominator perturbations [Kwa93], can be traced to [Vid84], [Vid85], where an alternative approach in modelling plant uncertainties was advocated for controller synthesis. This approach builds on *additive* uncertainty representations using stable unstructured perturbations (with bounded $\mathcal{H}_\infty$ norm) to the *coprime* factors in a *coprime* factorization of the (shaped/nominal) plant. Schematic representation[13] of the model error using a normalized *coprime* factorization of the nominal plant is shown in Figure 3.7.

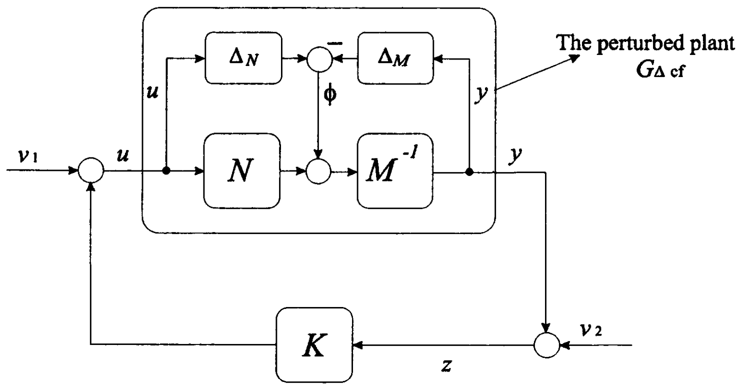

Figure 3.7: Coprime factor uncertainty

If the plant has an l.c.f as $\mathbf{G} = \widetilde{\mathbf{M}}^{-1}\widetilde{\mathbf{N}}$ where $\widetilde{\mathbf{M}}$ and $\widetilde{\mathbf{N}}$ are normalized such that $\widetilde{\mathbf{M}}\widetilde{\mathbf{M}}^* + \widetilde{\mathbf{N}}\widetilde{\mathbf{N}}^* = \mathbf{I}$ then the family of plants represented by perturbations to the *coprime*

[13]For convenience the same Figure will also be used on p.89.

factors of the nominal plant can be presented as in (equality 3.22), where $0 < \epsilon < 1 \rightarrow \gamma > 1$. Solution to the corresponding robust stabilization of a normalized *coprime* factor plant description is surprisingly explicit and intuitively appealing [GM89], and will be briefly considered later in Chapter 4 and also in this chapter.

The *coprime* factors $\tilde{\mathbf{N}}_s$ and $\tilde{\mathbf{M}}_s$ are normalized *coprime* factors of the shaped plant $\mathbf{G}_s$. In MIMO systems framework the motivation of using the weights $\mathbf{W}_1$ and $\mathbf{W}_2$ is to reflect on the closed loop objectives or specifications by modifying the shape of the nominal plant $\mathbf{G}$ in line with the requirements for low, mid and high frequency ranges underlined in section 3.1. Appropriate shaping will also facilitate tolerance against different types of *multiplicative* and *additve* uncertainties. For example, ensuring that the shaped plant's $\mathbf{G}_s$ gain is large at low frequencies, and in directions, for which the uncertainty is primarily of inverse multiplicative type; additionally that the plant's $\mathbf{G}_s$ gain is small at high frequencies, and in directions for which the uncertainty is primarily of *multiplicative* type. A good crossover can be provided, assuming that the plant's behaviour (dynamics) is well known in between these two frequency ranges.

3.3.6 Linear Fractional Transformation

Each of the previously mentioned four fundamental mathematical formulations for representing uncertainty can be embedded into a general form as illustrated in Figure 3.8 which depicts the so called *"big picture"* of control [Doy84a].

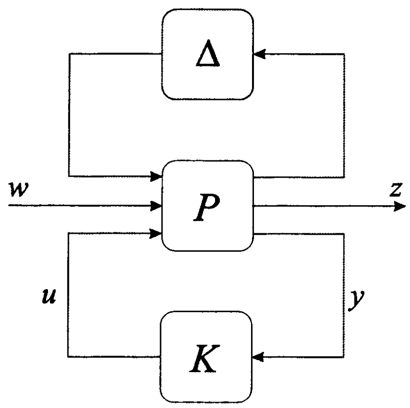

Figure 3.8: General framework: big picture of control

Linear Fractional Transformations denoted by (LFT's) also known as bilinear transformations are a commonly used mathematical framework in network and system theory for representing and standardizing a wide variety of feedback arrangements- the *"big picture"* of control represents one of them. Closed loop operators like sensitivity and co-sensitivity are linear fractional in character, as are solutions to the $\mathcal{H}_\infty$ control problem [DGKF89] and all solutions to the Hankel norm model reduction problem [Glo84]. The components of any interconnected system may be arranged to fit the configuration in Figure 3.8. Virtually any system or control problem can be cast in this *"big picture"* of control framework.

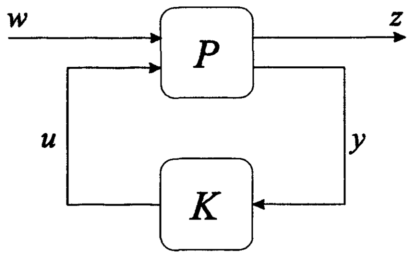

Figure 3.9: Synthesis Framework-LLFT

Figure 3.9 illustrates a feedback interconnection of a 'to be designed' internally stabilizing controller **K**, and a generalized plant **P** associated with a particular combination of objectives. **P** integrates not only the nominal plant **G**, but also the weighting functions and interconnections to form the required closed loop objective transfer function from the desired inputs to the desired outputs- $\mathbf{T}_{z\omega}$. **P** is called a generalized plant. **P** is usually partitioned to conform with the partitioning of the input and output vectors and maps the vector signals $\begin{bmatrix} \omega & u \end{bmatrix}^T$ *to* $\begin{bmatrix} z & y \end{bmatrix}^T$.

A useful physical interpretation of an LFT in the control sense is that it defines a closed loop transfer function matrix, $\mathbf{T}_{z\omega}$ from exogenous inputs ω to cost function or output signal z.

Many objectives can be combined into the framework in Figure 3.8. A fractional map of **P** and **K** can be written in the form
$\mathcal{F}_l(\mathbf{P},\mathbf{K}) = \mathbf{P}_{11} + \mathbf{P}_{12}\mathbf{K}(I - \mathbf{P}_{22}\mathbf{K})^{-1}\mathbf{P}_{21}$ where **P** and its components have compatible dimensions with **K**. $\mathcal{F}_l(\mathbf{P},\mathbf{K})$ denotes the *lower* linear fractional transformation (LLFT) and $\mathbf{P}_{11}$ is the nominal mapping of $\mathcal{F}_l(\mathbf{P},\mathbf{K})$, which is desirably *"modified"* or *"perturbed"* by **K**, and $\mathbf{P}_{12}$, $\mathbf{P}_{21}$, $\mathbf{P}_{22}$ reflect a prior knowledge as to how the controller affects the nominal map $\mathbf{P}_{11}$. In the case of $\mathbf{K} = [0]$, the map $\mathcal{F}_l(\mathbf{P},\mathbf{K})$ represents the nominal plant **G**, which is P_{11}. This is the form that will be used in this work as it suitably represents input-output relations of plant-controller interconnection. The LFT is called well-posed if $(I - \mathbf{P}_{22}\mathbf{K})^{-1}$ exists or equivalently that $(I - \mathbf{P}_{22}(\infty)\mathbf{K}(\infty))^{-1} \neq 0$. This theoretical mathematical framework facilitates a variety of closed loop and open-loop design problems, posed in terms of a linear fractional transformations involv-

ing a fixed system known as the generalized plant **P** and a to-be-designed system known as the controller (or compensator) **K**. For example a large class of controller synthesis problems can be described in the language of LFTs, and every LFT can be represented/reformulated as yet another LFT. Examples include the full information problem [PP01], $\mathcal{H}_\infty$ regulator problem and the four block problem [GL95].

$z = \mathcal{F}_l(\mathbf{P}, \mathbf{K})\omega \equiv \mathbf{T}_{z\omega}$ where the transfer function matrix **P** maps

$$\begin{bmatrix} \omega & u \end{bmatrix}^T \longrightarrow \begin{bmatrix} z & y \end{bmatrix}^T$$

in the following way

$$\begin{bmatrix} z \\ y \end{bmatrix} = \begin{bmatrix} \mathbf{P}_{11} & \mathbf{P}_{12} \\ \mathbf{P}_{21} & \mathbf{P}_{22} \end{bmatrix} \begin{bmatrix} \omega \\ u \end{bmatrix}$$

and $u = \mathbf{K}y$.

In the state-space domain, z and y are the solutions of ordinary linear differential equations driven by ω and u:

$$\begin{bmatrix} \dot{x} \\ z \\ y \end{bmatrix} = \left[\begin{array}{c|cc} A & B_1 & B_2 \\ \hline C_1 & D_{11} & D_{12} \\ C_2 & D_{21} & D_{22} \end{array}\right] \begin{bmatrix} x \\ \omega \\ u \end{bmatrix} \tag{3.23}$$

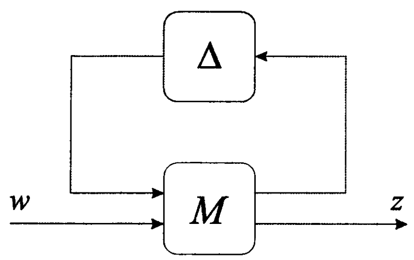

Figure 3.10: Analysis Framework-ULFT

Figure 3.10 shows a fractional map of **M** and Δ, where

$$z = \mathcal{F}_u(\mathbf{M}, \Delta)\omega \equiv \{\mathbf{M}_{22} + \mathbf{M}_{21}\Delta(I - \mathbf{M}_{11}\Delta)^{-1}\mathbf{M}_{12}\}\omega \tag{3.24}$$

The upper linear fractional transformation denoted by $\mathcal{F}_u(\mathbf{M}, \Delta)$ relates the generalized plant **M** with Δ and is the transfer function from w to z, where $\mathbf{M} = \mathcal{F}_l(\mathbf{P}, \mathbf{K})$.

Later, it will become obvious that LLFT $\mathcal{F}_l(\bullet,\bullet)$ offers a convenient configuration to facilitate formulation of different $\mathcal{H}_\infty$ controller synthesis problems, whereas the alternative ULFT $\mathcal{F}_u(\bullet,\bullet)$ provides a framework for integrating the uncertainty blocks into the generalized plant. For a more detailed account on LFTs the reader is referred to [Red60].

In the general control configuration in Figure 3.8, the signal ω contains all exogenous inputs: commands, disturbances and noises; z represents exogenous outputs, or objectives: *error* signals to be minimized, e.g. $y-r$; y contains the controller input signals: the measurements, references and other signals that are available for on-line control purposes and finally the control signals u are the manipulated variables.

In the controller synthesis problem we aim to select a causal linear controller **K** so that the closed loop system mapping ω to z, $\mathbf{T}_{z\omega} \equiv \mathcal{F}_l(\mathbf{P},\mathbf{K})$, is small in an $\mathcal{H}_\infty$ norm sense i.e.

$\min_{\omega\in\mathbb{R}} \|\mathbf{T}_{z\omega}\|_\infty < \gamma$ subject to the constraint that the closed loop is internally stable.

Since the objective is to make z, the exogenous outputs, small, the problem is often referred in the literature as a generalized regulator problem.

3.4 Robust stability and performance

3.4.1 Robust control

The feedback design problem centres around the trade off involved in reducing the overall impact of uncertainty.

Plant uncertainty and variability are formidable adversaries and the necessity to stabilize plant models which are uncertain motivates the idea of robust stability- the ability of a closed loop system to remain stable in the presence external unpredictable signals and errors in mathematical models.

In contrast to the traditional optimal control methods, like **LQG** [Kwa93] where the theory provides tools for performance optimization but not for robustness the need for a new theory emerges. This theory should offer a quantitative measure of performance and robustness that can be formulated into an optimization problem with a synthesis procedure available. The theory must also be tractable and accessible to practising engineers, but not least to be able to address the demands of real world problems. A theory that will incorporate all these requirements is bound to be multivariable in nature. The scope of the so called robust control theory is to present theory for the analysis, design and synthesis of feedback systems so as to combine performance optimization with the guarantees of robustness in a range of operating conditions of the system.

Robust control theory offers a toolbox of control techniques for the design of robust controllers. The design of a robust controller usually proceeds in 'two steps'. First a plant model set $\mathbf{G}_\Delta$, which represents the real hardware system, is characterized in terms of the nominal model $\mathbf{G}$ and uncertainty Δ. This characterization, as discussed earlier, can be achieved mathematically by means of *additive* model error Δ_A, *multiplicative* model error Δ_{mult} or *coprime* factor model errors $\Delta_{\widetilde{M}}$, $\Delta_{\widetilde{N}}$. A closed loop is called robustly stable if stability is ensured for every plant model $\mathbf{G} \in \mathbf{G}_\Delta$. The second step involves the design of a controller $\mathbf{K}$ that will stabilize every uncertain plant model represented in one of the following forms: $\mathbf{G}_{\Delta_A}$, $\mathbf{G}_{\Delta mult}$, $\mathbf{G}_{\Delta cf}$.

The process of finding such a compensator is greatly facilitated by two important analysis results: firstly, necessary and sufficient conditions for robust stability, and secondly, a sufficient condition for robust performance, where robust stability and robust performance are defined solely in terms of acceptable magnitudes for the nominal functions $\overline{\sigma}(\mathbf{T}(j\omega))$ and $\overline{\sigma}(\mathbf{S}(j\omega))$ [DS81], [DFT92].

Over the past few decades the $\mathcal{H}_\infty$ control design approach has provided some promising results in the area of robust stabilization of plants with unstructured uncertainties. The condition for robust stability involves a test on the $\mathcal{H}_\infty$ norm of a particular closed loop transfer function, and hence the existence of a robustly stabilizing controller can be determined via the $\mathcal{H}_\infty$ optimization techniques originated by [Zam81].

3.4.2 Robust stabilization

In real time applications, where the absence of a perfect model of the plant is almost certain, a controller design process must be posed as an iterative optimization problem with the most fundamental requirement being to design a controller that is stabilizing. It should operate safely and satisfactorily meet certain control loop performance specifications in the presence of modelling mismatch between the modelled plant and the real plant. The resulting controller will be a solution to the so called robust stabilization problem.

There are several ways- some of which have been covered- that can be used to form an enclosing set with structure to facilitate the solution of a robust stabilization problem. However, in addition to robust stability, a satisfactory controller must also satisfy performance specifications. $\mathcal{H}_\infty$ optimization offers a suitable framework for incorporating them. We have seen in the earlier sections (3.2.1) of the chapter that performance related issues such as disturbance rejection or precision tracking can be achieved by minimizing the $\mathcal{H}_\infty$ norm of a relevant closed loop transfer function. That is, by minimizing the maximum energy in the output signal to a set of signals of unit energy we can guarantee a level of nominal performance.

Robust stabilization problem can be a single-target or multi-target objective problem and can be stated as follows: Given a set of plants $\mathbf{G}_\Delta$ find, if one exists, a stabilizing controller $\mathbf{K}$ such that the interconnection $[\mathbf{G}_\Delta, \mathbf{K}]$ is well posed and internally stable for all plants $\mathbf{G} \in \mathbf{G}_\Delta$. Assuming that the generalized plant has a known state-space realization the aim is to synthesize an internally-stabilizing controller that satisfies a norm constraint on the closed loop operator $(\mathcal{F}_l(\mathbf{P}, \mathbf{K}) < \gamma)$[14]. These minimization problems can be rewritten in the *"big picture"* LFT framework as $\inf_{stab.\mathbf{K}} \|\mathcal{F}_l(\mathbf{P}, \mathbf{K})\|_\infty < \gamma$.

Assessing robust stability of an interconnected system as shown in Figure 3.3 can be done by using:

- the small-gain theorem: where the argument will rely on considering stable perturbations $\Delta \in \mathcal{RH}_\infty$

or

- homotopy arguments: where perturbations are assumed to have been bounded on the imaginary axis and on counting winding numbers *wno*, using relationships of the form;

$wno\ \ det(AB) = wno\ \ det(A) + wno\ \ det(B)$; if A, B, A^{-1} and $B^{-1} \in \mathcal{L}_\infty$ together with $wno\ det(I + A) = 0$, if $A \in \mathcal{L}_\infty$ and $\|A\|_\infty < 1$ [Vin00].

Remark 3.6 *Stronger results can be obtained and established using homotopy arguments [Vin00].*

[14] The problem can be scaled so that $\gamma = 1$, this can be done by dividing P_{11} and P_{12} by γ.

Theorem 3.2 *([MG90] p.33) K stabilizes $\mathcal{F}_u(\mathbf{P}, \Delta)$ for all $\|\Delta\|_\infty < \epsilon$ [when the generalized plant satisfies the assumptions that (A, B_2) is stabilizable and (C_2, A) is detectable], if and only if:*

- *K stabilizes the nominal plant* $\mathbf{G}$
- $\|\mathcal{F}_l(\boldsymbol{P}, \boldsymbol{K})\|_\infty \leq \epsilon^{-1}$.

Theorem 3.2 presents sufficient conditions for robust stability for the uncertain model $\mathbf{G}_\Delta = \mathcal{F}_u(\mathbf{P}, \Delta)$. Various robust stability tests for unstructured uncertainties under various assumptions can be developed depending on the type of mathematical model set used for representing the uncertainty in the plant; for these, the interested reader is referred to [GL95], [SP96], [ZDG96] for more details.

Here, we will present conditions for robust stability of systems described by uncertainty models previously considered. For brevity the presentation will omit the proofs. For all robust stability tests, which are a special version of Theorem 3.2, the following conditions hold:

- $\Delta \in \mathcal{RH}_\infty$, $\|\Delta\|_\infty < \epsilon$ and
- **K** stabilizes the nominal plant **G**

For the *additive* type of uncertainty where the perturbed plant is described by $\mathbf{G}_{\Delta A} = G + \Delta = \mathcal{F}_u(\mathbf{P}, \Delta_A)$, stability robustness of $\mathcal{F}_l(\mathbf{G}_{\Delta_A}, \mathbf{K})$ is ensured if and only if:

Corollary 3.1

- the transfer function $\mathbf{T}_{zw} = \|\mathbf{K}(I - \mathbf{GK})^{-1}\|_\infty \leq \gamma = \epsilon^{-1}$

□

Analogously, for the *multiplicative* type of uncertainty at the plant output where the perturbed plant is denoted by $\mathbf{G}_{\Delta_{mul}} = \mathbf{G} + \Delta\mathbf{G} = \mathcal{F}_u(\mathbf{P}, \Delta_{mul})$, stability robustness of $\mathcal{F}_l(\mathbf{G}_{\Delta_{mul}}, \mathbf{K})$ is ensured if and only if:

Corollary 3.2

- the transfer function $\mathbf{T}_{zw} = \|(I - \mathbf{GK})^{-1}\mathbf{GK}\|_\infty \leq \gamma = \epsilon^{-1}$

□

For *coprime* factor uncertainty where the perturbed plant is denoted by $\mathbf{G}_{\Delta_{cf}} = (\widetilde{\mathbf{M}} + \Delta_M)^{-1}(\widetilde{\mathbf{N}} + \Delta_N) = \mathcal{F}_u(\mathbf{P}, \Delta)$, and $\Delta = \|[\Delta_N \quad \Delta_M]\|_\infty < \epsilon$, where it can be shown that $(\Delta_N, \Delta_M) \in \mathcal{RH}_\infty$; then, stability robustness of $\mathcal{F}_l(\mathbf{G}_{\Delta cf}, \mathbf{K})$ is ensured if and only if:

Corollary 3.3

- the transfer function $\mathbf{T}_{\phi \to \begin{bmatrix} u & y \end{bmatrix}^T} = \left\| \begin{bmatrix} \mathbf{K} \\ \mathbf{I} \end{bmatrix} (\mathbf{I} - \mathbf{GK})^{-1} [\mathbf{G} \quad \mathbf{I}] \right\|_\infty \leq \gamma = \epsilon^{-1}$

□

As seen, robust stabilization problems can be phrased for perturbations that are embedded in the loop in *additive* or *multiplicative* form [GD88], and can be written in the form of an LFT problem and solved using $\mathcal{H}_\infty$ optimization.

3.4.3 Robust stabilization of normalized coprime factors

This section presents a summary of the theoretical background associated with the normalized *coprime* factor robust stabilization problem and its relevance to the loop-shaping design. Robust stabilization of the normalized *coprime* factor description of the (nominal/shaped) plant has both an elegant and sensible solution with an intuitive and relatively straightforward engineering implementation [MG90].

Let the nominal plant $\mathbf{G}$ be represented by normalized left *coprime* factorization in the form depicted in Figure 3.7 where $\mathbf{G} = \mathbf{M}^{-1}\mathbf{N}$. The motivation for the choice of this particular description will be briefly outlined in the next chapter; for mathematically more rigorous justification the reader is referred to [GM89].

A normalized *coprime* factor uncertainty description[15] offers distinct advantages over other methods as it allows a wider class of system uncertainty to be captured. In addition, it has been shown in [ES87] that the relations between the size of *coprime* factor perturbations $\|[\Delta_M \quad \Delta_N]\|_\infty$ and distance between the systems in the gap metric [Geo88] demonstrate robustness as a property of closed loop stability in the *coprime* factor framework.

[15] It may be the case that different representation of modelling error are useful over different frequency ranges.

It can be argued that for robust stabilization (in the absence of precise information on the nature of the uncertainty) the choice of the normalized *coprime* factors in fact gives an implicit weighting to the uncertainty [GSM90]. The implicit weighting function is, the numerator of the *coprime* factor plant description, $\mathbf{M}^{-1}$, as seen in the 2 (two) block standard $\mathcal{H}_\infty$ problem (Equation 3.25); where the left side corresponds to the transfer function from ϕ to $\begin{bmatrix} u & y \end{bmatrix}^T$ in Figure 4.2,

$$\left\| \begin{bmatrix} \mathbf{K} \\ I \end{bmatrix} (I - \mathbf{GK})^{-1} \tilde{\mathbf{M}}^{-1} \right\|_\infty = \left\| \tilde{\mathbf{M}}^{-1} (I - \mathbf{GK})^{-1} \begin{bmatrix} \mathbf{K} & I \end{bmatrix} \right\|_\infty \tag{3.25}$$

provides a balance on the closed loop objectives requirements about the *"natural"* bandwidth of the system [16]. Through this particular *coprime* factorization the aim is to alter the bandwidth of the closed loop system to that of the natural bandwidth of the shaped plant ($\underline{\sigma}(\mathbf{G}_s) \simeq 1$).

This, however, assumes that the nominal system has a desirable loop-shape. Unfortunately, this, in practice, is rarely the case and thus the designer must intervene in the loop-shape, modify it and by doing so compensate for performance before the stabilization procedure.

In the frequency domain, using an *unnormalized coprime* factorization of the plant implies weighting the transfer functions within the closed loop design objective [GSM90]. Whereas, using normalized *coprime* factorization of the plant ensures equal weighting on the allowable numerator and denominator perturbations, as well as the same norm bound on all the four relevant closed loop transfer functions.

$$\left\| \begin{bmatrix} \mathbf{K} \\ I \end{bmatrix} (I - \mathbf{GK})^{-1} \begin{bmatrix} \mathbf{G} & I \end{bmatrix} \right\|_\infty = \left\| \begin{bmatrix} \mathbf{KS}_o\mathbf{G} & \mathbf{KS}_o \\ \mathbf{S}_o\mathbf{G} & \mathbf{S}_o \end{bmatrix} \right\|_\infty < \gamma = \frac{1}{\epsilon} \tag{3.26}$$

This supports the claim that normalized *coprime* factorization allows balancing of the closed loop design objectives by placing equal emphasis on each of the closed loop transfer functions. Additionally, in general, it is not possible to obtain an exact solution for Equation 3.26 and an iterative procedure is recommended in [VK86]. However, if the *coprime* factors are normalized, then an exact and non-iterative solution becomes possible [GM89]. Since the solution of the NCFRS problem does not require iterations this also brings significant computational savings.

[16] $\underline{\sigma}(\mathbf{G}) \simeq 1$ is defined as the natural bandwidth of a system.

L.c.f and r.c.f of a given plant **G** always exist. Therefore, unlike other representations, no assumptions are required for this problem to have a well balanced solution. Poles and zeros on the imaginary axis can also be tolerated without creating any theoretical or numerical difficulties.

These features of the (normalized) *coprime* factors serve as primary motivations for the formulation of normalized *coprime* factor robust stabilization problem in terms of *additive* stable perturbations to the normalized *coprime* factors of a given plant.

By definition $\widetilde{\mathbf{N}}$ and $\widetilde{\mathbf{M}}$ are asymptotically stable thus $\overline{\sigma}(\widetilde{\mathbf{N}})$ and $\overline{\sigma}(\widetilde{\mathbf{M}})$ are bounded [GM89]. Through straightforward algebraic manipulations it can be shown that *coprime* factors also appear as bounds for allowable *additive* uncertainty

$$\overline{\sigma}(\Delta) \;<\; \frac{\overline{\sigma}(\widetilde{\mathbf{M}})}{\overline{\sigma}(\mathbf{K}(I-\mathbf{GK}))} \tag{3.27}$$

and allowable *multiplicative* uncertainty

$$\overline{\sigma}(\Delta) \;<\; \frac{\overline{\sigma}(\widetilde{\mathbf{M}})+\frac{1}{\gamma}}{\overline{\sigma}(\mathbf{GK}(I-\mathbf{GK}))}. \tag{3.28}$$

3.5 $\mathcal{H}_\infty$ Control

This section is primarily concerned with introducing and motivating the use of $\mathcal{H}_\infty$ *sub/optimal* control theory as a tool for controller synthesis and analysis.

3.5.1 From classical to modern control: Overview and motivation for new tools

The area of linear control system design has advanced rapidly since the first mathematically rigorous exposition on synthesis theory on optimal control and filtering by Norbert Wiener in [Wie49]. Wiener's work on prediction theory for stochastic processes proved that certain design problems involving integral performance indices may be solved analytically. Though still unable to cope with time-varying or MIMO systems Wiener-Hopf optimization as a frequency design optimization relieved the designer of the daunting thought that better solution might be possible by uncovering inconsistent design specifications[17]. The solution of the quadratic matrix equation

[17]Research carried out by [JKL97] and [YBJ00] in utilizing Wiener-Hopf design approach has shown its successful application in 1 Dof, 2 Dof and 3 Dof Multivariable control systems.

also known as a *Riccati* equation provides a solution to the Wiener-Hopf optimal control problem.

By the early 1950's, frequency response methods had developed into powerful tools for controller design and were commonly used by practising engineers. In the years until the 1960's most of the controller design work was based on graphics-based methods in the frequency domain [Nyq32], [Bod45]. The fundamental work of these two research scientists started the frequency domain approach to classical feedback design, where the measures used for performance and robustness assessment were gain and phase margins, the unit-step response and its overshoot. There were several reasons for the success of these frequency response methods: easily established connection between frequency response plots and acquired experimental data, the availability of a rich variety of diagnostic and manipulative aids that enable engineers to refine the design in a systematic way, the existence of simple rules-of-thumb for standard control configurations such as Ziegler-Nichols methods for tuning PID controllers, etc. However, the intrinsically complex nature of real world problems, and the inadequacy of these techniques to address the needs of control engineers in dealing with problems containing high degrees of inter-channel coupling between the control inputs and measured variables, challenged the applicability of these graphically based design methods to multivariable plants.

Some years later Kalman's [Kal60] introduction of state-space methods bridged the short fall of the Wiener-Hopf design theory in dealing with MIMO systems and introduced a new line of research. The Kalman filter and *Linear Quadratic Gaussian* (**LQG**) control design methods are still recognized to be the first procedures known to have successfully tackled multivariable control problems with applications mainly in the aerospace industry. However, the techniques assumed that the system's dynamical model was accurately known and this was soon recognized to be no longer feasible for output feedback control problems. Hence they could not guarantee the robustness of the controller to any unmodelled dynamics and external disturbances, unless they could be modelled as Gaussian white noise processes or filtered white noise processes which in practice will not hold for many applications. Full-state feedback **LQ** controllers and Kalman filters considered separately have very good robustness stability properties. Unfortunately, as the **LQG** method does not explicitly take into account uncertainties arising from the dynamics of the system under consideration it may compromise on the robustness of the resulting design. Optimality does not guarantee stability robustness and **LQG** controllers can exhibit poor stability robustness properties and the design's stability margins can be arbitrary small [Doy78]. Therefore **LQG** optimal design must be analysed aposteriori. Nevertheless **LQG** has been successfully used and implemented on industrial applications mainly in aerospace problems: e.g. optimal trajectory manoeuvring, optimal fuel use. This robustness problem and the increasing demands of the defence and aerospace industries has initiated a stream of research to develop extensions to multivariable systems based on state-space descriptions of the plant. Attention has been given to remedy these drawbacks of the state-space **LQG** optimal quadratic design method, and this has brought renewed interest in classical frequency response ideas, [DS81] e.g. multivariable phase and gain margins [Mac82]. Attempts have also been made to generalize the Nyquist stability criterion to fit into the MIMO design framework [PM79].

The capability of a system to cope with uncertainties in a satisfactory manner, while maintaining its stability and performance has been a key engineering objective throughout the entire development of feedback control theory.

With the work of [DS81] on the maximum singular value ($\bar{\sigma}(\bullet)$), investigating and assessing the degree of stability robustness, sensitivity reduction and disturbance attenuation of the linear multivariable systems became possible. The direct relationship between the size of the appropriate (closed/open) loop transfer function (or transfer function combinations) and bandwidth could be easily established. Further research had shown efforts to accommodate the peculiarities of multivariable systems leading to use of a mathematical notion in operator theory as a new measure for assessing a system's stability and performance: the notion was the $\mathcal{H}_\infty$ Hardy space operator norm. The roots of the contemporary methods for robustness analysis date back to the research in the late 1960's on feedback stability for nonlinear systems from an input-output perspective [Zam66a], [Zam66b].

Although in an engineering context the use of $\mathcal{H}_\infty$ optimization appears in the work of Helton in [HS89], it was George Zames, in [Zam81], that first elaborated on a solution to a specific $\mathcal{H}_\infty$ norm minimization, over the set of all stabilizing controllers, of a transfer function from a disturbance signal to the output for a SISO system. This was *sensitivity* minimization. However, it was the work of [ZF83] that had sparked considerable interest in $\mathcal{H}_\infty$ norm minimization methods which would later become the backbone of frequency based multivariable Robust Control Theory. Years later a solution to a general rational MIMO $\mathcal{H}_\infty$ optimal control problem was presented in [Doy84b]. This solution relied heavily on state-space formulae and suffered from severe problems with the high order of the *Riccati* equations. Due to existing requirement of solving several *Riccati* equations of increasing dimensions the associated computational complexity was immense. This has had overall implications on the order of resulting controllers which were practically infeasible to implement due to very high orders. In an effort to find a simpler solution to the problem based on the approach developed by [Doy84b], relatively simplified state-space $\mathcal{H}_\infty$ controller formulae were derived and presented in [GD88], which, constituted a basis for a more direct and simpler approach [DGKF89]. The key role was played by the connections established between frequency domain inequalities, spectral factorization of some frequency domain functions and *Riccati* equations.

Control system design and analysis based on the $\mathcal{H}_\infty$ norm concept has dominated much of control theory since the 1980's, and has gradually evolved to become a well established tool with applications in many areas of science and engineering; see [LWN03], [SMD88], [SP96] and relevant references therein.

The $\mathcal{H}_\infty$ norm has several attractive mathematical properties that have made it a suitable tool for controller synthesis and analysis in the control community. It has a frequency domain interpretation which allows more intuition into the design of the controller, and a more constructive approach to the assessment and analysis of the controller. A design approach based on $\mathcal{H}_\infty$ optimization is inherently multivariable and can simultaneously address both performance and robustness requirements in a single design metric framework with the benefit of a guaranteed level of robustness. Using the small gain theorem (Theorem 3.1) a bound on the $\mathcal{H}_\infty$ norm of a stable closed loop transfer function is sufficient to guarantee a level of robustness of the closed loop against the presence of a class of stable perturbations Δ on the plant. Since the technique is multivariable it can simultaneously and reliably stabilize several interacting feedback loops. It can naturally characterize uncertainty providing flexibility in representing unstructured model uncertainty and facilitating robust stability guarantees in the face of modelling errors.

The $\mathcal{H}_\infty$ norm is an induced norm (Equation 3.29) and therefore satisfies the multiplicative property which allows it to be used as a tool in the derivation of robust stability tests (and other results) see section 3.4:

$$\|A(s)B(s)\|_\infty \leq \|A(s)\|_\infty \cdot \|B(s)\|_\infty \tag{3.29}$$

3.5.2 The standard $\mathcal{H}_\infty$ problem

As opposed to analytic methods such as **LQG** which is an optimal control theory encompassing the minimization of integral quadratic performance indices subject to linear-state-space dynamics driven by Gaussian white noise, the $\mathcal{H}_\infty$ optimal control problem reduces to the design of a stabilizing controller, **K**, minimizing the $\mathcal{H}_\infty$ norm (maximum energy -worst case- signal gain) of the closed loop transfer function from external disturbance ω to the error signal z, usually denoted by $y - r$.

We have seen earlier that one can obtain an accurate representation of the uncertainty inherent in a plant model in the form presented in Figure 3.8- by pulling out the uncertainty in the plant to form Δ.

Recall that by taking the perturbation Δ out from the Figure 3.8 we create an LLFT framework suitable for controller synthesis. **K** is a controller constrained to provide internal stability- *admissible;* proper and stabilizing- and **P** is a generalized plant with the following transfer matrix realization:

$$\mathbf{P}(s) = \left[\begin{array}{c|cc} A & B_1 & B_2 \\ \hline C_1 & D_{11} & D_{12} \\ C_2 & D_{21} & D_{22} \end{array}\right] = \left[\begin{array}{c|c} A & B \\ \hline C & D \end{array}\right] \tag{3.30}$$

It can also be represented with the following structure:

$$\mathbf{P}(s) = \begin{bmatrix} \mathbf{P}_{11} & \mathbf{P}_{12} \\ \mathbf{P}_{21} & \mathbf{P}_{22} \end{bmatrix}$$

which is compatible with the dimensions of the control signal $u(t)$, measurement variables $y(t)$, the set of exogenous inputs $\omega(t)$, and the cost function (or exogenous output) $z(t)$. The generalized plant **P** maps

$$\begin{bmatrix} \omega & u \end{bmatrix}^T \longrightarrow \begin{bmatrix} z & y \end{bmatrix}^T \tag{3.31}$$

and substituting $u = \mathbf{K}y$ yields the transfer function, $\mathbf{T}_{z\omega}$, from the set of exogenous inputs ω to the set of exogenous outputs z. Expressed in the LFT framework:

$z = \mathcal{F}_l(\mathbf{P}, \mathbf{K})\omega$ and $\mathbf{T}_{z\omega} \equiv \mathcal{F}_l(\mathbf{P}, \mathbf{K}) = \mathbf{P}_{11} + \mathbf{P}_{12}\mathbf{K}(I - \mathbf{P}_{22}\mathbf{K})^{-1}\mathbf{P}_{21}$.

It is possible to formulate a number of practical design problems in the form:

$$\min_{stab.K} \|\mathcal{F}_l(\mathbf{P}, \mathbf{K})\|_\infty \equiv \min_{stab.K} \|\mathbf{T}_{z\omega}\|_\infty. \tag{3.32}$$

where the minimization is over all stabilizing controllers **K**. This is known as the $\mathcal{H}_\infty$ optimization problem. The term $\mathcal{H}_\infty$ problem arises from the fact that we are minimizing $\|\mathcal{F}_l(\mathbf{P},\mathbf{K})\|_\infty$, s.t. $\mathcal{F}_l(\mathbf{P},\mathbf{K}) \in \mathcal{H}_\infty$ and the feedback interconnection **P**, **K** is internally stable.

The optimal $\mathcal{H}_\infty$ control problem can be formally stated as follows:

Find all internally stabilizing (*admissible*) controllers **K**, such that $\|\mathbf{T}_{zw}\|_\infty$ is minimized; $\gamma_{min} = \gamma_{opt} := \min\{\|\mathbf{T}_{zw}\|_\infty : \mathbf{K}\ \textit{admissible}\}$.

However, in contrast to $\mathcal{H}_2$ optimal control theory[18], where the optimal controller is unique and can be found by solving only two *Riccati* equations without iterations, optimal $\mathcal{H}_\infty$ controllers do not pose uniqueness for MIMO systems and do require an iterative procedure for their solution. In point of fact, finding an $\mathcal{H}_\infty$ optimal controller involves significant theoretical and computational complexity [GD88] and the record of applications of $\mathcal{H}_\infty$ as a design tool shows that often, the design of optimal controller is not necessary. While having a knowledge of the optimum (minimal) $\mathcal{H}_\infty$ norm gives an insight of what may be achievable with a specific controller; a controller which is practically easier to implement, computationally less demanding, and is still very close (in an $\mathcal{H}_\infty$ norm sense) to the optimal one is to be preferred instead. This is in fact a suboptimal controller, and a suboptimal control problem can be formulated as:

Given $\gamma > 0$, synthesize an internally stabilizing, proper, LTI controller **K**, if there is one, such that the closed loop transfer matrix, $\min_{stab.K} \|\mathbf{T}_{zw}\|_\infty < \gamma$. where $\gamma > \gamma_{min} = \gamma_{opt}$.

Due to complicated algebraic manipulations involved in their derivations optimal $\mathcal{H}_\infty$ controllers are more difficult to characterize than suboptimal ones. Consider the transfer function matrix realization of **P**(s):

$$\mathbf{P}(s) = \left[\begin{array}{c|cc} A & B_1 & B_2 \\ \hline C_1 & 0 & D_{12} \\ C_2 & D_{21} & 0 \end{array}\right] \tag{3.33}$$

Suboptimal controllers owe their simplified solution to the following assumptions:

i) (A, B_1) is stabilizable and (C_1, A) is detectable;

[18] [DGKF89] unveils the link between $\mathcal{H}_2$ optimal control and LQG optimal control problem studied in the 1960's and 1970's.

ii) (A, B_2) is stabilizable and (C_2, A) is detectable;

iii) $D_{12}^* C_1 = 0$ and $D_{12}^* D_{12} = I$ where D_{12} has a full column rank

iv) $B_1 D_{21}^* = 0$ and $D_{21} D_{21}^* = I$ where D_{21} has full row rank

It is important to note that these assumptions still allow the essential features of the $\mathcal{H}_\infty$ theory to be retained. Assumption $i)$ is made for technical reasons: for the system to be stabilizable via output feedback. It simplifies the theory for the solution of the $\mathcal{H}_\infty$ suboptimal problem. Assumption $ii)$ together with assumption $i)$ is also made for technical reasons; it guarantees that the *control* and *filtering* Algebraic *Riccati* Equations (AREs) associated with the related $\mathcal{H}_2$ problem have positive definite stabilizing solutions. It is also necessary and sufficient for the plant **P** to be internally stabilizable. Orthogonality assumptions in $iii)$ and $iv)$ are made for simplicity. The rank assumption in $iv)$ guarantees that the $\mathcal{H}_\infty$ problem is nonsingular.

The assumptions on $D_{11} = 0$ and $D_{22} = 0$ are also made for simplicity. Relaxing the assumption $D_{11} = 0$ will complicate the controller formulae substantially (Chapter 17 [ZDG96]), whereas stating $D_{22} \neq 0$ does not pose any problems, since an equivalent problem with $D_{22} = 0$ can be formulated by a linear fractional transformation on the controller **K**.

Central, in the $\mathcal{H}_\infty$ optimal control synthesis, is the role of Algebraic *Riccati* Equations, which take the following form:

$$A^* X + X A^* + X R X + Q = 0 \tag{3.34}$$

where matrices A, Q, $R \in \mathcal{R}^{n \times n}$ with Q, R symmetric.

Associated with this Algebraic *Riccati* Equation is a *Hamiltonian* matrix:

$$H := \begin{bmatrix} A & R \\ -Q & -A^* \end{bmatrix} \tag{3.35}$$

The $\mathcal{H}_\infty$ solution involves the following two *Hamiltonian* matrices:

$$H_\infty := \begin{bmatrix} A & \gamma^{-2} B_1 B_1^* - B_2 B_2^* \\ -C_1^* C_1 & -A^* \end{bmatrix}, \quad J_\infty := \begin{bmatrix} A^* & \gamma^{-2} C_1^* C_1 - C_2^* C_2 \\ -B_1 B_1^* & -A \end{bmatrix} \tag{3.36}$$

where H_∞, J_∞ are $2n \times 2n$ matrices.

Theorem 3.3 *([ZDG96] p.419) There exists an admissible controller such that $\|T_{zw}\|_\infty < \gamma$ if and only if the following three conditions hold:*

i) $H_\infty \in dom(Ric)$ *and* $X_\infty := Ric(H_\infty) \geq 0$;

ii) $J_\infty \in dom(Ric)$ *and* $Y_\infty := Ric(J_\infty) \geq 0$;

iii) $\rho(X_\infty Y_\infty) < \gamma^2$.

where X_∞ satisfies the algebraic Riccati equation and is uniquely determined by H_∞, X_∞ is a function of H_∞; $H \to X$ is a function denoted by Ric. The domain of all Hamiltonian matrices

a) *whose eigenvalues are symmetric about the imaginary axis, and*

b) *which satisfy complementary property ([ZDG96] p.333)*

is defined as dom(Ric).

Whenever conditions $i), ii), iii)$ hold, there exists such an admissible controller which is also called a central or minimum entropy controller which has the following state space realization

$$K_{sub}(s) := \left[\begin{array}{c|c} \widehat{A}_\infty & -Z_\infty L_\infty \\ \hline F_\infty & 0 \end{array}\right]$$

where

$$\widehat{A}_\infty := A + \gamma^{-2} B_1 B_{1\infty}^* + B_2 F_\infty + Z_\infty L_\infty C_2$$

$$F_\infty := -B_2^* X_\infty, L_\infty := -Y_\infty C_2^*, Z_\infty := (I - \gamma^{-2} Y_\infty X_\infty)^{-1}.$$

For the solution of the optimal and general $\mathcal{H}_\infty$ problem the reader is referred to section 16.11 and Chapter 17 of [ZDG96].

In this work we shall only be interested in finding *suboptimal* controllers, controllers that make $\|\mathbf{T}_{zw}\|_\infty < \gamma$ where $\gamma > \gamma_{min} = \gamma_{opt}$, and when $\gamma \to \infty$ the $\mathcal{H}_\infty$ problem reduces to $\mathcal{H}_2$ problem.

3.5.2.1 Controller Synthesis

There are many approaches for solving the $\mathcal{H}_\infty$ control problem, and probably the most celebrated one is in terms of *Riccati* Equations. The controller that satisfies the specified objectives exists if and only if two *Riccati* equations namely (*Generalized Control Algebraic Riccati Equations*)- GCARE, and (*Generalized Filtering Algebraic Riccati Equations*)- GFARE have appropriate (positive definite) solutions [DGKF89].

We will be interested only in the search for a stabilizing controller that achieves

$$\min_{stab.\ K} \|\mathcal{F}_l(\mathbf{P},\mathbf{K})\|_\infty < \gamma, \gamma > \gamma_{opt} = \gamma_{min} \tag{3.37}$$

In general it may not be possible to solve the $\mathcal{H}_\infty$ optimization problem for γ_{min} exactly, in which case an iterative procedure must be adopted instead. A binary search (with a bisection algorithm) can be suitably used to approximate this norm. A faster, quadratically convergent algorithm is presented in [BB90].

The exact solution of the inequality in Equation 3.37 can be found in the case when $dim(\omega) = dim(y)$, and $dim(u) = dim(z)$; consider (Figure 3.9). This special case is called the one-block problem and is such that the *row* and *column* dimensions of $\mathbf{K}$ and $\mathcal{F}_l(\mathbf{P},\mathbf{K})$ are the same. In the other cases using the bounded real lemma [ZDG96] the question to be addressed is the existence of $\overline{\sigma}(\mathcal{F}_l(\mathbf{P},\mathbf{K})) < \gamma$. The bounded real lemma also provides an insight into the synthesis of the controllers that satisfy specified (open/closed) loop transfer function objectives in terms of singular values. Additionally the bounded real lemma gives a condition for a linear time-invariant system to have less than unity gain.

3.5.3 $\mathcal{H}_\infty$ control problem and frequency domain

The formulation of the $\mathcal{H}_\infty$ control problem is based on frequency domain performance measures and draws heavily from classical frequency domain design techniques. $\mathcal{H}_\infty$ sub/optimal control has evolved as a natural extension to existing feedback theory to address explicitly the needs of theoreticians and control design engineers for a unified theory that will be amenable to optimization, capable of dealing with modelling discrepancies and unknown, sporadic but bounded in magnitude disturbances, and most importantly applicable to real-world problems which are mostly multivariable in nature.

A fundamental requirement for an $\mathcal{H}_\infty$ design to take place is that all objectives for performance and robustness must be formulated in terms of desired frequency 'shapes' of appropriate (closed/open)-loop transfer function frequency response magnitudes.

Given a linear time-invariant closed loop transfer function the objective of $\mathcal{H}_\infty$ control optimization is technically two-fold:

- To synthesize a controller **K(s)** which will first internally stabilize a set of plants; the nominal plant and desirably the perturbed plant $\mathbf{G}_\Delta$
- To minimize only the *supremum* of the largest singular value *"worst direction"* or *"worst frequency"* of the given transfer function(s) (or functions which represent design objectives) over a given frequency range [19].

$$\min_{stab.K} \| \bullet \|_\infty \equiv \min_{stab.K} \sup_{\omega \in \mathbb{R} \bigcup \infty} \overline{\sigma}(\bullet). \tag{3.38}$$

A sensible question that a control designer may ask is: 'Why is there a need for minimization of the $\| \bullet \|_\infty$ norm of some (closed/open) loop transfer functions?'. Essentially it gives a measure of how hard it is to reach $x(t) = x_{des}$ from $x(0) = 0$, i.e. gives an indication of how large an input u is required to reach a desired state. $\mathcal{H}_\infty$ control is a worst-case design paradigm and minimum energy indicates less control effort to drive the system to where we want. The $\mathcal{H}_\infty$ norm of a transfer function matrix constitutes a bound on the maximum allowable energy of the output signals over a class of input signals of unit energy.

For example, by minimizing the $\mathcal{H}_\infty$ norm of a selected transfer function reflecting closed loop performance specifications we minimize the energy gain of the system and thus contribute towards satisfying the performance objectives (see Section 3.2.1).

Direct minimization utilizing $\mathcal{H}_\infty$ methods has been developed for synthesizing compensators which directly minimize $\|S(j\omega)\|_\infty$ or $\|T(j\omega)\|_\infty$ or singular values of weighted augmented combinations $\left\| \begin{bmatrix} S & KS & T \end{bmatrix}^T \right\|_\infty$, $\left\| \begin{bmatrix} S & T \end{bmatrix}^T \right\|_\infty$ or $\left\| \begin{bmatrix} S & KS \end{bmatrix}^T \right\|_\infty$.

[19] Minimizing the $\mathcal{H}_2$ norm corresponds to minimizing the sum of the square of all the singular values over all frequency range, and to pushing down all singular values over all frequencies.

3.6 Summary

This chapter has served as an introduction to many fundamental concepts in this thesis, taking the reader from basic principles of feedback control to modern mathematical tools for controller synthesis and analysis.

In the context of the suboptimal $\mathcal{H}_\infty$ operator framework controller design requirements, four types of uncertainty representations have been reviewed. Particular emphasis has been given to the normalized *coprime* factor uncertainty representation. It is a major tool in our controller design methods.

Necessary and sufficient conditions for a given controller $\mathbf{K}$ to stabilize robustly a perturbed plant under these forms have been presented.

The next chapter will expose the reader to important controller synthesis techniques with optimization criteria within a specific $\mathcal{H}_\infty$ framework, namely, $\mathcal{H}_\infty$ loop-shaping. We will attempt to elaborate on the implications of the structure of the weights in attaining the desired design characteristics. We also hope that the results will communicate on the authority the designer gains in loop-shaping, and the limitations s/he faces when using some of these optimization based techniques.

Chapter 4

Advanced control via $\mathcal{H}_\infty$ loop-shaping

The research presented herein is based on a single, intuitive, relatively straightforward approach to control system design- $\mathcal{H}_\infty$ loop-shaping. With its proven record in the field of engineering practice, $\mathcal{H}_\infty$ loop-shaping combines the performance benefits of classical control with the robustness characteristics of $\mathcal{H}_\infty$ optimization.

The normalized left *coprime* factorisation approach is used as a tool for obtaining robust stability using $\mathcal{H}_\infty$ optimal control. The stability margin ($\epsilon \equiv b_{\mathbf{G},\mathbf{K}}$) along with its pointwise version of $\rho_{\mathbf{G},\mathbf{K}}$ are introduced as measures to assess the success of the design procedure.

The impact of the structure of the weighting functions in the 1 Dof $\mathcal{H}_\infty$ LSDP is studied. The study is strengthened with a presentation of several algorithms for constructing weighting functions. This is followed by a presentation of two different (1 Dof and 2 Dof) controller architectures which utilize a realistic assessment of the benefits of the weighting function algorithms.

4.1 From classical to robust loop-shaping: in the SISO and MIMO context

The fundamental work of Bode who mathematically established the gain-phase integral relations (see [Bod45]) in the frequency domain response of a system forms an essential base for a frequency domain design method, the so called loop-shaping approach.

Theorem 4.1 *For every frequency* ω_0

$$\angle L(j\omega_0) = \frac{1}{\pi}\int_{-\infty}^{\infty} \frac{d\ln|L|}{d\nu} \ln\coth\frac{|\nu|}{2} d\nu \tag{4.1}$$

where the integration variable is $\nu = \ln(\frac{\omega}{\omega_0})$*, and the slope function* $\frac{d\ln|L|}{d\nu}$*, which is almost always negative, is weighted by the function* $\ln\coth\frac{\nu}{2} = \ln\left|\frac{\omega+\omega_0}{\omega-\omega_0}\right|$.◇

Careful analysis will lead to the conclusion that as $\omega \to \omega_0$ the values of the slope function $\frac{d\ln|L|}{d\nu}$ are more emphasised; L denotes the open loop transfer function. Thus, roughly speaking, the steeper the graph of $|L|$ near frequency ω_0, the smaller the value of the phase of L; this can be easily proved [DFT92] [p.113]. Thus, internal stability is directly related to the slope of $|L|$, and internal stability will be violated if $|L|$ rolls off too fast through crossover.

An extended version of Bode's gain-phase relationship, in Theorem 4.1, for an open loop stable and scalar system with possible non-minimum phase zeros follows from [ZDG96] [p.151] and is presented in Theorem 4.2:

Theorem 4.2

$$\angle L(j\omega_0) = \frac{1}{\pi}\int_{-\infty}^{\infty} \frac{d\ln|L|}{d\nu} \ln\coth\frac{|\nu|}{2} d\nu + \angle\prod_{i=1}^{k}\frac{j\omega_0+\overline{z}_i}{j\omega_0-z_i} \tag{4.2}$$

◇

Where the z_i's are the *RHP* zeros of L(s); then, for $\forall$ i, the second term on the right hand side in Equation 4.2

$$\angle\prod_{i=1}^{k}\frac{j\omega_0+\overline{z}_i}{j\omega_0-z_i} \leq 0$$

is the non-minimum phase part of L(s). It is widely known [SBG97] that an unstable zero in the system contributes an additional phase lag and thus, imposes limitations on how fast/slow the open loop gain can be rolled off. This makes blatant the clash between loop quality around ω_c and the attenuation rate.

In classical feedback control the robustness and performance design constraints expressed in terms of the magnitude of the frequency response of some closed loop transfer functions can be approximated, at appropriate frequency ranges, by the magnitude of the open loop transfer function L (in SISO problems), or by the magnitude of the transfer functions $\mathbf{L}_i$, $\mathbf{L}_o$ (in MIMO problems).

Shaping the open-loop system's singular values, however, does not guarantee that the closed loop system in Figure 3.1 will be internally stable. It has been shown by [Bod45] that for SISO systems, in general, closed loop stability can be determined from the open loop gain/phase relationship near crossover frequency (ω_c) or $|L| = 1$, and that in particular the rate of transition from high gain to low gain is limited by phase requirements. The greater the slope of $|L|$ near crossover, the smaller the angle of L. Therefore if $|L|$ drops too rapidly through crossover, internal instability will become unavoidable. Hence, a gentle slope, a slope of no more than 2, must be maintained at this region. In MIMO systems this condition cannot be determined from the frequency response shape of the open loop singular values.

Therefore, in the classical loop-shaping approach the need to ensure stability of the closed loop requires that open loop phase properties are also considered. It has been shown in [Bod45] for the SISO case and in [FL87] that for MIMO systems achievable loop shapes are limited by open loop poles and zeros located in the *RHP*. To provide relief to the constraints brought about by the plants phase properties, research was directed to incorporate mid-frequency multivariable plant open-loop phase manipulations along with its gains [HM81], [Mac82].

Although the absolute value of the respective complex-valued function at each frequency in a given frequency range is a suitable measure to represent the gains in single-input single-output systems, it is insufficient to capture and reflect the inherent complexities of multi-input multi-output systems. Singular values were introduced in Chapter 2 as appropriate measures of magnitude for matrix valued transfer functions. It was the derivation of mathematical inequality conditions for stability robustness and performance in terms of those (suitable) new measures of size for MIMO systems dynamics that made possible a successful generalization of the appealing loop-shaping technique to MIMO systems [DS81], [FL87], [SD91], [DFT92]. Notable links between classical frequency domain design and $\mathcal{H}_\infty$ design approaches were established which allowed the designer to utilize the intuition gained from the classical techniques in the $\mathcal{H}_\infty$ norm minimization based approaches. In both of the design approaches the designer can explicitly and graphically manipulate magnitudes of the frequency responses of some (open/closed) loop transfer functions.

Specifications can be also reduced to *spatially round* [1] requirements on S(s) and T(s).

[1] A transfer function is *spatially round* when its condition number $\kappa(\bullet) \doteq \frac{\overline{\sigma}(\bullet)}{\underline{\sigma}(\bullet)} \approx 1$.

4.1.1 Closed loop-shaping

Many linear and non linear MIMO design problems defined by pre-specified performance objectives, external signal sets and plant sets can be reduced to one of shaping Bode plots of sensitivity and complementary sensitivity transfer functions of the feedback system to achieve design targets of performance and robustness.

It was shown in Chapter 2 that the $\mathcal{H}_\infty$ norm of a real rational transfer function is the peak of the transfer function magnitude, and by introducing weights, the $\mathcal{H}_\infty$ norm can also be interpreted as the magnitude of some closed loop transfer function relative to a specified upper bound, which is usually what is desired.

Although at some cost, it is always possible and convenient to perform designs by directly shaping terms like $\mathbf{S}$ and $\mathbf{T}$ rather than translating specifications in constraints on the open loop shape. This leads to a specific configuration called weighted sensitivity where the designer has performance and robustness objectives "*stacked*" and tries to minimize the $\mathcal{H}_\infty$ norm of the weighted form of sensitivity, co-sensitivity and some other closed loop transfer functions [SP96] [p.59], [WH90].

In this approach, an uncertainty model description can be used to describe the set of plants $\mathbf{G}_\Delta$ over a wide frequency range, weights $\mathbf{W}_1$ and $\mathbf{W}_2$ can be chosen according to the information available about the frequency behaviour of the central plant $\mathbf{G}$ at various frequencies. That is at (usually low) frequencies where the frequency response of the plant's dynamics is well known Δ must be forced to be small by selecting $\mathbf{W}_1$ and $\mathbf{W}_2$ large. Whereas at frequencies (usually high) for which the plant is highly uncertain, Δ shall be allowed to be large by appropriately manipulating with $\mathbf{W}_1$ and $\mathbf{W}_2$ such that their magnitude is small. This mathematical representation of the uncertainty in the plant does fully capture the nature of the feedback.

In the context of $\mathcal{H}_\infty$ design an alternative approach to linear MIMO control systems design is the so called mixed sensitivity approach. It was first introduced in [Kwa83] and [VJ84], and the fact that it relied on optimization of a criterion which involved two or more sensitivity transfer functions served as a motivation for the name "*mixed*" sensitivity. The designer specifies closed loop objectives in terms of the requirements on the singular values of the weighted closed loop transfer functions with design significance. The advantage of controller synthesis based on an $\mathcal{H}_\infty$ closed loop approach method is that specifications apply at all frequencies, whereas open loop-shaping is usually restricted to frequencies of low and high loop gain. Additionally, robustness and performance properties can be traded both at the plant input and plant output. Furthermore, an important advantage over open loop-shaping is that shaping the closed loop by weighting functions allows the designer to graphically manipulate with what s/he sees until s/he gets what s/he wants, whereas in $\mathcal{H}_\infty$ loop-shaping the manipulated open loop is only an indication of the closed loop. Therefore, it is common that open loop shape (requirements) do not translate as desired to the closed loop shape. However, there are several disadvantages of closed loop design: arriving at stabilizing controller to ensure that closed loop performance and robustness specifications are met, requires the well known, γ iterations. It was shown in [SG90] that ("*mixed*" sensitivity) $\mathcal{H}_\infty$ norm minimization design procedures can produce controllers whose zeros cancel all stable poles of the plant. This is unacceptable in the case when the plant has lightly damped modes, i.e poles close to imaginary axis (and most systems with flexible appendages: satellites, robotic manipulators fall into this category; helicopter's main rotor blades are also flexible but practice has shown that they do not pose the same effect as in aforementioned systems). Along with that, the appropriate selection of the closed loop objectives and weighting functions is not trivial and tends to be developed for each particular example. This is a drawback of all loop-shaping methods, but is particularly so, as we will see later, in open loop-shaping.

A design approach that also exploits the fundamental principles of loop-shaping is Loop Transfer Recovery (**LTR**). The technique is a specialized application of **LQG** control that aims at recovering the desirable features of full state feedback [KS72], [SA87]. In this method the designer specifies the desired loop shape by manipulating the singular values of MIMO systems. Whilst it can successfully be applied to both unstable and non-minimum phase plants [ZF90], as a multivariable loop-shaping method, it has found only limited use in practical applications. The method necessitates an assumption that the number of inputs is at least equal to the number of outputs [SP96]. The full state feedback recovery in the **LTR** procedure introduces high gains which can initiate problems with unmodelled dynamics; and the method can only guarantee performance and robustness properties at the either plant input or plant output.

4.1.2 Open loop-shaping

The loop-shaping design technique is conceptually simple as it involves finding a controller that shapes the loop transfer function[2] $\mathbf{L}_o = \mathbf{GK}$ so that the loop gains $\underline{\sigma}(\mathbf{L}_o)$ and $\overline{\sigma}(\mathbf{L}_o)$, as depicted in Figure 4.1, clear the boundaries specified by the performance and robustness requirements respectively at low (up to ω_l) and high (above ω_h) frequencies.

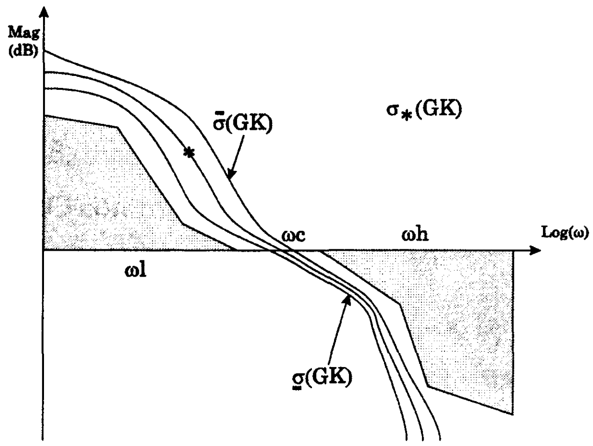

Figure 4.1: Desired Open Loop Singular Values

In scalar (SISO) control system design, the frequency response is only a function of the frequency of the input signal $u(j\omega) \in \mathbb{C}^n$, and the design procedure is effective and relatively straightforward to use since the minimum singular value and maximum singular value are identical at each frequency of consideration $\overline{\sigma}(L) = \underline{\sigma}(L) = |L|$. This leaves the control law designer with only one frequency response magnitude shape to manipulate. However, in multivariable systems the frequency response of the system does not only depend on the frequency but also on the direction of the input signal $u(j\omega)$. This property adds a significant challenge to MIMO controller design.

Therefore, when loop-shaping is extended to MIMO systems, this will inevitably introduce a level of conservatism in the loop-shaping procedure. Some limitations are as outlined below:

- The technique alone cannot effectively deal with problems arising from the combination of different specifications in different channels and/or problems with

[2]Here we have expressed the desired open loop shape in terms of the open loop singular values at the plant output, however without loss of generality the principle of loop-shaping applies identically to the open loop singular values at the plant input as well, simply replacing $\mathbf{L}_o$ by $\mathbf{L}_i$.

different uncertainty characteristics in different channels without introducing significant conservatism.

- In Figure 4.1 the frequency range ω_l, ω_h cannot be chosen arbitrarily small; their boundaries and geometry, similar to the weighting functions, are problem dependent and dictated by the requirements of the system being considered.
- The possibility of interference between the low frequency performance region (up to ω_l) and the high frequency robustness region (above ω_h) at frequencies usually around crossover (ω_c) or mid range always exists.

We will see in Chapter 5, that none of these potential constraints imply the nonexistence of (such) a MIMO controller that will satisfy both nominal performance and robust stability requirements in the design.

Alternatively the designer can perform design on a loop by loop basis but when cross-coupling between feedback loops becomes significant this can be both laborious, inefficient and not very realistic, which may consequently lead to a poor design.

In [DFT92] guidelines for loop-shaping of SISO systems are provided where it is suggested that in order to get the right loop-shape of $|L|$ where $L = GK$ to begin with K is chosen as a *constant*, which is usually 1, and then dynamics is added to the K. Performance and robustness specifications on S and T are converted into specifications on the loop transfer function L, with reasonable crossover characteristics. This method has attracted a significant amount of research study, however, the restrictions to SISO systems and the requirement for G to be invertible were disadvantages. It is difficult to tune for complex problems since the open loop is only indirectly shaped by low frequency weighting function W_1 and high frequency robustness weighting function W_2 which form correspondingly the low frequency and high frequency regions to be avoided. The underlying idea of loop-shaping was extended by the same authors to perform loop-shaping directly with K or other quantities for plants with *RHP* poles and *RHP* zeros.

In contrast to loop-shaping treated in [DFT92], a more systematic as well as rigorous approach must be taken to address the needs of the designer in terms of transparency and ease of use of the loop-shaping method in MIMO systems. One, and nowadays widely used, approach is direct and effective shaping of the system's loop-gain operator GK as a function of frequency over the frequency range of interest with the aid of frequency dependant weighting functions.

A method which is based on governing principles of classical loop-shaping and combines the stability guarantee of $\mathcal{H}_\infty$ control to overcome the existing limitations present in techniques like **LTR** procedure and $\mathcal{H}_\infty$ *"mixed"* sensitivity is the $\mathcal{H}_\infty$ loop-shaping method.

4.2 Loop-shaping via $\mathcal{H}_\infty$ synthesis

A novel method for robust controller design, known as $\mathcal{H}_\infty$ loop-shaping, which incorporates notions of classical loop-shaping with the characteristics of $\mathcal{H}_\infty$ control, was first proposed in [MGN88], further developed in [GM89] and extended into a controller synthesis in [MG90], [MG92]. This elegant method blends, in a systematic way, the *normalized* l.c.f. robust stabilization problem as a means of guaranteeing closed loop stability with the philosophy of classical loop-shaping as a tool to meet closed loop performance requirements. It has gradually established itself in the last decade as a tool that practising engineers nowadays use in a wide range of applications. Although the technique does not explicitly guarantee robust performance, extensive practical experience has shown that it also provides some level of robust performance. Research carried out in [PG02] has shown that the 2 Dof controller design procedure can integrate tools for ensuring a level of robust performance subject to robust stability constraints.

$\mathcal{H}_\infty$ loop-shaping design is, essentially, a two step design procedure, namely:

1) Loop-shaping: where the designer aims to give the nominal plant's singular values a desired shape at low and high frequencies to meet performance and robustness requirements. The shaping is done so that the crossover frequency corresponds to the desired closed loop bandwidth, and low and high frequency gains are as desired.

2) Robust Stabilization: The normalized *coprime* factor $\mathcal{H}_\infty$ robust stabilization problem, solved explicitly in [GM89], is used to stabilize robustly the shaped plant against the presence of stable and bounded perturbations on the normalized *coprime* factors of the shaped plant.

In each of the two steps the designer must ensure various objectives are met in order to extract most benefit out of the method.

4.2.1 Loop-shaping

After an initial inspection of the frequency response of the scaled nominal plant **G**, the first step a designer will take is to determine the desired loop-shape which is derived from requirements in the time domain.

After that by augmenting the nominal plant with the aid of diagonal or non-diagonal pre-/post-filters $\mathbf{W}_1$, W_2 s/he will aim to attain high gain of singular values at low frequencies (for good disturbance rejection and tracking), and low gain at high frequencies (for good robust stability and noise attenuation)[3]. From classical loop-shaping an equally important objective is that the gain around cross-over at the desired bandwidth does not fall off quicker than 40 dB/dec corresponding to a slope of -2, ensuring good phase margin. In view of the Bode gain-phase relationship, steeper transition from low frequency high gain region to high frequency low gain region will reduce the available phase margin. To rectify this the designer will need to increase the gain in appropriate channels which might not be tolerated well by the system.

The designer must also ensure that the loop gain is large around the frequencies and in the directions of open loop unstable poles and small around the frequencies and in the directions of open loop unstable zeros [Vin00]. This is because *RHP* poles, together with *RHP* zeros and time-delays impose, respectively, lower and upper bounds on the achievable bandwidth [FL85], [SBG97], [Ast00]. Violating these bounds, for example, pushing the bandwidth in one of the channels too high and having it above the frequencies of *RHP* zeros will violate physically achievable bandwidth.

Remark 4.1 *In contrast to the classical loop-shaping approach $\mathcal{H}_\infty$ loop-shaping is performed without consideration of nominal plant phase information. At this stage closed loop stability requirements are dismissed. However, for this, care will be taken in the next step of the procedure.*

After completing the loop-shaping, and the designer is satisfied that the weighted plant's frequency response will adequately capture the performance specifications s/he can proceed to the second phase of the loop-shaping design procedure $\mathcal{H}_\infty$ LSDP. Namely, robust stabilization of the shaped plant in the presence of stable perturbations on its normalized *coprime* factors; this phase has several sub-steps as follow.

[3] Figure 4.7 depicts a schematic representation of augmenting a nominal plant in loop-shaping.

4.2.2 Normalized coprime factorization robust loop-shaping controller synthesis

Consider the configuration in Figure 4.2 where $\mathbf{G}$ is an LTI plant, and $\mathbf{G}_s(s) = \widetilde{\mathbf{M}}_s^{-1}\widetilde{\mathbf{N}}_s$ is a normalized l.c.f. of $\mathbf{G}_s = \mathbf{W}_1\mathbf{G}\mathbf{W}_2$.

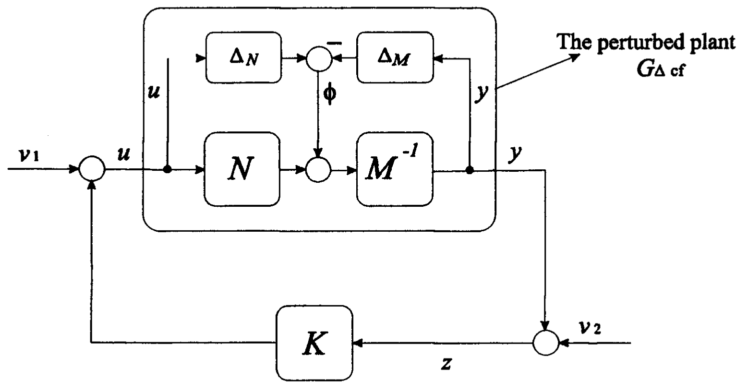

Figure 4.2: Coprime factor uncertainty

Recall that $\mathbf{G}_{\Delta_{cf}}$ is a family of perturbed plants previously defined as:

$$\mathbf{G}_{\Delta_{cf}} = \{(\widetilde{\mathbf{M}} + \Delta_{\widetilde{M}})^{-1}(\widetilde{\mathbf{N}} + \Delta_{\widetilde{M}}) : \ [\Delta_{\widetilde{M}} \ \ \Delta_{\widetilde{N}}] \in \mathcal{RH}_\infty, \ \ \|[\Delta_{\widetilde{M}} \ \ \Delta_{\widetilde{N}}]\|_\infty < \epsilon = \gamma^{-1}\}$$

Necessary and sufficient conditions for the robust stability of plants represented in the normalized left *coprime* factor framework were given in Corollary 3.3. Minimizing the $\mathcal{H}_\infty$ norm of the transfer function from $\phi \rightarrow \begin{bmatrix} u & y \end{bmatrix}^T$ maximizes the size of *coprime* factor perturbations $\left\| \begin{bmatrix} \Delta_M & \Delta_N \end{bmatrix} \right\|_\infty$ which will destabilize the closed loop. This immediately gives a design objective in the normalized *coprime* framework; to design a controller $\mathbf{K}$ that stabilizes the perturbed plant $\mathbf{G}_{\Delta_{cf}}$ for a given ϵ where the optimal solution to the normalized l.c.f robust stabilization problem over all stabilizing controllers is given by:

a) Calculate ϵ_{max}

$$\inf_{stab.\mathbf{K}} \left\| \begin{bmatrix} \mathbf{K} \\ I \end{bmatrix} (I - \mathbf{G}_s\mathbf{K})^{-1}\widetilde{\mathbf{M}}_s^{-1} \right\|_\infty := \gamma_{min} = \epsilon_{max}^{-1} \tag{4.3}$$

where the *infimum* is taken over all stabilizing controllers. For any controller $\mathbf{K}$ stabilizing a system $\mathbf{G}$, it can be proved that it achieves the same stability margin ϵ_{max} for systems described by both left and right *coprime* factorization [GS90], [ZDG96] (Corollary 18.8-p.485).

b) Select $\epsilon \leq \epsilon_{max}$ (then $\gamma \geq \gamma_{min}$), and synthesize a stabilizing controller $\mathbf{K}_\infty$ which will stabilize the normalized l.c.f. of $\mathbf{G}_s$ with stability margin ϵ and satisfy:

$$\left\| \begin{bmatrix} \mathbf{K}_\infty \\ I \end{bmatrix} (I - \mathbf{G}_s\mathbf{K}_\infty)^{-1}\widetilde{\mathbf{M}}_s^{-1} \right\|_\infty \leq \gamma = \epsilon^{-1} \tag{4.4}$$

For this purpose the designer can use a readily available command `ncfsyn` in the μ-Analysis and Synthesis Toolbox, which requires as inputs only the shaped plant and a specified factor percentage of the suboptimal controller achieving a performance factor less than optimal[4].

c) Obtain the actual controller $\mathbf{K}$ by augmenting $\mathbf{K}_\infty$ with pre-/post filters $\mathbf{W}_1$ and $\mathbf{W}_2$ such that $\mathbf{K} = \mathbf{W}_1\mathbf{K}_\infty\mathbf{W}_2$.

Remark 4.2 *The problem of minimizing (Equation 4.3) is always well-posed, even in the case when the nominal plant has poles on the imaginary axis.*

4.2.2.1 Stability margin

The key variable in assessing the success of the $\mathcal{H}_\infty$ LSDP is the parameter ϵ_{max} - maximum (optimal) stability margin. It can be regarded as a multipurpose design indicator of the success of the loop-shaping design procedure. It bridges stage 1 and stage 2 of the $\mathcal{H}_\infty$ LSDP. If ϵ_{max} is too small (γ_{min} large); $\epsilon_{max} \ll 1 \Longrightarrow \gamma_{min} \gg 1$, this indicates incompatibility between the specified loop shape (conceived as desired loop shape), nominal plant phase and thus closed loop robust stability requirements. That is, ϵ_{max} is not only an indicator of the success of the synthesis procedure in meeting the specifications reflected via the loop shapes, but is also a measure of robust stability of the closed loop. Therefore as large as possible value of ϵ_{max} is desired, but always $\epsilon_{max} < 1$. If $\epsilon \ll 1$ this indicates violation on both performance and robustness requirements and leads to an unsuccessful loop-shaping design.

High stability margin is generally thought as $\epsilon_{max} \geq 0.25$ and will guarantee that the actual loop-shapes at the plant output $\mathbf{L}_o = \mathbf{G}\mathbf{W}_1\mathbf{K}_\infty\mathbf{W}_2$, and at the plant input $\mathbf{L}_i = \mathbf{W}_1\mathbf{K}_\infty\mathbf{W}_2\mathbf{G}$ do not change significantly after the controller is augmented with the plant.

[4]Factor= 1 implies that an optimal controller is required; 1 <factor< 2 implies that a suboptimal controller is needed.

Practical experience in using $\mathcal{H}_\infty$ LSDP in [MG90], [HG93], [SP96], [SWP+01] and [PPT+05] shows that a value of ϵ_{max} in the range $0.25 \leq \epsilon_{max} < 0.4$, or $\gamma_{min} < 4$, is desirable and usually leads to a successful design.

Since the robust stabilization problem requires minimization of Equation 4.3, it can be observed that when the norm is small the stability margin is large (good), and when the norm is large the stability margin is small (bad).

Remark 4.3 *In fact we can tighten the bound on γ and consequently on $\epsilon \equiv b_{\mathbf{G,K}}$ because it has been shown in [Vin00] that for most of the plants $\mathbf{G}$ it is impossible to stabilize the set of perturbed plants $\mathbf{G}_{\Delta_{A,mult,cf}}$ if $\gamma < \sqrt{2}$, therefore it will be assumed that $\gamma > \sqrt{2}$. Later in the thesis, through applications, it will become obvious that $\sqrt{2} < \gamma < 4 \Rightarrow \epsilon < 0.7$.*

Stability margin ϵ_{max} has an alternative notational representation as in Definition 4.1.

Definition 4.1

$$b_{\mathbf{G,K}} := \begin{cases} \left\| \begin{bmatrix} K \\ I \end{bmatrix} (I - GK)^{-1} \begin{bmatrix} G & I \end{bmatrix} \right\|_\infty^{-1}, & if \begin{bmatrix} G, K \end{bmatrix} \text{ is stable;} \\ 0, & \text{otherwise.} \end{cases} \tag{4.5}$$

where $\mathbf{G}$ is the nominal plant, and $\mathbf{K}$ is the controller, also $\sup_{stab.K} b_{\mathbf{G,K}} = b_{opt}(\mathbf{G})$.
If the interconnection [G,K] is stable, $b_{\mathbf{G,K}}$ also represents the smallest distance between the frequency responses of $\mathbf{G}$ and $\mathbf{K}$. This is measured by a function ρ as a pointwise version of $b_{\mathbf{G,K}}$ and defined as follows:

Definition 4.2 *([Vin00] p.68) For given $\mathbf{G} \in \mathbb{C}^{q\times p}$ and $\mathbf{K} \in \mathbb{C}^{p\times q}$ we can define*

$$\rho(G,K) := 1/\overline{\sigma}\left(\begin{bmatrix} K \\ I \end{bmatrix} (I - GK)^{-1} \begin{bmatrix} G & I \end{bmatrix} \right) \tag{4.6}$$

A few algebraic manipulations combined with Equation 4.5 lead to:
$b_{\mathbf{G,K}} := \inf_{\omega\in\mathbb{R}} \rho(\mathbf{G}(j\omega), \mathbf{K}(j\omega))$.

There is a frequency domain interpretation of an upper bound on $b_{opt}(\mathbf{G})$ which facilitates a relationship between the nominal plant $\mathbf{G}$ and the optimal stability margin to be established. This is shown in the following proposition:

Proposition 4.1 *[GS90]*
$b_{opt}(G) := \inf_{s:\Re(s)>0} \underline{\sigma}(\mathcal{G}_{\mathbf{G}})$. $\diamond$

$\mathcal{G}_{\mathbf{G}} = \begin{bmatrix} \tilde{\mathbf{M}} \\ \tilde{\mathbf{N}} \end{bmatrix}$ denotes normalized right graph symbol for **G**.

Given a minimal state-space realization (A, B, C, D) of **G**, it has been shown that the lowest achievable value of γ, denoted by γ_{min} gives the *optimal* solution of the normalized l.c.f robust stabilization problem (Equation 4.3).

The solution for the optimal stability margin ϵ_{max} is generally iterative [VK86], but if the *coprime* factors of the shaped plant $\mathbf{G}_s$ are normalized, it has been shown in [GM89] that a noniterative solution is, indeed, possible through an elegant formula given by:

$$\gamma_{min} = \epsilon_{max}^{-1} = (1 + \rho(ZX))^{1/2} = (1 - \left\| \begin{bmatrix} \tilde{\mathbf{N}} & \tilde{\mathbf{M}} \end{bmatrix} \right\|_H^2)^{-1/2} = (1 - \lambda_{max}(PQ))^{-1/2} \quad (4.7)$$

where ϵ_{max} >0; $\left\| \begin{bmatrix} \tilde{\mathbf{N}} & \tilde{\mathbf{M}} \end{bmatrix} \right\|_H$ denotes the *Hankel* norm of $\begin{bmatrix} \tilde{\mathbf{N}} & \tilde{\mathbf{M}} \end{bmatrix}$ and satisfies $\left\| \begin{bmatrix} \tilde{\mathbf{N}} & \tilde{\mathbf{M}} \end{bmatrix} \right\|_H < 1$; ρ denotes the spectral radius (magnitude of the maximum singular value) $\rho(ZX) = |\lambda_{max}(ZX)| < \gamma$; P and Q are controllability and observability grammians respectively. $X \geq 0, Z \geq 0$ are unique positive semi-definite stabilizing solutions correspondingly to the Generalized Control Algebraic *Riccati* Equation:

$$(A - BS^{-1}D^*C)^*X + X(A - BS^{-1}D^*C) - XBS^{-1}B^*X + C^*R^{-1}C = 0 \quad (4.8)$$

and to the Generalized Filter Algebraic *Riccati* Equation:

$$(A - BD^*R^{-1}C)Z + Z(A - BD^*R^{-1}C)^* - ZC^*R^{-1}CZ + BS^{-1}B^* = 0 \quad (4.9)$$

where $R := I + DD^*$, $S := I + D^*D$ and by inspection $R^{-1} = I - DS^{-1}D^*$ and $S^{-1} = I - D^*R^{-1}D$.

The "*central*" controller in [MG90] which guarantees a solution of Equation 4.3 for a specified $\gamma > \gamma_{min}$ has the following state space form:

$$\mathbf{K} =: \left[\begin{array}{c|c} A + BF + \gamma_{min}^2 (Q^*)^{-1} ZC^*(C + DF) & \gamma_{min}^2 (Q^*)^{-1} ZC^* \\ \hline B^*X & -D^* \end{array}\right] \quad (4.10)$$

where $F = -S^{-1}(D^*C + B^*X)$ and $Q = (1-\gamma_{min}^2)I + XZ$.

These formulas simplify for the case where the plant is strictly proper, i.e. $D = 0$.

The robust stabilization problem can also be solved by having it reduced to a *Nehari* extension problem. This approach was explored by [GM89] with the aim to find the largest class of perturbations such that $\mathbf{G}_{\Delta_{cf}}$ will remain stable.

In the same article of [GM89] it was also concluded that the *coprime* factors of the controller can be directly generated from the normalized *coprime* factors of the plant by obtaining the *Nehari extension* of the matrix transfer function $\begin{bmatrix} -\tilde{\mathbf{N}}^* \\ \tilde{\mathbf{M}}^* \end{bmatrix}$.

Thus $\mathcal{H}_\infty$ optimal controllers for the robust stabilization problem taken over all stabilizing controllers could, then, be described by $\mathbf{K} = \mathbf{U}\mathbf{V}^{-1}$ where $\mathbf{U}, \mathbf{V} \in \mathcal{RH}_\infty$ are right *coprime* factors and satisfy

$$\left\| \begin{bmatrix} -\tilde{\mathbf{N}}^* \\ \tilde{\mathbf{M}}^* \end{bmatrix} + \begin{bmatrix} \mathbf{U} \\ \mathbf{V} \end{bmatrix} \right\|_\infty = \left\| \begin{bmatrix} \tilde{\mathbf{N}} & \tilde{\mathbf{M}} \end{bmatrix} \right\|_H < 1 \tag{4.11}$$

The normalized l.c.f (r.c.f) robust stabilization problem (RSP) is a rigorous approach to robust controller design, however, the trade-off is that robust performance objectives can not be included directly, and only guarantees for robust stability are provided [VK86], [Vid88]. Therefore, in practice, designing control systems using only normalized l.c.f. (r.c.f) will not be sufficient to meet closed loop performance objectives. However, this is not a concern in the context of $\mathcal{H}_\infty$ LSDP as the loop-shaping stage of the procedure does give the designer the freedom to specify and incorporate performance objectives.

The so-called normalized *coprime* factor robust stabilization problem in Equation 4.3 is a two-block $\mathcal{H}_\infty$ norm minimization problem.

Recalling that the $\mathcal{H}_\infty$ norm is an invariant under right multiplication by a *co-inner* function $\left\| \begin{bmatrix} \tilde{\mathbf{M}}_s & \tilde{\mathbf{N}}_s \end{bmatrix} \right\|_\infty = 1$ after a few but straightforward mathematical manipulations an equivalent to Equation 4.3 but four-block problem can be obtained. It takes the following form ($\mathbf{G}_s$ is replaced by $\mathbf{G}$ without loss of generality):

$$\left\| \begin{bmatrix} \mathbf{K} \\ I \end{bmatrix} (I - \mathbf{G}\mathbf{K})^{-1} \begin{bmatrix} \mathbf{G} & I \end{bmatrix} \right\|_\infty < \gamma = \epsilon^{-1} \tag{4.12}$$

Then it can be easily proved that:

$$\left\| \begin{bmatrix} \mathbf{K} \\ I \end{bmatrix} (I - \mathbf{GK})^{-1} \begin{bmatrix} \mathbf{G} & I \end{bmatrix} \right\|_\infty = \left\| \begin{bmatrix} \mathbf{G} \\ I \end{bmatrix} (I - \mathbf{KG})^{-1} \begin{bmatrix} \mathbf{K} & I \end{bmatrix} \right\|_\infty =$$
$$\left\| \begin{bmatrix} \mathbf{GS}_i\mathbf{K} & \mathbf{GS}_i \\ \mathbf{S}_i\mathbf{K} & \mathbf{S}_i \end{bmatrix} \right\|_\infty = \left\| \begin{bmatrix} \mathbf{KS}_o\mathbf{G} & \mathbf{KS}_o \\ \mathbf{S}_o\mathbf{G} & \mathbf{S}_o \end{bmatrix} \right\|_\infty < \epsilon^{-1} \tag{4.13}$$

It can be seen that the stability margin provides a bound on the gain of eight closed loop transfer functions between inputs and outputs in the feedback loop depicted in Figure 3.1. This way it allows the design engineer to balance robustness and performance design indicators at various input and output points of the feedback system.

This follows from *Proposition* 3.5 in [Vin00], which states that

$$\left\| \mathbf{T}_{\begin{bmatrix} \omega_1 & \omega_2 \end{bmatrix}^T \to \begin{bmatrix} u & y \end{bmatrix}^T} \right\|_\infty = \left\| \mathbf{T}_{\begin{bmatrix} v_1 & v_2 \end{bmatrix}^T \to \begin{bmatrix} u & y \end{bmatrix}^T} \right\|_\infty \tag{4.14}$$

Remark 4.4 *This is in contrast to other 2 block $\mathcal{H}_\infty$ optimization control system design procedures like "mixed" sensitivity S/KS, S/T or even S/KGS. In all of these problem formulations, bounds, only on the transfer functions within the closed loop design objectives are given. This leaves the 'door open' for bounds on other transfer functions (also of interest but left outside due to the structure of the 2 block problem) to be arbitrarily undesirable due to pole/zero cancellations in the closed loop transfer functions as described in [SG90].*

Remark 4.5 *The robust stabilization in $\mathcal{H}_\infty$ LSDP, in contrast to other standard $\mathcal{H}_\infty$ design techniques, is done without frequency weighting. An alternative $\mathcal{H}_\infty$ formulation for the problem of minimizing $\mathcal{H}_\infty$ frequency weighted gain from the disturbances on the plant input and output to the controller output and input is presented in [MG92].*

4.2.2.2 Bounds on the normalized coprime factors

Earlier in this chapter we have emphasised that the asymptotic stability property of *coprime* factors provides guarantees on normalized or non-normalized *coprime* factors to be bounded. The following are expressions for the explicit upper bounds of the *coprime* factors.

$$\overline{\sigma}(\widetilde{\mathbf{N}}_s) = \left(\frac{\overline{\sigma}^2(\mathbf{W}_2\mathbf{G}\mathbf{W}_1)}{1 + \overline{\sigma}^2(\mathbf{W}_2\mathbf{G}\mathbf{W}_1)} \right)^{\frac{1}{2}} \leq 1 \tag{4.15}$$

and

$$\overline{\sigma}(\widetilde{\mathbf{N}}_s) = \overline{\sigma}(\mathbf{N}_s) \tag{4.16}$$

$$\overline{\sigma}(\widetilde{\mathbf{M}}_s) = \left(\frac{1}{1+\overline{\sigma}^2(\mathbf{W}_2\mathbf{G}\mathbf{W}_1)}\right)^{\frac{1}{2}} \leq 1 \tag{4.17}$$

and

$$\overline{\sigma}(\widetilde{\mathbf{M}}_s) = \overline{\sigma}(\mathbf{M}_s) \tag{4.18}$$

At frequencies of high loop gain (low frequencies) we have

$$\overline{\sigma}(\widetilde{\mathbf{N}}_s) = \overline{\sigma}(\mathbf{N}_s) \simeq 1$$

whereas at frequencies of low loop gain (high frequencies) we have

$$\overline{\sigma}(\widetilde{\mathbf{M}}_s) = \overline{\sigma}(\mathbf{M}_s) \simeq 1.$$

Where $\widetilde{\mathbf{N}}_s$ and $\widetilde{\mathbf{M}}_s$ are normalized *coprime* factors of the shaped plant $\mathbf{G}_s = \widetilde{\mathbf{M}}_s^{-1}\widetilde{\mathbf{N}}_s$ and satisfy $\widetilde{\mathbf{N}}_s\widetilde{\mathbf{N}}_s^* + \widetilde{\mathbf{M}}_s\widetilde{\mathbf{M}}_s^* = \mathbf{I}$

At frequencies where $\widetilde{\mathbf{M}}_s$ is small that indicates a pole of the shaped plant near the imaginary axis [MG90].

It is intuitive to conclude that $\overline{\sigma}(\widetilde{\mathbf{N}}_s)$ and $\overline{\sigma}(\widetilde{\mathbf{M}}_s)$ are only directly dependent on the nominal plant $\mathbf{G}$ and the loop-shaping functions $\mathbf{W}_1$ and $\mathbf{W}_2$.

In the loop-shaping design procedure, the open-loop-shaping transfer function matrices $\mathbf{W}_1$, $\mathbf{W}_2$ modify the dynamics of the system for which a controller is going to be designed. As we will see later, they are the only tools not only in $\mathcal{H}_\infty$ LSDP but also in the $\mathcal{H}_\infty$ "*stacked*" problem formulation that can be directly manipulated by the designer to affect indirectly (directly) the behaviour of the closed loop transfer functions, and thus to emphasise and facilitate trade-offs of performance with robustness. Therefore it can confidently be said that good engineering practice and appropriate selection of the structure of the weighting functions is key to a successful design.

4.3 Weighting functions in $\mathcal{H}_\infty$ Loop-shaping

In earlier chapters we have underlined the benefits of performing design in the frequency domain where performance measures such as: control bandwidth (ω_B or ω_{BT}) [5]- determined by the choice of the crossover frequency (ω_c); the trade off between the degradation in the desired loop shape and stability margins (indicated by $b_{opt}(\mathbf{G})$) can be appropriately captured through the dynamics of the weighting functions. The use of weights or linear multipliers [GL95] is a common practice in control system design (optimization), particularly in infinity norm optimization. The weights are frequency dependent and in general can be viewed as augmenting the dynamics of the plant. Dynamic weights allow the designer not only to capture frequency dependent characteristics of signals or systems, but also to establish bounds on the size of the various closed loop transfer functions which determine performance and robustness. For example, if a given closed/open loop transfer function $\mathbf{Q}$ is known to be a low pass system (like $\mathbf{T}$ or $\mathbf{KS}$) where (for every ω) $\overline{\sigma}(\mathbf{Q}(j\omega)) < \underline{\sigma}(\mathbf{W}^{-1}(j\omega))$, then $\mathbf{W}^{-1}$ is a constant or dynamic weight satisfying $\|\mathbf{WQ}\|_\infty < 1$ and capturing this information in a compact way.

It is very common in practical applications that the plant's frequency response does not possess the "*shape*" that will capture good closed loop performance or robust stability requirements or both. This necessitates the plant's singular values, as functions of frequency, to be reshaped and brought to comply with the design objectives at low and high frequencies. In the $\mathcal{H}_\infty$ loop-shaping framework, this can be achieved by pre-multiplying the nominal plant $\mathbf{G}$ with a pre-filter $\mathbf{W}_1$ to alter and remedy the low frequency associated characteristics (e.g. disturbance rejection, command tracking), and then post-multiplying the augmented system $\mathbf{GW}_1$ with $\mathbf{W}_2$ to modify properties at high frequencies (e.g. noise mitigation or rejection, and robustness to unmodelled dynamics). It is usually $\mathbf{W}_1$ that accommodates the elements which modify the dynamics of the plant; $\mathbf{W}_2$ is often a constant matrix. Finally, it is the shaped plant $W_2\mathbf{GW}_1$ that is optimally robustly stabilized and not the plant $\mathbf{G}$.

The lack of a unifying theory and a universal algorithm for weight selection in $\mathcal{H}_\infty$ control is understandable. Every dynamical system will embed different characteristics and hence so will the dynamical weights. Therefore, for years, weights have been con-

[5]Although there are different interpretations of the bandwidth in [SP96] and [Oga02] we will use ω_B which is defined with respect to the sensitivity transfer function.

structed for every specific problem at hand based on rules of *"thumb"* and some well established guidelines [SP96], [Hyd95]. These guidelines simply reflect on performance and robustness design tradeoffs (outlined in section 3.2.1).

The selection of weights evolves as a multi objective procedure and thus has several objectives. Weights are designed to address performance (via $\mathbf{W}_1$) in the system, for robustness (via $\mathbf{W}_1, \mathbf{W}_2$) and for feasibility [Vin00].

Therefore a procedure for weight design must reflect on all these trade-offs. It is not trivial to unify all these in a single criterion. Insight on justification of the complexity of trade off between frequency objectives can be gained from section 3.2.1.

It must be born in mind that the construction of weighting functions in $\mathcal{H}_\infty$ loop-shaping and in $\mathcal{H}_\infty$ *"mixed"* (*"stacked"*)- sensitivity are distinct from one another.

In the following section we will present a brief summary of the advantages and disadvantages of diagonal (or structured) weighting functions within the $\mathcal{H}_\infty$ LSDP context followed by an overview of the existing algorithm for designing non-diagonal (or unstructured) pre/post- filters proposed in [PG97]. A presentation of a modified- LMI optimized algorithm for the unstructured weight design developed in [Lan01] will be briefly mentioned.

4.3.1 Diagonal (structured) weights

A square transfer function matrix $\mathbf{W}_j \in \mathcal{RH}_\infty$, ($j = 1, 2$), is called diagonal, if all non-diagonal entries of the matrix are zero.
Weights with diagonal structure have been used extensively in $\mathcal{H}_\infty$ *sub/optimal* control as tools to modify the frequency response magnitude shape of various closed loop transfer functions (**S**, **T**, **KS**) [Kwa93], [WH90]. The transparency (of shaping singular values) and ease that diagonal weights provide in shaping a closed loop transfer function's singular values have also put them forward as a favourable candidate in shaping the nominal plant's singular values in the $\mathcal{H}_\infty$ loop-shaping controller design procedure.

Over the years their usefulness in $\mathcal{H}_\infty$ LSDP has been illustrated by the extensive number of applications in a wide range of (mostly) engineering disciplines that they have been used in.

Intrinsic to many complex dynamical systems characteristics such as severe inter-channel cross-coupling, ill-conditioning, and directionality (distinctive to MIMO systems) are some of those factors that would challenge even the experienced designer in arriving to relatively good shapes by using diagonally structured weights. This leaves the possibility that some of the performance and robustness requirements in the design are likely to be compromised. Nonetheless, in the absence of some of those characteristics, within the context of $\mathcal{H}_\infty$ loop-shaping, diagonal structured weights continue to remain popular as the first choice of weight. They are simple to construct, easy to tune by hand, straightforward to interpolate in gain scheduling and transparent in the way each diagonal element in the weight scales only the corresponding diagonal element in the nominal/shaped plant.

4.3.2 Non-Diagonal (unstructured) weights

A transfer function matrix $\mathbf{W}_j \in \mathcal{RH}_\infty$ ($j = 1, 2$) is called non-diagonal if it has non-zero non-diagonal elements. A sparse matrix can accommodate non-diagonal elements which are zero [HJ85], and it is considered non-diagonal.

In relatively high order plants with complex aerodynamic and mechanical structures exhibiting high levels of cross-coupling (between control input and measurement output channels), high condition numbers (different gains in different directions at the same frequency) the designer can easily lose insight into how each diagonal element in the weights affects the singular values of the scaled nominal plant. In this way, the design problem becomes very difficult. The task of choosing diagonal (structured) weights, unless posed as an optimization problem, is an iterative, time consuming process, that can be quite onerous if done in an *ad-hoc* manner. In order to surmount the difficulty posed by the system's high condition number, and in line with this, to establish more "*authority*" in shaping the singular values of the open loop plant, Papageorgiou in [PG97] proposed a systematic procedure to facilitate the construction of non-diagonal (or unstructured weights) in the $\mathcal{H}_\infty$ LSDP context. Their work was demonstrated on the design of a 1 Dof controller for a 4 state 2×2 sized plant. Earlier, a relatively simplified version of this procedure was reported in [PGH97]. Later in [PG02] the procedure was extended to the design of a 2 Dof controller with robust performance guarantees. The roots of this idea, however, can be found in the Reverse Normalization Framework (RNF) for controller design in [HM81].

A few years later Lanzon [Lan01] combined steps of the procedure presented in [PG97] with the steps of standard $\mathcal{H}_\infty$ loop-shaping design procedure to formulate an optimization problem in terms of linear matrix inequalities (LMI) to maximize the robust stability margin over the loop-shaping weights and associated constraints. Considering time domain performance specifications, robust performance and robust stability regions (at low and high frequencies) have been created by setting constraints on $\sigma(\mathbf{G}_s)$, $\sigma(\mathbf{W}_1)$, $\sigma(\mathbf{W}_2)$; $k(W_1)$ and $k(W_2)$.

4.4 Algorithms for weight construction

4.4.1 Algorithm of Papageorgiou

This particular algorithm constitutes our main tool for designing non-diagonal weights. It will therefore be considered in more detail in the course of its review. In alignment with the principles of classical loop-shaping the first step a designer will take is to inspect the singular values of the nominal plant $\mathbf{G}$ and to estimate the loop shape that will capture the performance and robustness requirements.

The so called "*desired*" loop shape can be achieved by augmenting the dynamics of the nominal plant with frequency dependent weighting functions. This is performed after careful inspection of the singular values of the nominal plant $\mathbf{G}$ depicted in Figure 4.3.

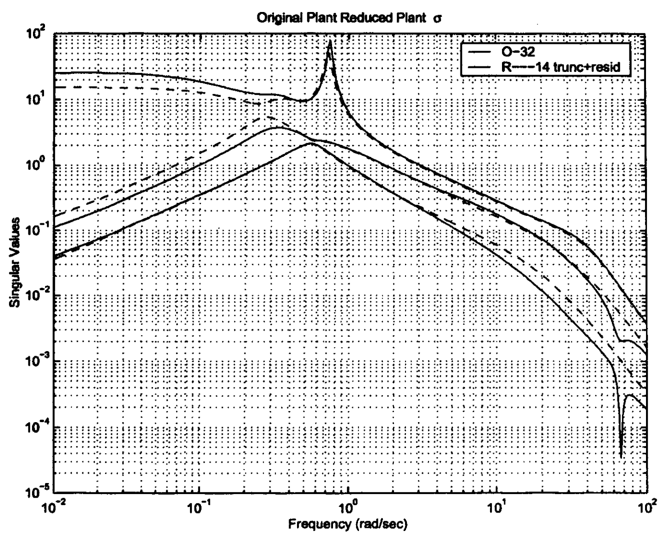

Figure 4.3: Shapes of actual (32 state) and reduced order (14 states) plant's singular values; (continuous line-actual), (dashed line- reduced)

Figure 4.3 depicts with continuous line the singular values of the original helicopter plant $\mathbf{G}$, and with dashed line the reduced order plant's singular values as function of frequency. The structure of the weighting transfer functions $\mathbf{W}_1$ and (if necessary $\mathbf{W}_2$) that will weight elements, $\sigma_i(\mathbf{G})$ of $\mathbf{G} \in \mathcal{RL}_\infty$ needs to be decided. Augmentation with both will result in $\sigma_j(\mathbf{W}_2)\sigma_i(\mathbf{G})\sigma_i(\mathbf{W}_1)$. Here the i-th singular value of the desired loop shape, Σ_s^{des}, is approximately $\sigma_j(\mathbf{W}_2)\sigma_i(\mathbf{G})\sigma_i(\mathbf{W}_1)$ where $(i \neq j)$ for non-square systems. The set of "*desired*" loop shapes encloses all the loop shapes (which may be infinite) that will meet the robustness and performance requirements dictated by the plant's intrinsic constraints, by the operational environment and by design objectives. In effect the designer has chosen a diagonal transfer function matrix $\mathbf{W} = diag(w_1, ..., w_m)$ that augments the singular values of the nominal plant $diag(\sigma_1, \ldots, \sigma_m)$ to give the "*desired*" loop-shape. A careful thought should be spent on the fact that the singular values of the nominal plant may not be arranged in decreasing order at all frequencies.

$\mathbf{W}_1^d$ and $\mathbf{W}_2^d$ must be chosen such that the shaped plant $(\mathbf{G}_s)$ contains no unstable hidden modes, i.e. the shaped plant $(\mathbf{G}_s)$ is state stabilisable and state detectable; conditions that will ensure internal stability of the closed loop system. This leaves open the possibility of unstable and/or non-minimum phase weights. The use of unstable and non-proper weights in the $\mathcal{H}_\infty$ design framework has been studied in [Mei95], [PTG90]. In the proposed algorithm $\mathbf{W}_{1,2}{}^d \in \mathcal{RH}_\infty$, with the possible exception of integrators, the weighting functions are stable, minimum phase, and units in $\mathcal{RH}_\infty$. Pole-zero cancellations between the nominal plant and the weights in the *LHP* do not affect internal stability but can lead to poor robust performance [SG90].

Procedure Requirements:

Assume that the nominal plant model $\mathbf{G}$ with n inputs and m outputs is linear time invariant (LTI), $\mathbf{G} \in \mathcal{RL}_\infty$ and has a minimal state space realization A, B, C, D.

The Design Procedure:

Given structured diagonal weights $\mathbf{W}_1^d$ and $\mathbf{W}_2^d$, the following procedure enables the designer to select non-diagonal weights $\mathbf{W}_1^{nd}$, $\mathbf{W}_2^{nd}$ that are stable and minimum phase, such that $\sigma_i(\mathbf{W}_2^d\mathbf{G}\mathbf{W}_1^d\mathbf{W}_1^{nd}) \simeq \sigma_i(\mathbf{G}_s)\sigma_i(\mathbf{W}_1^{nd})$ for all $i = 1, \ldots, r; r = rank(\mathbf{G})$.

The design procedure in [PG97] is outlined below for completeness and is complemented with some additional comments gathered from the author's own experience of using it:

1 a) Select a frequency range of interest $[\omega_l, \omega_h]$ that contains the dynamics of $\mathbf{G}$ around the tentative closed loop bandwidths. Although the range can be problem dependent, experience has shown that the range 0.01 rad/sec to 100 rad/sec is usually sufficient to capture the salient dynamic characteristics of the system plant.

b) Grid the range sufficiently densely. At each frequency ω of the selected grid frequency range perform a singular value decomposition *SVD* of $\mathbf{G}(j\omega)$:

$$\mathbf{G}(j\omega) = U(j\omega)\Sigma(j\omega)V(j\omega)^*,$$

such that the ordering of the singular values in $\Sigma(j\omega)$ is uniform across the frequency range considered. By uniform it is meant that each singular value as a function of frequency varies continuously with frequency.

The μ-Toolbox command *vsvd* [BDG+98] arranges the singular values in decreasing order at each frequency and as such can not be used directly. However, it can easily be modified to guarantee uniform ordering of the singular values over the frequency range of interest. We have seen in Chapter 2 that in *SVD* the left (*U*) and the right (*V*) singular vector matrices are not unique, hence they vary discontinuously with frequency.

However, ensuring the uniform ordering of the singular values when combined with careful selection, frequency by frequency, of the all-pass factors [HJ85] (Lemma 7.3.1) up to which (*U* and/or,*V*) is unique, also ensures that elements U_{ω_k} and V_{ω_k}, respectively of *U* and *V*, vary continuously across the pre-defined frequency range of interest $[\omega_l, \omega_h]$. By continuous variation we mean continuous when the grid is infinitely dense. Continuous variation of an element of *V* is shown in Figure 4.4.

2. If $\mathbf{G}(j\omega)$ has distinct singular values then V is determined up to a right diagonal all pass factor. $\Phi = e^{j\theta_i}I$ where $i = 1, \ldots, r$ with all $\theta_i \in \mathbb{R}$.

Solve the second norm minimization:

$$\alpha_{k,i}^{opt} = arg \min_{\|\alpha\|=1} \|v_{\omega_k,i} - v_{\omega_{k+1},i}\alpha\|_2 \tag{4.19}$$

where its analytical solution is $\alpha_{k,i}^{opt} = -\angle(v^*_{\omega_k,i}v_{\omega_{k+1},i})$ at each pair of grid frequencies (ω_k, ω_{k+1}) where $v_{\omega_k,i}$ denotes the i-th column of $V(j\omega_k)$. Then post-multiplying $V(j\omega_{k+1})$ by the all pass factor $e^{j(diag(\alpha_{k,1}^{opt},\ldots,\alpha_{k,m}^{opt}))}$, guarantees continuous variation of the elements of V.

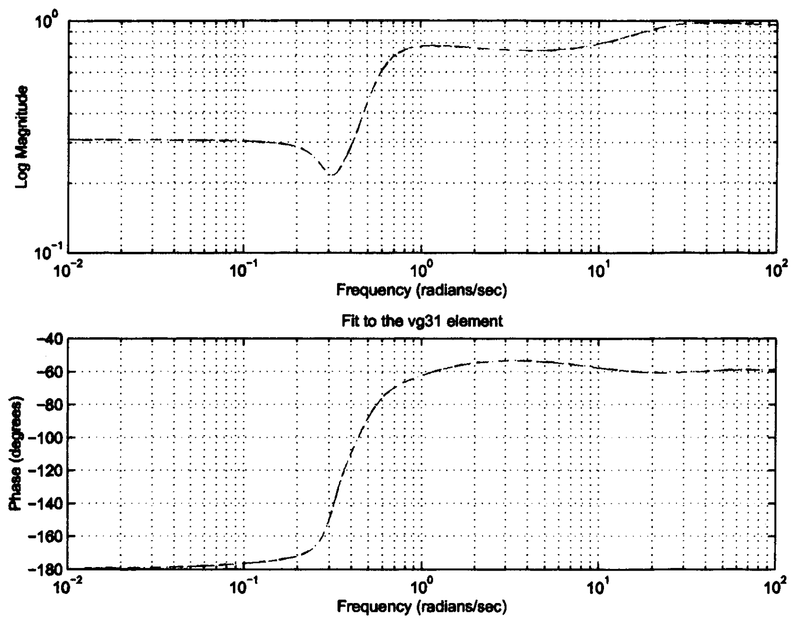

Figure 4.4: Continuous variation of an element of V

However, at frequencies of repeated singular values, ensuring the continuous variation of the elements of U and V is not possible since at these frequencies there are multiple vectors which can be used as perfectly valid singular vectors. After determining the all-pass factors that make the singular vectors in U_{ω_k} and V_{ω_k} piecewise continuous [Lan01] high order transfer function matrices **U**(s) and **V**(s) are found by arranging u_{jk} and v_{jk}.

3. Fit a transfer function to each of the elements $v_{jk}(j\omega)$ of V, where $j = 1, \ldots, m$ and $k = 1, \ldots, n$, without restricting the transfer functions to be stable and minimum phase. Experience with fitting stable and minimum phase transfer functions will be revealed in Chapter 5. Create a transfer function matrix from all the elements $\hat{v}_{jk}$ and denote the resulting matrix by $\widehat{V}$. Note that $\widehat{V}$ may be unstable. The designer is essentially inverting the right singular vector matrix V of the plant, but this inverting should not lead to poor robustness [PG97]. The better the fit, the closer $V^*\widehat{V}$ will be to identity. The infinity norm of the difference between $\widehat{V}$ and V can be used as a measure of the success of the fit, $\|V - \widehat{V}\|_\infty < \delta$. The smaller δ is, the better the fit will be.

   It can be fairly easily shown that for a perfect fit the ratio $\frac{\kappa(V)}{\kappa(\widehat{V})} = 1$; or $\frac{\overline{\sigma}(\widehat{V})}{\underline{\sigma}(V)} = 1$.

   The designer must be aware that a highly accurate fit, however, may result in a high order of $\widehat{V}$. Figure 4.5 is a Bode plot of the product $V^*\widehat{V}$ and serves as an illustrative example of the success of the fit; it would have been preferred to have singular values aligned. Misaligned singular values in the Log Magnitude plot in Figure 4.5 indicate that the fit has not been perfect; a perfect fit may be possible if high order fitting is performed on the elements of the singular vector matrix.

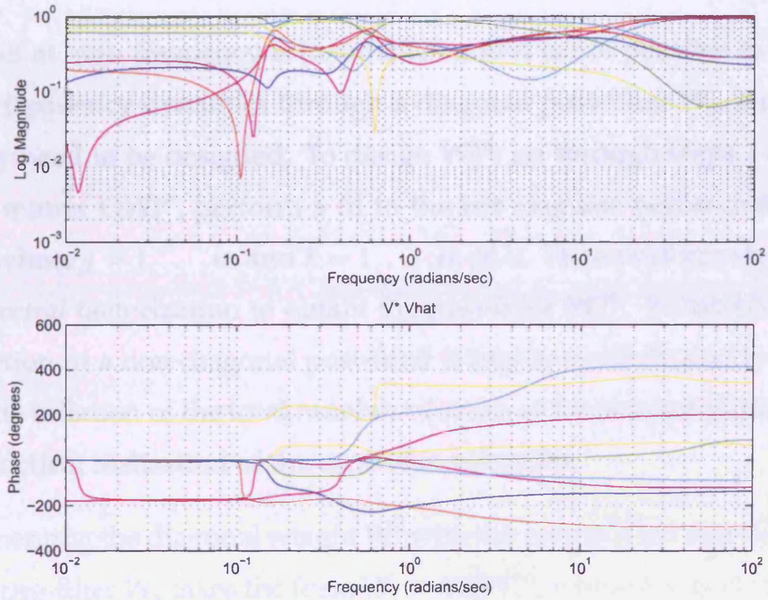

Figure 4.5: Frequency response of alignment product: $V^* \cdot \widehat{V}$

In most industrial systems a high order fit of $\widehat{V}$ will become inevitable. Therefore the designer will inevitably face the cumbersome task of selecting the most suitable model reduction algorithm to ensure the minimum impact on the structure of $\widehat{V}$. After all, it is the structure of $\widehat{V}$ that will matter in the design.

Two ways can be followed to reduce the order of $\widehat{V}$:

a) Element by element v_{jk} model order reduction, or

b) Direct reduction of the $\widehat{V}$

4. Construct a diagonal transfer function matrix $\Gamma = diag(\gamma_{11}, \gamma_{22}, \ldots, \gamma_{nn})$ (or $\Pi = diag(\pi_{11}, \pi_{22}, \ldots, \pi_{mm})$) the elements of which correspondingly emphasize the desired conditioning and the singular values of $\mathbf{W}_1^{nd}$ and ($\mathbf{W}_2^{nd}$). This allows the designer to specify closed loop performance at the input and output of the plant respectively.

5. Check if $\sigma_i(\mathbf{G}\widehat{V}\Gamma) \simeq \sigma_i\gamma_i$; the transfer function $\widehat{V}\Gamma$ does not need to be stable and minimum phase, as the *co-spectral* factorisation of $\widehat{V}\Gamma(\widehat{V}\Gamma)^{\sim}$ produces stable co-

spectral factors $\widehat{V}\Gamma(\widehat{V}\Gamma)^\sim = \mathbf{W}_1^{nd}(\mathbf{W}_1^{nd})^\sim$ where $\mathbf{W}_1^{nd}$ denotes the *co-spectral* factor, and is unit ($\mathbf{W}_1^{nd}, \mathbf{W}_1^{nd-1} \in \mathcal{RH}_\infty$), then $\sigma_i(\mathbf{G}\mathbf{W}_1^{nd}) = \sigma_i(\mathbf{G}\widehat{V}\Gamma) \simeq \sigma_i\gamma_i$. The closer the fit of $\widehat{V}$ to V the more decoupled will be the product $V^*\widehat{V}\Gamma$ which allows direct manipulation of singular values $\sigma_i(\mathbf{G})$ through the singular values of $\sigma_i(\Gamma)$.

6. If the roll off at high frequency is insufficient and it is not possible to desirably alter high frequency dynamics through a diagonal post-filter $\mathbf{W}_2$, a non-diagonal $\mathbf{W}_2^{nd}$ may need to be designed. To design $\mathbf{W}_2^{nd}$, go through steps 1 and 2 for the transfer matrix $\mathbf{G}\mathbf{W}_1^{nd}$, perform a fit to the left singular vector matrix elements $u_{jk}(j\omega)$ where $j = 1, \ldots, m$ and $k = 1, \ldots, m$ of U. Then perform step 4, this time using *spectral* factorization to obtain the post-filter $\mathbf{W}_2^{nd}$. In complex systems, a construction of a non-diagonal post-filter is highly unlikely due to its contribution to the inflation of the total number of states of the shaped plant. This would make practical realisation of the controller infeasible.

7. After augmenting the diagonal weight $\mathbf{W}_1^d$ with the constructed non-diagonal weight $\mathbf{W}_1^{nd}$ the pre-filter $\mathbf{W}_1$ takes the form $\mathbf{W}_1 = \mathbf{W}_1^d\mathbf{W}_1^{nd}$, where the post-filter takes the form $\mathbf{W}_2^{nd}\mathbf{W}_2^d$.

Augmented with diagonal and non-diagonal weights, the shaped plant will become $\mathbf{G}_s = \mathbf{W}_2^{nd}\mathbf{W}_2^d\mathbf{G}\mathbf{W}_1^d\mathbf{W}_1^{nd}$.

The *co/spectral* factorizations in steps 5 and 6 can be obtained using formulae stated in [Fra87]. These standard formulae, however, do not allow poles and zeros on the imaginary axis. The presence of imaginary axis poles and/or zeros either in the nominal plant or any of the weighting functions will lead to numerical complications. In order to circumvent this numerical difficulty it was initially assumed that $\mathbf{G}, \mathbf{G}^{-1} \in \mathcal{RL}_\infty$. It is common for the pre-filter $\mathbf{W}_1$ to contain integrators to increase low frequency gain and enhance performance. If all channels have integrators then they can be factored out of $\mathbf{W}_1^d, \mathbf{W}_2^d$ and absorbed into $\mathbf{W}_1, \mathbf{W}_2$ once $\mathbf{W}_1^{nd}$ and $\mathbf{W}_2^{nd}$ have been computed. If integrators are not placed in all channels then it is suggested that before performing the *co/spectral* factorization each integrator be approximated by a constant at frequencies lower than the dynamics of the nominal plant. Alternatively, the designer can use more elaborate but computationally demanding spectral factorization methods via Hermitian pencils [CG89] but allow for the presence of imaginary axis poles and zeros in $\mathbf{G}$ and $\mathbf{W}_1^d$. The design algorithm can be successfully applied to systems that exhibit strong directionality properties, i.e. with high condition number

($\kappa \gg 1$).

However, it is not known whether there are any pole/zero cancellations between the weights $\mathbf{W}_1$, $\mathbf{W}_2$ and the nominal plant $\mathbf{G}$ in the *LHP* which can lead to poor robust performance.

4.4.2 Algorithm of Lanzon

This section is a summary of a sub-optimal iterative algorithm proposed in [Lan01] for the design of unstructured weights $\mathbf{W}_1^{nd}$, $\mathbf{W}_2^{nd}$ such that $b_{opt}(\mathbf{G}_s)$ is maximized (γ minimized) within the context of $\mathcal{H}_\infty$ loop-shaping. Inputs to the algorithm are:

1. Appropriately scaled nominal plant $\mathbf{G}_s$.
2. Frequency functions $s_{min}(j\omega)$ and $s_{max}(j\omega)$ that define the boundaries for the low frequency performance and high frequency robustness regions, and thus confines the principle gains of the singular values of $\mathbf{G}_s$.
3. $|w_{max(i)}|$ and $|w_{min(i)}|$, that delimit the allowable region for the singular values of the loop-shaping weight $\mathbf{W}_i(j\omega)$,$(i = 1, 2)$. These can be constant or dynamic.
4. $k_i(j\omega)$ that bounds the condition number of the loop-shaping weights $\mathbf{W}_i(j\omega)$,$(i = 1, 2)$.

The algorithm aims to:

$$\textit{minimize} \quad \gamma$$

such that

1. $(\mathbf{G}_s, \mathbf{K}_\infty)$ interconnection is internally stable for $\mathbf{W}_1, \mathbf{W}_1^{-1} \in \mathcal{RH}_\infty$,$\mathbf{W}_2, \mathbf{W}_2^{-1} \in \mathcal{RH}_\infty$.
2. $\left\| \begin{bmatrix} \mathbf{K}_\infty \\ I \end{bmatrix} (I - \mathbf{G}_s\mathbf{K}_\infty)^{-1}\widetilde{\mathbf{M}}_s^{-1} \right\|_\infty \leq \gamma, \quad \gamma > \gamma_{min}.$
3. $|s_{min}(j\omega)| < \sigma_i(\mathbf{G}_s(j\omega)) < |s_{max}(j\omega)|$ *for every i* and ω.
4. $|w_{min(1)}(j\omega)| < \sigma_i(\mathbf{W}_1(j\omega)) < |w_{max(1)}(j\omega)|$ and $|w_{min(2)}(j\omega)| < \sigma_i(\mathbf{W}_2(j\omega)) < |w_{max(2)}(j\omega)|$ *for every i* and ω.

5. $\kappa(\mathbf{W}_1(j\omega)) < |k_1(j\omega)|$ and $\kappa(\mathbf{W}_2(j\omega)) < |k_2(j\omega)|$ *for every* ω.

where s_{min}, s_{max}, $w_{min(i)}$, $w_{max(i)}$ and k_i (i=1, 2) are SISO transfer functions that are sensibly selected by the design engineer to reflect the desired specifications.

After some cumbersome algebraic manipulations [Lan01] the optimization problem can be brought into a form of a *quasi-convex generalized eigenvalue* minimization problem, which can be effectively solved using the relevant solver provided in [GNLC95].

The objective of the algorithm is to maximize the robust stability margin ϵ_{max} in the presence of constraints on various static/dynamic variable structures. The maximization of the robust stability margin in this algorithm results in aligning the shaped plant's singular values at crossover frequency. Aligning of the singular values of the shaped plant is not a frequently encountered phenomenon. While this may prove effective in improving the time response in some, amongst all, controlled channels; on the other side, this forceful bring-together of the principal gains may have an adverse impact on the response characteristics of some other controlled channels. From a realistic and industrial point of view, rarely do time domain specifications translate into exactly the same (for all channels) objectives in the frequency domain. Particularly careful assessment must be conducted prior to any decision to align the singular values of an ill-conditioned plant.

The alignment resulting from the application of the LMI optimization algorithm can be avoided by removing the bounds imposed on $|\omega_{max(i)}|$, $|\omega_{min(i)}|$ and $k_i(j\omega), i = 1, 2$. This relaxes the design optimization constraints. However, the absence of a constraint on the condition number in the algorithm may lead to weighting function(s) with high condition number(s). This would result from an attempt to rectify the ill-conditioning of the plant. The use of ill-conditioned weights for ill-conditioned plants, due to performance concerns, is not advised. A result would be increased control actuator activity, which can lead to actuator saturation problems and even loss of stability.

The algorithm is an ascent algorithm, that is, the value $\epsilon_{max}(i)$ is monotonically non-decreasing with every increment (i) in the iteration, and at each iteration (i) the reciprocal of the square root of the minimum cost satisfies $\gamma\omega^2 \geq \epsilon_{max}(i-1)$ for every ω. The problem is not simultaneously convex in all variables and, convergence to a global maximum cannot be guaranteed; however, monotonicity properties can be ensured [Lan01]. Therefore the generalized eigenvalue optimization problem is caste in the form of an iterative algorithm. This approach provides insight into how non-diagonal weights can be constructed using LMI optimization in the frequency domain.

The algorithm presented in [Lan01] can be suitably manipulated by the designer towards use of diagonal weighting functions as well.

Remark 4.6 *Both of the algorithms enable the designer to get a feel for the achievable performance, and determine whether diagonal weights would be sufficient. The algorithm in [PG97] still requires a significant manipulation of the singular values mainly through the transfer function matrix Γ (and/or Π) which reflects on the relative conditioning and singular values of the weight(s). In complex plants shaping the singular values and attaining a "desired" shape will still be challenging.*

A distinctive feature of the algorithm in [Lan01] is that it reduces drastically the amount of engineering "labour" to be spent by the designer on the iterations of the weights in successfully arriving at desired weighting functions. It is assumed that the designer is acquainted with the basic principles of loop-shaping and possesses sufficient information about the plant to provide sensible bounds on the design parameters (1, 2, 3, 4) stated earlier as inputs to the algorithm. The algorithm presented in [Lan01] substitutes the designer effort with computationally expensive LMI manipulations, often arising from the complexity of the plant. This computational demand emerges as a threat to the practical feasibility of the problem and synthesized controller.

Remark 4.7 *Since both of the weight design algorithms are frequency based, a crucial stage is to ensure that the order of the singular values is uniform across frequency [PG97]. That is, the ordering of the singular values at each frequency and at zero DC gain is the same. This will consequently ensure the correct ordering of the singular vectors in U_{ω_k} and V_{ω_k} in the frequency range of interest.*

Remark 4.8 *The designer should note that both algorithms generate weighting functions which are units in $\mathcal{H}_\infty$. Therefore, any integral element must be accommodated in the diagonal weight $\boldsymbol{W}_1^d$ a-priori to produce $\boldsymbol{W}_1^{nd}$. The second iterative algorithm requires an initial controller $\boldsymbol{K}_\infty^0$ (as a starting point) such that the interconnection $(\boldsymbol{G}_s, \boldsymbol{K}_\infty)$ is internally stable. The first conclusion provides an intuitive and plausible justification to application of the algorithm on the shaped plant rather than on the nominal plant. This is simply because high gain of the frequency response at low frequencies can hardly be ensured without a (near or pure) integral element, and if it can, this will be possible only with insertion of high gain in the loop which is limited by actuator bandwidth.*

4.5 Weighting functions' impact on the open/closed loop behaviour

4.5.1 Weighting functions and the achievable open loop shape

It was shown in [MG92] that a suboptimal controller $\mathbf{K}_\infty$ that satisfies Equation 4.4 and achieves a stability margin $\epsilon \leq \epsilon_{max}$ will change the specified ("*desired*") loop shape of $\mathbf{G}_s$. However, providing that ϵ is sufficiently large, the deterioration in the loop shape at the plant input and plant output at low frequencies ($(0, \omega_l]$) is limited by:

$$\underline{\sigma}(\mathbf{L}_i) = \underline{\sigma}(\mathbf{KG}) = \underline{\sigma}(\mathbf{W}_1\mathbf{K}_\infty\mathbf{W}_2\mathbf{G}) \geq \frac{\underline{\sigma}(\mathbf{W}_2\mathbf{G}\mathbf{W}_1)\underline{\sigma}(\mathbf{K}_\infty)}{k(\mathbf{W}_1)} \tag{4.20}$$

$$\underline{\sigma}(\mathbf{L}_o) = \underline{\sigma}(\mathbf{GK}) = \underline{\sigma}(\mathbf{G}\mathbf{W}_1\mathbf{K}_\infty\mathbf{W}_2) \geq \frac{\underline{\sigma}(\mathbf{W}_2\mathbf{G}\mathbf{W}_1)\underline{\sigma}(\mathbf{K}_\infty)}{k(\mathbf{W}_2)} \tag{4.21}$$

and at high frequencies ($[\omega_h, \infty)$) by:

$$\overline{\sigma}(\mathbf{L}_i) = \overline{\sigma}(\mathbf{KG}) = \overline{\sigma}(\mathbf{W}_1\mathbf{K}_\infty\mathbf{W}_2\mathbf{G}) \leq \frac{\overline{\sigma}(\mathbf{W}_2\mathbf{G}\mathbf{W}_1)\overline{\sigma}(\mathbf{K}_\infty)}{k(\mathbf{W}_1)} \tag{4.22}$$

$$\overline{\sigma}(\mathbf{L}_o) = \overline{\sigma}(\mathbf{GK}) = \overline{\sigma}(\mathbf{G}\mathbf{W}_1\mathbf{K}_\infty\mathbf{W}_2) \leq \frac{\overline{\sigma}(\mathbf{W}_2\mathbf{G}\mathbf{W}_1)\overline{\sigma}(\mathbf{K}_\infty)}{k(\mathbf{W}_2)} \tag{4.23}$$

For example, inequalities 4.20 and 4.21 indicate that inclusion of $\mathbf{K}_\infty$ to form the actual loop shape will result in a decrease in loop gain at frequencies of high loop gain (low frequencies).

The above arguments follow from two observations: firstly, that for square plants $\mathbf{G}$, $\overline{\sigma}(\mathbf{K}_\infty)$ (and $\underline{\sigma}(\mathbf{K}_\infty)$) are explicitly bounded by functions of γ, $\overline{\sigma}(\mathbf{G}_s)$, (and $\underline{\sigma}(\mathbf{G}_s)$) [ZDG96] [p.490 and p.492], and secondly that the designer can reduce the amount of change through the weighting functions.

4.5.1.1 Behaviour of the standard closed loop objectives

Theorem 4.3 *[MG92]*

Let G be the nominal plant and let $\mathbf{K} = \mathbf{W}_1\mathbf{K}_\infty\mathbf{W}_2$ be the associated controller obtained from the loop-shaping design procedure. Then if

$$\left\| \begin{bmatrix} K_\infty \\ I \end{bmatrix} (I - G_s K_\infty)^{-1} \widetilde{M}_s^{-1} \right\|_\infty \leq \gamma \tag{4.24}$$

We have

$$\overline{\sigma}(KS_o) = \overline{\sigma}(K(I - GK)^{-1}) \leq \gamma \overline{\sigma}(\widetilde{M}_s) \overline{\sigma}(W_1) \overline{\sigma}(W_2) \tag{4.25}$$

$$\overline{\sigma}(S_o) = \overline{\sigma}((I - GK)^{-1}) \leq \min\{\gamma \overline{\sigma}(\widetilde{M}_s) k(W_2), 1 + \gamma \overline{\sigma}(N_s) k(W_2)\} \tag{4.26}$$

$$\overline{\sigma}(S_i) = \overline{\sigma}((I - KG)^{-1}) \leq \min\{\gamma \overline{\sigma}(M_s) k(W_1), 1 + \gamma \overline{\sigma}(\widetilde{N}_s) k(W_1)\} \tag{4.27}$$

$$\overline{\sigma}(T_o) = \overline{\sigma}((I - GK)^{-1}(GK)) \leq \min\{\gamma \overline{\sigma}(\widetilde{N}_s) k(W_1), 1 + \gamma \overline{\sigma}(M_s) k(W_1)\} \tag{4.28}$$

$$\overline{\sigma}((I - GK)^{-1} G) \leq \frac{\gamma \overline{\sigma}(\widetilde{N}_s)}{\underline{\sigma}(W_1) \underline{\sigma}(W_2)} \tag{4.29}$$

$$\overline{\sigma}(T_i) = \overline{\sigma}(KG(I - KG)^{-1}) \leq \min\{\gamma \overline{\sigma}(N_s) k(W_2), 1 + \gamma \overline{\sigma}(\widetilde{M}_s) k(W_2)\} \tag{4.30}$$

where $\gamma = \epsilon^{-1}$, $(\widetilde{\mathbf{N}}_s, \widetilde{\mathbf{M}}_s)$, respectively, $(\mathbf{N}_s, \mathbf{M}_s)$, is a normalized l.c.f., respectively, r.c.f., of $G_s = W_2 G W_1$, and $k(\bullet) = \frac{\overline{\sigma}(\bullet)}{\underline{\sigma}(\bullet)}$, denotes the frequency-dependent condition number of a given transfer function.

Careful attention to inequalities in Theorem 4.3 once again confirms that, it is through appropriate selection of weighting functions, that a designer can attain the design objectives.

Selection of $\mathbf{W}_1$ and $\mathbf{W}_2$ allows the designer to manipulate directly $\kappa(\mathbf{W}_1)$, $\kappa(\mathbf{W}_2)$, and indirectly $\gamma = \epsilon^{-1}, \overline{\sigma}(\widetilde{\mathbf{N}}_s) = \overline{\sigma}(\mathbf{N}_s)$ and $\overline{\sigma}(\widetilde{\mathbf{M}}_s) = \overline{\sigma}(\mathbf{M}_s)$ which are bounded.

Tighter bounds on the sensitivity and co-sensitivity operators were derived in [Vin00], but these can be conservative.

4.6 Control system design

4.6.1 Translation of time domain specifications into the frequency domain

Translation of the time domain performance requirements (specifications) into frequency domain specifications, due to the nature of individual problems, is a non-trivial task and comprises the very first step of not only the $\mathcal{H}_\infty$ loop-shaping procedure but of every frequency domain based design method. Interpretation and translation of the time domain requirements relies mostly on engineering experience and intuition and rarely on referral to a written reference manual. Rotorcraft industries have been fortunate to possess written reference manual [Ano00] to establish and describe in general language the link between time domain requirements, and their correspondence in the frequency domain. Time domain requirements usually expressed with (rise time- t_r, settling time- t_s, overshoot- M_p and steady-state -e_{ss}) can be reflected on the open/(closed) loop shapes at low and high frequencies and at the cross-over (bandwidth) frequencies, or they can be used directly as an integral part of the design as in 2 Dof controller architecture.

While for 2^{nd} order systems there are explicit formulae [FPEN02] relating time domain specifications (t_r, t_s, M_p, e_{ss}) to frequency domain objectives, for (lower/higher) order systems translations will be only approximate. Therefore, it may become necessary to validate the feasibility of the design through extensive time domain simulations and assess if the original objectives are met. If they are not, then the design process (in the $\mathcal{H}_\infty$ context) is repeated for slightly modified weights, therefore, altering the frequency domain response magnitudes.

4.6.2 Common structures of weights in $\mathcal{H}_\infty$ loop-shaping

We have seen that structures of weighting functions can vary with the complexity of the problem in hand, as well as with personal preference and experience of the designer with tools to construct such weighting functions. The following weighting structures, however, are representative of those well established and frequently used in practice. $\mathbf{W}_1$ is in the form of a simple Proportional Integral element $\frac{\alpha s+\beta}{s+\delta}$ with $\alpha, \beta, \delta \in \mathbb{R}$. In some cases $\delta \ll 1$ is used as a buffer to circumvent numerical difficulties in integration. For low frequency performance, in $\mathbf{W}_1$, the designer can also include phase-lead for reducing the roll off rates at crossover and phase-lag to increase the roll-off rates at high frequencies. In the case of a pure Proportional Integral structure, the integrator in $\mathbf{W}_1$ is also used to ensure zero steady-state, good tracking of attitude, disturbance rejection. The proportional element is used to reduce the phase lag around cross-over introduced by the integrator and to increase robust stability. This value is a trade-off between speed of response, authority on actuator usage and robustness. The post-filter $\mathbf{W}_2$ has several possible structures. It is either chosen to be a constant, to reflect the relative importance of the outputs aimed to be controlled; as a selector of measurements being fed back to the controller- mostly in 2 Dof controller architecture; or as a diagonal transfer matrix with low pass filters to desensitize the system to high frequency measurement noise. Rarely can they accommodate lead-lag filters to reduce the phase-lag at cross-over. $\mathbf{W}_1$ and $\mathbf{W}_2$ must be chosen such that the shaped plant $\mathbf{G}_s$ contains no unstable hidden modes, i.e the shaped plant is state stabilizable and state detectable. This is required to ensure internal stability of the closed loop system. Although $\mathbf{W}_1$ and $\mathbf{W}_2$ do not have to be necessarily diagonal, having diagonal weights usually seems sufficient. An algorithm for construction of unstructured weights has been proposed in [PG97] (and covered in section 4.4.1).

4.6.3 Procedure

After a preliminary inspection of the frequency response of the nominal plant, the designer will be required to reshape the nominal plant's singular values by introducing pre/post weighting functions. This is done in accordance with the requirements imposed on the nominal plant; to acquire a desired frequency response shape that will capture the nominal performance objectives (disturbance rejection, tracking, input/output decoupling); and to reflect on the actuator authority, noise rejection and (to some extent) robust stability properties of the control system design.

Prior to the weight selection in loop-shaping some preliminary steps may need to be performed; for example, scaling, diagonalizing or decoupling of the system. A particular emphasis must be given to scaling. Proper scaling (as outlined in [SP96], p.5- p.6; [Hyd95], p.39) can make model analysis, controller design and even weight selection easier.

4.7 Controller architecture

This section will present, various degrees of freedom controller architectures that will find use in the controller designs presented in Chapter 5.

4.7.1 One Degree-of-freedom controller

Figure 4.6 illustrates a 1 Dof $\mathcal{H}_\infty$ loop-shaping controller architecture.

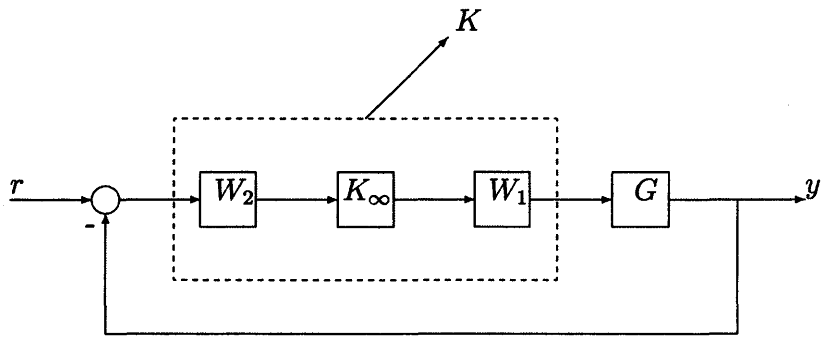

Figure 4.6: Unity Feedback for Loop-shaping

An outline of the $\mathcal{H}_\infty$ LSDP was given earlier (in Section 4.2), but more detailed presentation can be found in several references but in particular in [MG90], [Hyd95] and [SP96].

Design procedure:

1) The nominal plant **G** is augmented with pre and post (weighting functions) $\mathbf{W}_1$ and $\mathbf{W}_2$ so that the weighted ("*shaped*") plant has the open loop shape which will meet the specified closed loop performance/robustness objectives. These will normally mean high gain at low frequency, roll-off rates of approximately 20 dB/dec (a slope of -1) at the desired bandwidth, and high frequency roll-off. For example ensuring a cross-over roll-off close to 20 dB/dec corresponds to 90 degrees phase, which will ensure good phase margin. In practice, the maximum rate of transition from low frequency to high frequency regions (also named as roll-off rate) is 40 dB/dec, however 20 dB/dec is the preferable rate. Higher roll-off rates, introduce second (or higher) order integrators, and improve the disturbance rejection- and conditioning- at low frequency, however, this is at the expense of increased phase lag, reduced phase margin, and increased oscillatory behaviour of the (time) response.

The selection of the weights is not straightforward, designers usually rely on past experience and intuition provided by classical loop-shaping concepts. This procedure involves some trial and error, there is not any systematic and scientific way yet of doing this. The designer may use the traditional manual design of $\mathbf{W}_1$, $\mathbf{W}_2$ or one of the methods available presented earlier in this chapter. In [GPGC] an expert system was developed for selecting a pre-compensator $\mathbf{W}_1$, by translating time domain response requirements into the frequency domain. Although the proposed procedure eases the process of weight selection, in fact it still does not make the designer intervention void, and requires further tuning by the designer.

A schematic representation of the shaped plant and the $\mathbf{K}_\infty$ controllers is shown in Figure 4.7.

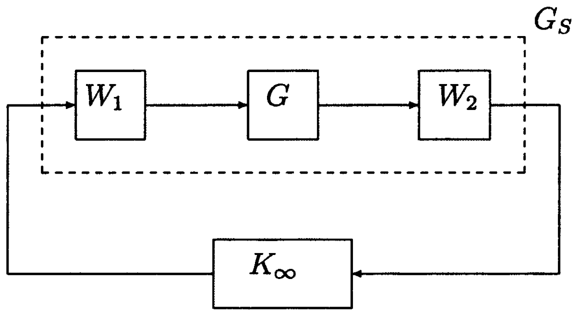

Figure 4.7: Shaped Plant $\mathbf{G}_s$ in the Loop-shaping approach

2) To synthesize a robustly stabilizing $\mathcal{H}_\infty$ LS controller ($\mathbf{K}_\infty$) the design engineer can use the command `ncfsyn.m` in μ Analysis and Synthesis Toolbox. The final controller $\mathbf{K}$ that will be implemented on the real system is constructed by combining the $\mathcal{H}_\infty$ controller $\mathbf{K}_\infty$ with the pre/post-filters chosen in the first step of LSDP. As a result, the final controller takes the form $\mathbf{K} = \mathbf{W}_1\mathbf{K}_\infty\mathbf{W}_2$, which is schematically shown in the Figure 4.8. However, as we will see in Section 4.8 the structure of the controller that will finally be implemented on the system will be rather different.

The controller $\mathbf{K} = \mathbf{W}_2\mathbf{K}_\infty\mathbf{W}_1$ will take care of both nominal performance and stability robustness. Although it can accommodate plants with more outputs than inputs, it does not possess the architecture to facilitate fully the efficient use of more measurements than those actively controlled ones. An advantageous property that the 2 Dof controller architecture possesses.

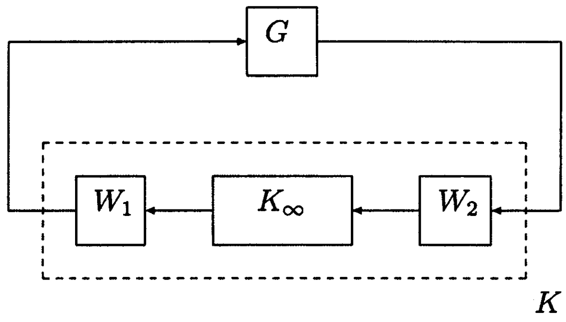

Figure 4.8: Final Controller

4.7.2 Two Degree-of-freedom controller

Although $\mathcal{H}_\infty$ is a frequency domain based design method a specific (controller) architecture namely two Degree-of-freedom-(Dof) controller architecture allows time domain specifications and frequency domain (robust) performance tracking to be successfully combined and integrated in the synthesis of a robustly stabilizing controller.

Improved performance for systems may be obtained by implementing a 2 Dof controller architecture. The research of [YBJ85] on the two Degree-of-Freedom parametrization theory initiated a stream of further research extending the use of 2 Dof controller architectures in $\mathcal{H}_\infty$ optimization. The design framework was successfully employed in the design of $\mathcal{H}_\infty$ loop-shaping controllers in [HHL91] with further investigations carried out in [LKP93]. The most distinguished feature of this combined controller design framework is that: in addition to robustness of stability, it also provides guarantees of closed loop robust tracking performance with respect to an ideal reference model $\mathbf{T}_{ref}$. Figure 4.9 illustrates a 2 Dof controller architecture which interlinks several components; the model of the system (**G**) in its *coprime* factors for which the controller is going to be designed; a reference (or ideal model) $\mathbf{T}_{ref}$ which embeds desired (ideal) time domain specifications, and a controller **K** which comprises two controllers: $\mathbf{K}_1$, for model matching, and $\mathbf{K}_2 \equiv \mathbf{K}_\infty$ for robust stability requirements.

The 2 Dof $\mathcal{H}_\infty$ controller **K** can be synthesized in two different ways: in one single step, or in two separate steps [LKP93]. In this thesis all 2 Dof controllers are synthesised in a single step. The single step approach offers two distinct advantages among many, when compared to the two step approach. The algorithm is easier to use and the resulting controller is of lower order. The second advantage comes as a result that both $\mathbf{K}_1$ and $\mathbf{K}_2$ controllers share the same state-space which, in the sub-optimal

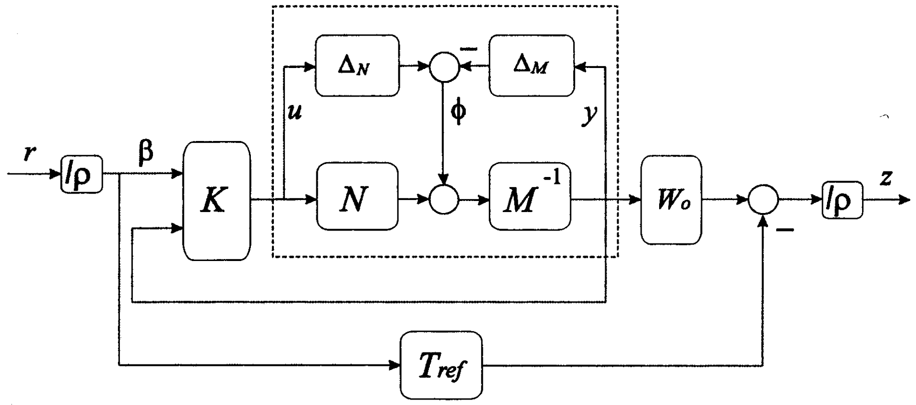

Figure 4.9: Two Degree-of-freedom design architecture

case, has the dimension of the generalized plant. No additional states are introduced by the pre-filter $\mathbf{K}_1$ compensator. However, its robust stability and robust tracking performance properties may not be as good as in the two step approach. The state estimator part of the controller is a Kalman filter, because the $\mathcal{H}_\infty$ filter *Riccati* equation has a zero solution [HHL91]. The resulting controller $\mathbf{K}$ has a partitioned structure $\mathbf{K} = \begin{bmatrix} \mathbf{K}_1 & \mathbf{K}_2 \end{bmatrix}$ where $\mathbf{K}_2$ is the feedback controller designed to guarantee robust stability and disturbance rejection specifications, while the pre-filter $\mathbf{K}_1$ compensator is to meet performance specifications and, at the same time, to ensure that the robust model matching inequality in Equation 4.31

$$\left\|(I - \mathbf{G}_s\mathbf{K}_2)^{-1}\mathbf{G}_s\mathbf{K}_1 - \mathbf{T}_{ref}\right\|_\infty \leq \gamma\rho^{-2} \tag{4.31}$$

is satisfied. Here ρ is a positive scalar model matching parameter accommodated in the input and output of the 2 Dof feedback configuration. Its value can be set by the designer, usually in the range $1 \leq \rho \leq 3$. It can be deduced from Equation 4.31 that higher values of ρ, hence smaller $\mathcal{H}_\infty$ norms, will make $\mathbf{T}_{r\to y}$ approximate $\mathbf{T}_{ref}$ thus placing more emphasis on robust model matching. This, however, will be at the expense of decreased robustness to uncertainties in the system and perturbations. Setting $\rho = 0$ reduces the 2 Dof problem to a 1 Degree-of-freedom controller architecture-normalized *coprime* factor robust stabilization problem.

Time domain specifications dictated on each channel can be diagonal and integrated into the controller design procedure by the designer through a transfer function matrix $\mathbf{T}_{ref} \in \mathcal{RH}_\infty$ chosen to have the time response characteristics of the model that would lead to desired design objectives. $\mathbf{T}_{ref}$ may, for example, include first or second order lag transfer functions correspondingly defined as $\frac{\alpha}{s+\beta}$ and $\frac{\omega_n^2}{s^2+2\zeta\omega_n+\omega_n^2}$; $\omega_n \in \mathbb{R}$

corresponds to undamped natural frequency, $0 \leq \zeta \leq 1$ is damping coefficient and $\alpha, \beta \in \mathbb{R}$. First order lag transfer functions are used when slower response is required. The flexibility that allows time domain requirements to be integrated in the design emerges as an additional (in this case second) degree-of-freedom in addition to the the degree of freedom in the conventional (1 Dof) $\mathcal{H}_\infty$ LSDP setup.

A 2 Dof controller architecture application does not necessarily need to make use of a reference model. An alternative configuration that does not make use of a reference model was presented in [IU00].

However, there is more in the 2 Dof controller architecture that really makes it favourable to its 1 Dof counterpart. It does not only allow the designer to integrate time domain requirements into the ideal model to be matched, but it also allows, by defining suitable constant quadratic performance index, denoted by W_o, to emphasise the relative importance of the measurements. While the controller architecture allows extra measurements to be effectively used in the synthesis of the controller $\mathbf{K}_2$, the output selection matrix will utilize only those output measurements which are to be controlled and included in the synthesis of the pre-filter $\mathbf{K}_1$ compensator. This manipulation exploits the availability of extra measurements which is more frequently encountered in industrial applications where the designer, for a variety of reasons, may need to include in the controller synthesis only those outputs of interest to be controlled. However it should be known that as the integral action can not be applied to more channels than the number of inputs, zero steady-state error can not be guaranteed in all loops. The approach of defining a performance index is also noted in the control literature as *soft* control [GGS00]. We will endeavour to cover more features (points) of 2 Dof $\mathcal{H}_\infty$ loop-shaping in the diagonal weight design procedure presented in Chapter 5. For more in-depth discussions, design analysis and references on 2 Dof controller architecture the reader is referred to [LKP93], [SP96], [GL95], [PG02].

Design procedure:

In the following we present an outline of the general 2 Dof one step controller design procedure. Since it is built on $\mathcal{H}_\infty$ loop-shaping ideas it should come as no surprise to the reader that some of the steps are identical to the 1 Dof controller design procedure.

For a detailed account on the mathematics behind the procedure the reader can consult [LKP93] and for a more practical oriented exposition [HHL91] and [SP96].

The procedure includes the following steps:

1) Shape the nominal plant frequency response by pre and post (if necessary) filters, and obtain the shaped transfer function $\mathbf{G}_s = \mathbf{W}_2\mathbf{G}\mathbf{W}_1 = \widetilde{\mathbf{M}}_s^{-1}\widetilde{\mathbf{N}}_s$. This is done in line with the instructions in Section 4.7.1. When the loop-shaping controller is to be implemented in the observer form [Vin00], the weights should be selected such that the bandwidth/(s) of $\widetilde{\mathbf{N}}_s$ is/(are not smaller than the bandwidth/(s) of $\mathbf{T}_{ref}$, because this will lead to poor robust performance. Make sure the stability margin is sufficiently large, this will ensure that $\mathbf{K}_2 = \mathbf{K}_\infty$ will be robustly stabilising.

   Where γ_{min} or ϵ_{max} is an indicator of robustness of the shaped plant to perturbations $\Delta_{\widetilde{M}}$ and $\Delta_{\widetilde{N}} \in \mathcal{RH}_\infty$ to the normalized *coprime* factors of the shaped plant such that: $\left\| \begin{bmatrix} \Delta_{\widetilde{M}} & \Delta_{\widetilde{N}} \end{bmatrix} \right\|_\infty < \epsilon$. Here $\Delta_{\widetilde{M}}$ and $\Delta_{\widetilde{N}}$ can be considered as low and high frequency perturbations to the output $\mathbf{G}_s\mathbf{K}_\infty$ and input $\mathbf{K}_\infty\mathbf{G}_s$ loop transfer matrices.

2) To enforce nominal and robust tracking requirements create an *"ideal"* reference model $\mathbf{T}_{ref}$ defined as a diagonal transfer matrix, $diag(T^{11}_{ref}, T^{22}_{ref}, \ldots, T^{mn}_{ref})$ to emphasize good output decoupling. The ideal but realistic transfer function which is usually formed of first $\frac{\alpha}{s+\beta}$ or second order lags $\frac{\omega_n^2}{s^2+2\zeta\omega_n^2+\omega_n^2}$ with $\alpha, \beta, \omega_n, \zeta \in \mathbb{R}$ and the speed of the response defined by $t_r = \frac{1.8}{\omega_n}$ for second order systems must not be too fast; an unrealistic speed of response will lead to excessive control signals and actuator activity, which will at some stage lead to poor robust stability.

3) Obtain an $\mathcal{H}_\infty$ loop-shaping controller $\mathbf{K}_\infty$ and choose its position (see next section for details). If necessary, reduce the order of the controller, and design a command pre-filter.

4) Select a scaling matrix W_o in view of variables to be controlled.

5) Select an appropriate scaling factor ρ (from the practical sensible range $1 \leq \rho \leq 3$). The scaling is performed through the stability margin ($\epsilon^{-1} = \gamma$) Equation 4.31. An alternative scaling, which may prove useful in some applications, can be performed through the time domain reference model $\mathbf{T}_{ref}$ [HHL91] [6].

6) Synthesise a sub-optimal controller $\mathbf{K}$ using the one step design. A `Matlab`® source code to synthesise a 2 Dof $\mathcal{H}_\infty$ controller can be found in [SP96] [p.389].

7) Partition the resulting controller $\mathbf{K}$ into $\mathbf{K}_1$ and $\mathbf{K}_2$ such that $\mathbf{K} = \begin{bmatrix} \mathbf{K}_1 & \mathbf{K}_2 \end{bmatrix}$.

[6] In this thesis scaling will be performed on the frequency domain.

If necessary reduce the order of $\mathbf{K}_\infty$, however this may affect the robustness properties of the closed loop $\mathbf{T}_{\beta\rightarrow y}$.

8) The pre-filter $\mathbf{K}_1$ can be scaled by a constant matrix S, as $\mathbf{K}_1 = \mathbf{K}S$, so that $\mathbf{T}_{r\rightarrow y}(j0) = \mathbf{T}_{ref}(j0) = I$. The constant matrix S evaluated at $\omega = 0$ is $S := \mathbf{T}^{-1}_{r\rightarrow y}(j0)\mathbf{T}_{ref}(j0)$. This will improve model matching over a broader range of the frequency domain, since $\mathcal{H}_\infty$ optimization tends to give $\mathbf{T}_{r\rightarrow y}$ the same frequency response magnitude shape as $\mathbf{T}_{ref}$. The order of the generated controller is bounded: $\partial(\mathbf{K}) \leq \partial(\mathbf{G}) + \partial(\mathbf{W}_1) + \partial(W_2) + \partial(\mathbf{T}_{ref})$, where $\partial(\star)$ denotes the order of the given transfer function. It can be seen that the order of the final controller differs from its 1 Dof counterpart by only $\partial(\mathbf{T}_{ref})$.

9) The controller must be evaluated in terms of robust stability and robust performance characteristics. Evaluate the time and frequency responses of relevant closed loop transfer functions to assess the robustness and performance properties of the designed controller. Depending on the nature of the violated closed loop properties, the designer may need to go back to Step 1 or Step 2 of the procedure.

10) Depending on the control strategy, the synthesized controller $\mathbf{K}$ can be implemented in three different ways: correspondingly in the feedback part of the loop, in the forward part of the loop, or in the observer form of $\mathbf{G}_s$ with the state feedback [A.91], [Vin00].

The 2 Dof design problem in Figure 4.9 is to find a controller $\mathbf{K}$ for the shaped plant $\mathbf{G}_s$ which will internally and robustly stabilise the closed loop, and will also ensure a level of robust performance in model matching context. All of these objectives are embedded in the minimization of the $\mathcal{H}_\infty$ norm of the mapping $\begin{bmatrix} r^T & \phi^T \end{bmatrix}^T \rightarrow \begin{bmatrix} u^T & y^T & z^T \end{bmatrix}^T$.

Consider this mapping as $\begin{bmatrix} \mathbf{P}_{11} & \mathbf{P}_{12} \\ \mathbf{P}_{21} & \mathbf{P}_{22} \end{bmatrix}$ then the elements and their interpretation in the design are as following:

$\mathbf{P}_{11} = \rho \begin{bmatrix} (I - \mathbf{K}_2\mathbf{G})^{-1}\mathbf{K}_1 \\ (I - \mathbf{G}\mathbf{K}_2)^{-1}\mathbf{G}\mathbf{K}_1 \end{bmatrix}$ - establishing authority on the actuator activity.

$\mathbf{P}_{12} = \begin{bmatrix} \mathbf{K}_2 \\ I \end{bmatrix} (I - \mathbf{G}\mathbf{K}_2)^{-1}\mathbf{M}^{-1}$ - associated with normalized *coprime* factor robust stability optimization.

$\mathbf{P}_{21} = \rho^2\left((I - \mathbf{G}\mathbf{K}_2)^{-1}\mathbf{G}\mathbf{K}_1 - \mathbf{T}_{ref}\right)$ - associated with closed loop desired model matching.

$\mathbf{P}_{22} = \rho\,(I - \mathbf{G}\mathbf{K}_2)^{-1}\,\mathbf{M}^{-1}$ - associated with robust stabilization.

The scaling factor ρ is introduced with the aim of emphasizing the model matching part of the problem (hence ρ^2 in element $\mathbf{P}_{21}$), at the expense of reduced robustness (elements $\mathbf{P}_{11}$ and $\mathbf{P}_{22}$).

The aims of the procedure, as the name suggests, are two fold:

- Robust stability- to ensure a satisfactory stability margin ϵ

- Robust performance in a tracking sense-by satisfying a bound on $\|\mathbf{T}_{r\to y} - \mathbf{T}_{ref}\|_\infty$.

The optimization problem in inequality 4.31 will force the closed loop (which is the operator on the left hand of the minus sign) to match the ideal model.

Remark 4.9 *In its standard form, the 2 Dof $\mathcal{H}_\infty$ loop-shaping controller architecture does not explicitly provide guaranteed robustness in the time domain. It does guarantee nominal tracking. Experience shows that if $\mathbf{T}_{ref}$ is selected reasonably then robust performance can also be expected. As a way to rectify this disadvantage of only expecting that robust performance will be met [PG02] introduced a procedure, which based on the standard 2 Dof $\mathcal{H}_\infty$ loop-shaping set-up, exploits μ-synthesis and ν-gap techniques with a robust stability constraint included to ensure that time domain specifications are also met accurately and robustly.*

4.8 Controller positioning in the loop and implementation

So far we have presented two algorithms, namely 1 Dof and 2 Dof, for the design and synthesis of controllers via the $\mathcal{H}_\infty$ loop-shaping method. Once a controller achieving the lowest possible infinity norm on the set of combined closed loop transfer functions has been synthesized, attention must be given to evaluation of the controller characteristics. This is done via extensive desk top simulations run on a representative mathematical model of the system. This is followed by implementation on a real test-bed or the actual system.

Although the necessary requirements on the various open/closed loop transfer functions are met and guarantee the existence of a controller, the implementation stage is yet to unveil the practical feasibility and functionality of this controller. Human factors play a critical and crucial role in interfacing the engineering requirements with the mathematical framework of the optimization process.

There are several ways of feeding the references into the loop and appropriately locating the controller in the loop. Three of the most commonly encountered controller positioning configurations in industrial applications are: *forward* path, *feedback* path, and in the *observer* form. For completeness and establishing a base for comparisons all three will be presented, however, implementations were based on one of them only.

The one regarded as conventional in a control sense is the unity feedback as depicted in Figure 4.10, where the controller is placed in the *forward* path of the loop.

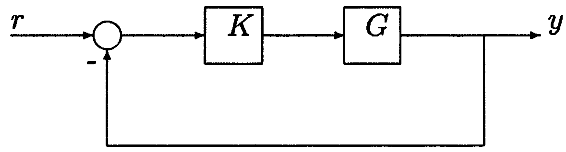

Figure 4.10: Unity Feedback implementation of K

For the standard $\mathcal{H}_\infty$ 1 Dof controller design set-up, if $\mathbf{K}_\infty$ has an integrator in its dynamics, this is the only place the controller can be located. Implementation of unity feedback leads to faster response, however, at the expense of large amount of overshoot (M_p) as the references directly excite the dynamics of $\mathbf{K}_\infty$ controller.

Figure 4.11 also illustrates a unity feedback set-up but, for a $\mathcal{H}_\infty$ loop-shaping design. A distinction, from the standard unity feedback configuration is that it offers more flexibility by allowing the loop-shaping weighting functions to be kept separate from the $\mathbf{K}_\infty$ controller.

The plant-controller feedback configuration can also be arranged such that the controller $\mathbf{K} = \mathbf{W}_1\mathbf{K}_\infty\mathbf{W}_2$ is located in the feedback loop as depicted in Figure 4.8. This type of set up will allow $\mathbf{W}_1$ and $\mathbf{W}_2$ to accommodate poles and zeros on the imaginary axis [MG92]. Positioning of the weighting functions in the feedback loop will also facilitate circumventing possible numerical problems. However, a controller in the feedback loop will (generally) lead to a slower and more damped response.

An alternative *feedback* path arrangement as shown in Figure 4.12 allows the designer to integrate weighting functions and $\mathbf{K}_\infty$ controller in different loops. Integral action

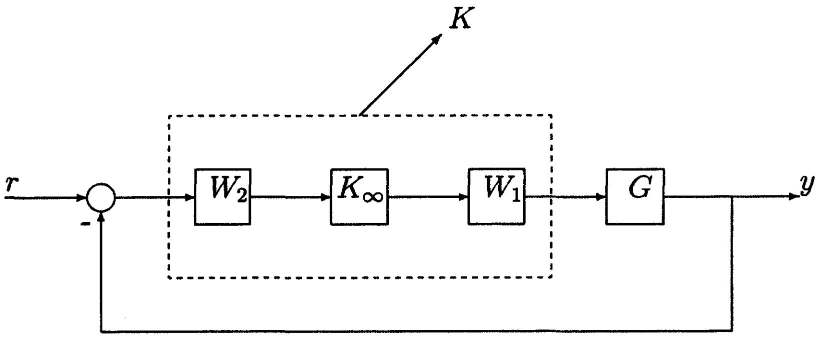

Figure 4.11: Unity Feedback for Loop Shaping

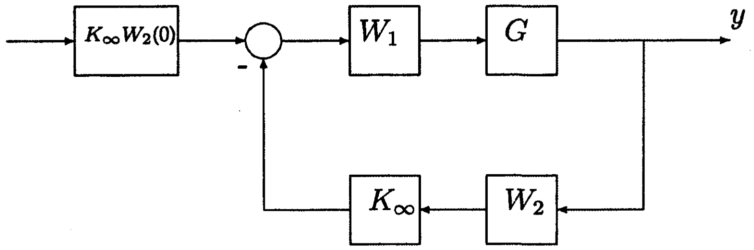

Figure 4.12: A practical implementation of the loop-shaping controller

will be accommodated in $\mathbf{W}_1$, so the steady-state error will be zero as required[7]. The constant (static) pre-filter $\mathbf{K}_\infty(0)\mathbf{W}_2(0)$, where $\mathbf{K}_\infty(0)\mathbf{W}_2(0) = \lim_{s\to 0}\mathbf{K}_\infty(s)\mathbf{W}_2(s)$, ensures steady-state gain of 1 between the reference commands r and measurement outputs y. The main motivation behind the use of this particular structure in implementing our controllers is that it is not (or it is less) prone to produce large amount of overshoots- described also as classical derivative kick- as the set of reference commands will not directly excite the dynamics of $\mathbf{K}_\infty$. We are assuming $\mathbf{W}_2$ is constant (not dynamic), which in most cases is true.

In general, $\mathcal{H}_\infty$ controllers cannot be written as an exact plant state observer and state feedback since there will be a worst disturbance term entering the observer state equation [DGKF89]. However, this is not the case in $\mathcal{H}_\infty$ loop-shaping. In [SG90] it was shown that the $\mathcal{H}_\infty$ loop-shaping controller can be partitioned as an exact plant observer with state feedback:

$$\begin{aligned}\dot{\hat{x}} &= A\hat{x} + H(C\hat{x} - y) + Bu \\ u &= F\hat{x}\end{aligned} \tag{4.32}$$

where (A, B, C) is a state-space realization of the weighted plant $\mathbf{G}_s$; $H = -ZC^*$ and

[7]This may not be always the case for systems with number of outputs higher than the number of inputs.

$F = B^*\gamma^2(I + XZ - \gamma^2 I)^{-1}X$, where $X > 0$ and $Z > 0$ are unique solutions to *GCARE* in Equation 4.8 and *GFARE* in Equation 4.9 respectively.

It must be noted that the observer based structure is with respect to the shaped plant $\mathbf{G}_s$, and not $\mathbf{G}$. In this configuration, references enter the loop at an unconventional place [Hyd95] compared to the *feedback* loop and *forward* loop controller positioning. But common to both the *observer* based and the $\mathcal{H}_\infty$ loop-shaping type *feedback* path configuration is that, due to the positioning of $\mathbf{K}_\infty$, neither of them is prone to produce overshoot to step responses.

An $\mathcal{H}_\infty$ loop-shaping observer based controller has a structure that is technically suitable to gain scheduling, where gains in F and H can be scheduled as a function of appropriate variables. It has also been shown that it can guarantee robust performance [PG99].

It is shown in [Vin00] that the observer based structure of the $\mathcal{H}_\infty$ loop-shaping controller can produce a closed loop which is equal to $\widetilde{\mathbf{N}}$, that is $\mathbf{T}_{r \to y} = \widetilde{\mathbf{N}}$. Given the frequency domain magnitude dynamics of $\widetilde{\mathbf{N}}$, (near) unity at low frequency and rolling off at high frequency, the plant-controller system's time domain response properties will be very good.

Remark 4.10 *When the controller is implemented in the observer form the nominal tracking problem can be decoupled from the disturbance rejection problem.*

4.9 Real implementation of the controller

It is customary that prior to real implementation all the controllers are discretised. Whilst there are several methods such as Zero Order Hold, Triangle Approximation, Tustin approximation etc. of carrying out the discretisation, in our problem this was done by using Tustin's algorithm (or bilinear transformation) ($s \leftarrow \frac{2}{T}\frac{z-1}{z+1}$)- see the `c2d` command in the μ Analysis and Synthesis Toolbox. This maps the left half (stable region) of the s-plane exactly into the stable region of the z-plane (unit circle). Interestingly, the entire $j\omega$ axis of the s-plane is compressed into the 2π-length of the unit circle. The sampling rate was 64 Hz. In view of the limitations imposed by the on-board C compiler, and concerns for deteriorated responses due to lack of decimal numerical accuracy, state-space realizations representing the dynamics of the controller were truncated to between five and eight decimal places, see [PPT+05]. Once truncated the state-space realizations of the controllers have been incorporated into a C programming language code which had to be compiled on a *VAX* machine to produce a code which would "*communicate*" with the on-board *Bell 205* computer. For safety precautions prior to flight the controller was subjected to ground testing by having it implemented on a *NASA* model built in the *Bell 205* flight computer system which operates using floating point arithmetic. This procedure would allow any software (code) related issues to be addressed, and also, give a feel to the pilots of the stiffness of the cyclic sticks and activity of the actuators prior to flight.

Experience from numerous flight tests have brought to our attention a limitation which is important to underline; the computational power of the on-board computer imposed an upper bound on the size of the implementable control algorithms. A 30-state controller has been accommodated and flight tested successfully [PPT+05].

4.10 Challenges in control systems design

4.10.1 Ill-conditioning and control

Earlier in Chapter 2 we have stated that whenever the plant's transfer function is evaluated at a frequency of interest and has high condition number $\kappa(\bullet) \gg 1$ it is said to be ill-conditioned. Ill-conditioned systems can be encountered in many fields of science and engineering but mostly in chemical process control [SM34]. It is widely known that the control of ill-conditioned plants is generally difficult and problematic due to the presence of uncertainty [SMD88], [SM34]. In [Fre90] multivariable loop-shaping is examined for ill-conditioned plants, providing conditions and guidelines to shape the singular values at one break point and to achieve properties both at the plant input and output.

From a control perspective ill-conditioning at a certain frequency indicates that the gain of the plant exhibits strong dependence on the direction of the input vector $u(\mathrm{t})$; therefore some input signals will be amplified with much greater gain than others. This also characterizes a property unique for MIMO systems namely *directionality*, where the inputs in the directions corresponding to high plant gains are strongly amplified by the plant, while the inputs in the directions corresponding to low plant gains are not. For $\mathbf{G} \in \mathbb{R}^{m \times n}$, inputs in the direction corresponding to high plant gain are those input vectors $u(\mathrm{t})$ that align with the right singular vectors $v_j, (j = 1, \cdots, n)$, that are scaled by the maximum singular value $\overline{\sigma}$. Similarly, inputs in the direction corresponding to smallest plant gain are those input vectors that align with the right singular vector v_n scaled by the minimum singular value $\underline{\sigma}$. An input vector $u(t)$ is said to be aligned with v_i if and only if the pair satisfies the following condition:

$$acos\left\{\frac{<u|v_i>}{\|u\|_2\|v_i\|_2}\right\} = 0 \tag{4.33}$$

which states that the $\angle(u(t), v_i) = 0°$. Singular value analysis represents an important tool for characterizing robustness of control systems. The singular value decomposition has been commonly used in process control to effectively design controllers to eliminate directionality of the process, or to achieve a trade-off between the nominal performance and its sensitivity to the model uncertainty [BD92] and disturbance directionality. To compensate for the strong directionality present in ill-conditioned plants, the controller must apply large input signals in the directions where the plant gain is low, this leads to a controller similar to $\mathbf{K} = \mathbf{G}^{-1}$, where $\mathbf{G}$ is the plant. However, due to uncertainty, the direction of the large input may not exactly correspond to the direction in which plant gain is low. This characteristic may first cause an excessive amplification in the output signals which are already scaled by large singular values, and then result in large values of controlled variables, quite possibly giving rise to poor performance or even instability. To rectify this in an ill-conditioned plant a pre-filter (consider a weighting function $\mathbf{W}_1$) can be designed to ensure that all signals are amplified in the same way (or in view of the needs). Since a dynamic weighting function performs a spatial rotation of a given input/s signal, this can be accomplished by redirecting the input signal vectors of primary concern in the directions of high plant gain, and those of secondary concern in the directions corresponding to the low plant gain. Alternatively one can reduce directionality by reducing the condition number (κ) of $\mathbf{G}_s$. The directionality property of inputs (references, uncertainty, disturbance) and their stochastic nature make it extremely hard to estimate their direction. In this case, the second approach makes more sense in practice. This, once again, only reinforces the importance of a weighting function as a tool to tackle ill-conditioning at given frequencies. However, this adjustment of the $\kappa(\mathbf{G}_s)$ has to be done by closely monitoring the impact it will have on robustness and nominal performance indicators- see inequalities in Theorem 4.3.

4.10.2 Model reduction

Irrespective of the advances being continuously made in expanding the computational power of the controlling units- computers; simple, low order linear controllers are usually preferred over their complex, high order counterparts. Central behind this motivation is the relatively reduced demand in computations of the controller, and from the software and hardware perspectives less things that can go wrong, and purely from the software point of view there will be fewer bugs to fix, i.e. verification and validation of software will be easier. There are several model reduction techniques available in the control literature each of which has its preferable areas of application. In the course of the controller design we will familiarize the reader only with those techniques that we have found useful.

$\mathcal{H}_\infty$ control theory is a powerful tool for the design of robust controllers for uncertain, complex, multivariable systems. However, it is foreseeable that this powerful tool, so to say, will have its own disadvantages in embracing all the qualities as a controller design tool. It is typical that controllers designed with this methodology will have orders comparable to those of the plants which the design has been based on. While properties guaranteeing closed loop stability, and performance are a *"must"* for a controller to be considered for implementation on the real system, feasibility of the controller in the implementation phase does strongly depend on its order. This underlines the order of the resulting controller as a constraint which may need to be integrated into the controller synthesis procedure.

Chapter 5

Flight control law design for Bell 205

This chapter presents the design (analysis and synthesis) of various $\mathcal{H}_\infty$ loop-shaping control laws for a multi-purpose variable stability teetering *Bell 205* helicopter in the low speed region (up to 45 *knots*). These control laws utilize both the diagonal and non-diagonal weighting functions in the process of attaining the desired shaped plant ($\mathbf{G}_s$) frequency response. Design stages are complemented with relevant performance and robustness assessment indicators; the challenges encountered with different controller architectures, weight selection and construction techniques are discussed, and some approaches for their remedies are suggested.

5.1 Introduction

The theory presented in the previous chapters underlined the importance of $\mathcal{H}_\infty$ robust control as a design tool amongst many others available. In this chapter our aims are several: to study the effect of the weighting functions in the process of the design of various degrees of freedom $\mathcal{H}_\infty$ loop-shaping controllers; to utilize the frequency domain robustness and performance analysis indicators in the design stages; and, to assess the synthesised control laws on the *Bell 205* multipurpose, variable stability FbW helicopter.

The application of $\mathcal{H}_\infty$ loop-shaping to the design of flight control laws for the *Bell 205* is a continuation of several years research. The designs presented herein cover most, if not all, of the topics the reader was familiarized with in the preceding chapters of this thesis.

5.2 Helicopter aeromechanic model

The control object in this research is the *Bell 205* helicopter based at National Research Council of Canada's Institute for Aerospace Research; a profile view of the helicopter is shown in Figure 5.1. The *Bell 205* is an extensively modified version of *Bell 205 A1*.

Figure 5.1: The NRC Bell 205 research helicopter

The *Bell 205* has a full authority, fly-by-wire instrumented Flight Control System (FCS), with a single-turbine, two-blade teetering[1] rotor and an anti-torque tail rotor. There are several components that exhibit flexibility, but principally these effects arise from the blades and the tail boom. Flexible modes can in general be distinguished (on the complex plane) by possession of very lightly damped characteristic eigenvalues, and in the frequency domain by sharp peaks or spikes. The teetering rotor helicopter is a low bandwidth, modernised over the years, highly nonlinear aero-mechanical structure, with high cross-axis couplings and significant time delays. The time delays are mainly introduced by the dynamics of the teetering rotor system and the fuselage, which is pendulously suspended below the rotor.

The helicopter with such characteristics represents a challenging problem to any control system design method. Most of the helicopters, due to their asymmetric aerodynamics, are unstable in hover flying conditions and, thus, require high pilot workload in order to reduce couplings while performing various Mission Task Elements. Reduced workload will allow the pilot to give more attention to tasks that are secondary and which can become primary at any moment during the flight.

The mathematical model (*nrcbemfinal.mat*), a representation of the NRC *Bell 205* fly-by-wire research helicopter, was built and improved by *QinetiQ*, Bedford (United King-

[1]Teetering rotor helicopters are characterised by low roll damping, and it is in this type of helicopters where bandwidth reduction due to presence of time delay is much less significant.

dom) using the highly flexible Matlab®/Simulink system modelling and analysis environment. The model includes numerous graphical block diagrams, s-functions and is complemented by several custom build Matlab® (*mat*) files.

Some characteristics of the helicopters aeromechanical structure follow [Hc01]:

- **The main rotor**: is of the blade element type configured using two blades to approximate the two-blade teetering rotor configuration found on the real aircraft. The blades are assumed rigid and are free to move in the flap direction only. Thus no twist, lead-lag or elastic motion is included. The blades are assumed to be hinged at the centre of the hub and it is thought that this gives an adequate approximation to the blade retention system used on the real-aircraft. Blade section aerodynamics are modelled using lookup tables of data gathered in wind tunnel tests on a NACA 0012 section. Trigonometric functions are used to approximate regions outside the range of incidences measured in the wind tunnel. Pitching moment coefficient data are not used.

- **The tail rotor**: is represented using a rotor disk model, based on that developed for the *DERA* Helisim model. When used as a tail rotor, it operated in quasi-steady form, meaning that the blade flapping is assumed to respond instantaneously to changes in control setting of flight condition.

- **Fuselage, Fin and tail-plane**: These are all represented using lookup tables to give aerodynamics loads as functions of local incidence and sideslip

- **Engine**: No engine configuration data were available for the *Bell 205* engine/rotorspeed governor. During *QinetiQ*'s tuning exercise, a model of the Lynx Gem engine was adapted to provide improved prediction of collective to yaw cross coupling. At best this component is an emulation of the real aircraft system.

- **Primary Flight Control System**: is based on aircraft data provided by *NRC* (e.g. stick offsets and gradients). The main and tail rotor actuators are modelled using second order transfer functions.

The basis for the controller design was a 32-state nonlinear flight mechanic model of the *Bell 205*. The model integrates 9 states (ϕ, θ, ψ, u, v, w, p, q, r) describing the rigid-body dynamics of the helicopter fuselage, 3 states representing the dynamic inflow on the main rotor (λ_0, λ_{1c}, λ_{1s}), 8 states governing the rotor flapping motions of the non-rotating frame (β_0, β_{1c}, β_{1s}, $\dot{\beta}_0$, $\dot{\beta}_{1c}$, $\dot{\beta}_{1s}$, β_d, $\dot{\beta}_d$), 8 states describing engine and main rotor actuator dynamics (Q_e, θ_0, θ_{1c}, θ_{1s}, $\dot{Q}_e$, $\dot{\theta}_0$, $\dot{\theta}_{1c}$, $\dot{\theta}_{1s}$), 2 states representing rotor position and velocity ($\psi_{heading}$, $\Omega\dot{t}$), and 2 states mapping the dynamics of the tail rotor servo (θ_{0tr}, $\dot{\theta}_{0tr}$) [PPT+05]. Additional physical characteristics for the helicopter can be obtained from [SH98].

Blade element model representation of the main rotor differ from disk-based model in that the equations of motion of the vehicle are periodic in nature, due to each rotor blade driving the fuselage once per rev. An N-bladed helicopter contains periodicity at a frequency of N/rev. Equilibrium conditions cannot therefore be achieved simply by setting the state derivatives to zero, as would be the case for non-blade-element models. Instead, conditions under which the state derivatives are zero when averaged across a rotor rev are required. Hence, for these reasons the Simulink package trim function could not be used with *nrcbemfinal.mat* model.

The periodic nature of the equations of motion required the system model to be trimmed[2] using the periodic trim algorithm presented in [MB97]. Linearising a blade-element model to generate LTI state-space models requires a conversion from states representing the individual blades to states representing the average motion of all blades (the so-called multiblade or Coleman coordinates). This procedure is relatively straightforward for rotors with three or more blades, but for the teetering rotor it is impossible to find a transformation that eliminates periodicity from the equations of motion. To circumvent this problem, for the specific purpose of creating an LTI model, the *nrcbemfinal.mat* model was trimmed using four blades (rather than two) but modified such that the loads they impart to the fuselage are equivalent to those generated by a two blade system. The nonlinear flight mechanic model was linearised at 30 ft/sec forward airspeed, level flight, to obtain an LTI model suitable for $\mathcal{H}_\infty$ controller synthesis and analysis. Attempts to linearize the model around hover (speed of 5 ft/sec) or closer to hover (0.1 ft/sec) resulted in unobservable modes.

Table 5.1 shows the primary input actuators and controlled outputs used in the design procedure.

The MIMO LTI nominal plant has three control inputs[3]: longitudinal cyclic θ_{1s} to control pitch attitude, lateral cyclic θ_{1c} to control roll attitude, and pedal θ_{0tr} for yaw

[2]A custom made file for trimming was provided by *QinetiQ*, which nevertheless required some adjustments by the designer.

[3]Collective was left un-augmented (open loop) due to pilot preferences and safety reasons.

Primary input actuator	Primarily influenced axis	Controlled variable
Main rotor collective (θ_0)	Height	N/A
Longitudinal cyclic (θ_{1s})	Longitudinal	Pitch attitude (θ)
Lateral cyclic (θ_{1c})	Lateral	Roll attitude (ϕ)
Tail rotor collective (θ_{0tr})	Directional	Yaw rate (r)

Table 5.1: Actuators vs. controlled variables

control. Control inputs are in terms of pilot stick movement measured in *inches*. There are five outputs being measured: Pitch (θ) and Roll (ϕ) angles (measured in rad) and Yaw (r), Roll (p) and Pitch (q) rates (measured in rad/sec). The first three are to be controlled (as primary measurements) leaving the rest, as secondary measurements, only to be used in the controller synthesis- as it is the case in the **1sqNDW** design described later in this chapter.

To make the system, from input to output perspective, as diagonal[4] as possible before the model reduction, the third input -lateral- was changed with the second input - which is longitudinal. This is in full compliance with ACAH response type control law design.

The open loop model with 3 inputs and 5 outputs initially had 32 states. However, to prevent higher order controllers, to ease both the process of synthesis and most importantly the implementation of the resulting controller[5], the model was subjected to model reduction. The system's three states were truncated by inspection, using *strunc* [BDG+98]; the resulting model then had 29 states. The states removed by truncation were uniform inflow- λ, rotor azimuth- ψ and heading- $\psi_{heading}$. Heading was removed, because it is discontinuous at modulo 2π rad.The 29-state model was then residualised with *sresid* [BDG+98] to 14 states while retaining the dominant rigid-body dynamics ($\theta, \phi, u, v, w, p, q, r$) states and the salient main and tail rotor actuator dynamics ($\theta_{1c}, \theta_{1s}, \dot{\theta}_{1c}, \dot{\theta}_{1s}, \theta_{0tr}, \dot{\theta}_{0tr}$) states. The residualised states were mainly those associated with the rotors, which could be replaced with their steady-state values[6]. Residualisation replaces states with their steady-state values (unlike with truncation which sets the states to zero), and was chosen on the basis of its property of preserving

[4]In this case we refer to diagonal, when actuator in every input axis drives the output from the same axis.

[5]Due to the restrictions posed by the onboard computer computational capacity- software and hardware, the maximum number of states that the controller would be allowed to possess is 30.

[6]Figure 4.3 shows the original (nominal) plant and the truncated-residualised model plant singular values as a function of frequency.

the low frequency frequency response characteristics.

The selection of model reduction techniques and of states to be residualised or truncated were based on one, or a combination of several from the following: the past experience (in model reduction) with the same helicopter [SWP+01], [PSW+99]; the size of the gap (measured by the appropriate norm) between the original and reduced order models, and the frequency response Bode magnitude characteristics of the original and reduced order models. For more detailed expositions on the motivation for both the choice of the model reduction methods and the selection of appropriate modes in the model reductions the reader is referred to [SP96] and [Pad00] respectively, as well as references therein.

All measurements were antialiased with second order 10 Hz cut-off frequency Butterworth filters. Aircraft instrumentation systems usually employ analog antialiasing filters. They should be used carefully as they can distort the data unacceptably, because their properties are often not well defined. The time delays introduced by filters greatly influence the frequency-response phase curves derived from the flight-test data. Additional filtering can also be performed with digital filters after the data are recorded. It has been suggested in [HGT95] that the data sample rate must be at least twice the filter cutoff frequency, and a sample rate of 5 times the filter cut off frequency is preferable to avoid aliasing effects. The helicopter's mathematical model did not require any scaling. The choice of scaling usually requires some engineering insight into the capabilities of the real physical system.

To account for the computational and structural time delays and to establish consistency with the nonlinear model each channel of the linear model was also augmented with first order *Padé* transfer functions corresponding to a 75 ms time delay. Actuator gains in the linear analysis and design model were set to unity (magnitude), whereas the nonlinear Simulink model had sliding actuator gains as well as variable time delays (to serve for empirical robustness analysis) with values compliant to design specifications[7]. Actuators as part of the nonlinear model were modelled as first order lags with magnitude and rate limits, and affect all axes equally.

[7] This is unlikely to be the case in reality, however, for ease of analysis and lack of precise information about the mechanical structure all channels were augmented with the same amount of time delay.

5.2.1 Design stage

5.2.1.1 Helicopter control design objectives

The stability of a feedback system is a very important concept and in order that the feedback to be of any further use, the feedback controller **K** should certainly stabilize the set of possible plants. However, it would be misleading to consider the guarantee of stability alone as the most crucial objective of feedback control. In our effort to achieve our goals- *Level 1* handling qualities (HQ)- we will consider the reduction of sensitivity as another fundamental objective of feedback control. The importance of sensitivity was emphasised in earlier chapters, but for a more detailed account the reader can refer to references like [Kwa93], [Zam81], [Vin00], [SP96]. Note that sensitivity is chiefly a performance indicator. Specifications for a control law synthesis can be derived from the control perspective and in view of the ADS-33E handling qualities requirements. For this problem, the controller design specifications were as follow:

- The design should allow for a worst case time delay of up to 75 ms on the control action and for 30 per cent uncertainty on the actuators, where actuators should not exceed their limits.
- The final steady-state values of all measurements, directly associated with the corresponding demand, should be reasonably accurate- within acceptable error margin.
- Stability should be achieved throughout the operating envelope with reduced pilot workload.
- Good attitude tracking.
- Good input-output decoupling.
- Insensitivity to noise on the measurement sensors.
- The closed loop bandwidth ω_{bw}, and phase delay τ_p should satisfy *Level 1* Target Acquisition and Tracking in a Usable Cue Environment of 1, and preferably in UCE> 1.

These should be satisfied both for linearised and full nonlinear systems. Effectively, we would like to achieve as high as possible bandwidth within the control power of the actuators, and have small phase delay[8].

5.2.1.2 Bandwidth

In real applications, the closed loop bandwidths of a (MIMO) system are limited by various system configuration and architecture related factors such as: sensor noise, sampling frequency of the controller, time delays in the system, locations of poles and zeros, their directions, the actuator bandwidth and control power[9] available as well as unmodelled high-frequency dynamics. External factors such as uncertain responses due to gusty wind conditions are also important. In the presence of these factors, flying is possible however, in order to achieve high precision in challenging manoeuvres and to reduce pilot workload some sort of augmentation is required.

A peculiar characteristic of the *Bell 205* helicopter is the rotor mast-flexing mode, which is quite fast and involves movement of the transmission and rotor mast constrained by the engine mounts and other linkages [TP01].

5.2.1.3 Open loop analysis

State space analysis of the nominal plant's transfer function indicates of the presence of an unstable pole, and serves as a motivation for employing feedback in order to re-locate the unstable pole in the stable part of the complex plane- *LHP*; relocation of an unstable pole is only possible by feedback. The interested reader can find more in [SP96] about which of the controller positioning configurations: cascade, feedforward or feedback could be used as a means of stabilizing an unstable linear system.

Eigenvalue		ω	ζ
$\Re$	$\Im$	rad/sec	
1.0906e-001	-3.25e-001	3.4282e-001	-3.1814e-001
1.0906e-001	3.25e-001	3.4282e-001	-3.1814e-001

Table 5.2: Open loop unstable poles

[8]Bandwidth and phase delay in terms of applications to rotorcraft flight dynamics control are described in Appendix I.

[9]Note that high gain may aggravate high frequency uncertainty, and therefore the designer must pay attention to the power that actuators are generating.

Eigenvalue		ω	ζ
$\Re$	$\Im$	rad/sec	
7.3088e-003	0.0000e+000	7.3088e-003	-1.0000e+000
3.9062e-002	-6.6630e+001	6.6630e+001	-5.8625e-004
3.9062e-002	6.6630e+001	6.6630e+001	-5.8625e-004

Table 5.3: Open loop unstable zeros

The nominal helicopter plant accommodates poles and zeros in the *RHP* of the complex plane and, thus, is both unstable and non-minimum phase.

Table 5.2 and Table 5.3 show the locations of the unstable poles and non-minimum phase zeros respectively along with the undamped frequencies and damping characteristics of the plant -with embedded time delays of value 75 ms. The unstable poles are complex, near the origin and thus, lightly damped; the unstable zeros are also very slow[10]. These *RHP* poles and zeros [SL02] along with the modelled time delays [Ast00], and the non-square structure of the plant [CCM02], restrict (with low and high frequency bounds) the closed loop bandwidth of each channel. Inspection of the frequencies of the *RHP* poles and zeros suggests possible restrictions in the frequency range between 0.34 rad/sec and 66 rad/sec. It is also well known that open loop *RHP* poles outside the closed loop bandwidth and *RHP* zeros within the closed loop bandwidth restrict the achievable closed loop performance- see [Vin00], [FL85] and [SBG97]. Later in the chapter, when closed loop bandwidths will become known, careful analysis will reveal that not only the unstable poles are within the closed loop bandwidths' region, but also the unstable zeros are within this region. In view of this, and the *Level 1* handling quality requirements for military rotorcraft described in [Ano00], in this problem, only the loci of the non-minimum phase zeros may manifest themselves (in a performance context) by limiting the achievable bandwidth in one or several of the channels.

Subplot a) in Figure 5.2 shows the original and model reduced (by truncation and residualisation) helicopter plant's singular values (as a function of frequency). Inspecting subplot b), in the same figure, brings to evidence the change of condition number $\kappa(j\omega)$ of the nominal plant with frequency. The plant has high condition number at some frequencies, reflecting on its sensitivity to a relative change (or er-

[10]Systems with slow zeros are known to be more difficult to control than systems with fast zeros [Ast00].

ror) in itself; i.e. making it an ill-conditioned plant. This brings several, and equally important interpretations; the plant is difficult to invert; the plant may be difficult to control; the dependency of the plant's gain to the direction of input. It is clear that at low frequency (the *performance region*) the plant's gain varies significantly with the direction of the input signal. Naturally, the gains at the system plant input and output also differ from one another. In the construction of the pre-filters, $\kappa(j\omega)$ variability has to be taken into account and the weighting function dynamics should compensate for this high conditioning, particularly at low frequency.

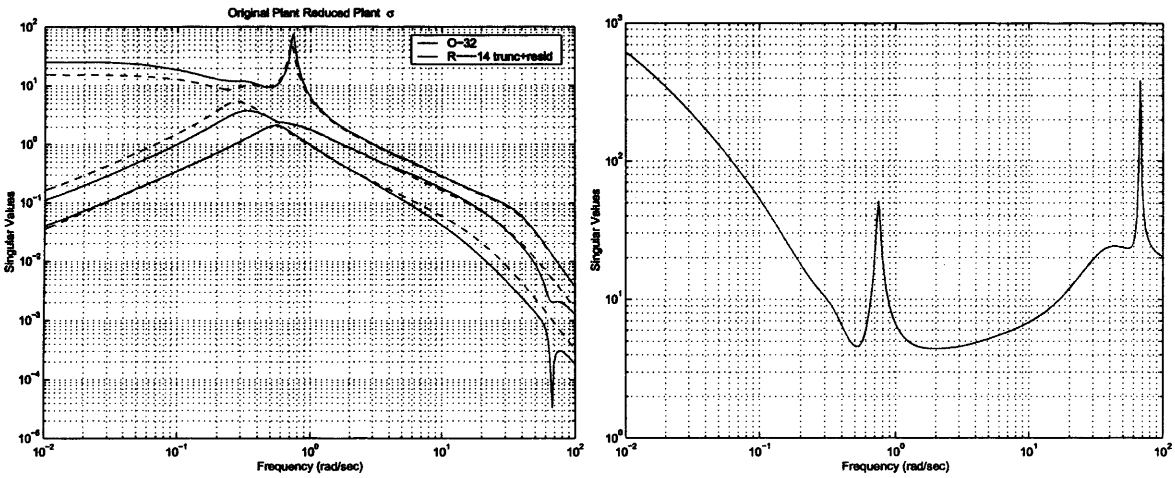

Figure 5.2: Loop shapes of **a)** solid- actual (32 state), dashed- reduced order plant's singular values (14 state); **b)** condition number

The high condition number and directionality property of the plant will also manifest itself in misaligning the range subspace (or column space) $R(\mathbf{K})$ of the controller with the row space of the shaped (or nominal) plant, $R(\mathbf{G}_s^*)$ [WFM01] which will adversely affect some of the (performance/robustness) properties of the closed loop system.

In the frequency range of $[0.01, 100]$ rad/sec the highest condition number (κ) has a value of 610 (at low frequency) at ω=0.01 rad/sec indicating very poor closed loop tracking (in two channels); the condition number gradually decreases, thus improving the conditioning of the plant, but around cross over at ω=0.75 rad/sec, due to the first resonant peak, the condition number peaks to a second larger value of κ=51. Additionally, the plant exhibits high singularity at high frequency (ω=68 rad/sec) with condition number of value κ=380 due to an anti-resonant peak. However, a closer look in subplot *b*) in Figure 5.2 reveals that the plant is relatively well conditioned around the range of the desired bandwidth (1.5 rad/sec to 4.5 rad/sec).

Although the condition number is scaling dependent, i.e. its value is not independent of input and output scaling of the plant, given that the scaling is performed correctly, a reasonable explanation (from a physical point of view) for the highest condition number can be the asymmetric aerodynamics of the helicopter. More precisely the fact that principal moment of inertia I_{xx} is much smaller than I_{zz} and I_{yy}; $I_{yy} > I_{zz} \gg I_{xx} > I_{xy}$.

5.2.1.4 Control law characteristics

Several types of longitudinally and laterally coupled linear controllers were designed for the *Bell 205* helicopter. It must be noted that, for their synthesis, the controllers presented herein used the same reduced (truncated-residualised) LTI model of the rotary-wing aircraft and were designed principally around a body axis referenced low forward speed of 30 feet/s ($\approx$ 20 *knots*) linearisation.

Two systems will be used as a platform of our research. One mapping a 3 dimensional input space to a 3 dimensional output space, a square transfer matrix. The other, mapping a 3 dimensional input space onto a 5 dimensional output space, represented by a non-square transfer function matrix. Both systems possess equal numbers of states before, and after the model reduction.

All controllers have been designed essentially on Attitude Command Attitude Hold (ACAH) response type with Rate Command Attitude Hold (RCAH) for the Yaw axis. Four LTI controllers were designed and flight tested in the facilities at NRC IAR Laboratories in Ottawa, Canada. Based on the following:

1. The geometrical structure of the plant (square, non-square).
2. The structure of the plant shaping filters ($\mathbf{W}_1$,$\mathbf{W}_2$); diagonal or non-diagonal.
3. The controller architecture employed (1 Dof, 2 Dof).

the controllers have been code named as following:

1. **1sqDW**- One degree-of-freedom controller synthesised for square plant that had been "*shaped*" with diagonal weights.
2. **1nsqDW**[11]- One degree-of-freedom controller synthesised for non-square plant that had been shaped with diagonal weights.

[11]The size of the non-square plant has affected the structure of the pre-filter used, hence the pre-filters - weighting- functions for the square and non-square systems were different.

3. **1nsqNDW**- One degree-of-freedom controller synthesised for non-square plant that had been "*shaped*" with non-diagonal and diagonal weights.

4. **2nsqDW**[12]- Two degree-of-freedom controller synthesised for non-square plant that had been "*shaped*" with diagonal weights.

This notational labeling is aimed at providing brevity, clarity and to ease the comprehension of comparative analysis results in the remaining sections of the thesis.

A linear time invariant model that describes the low speed dynamics of the helicopter plant was used in the control law design, whereas the full nonlinear model, augmented with variable actuator gains and variable time delays compliant to the design specification, was used in the closed loop (performance and robustness) analysis.

All the designs were three axis control laws: the Pitch, Roll and Yaw axes were controlled; the collective channel (used to control heave) was not closed (this was partly due to safety reasons and partly due to pilot preference as this channel is stable).

All the controllers had three control channels: the longitudinal and lateral cyclic to control pitch and roll manoeuvres respectively, and tail rotor collective to control yaw. The measured outputs were: Pitch (θ) and Roll (ϕ) angles together with Yaw (r), Roll (p) and Pitch (q) rates (the last two were excluded in the design of control law **1sqDW**), whereas, the controlled outputs were only three of the measured variables: Pitch (θ) and Roll (ϕ) angles, and Yaw rate (r).

We are now in a position to proceed with the design of a robustly stabilising compensator **K** for a normalized *coprime* factor description of a shaped plant.

5.3 One degree-of-freedom controller synthesis

5.3.1 Diagonal weights: Square nominal model- 1sqDW

In the first stage of the design we will aim to construct a transfer function matrix, called a weighting (or loop-shaping) function hereafter, such that performance requirements on the helicopter are imposed on the design.

In this control law synthesis we did not include two of the measurement outputs, namely Roll rate (p) and Pitch rate (q). However, in some of the control laws presented

[12]The two degree-of-freedom controller is designed in one step.

in this thesis these variables will be used to dampen the response -through derivative type of effect, and to assist in investigating the effects of the extra measurements on attaining control design objectives.

The role of the weighting functions $\mathbf{W}_1$, $\mathbf{W}_2$ will be to ensure that the loop-shape **GK** is compatible with the performance and robustness objectives in the low- $(0, \omega_l]$, medium and high- $[\omega_h, \infty)$ frequency ranges; these usually translate to high gain at low frequency, a smooth (not too fast) transition through ω_c, and low gain at high frequency. In view of these and previously outlined helicopter control design objectives the loop-shaping transfer functions for each channel were selected as follows. The weighting transfer functions $\omega_1^i, i = 1, 2, 3$ located on the diagonal of the (3×3) pre-filter square matrix $\mathbf{W}_1$ will be selected by considering low and intermediate frequency ranges, whilst transfer functions $\omega_2^i, i = 1, 2, 3$ located on the diagonal of the square matrix $\mathbf{W}_2$, will be chosen in accordance with requirements for the high frequency range.

5.3.1.1 Selection of $\mathbf{W}_1$

An initial assessment of subplot a) in Figure 5.2 (of the lowest singular value- as an indicator of performance- of the nominal plant at low frequencies) indicates the need for an integrator in the channel corresponding to $\underline{\sigma}(\mathbf{G})$ and for most of the time in all channels. This aims to increase the plant's gain equally in all directions in the low frequency range, ensuring that all input signals in these directions will get amplified so as to provide good disturbance rejection, good input/output decoupling and (reference) command tracking.

However, the integrator transfer function comes at the expense of introducing a phase lag of -90^o in the same frequency range, which adversely affects the stability margin (ϵ). Therefore, in order to maintain the robustness properties of the augmented plant a dynamic element, which will rectify this reduction in the phase margin, ought to be introduced. This can be achieved by a proportional gain element, resulting in a **PI** (Proportional and Integral) transfer function combination.

If the rate of attenuation of the (open) loop gain at unity magnitude gain crossover is high ($>$ 40 db/dec), in order to ensure good command decoupling (and tracking) it must be reduced to about 20 db/dec. The lower the rate of gain reduction through crossover, the smaller the phase lag; this can be deduced from the Bode gain-phase relationship, Equation 4.1 in Chapter 4. The designer should be mindful of the fact that high rate of gain reduction through crossover will bring a large phase-lag penalty which will lead to small phase margins, and then a poorly damped closed loop response.

After inspection of the singular values in the frequency range of interest, and after performing iterations (on the values of zeros, and gains of the transfer functions) in-line with (previously outlined) control law design objectives the pre-filter loop-shaping transfer function ($\mathbf{W}_1$) has taken the following structure:

$$\mathbf{W}_1 = \begin{bmatrix} \frac{3(s+0.65)}{s} & 0 & 0 \\ 0 & \frac{3.25(s+0.65)}{s} & 0 \\ 0 & 0 & \frac{3.95(s+0.9)}{s} \end{bmatrix}. \tag{5.1}$$

A zero at -0.65 was introduced in the first and second channels, and a minimum phase zero at -0.9 in the third channel. These will facilitate reduction of the transition roll-off rate through the crossover frequency region, and will also reflect on the damping of the closed loop response.

Each channel introduces integral action which will increase the low frequency gain and facilitate desirable disturbance attenuation properties, which in turn will provide improved (low-frequency) performance characteristics and ensure a zero steady-state error e_{ss}.

Different time domain specifications on each of the controlled outputs indicate different frequency domain requirements, and hence different bandwidths. The gains of 3, 3.25 and 3.95 in the three channels were selected to increase the crossover frequencies and to adjust the bandwidths accordingly.

The weight is well conditioned with $1 < \kappa(\mathbf{W}_1(j\omega)) < 2$ and was chosen to be diagonal which is often adequate, however for plants with strong cross-couplings between channels this approach may not be sufficient. Inclusion of non-diagonal weighting functions to facilitate singular value shaping will be investigated later with control law **1nsqNDW**.

5.3.1.2 Selection of $\mathbf{W}_2$

The pre-compensated shaped plant ($\mathbf{GW}_1$) was augmented with the diagonal post-filter ($\mathbf{W}_2$) with the following structure:

$$W_2 = \begin{bmatrix} 1 & 0 & 0 \\ 0 & 1 & 0 \\ 0 & 0 & \frac{11.5}{s+11.5} \end{bmatrix} \tag{5.2}$$

A low pass filter with cut-off frequency of 11.5 rad/sec was employed in the third output channel; it was observed that augmenting this channel will influence most the (roll-off) dynamics of the maximum singular value at high frequencies. The pole of the post-filter at -11.5 is selected to increase the roll-off rate at high frequencies, beyond 11.5 rad/sec, for better noise mitigation and, improved robustness. In order to reduce the control effort in response to any disturbances at the plant output, the open loop gain beyond cross over frequency (ω_c) must be rolled off sharply. The first two channels were left unaugmented as their roll-off rate was found to be satisfactory. The DC gain of $\mathbf{W}_2$ is 1.

The post-filter $\mathbf{W}_2$ is also used to ensure fast roll-off in the (high) frequency region where the modelled dynamics is least reliable. In this frequency region, limits on actuator bandwidths will also require that the high frequency gain is kept low. High roll-off will reduce the controller bandwidth, and thus will also limit high frequency actuator activity and act as an appropriate measure for actuator saturation prevention. In the high frequency region, where $(\overline{\sigma}(\widetilde{\mathbf{M}}_s) = 1)$, the inequality in Equation 4.25 simplifies to inequality in Equation 5.3 (where $\overline{\sigma}(\mathbf{W}_1) = \beta$, $\overline{\sigma}(\mathbf{W}_2) = \alpha$; α and β are constants, $\gamma = \epsilon^{-1}$).

$$\overline{\sigma}(\mathbf{KS}_o) < \gamma\overline{\sigma}(\mathbf{W}_1)\overline{\sigma}(\mathbf{W}_2) \tag{5.3}$$

It can be seen that the high frequency dynamics of the transfer function $\mathbf{W}_2$ is dominant in manipulating and defining the actuator bandwidth. Therefore the selection of the post-filter $\mathbf{W}_2$ is as important as the selection of the pre-filter $\mathbf{W}_1$.

Figure 5.3 depicts pre and post-compensated (shaped) system's frequency response;

subplot a) shows the frequency response Bode magnitude plots of $\mathbf{W}_1$ (dashed), $\mathbf{W}_2$ (dash dot) and the (model reduced) nominal system (G); subplot b) illustrates the singular values of the shaped plant $\mathbf{G}_s$.

From Figure 5.3 one can also deduce that the condition number of the pre-filter is very small ($\kappa(\mathbf{W}_1) < 2$). Care must be taken when designing ill-conditioned weighting

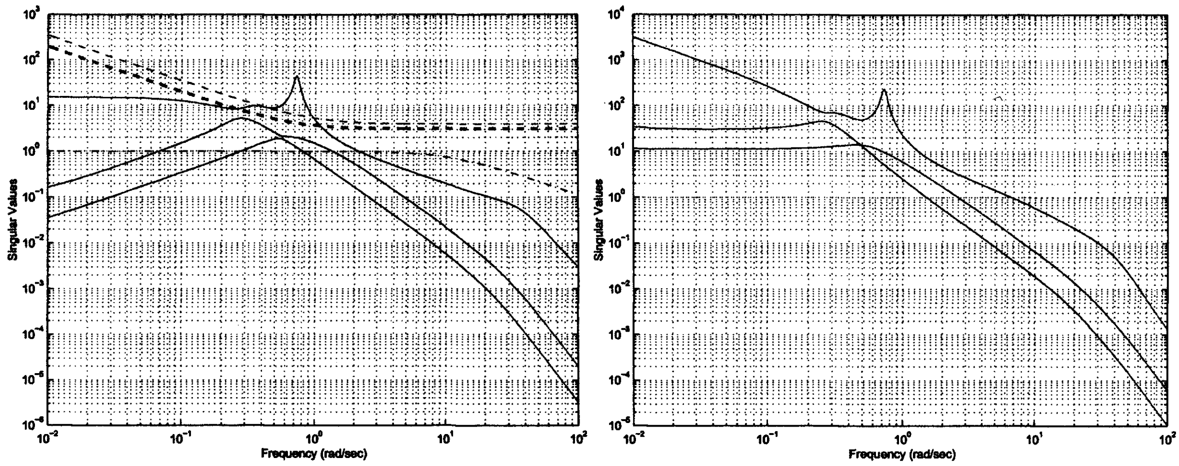

Figure 5.3: **a)** Nominal plant (*continuous*) and loop-shaping weights (*dashed*) **b)** Shaped plant

functions for ill-conditioned plants as this can lead to poor robustness at other (e.g. output) break-points in the loop [FL85].

5.3.1.3 $\mathbf{K}_\infty$ Controller synthesis

The loop-shaping performed so far accounts for performance and disregards the phase and robustness to uncertainties. In order to secure the stability robustness of the closed loop explicitly, and to take account of the phase of $\mathbf{G}_s$, a sub-optimal controller (with 9 per cent sub-optimality scale) was synthesised for the shaped plant using Matlab®'s μ-Toolbox command $[\mathbf{K}_\infty, e_{max}] = \mathtt{ncfsyn}(\mathbf{G}_s, 1.09)$. The optimal stability margin ϵ_{max} was 0.30042, but a normalized *coprime* factor robustly stabilizing controller $\mathbf{K}_\infty$ for the resulting shaped system $\mathbf{G}_s = \mathbf{W}_2\mathbf{G}\mathbf{W}_1$ guaranteed a stability margin of $\epsilon = 0.27769$. This indicates that $\epsilon * 100 = 27.7$ per cent of additive or proportional uncertainty in the *coprime* factors $\widetilde{\mathbf{N}}_s$ and $\widetilde{\mathbf{M}}_s$ of the shaped plant can be tolerated in the crossover frequency range. This synthesis is associated with an upper bound on the infinity norm (see Equation 4.3), which can be used to assess the effectiveness of the design. The stability margin (ϵ) has already been recognized as a good design indicator from several perspectives, such as:

- consistency between specified (desired) loop-shape and achieved loop-shape
- guarantee of high level of stability robustness
- good performance

where $\mathbf{K}_\infty$ is the resulting controller, which is designed to increase the gain in certain directions and to reduce it in others.

A Bode magnitude plot of the synthesised $\mathbf{K}_\infty$ controller can be seen in Figure 5.4 subplot a).

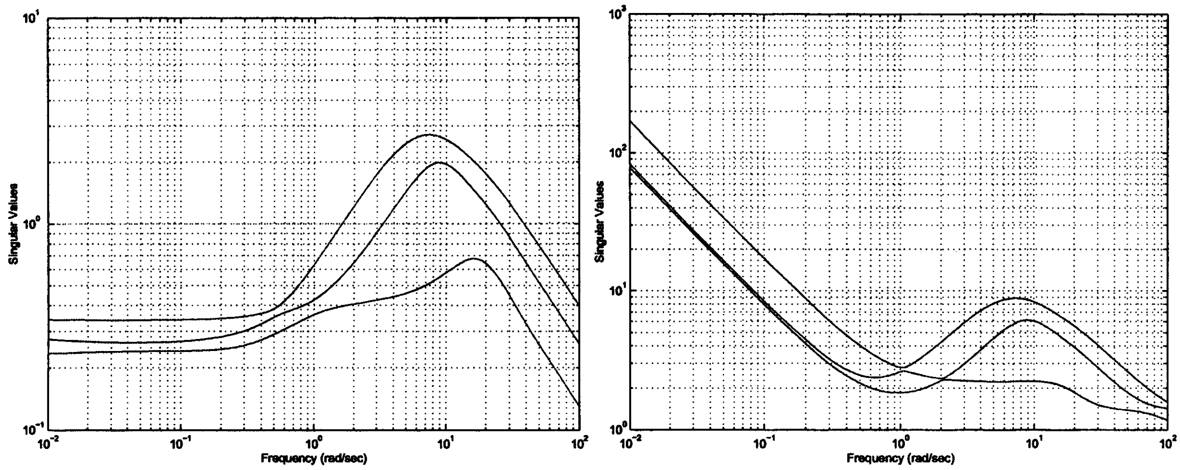

Figure 5.4: Singular values: a) Loop shaping controller $\mathbf{K}_\infty$ b) Implemented controller $\mathbf{K}_{imp}$

Weighting functions, although part of the design, are not part of the plant, and therefore they must be absorbed into the controller by replacing $\mathbf{K}_\infty$ by $\mathbf{K} = \mathbf{W}_1\mathbf{K}_\infty\mathbf{W}_2$. The final controller $\mathbf{K}$ has 25 states. Preserving the states of the controller is advisable whenever possible. The controller could be easily accommodated on the on-board computer of the *Bell 205*, and therefore no model reduction was applied.

The reciprocal of the stability margin ($\gamma = \epsilon^{-1}$) can be used to provide information on the degree of mismatch between the desired and actual loop shapes at low and high frequencies. For example, since at high frequency $\overline{\sigma}^2(\mathbf{G}(j\omega)) \ll 1$ then $\overline{\sigma}(\mathbf{K}_\infty(j\omega)) \lesssim \sqrt{\gamma^2 - 1}$, and at low frequencies, if $\underline{\sigma}^2(\mathbf{G}(j\omega)) \gg 1$ then $\underline{\sigma}(\mathbf{K}_\infty(j\omega)) \gtrsim \left(\sqrt{\gamma^2 - 1}\right)^{-1}$ [GM89]. Indeed, this is reinforced by inspecting Figure 5.4. It can be concluded that the achieved loop shape will differ from the desired one by a factor of $\sqrt{\gamma^2 - 1} = 3.46$ at high frequencies; note that $\overline{\sigma}(\mathbf{K}_\infty) = 2.7203$. It can be also inferred that the smaller the γ (larger ϵ), the smaller the deterioration of the loop shape after inclusion of the controller $\mathbf{K}$.

The achieved -actual- loop shapes at the plant input denoted by $\mathbf{L}_i = \mathbf{KG}$, and at the plant output by $\mathbf{L}_o = \mathbf{GK}$ can be seen in Figure 5.5 subplots a) and b).

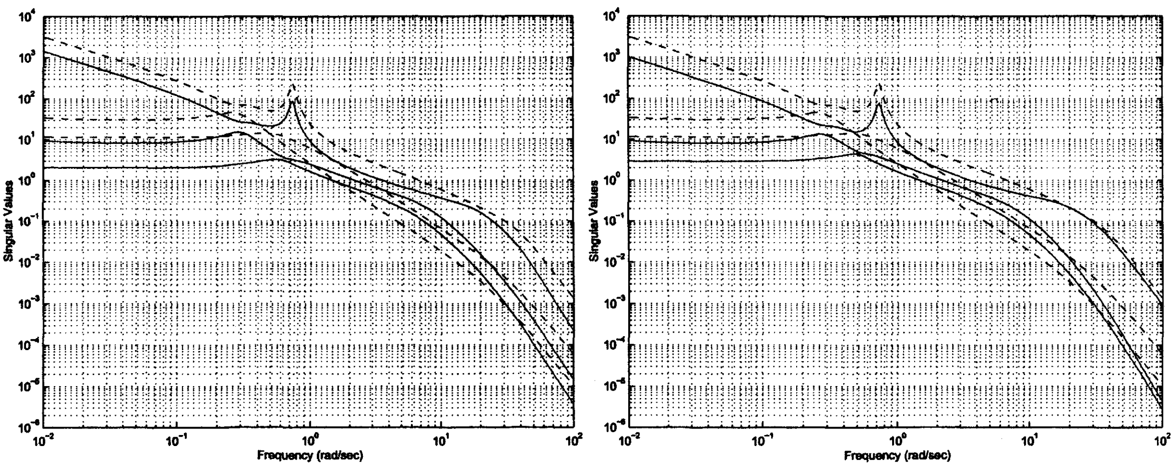

Figure 5.5: Shaped (*dashed*) vs. actual (*solid*) loop shapes: **a)** at the plant input $\mathbf{L}_i$ **b)** at the plant output $\mathbf{L}_o$

To achieve accurate closed loop tracking, (i.e. DC gain of 1 between inputs r and outputs y) in $\mathcal{H}_\infty$ loop-shaping, a constant pre-filter $\mathbf{K}_\infty(0)W_2(0)$ can be introduced and positioned as in Figure 4.12. Finally, the controller, which will be used in the analysis of the properties of the closed loop system, is the one that will be practically implemented and is denoted by $\mathbf{K}_{imp}$. It is derived by combining the constant $(\mathbf{K}_\infty(0)W_2(0))$, and dynamic ($\mathbf{W}_1, \mathbf{W}_2$ and $\mathbf{K}_\infty$) elements except $\mathbf{G}$ into a system interconnection structure, as shown in Figure 4.12.

Figure 5.4 subplot *b*) illustrates the frequency response of the implemented controller; it modifies the low frequency gain and high frequency gain. Note that the low frequency modification is satisfactory and the high frequency gain is small. However the roll-off in one of the channels is not very fast, which may affect some of the robustness properties of the system, although slow roll-off is usually good.

5.3.2 Linear frequency domain analysis

Performance and robustness analysis of the augmented system will be carried out using frequency responses of some of the closed loop transfer functions. Although some linear results may be conservative due to the nature of the assumptions on which they are based, they nevertheless provide sufficient insight and indicators to conclude whether or not the control law possesses the desired characteristics to be flight-tested.

Remark 5.1 *An intrinsic effect of ill-conditioning, and thus directionality, in MIMO systems* *is that a controller $\mathbf{K}_\infty$ that provides desirable performance and robustness at one break point-before the nominal plant, may not provide the same level of "service" at another break point-at the plant output. It is therefore essential that in the design process, properties at both the plant input and plant output are evaluated.*

5.3.2.1 Performance analysis

Inspection of some of the frequency domain indicators for disturbance attenuation and tracking performance (input sensitivity $\mathbf{S}_i$, output sensitivity $\mathbf{S}_o$ and $\mathbf{S}_o\mathbf{G}$) in Figure 5.6 reveal that the system provides an acceptable but not very satisfactory level of disturbance rejection and reference signal tracking at low frequencies in two channels, but with very small steady-state error in one controlled channel. Subplots a) and b) also indicate that the augmented system exhibits very good immunity to disturbances acting on the Yaw channel.

The following is a further interpretation of the frequency responses; Figure 5.6 highlights the effect of the integral action (s^{-1}) on the input/output sensitivity transfer function. Input/output disturbance attenuation is good in the low frequency range up to 0.5 rad/sec. The peak value of the sensitivity at the output $\|\mathbf{S}_o\|_\infty = 2.4840$ is slightly greater than at the input $\|\mathbf{S}_i\|_\infty = 2.1924$. This points to slightly better robustness to unstructured input inverse multiplicative uncertainty, than unstructured output inverse multiplicative uncertainty.

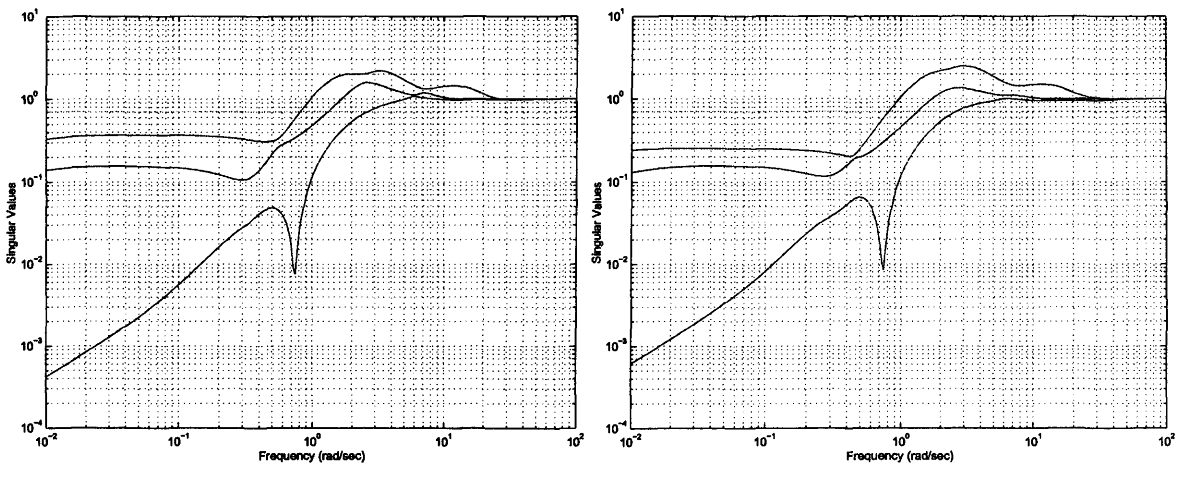

Figure 5.6: **a)** Input sensitivity $\mathbf{S}_i$ **b)** Output sensitivity $\mathbf{S}_o$ singular values

The frequency response of $\mathbf{S}_o\mathbf{G}$ in Figure 5.7 indicates that the compensated closed loop system is able to attenuate both low and high frequency disturbances acting on the plant input, but it is much better at high frequencies. One of the channels exhibits slightly higher sensitivity to disturbances at high frequencies. It is worth clarifying that low frequency disturbance attenuation is due to an integral action in $\hat{\mathbf{K}}$ (via $\mathbf{W}_1$), whereas high frequency input disturbance attenuation at the plant output takes place due to the strictly proper nature of the shaped plant $\mathbf{G}_s$.

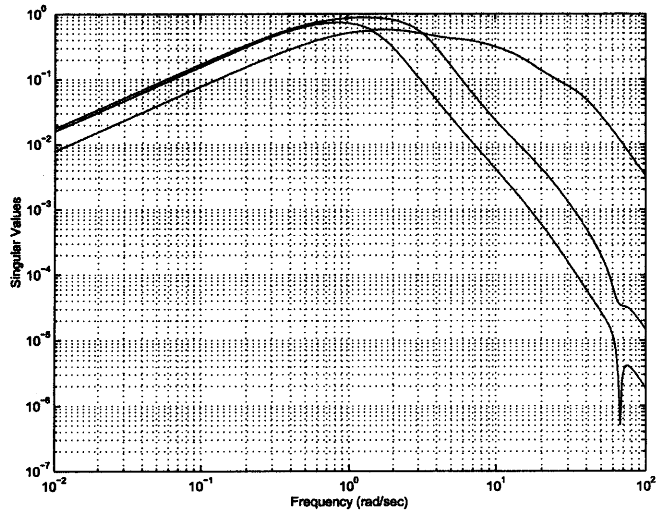

Figure 5.7: Singular values $\mathbf{S}_o\mathbf{G}$

5.3.2.2 Robustness analysis

Figure 5.8 shows the frequency response history of the robustness of the closed loop to multiplicative input and output uncertainties- $\mathbf{T}_i$ and $\mathbf{T}_o$; good roll-off at high frequency confirms the system's robustness ability to mitigate high frequency measurement noise. Values of $\overline{\sigma}(\mathbf{T}_i)$ (and $\overline{\sigma}(\mathbf{T}_o)$) determine the size of the smallest unstructured input (and output) perturbation Δ_i (Δ_o) modelled in multiplicative form that could destabilize the system.

The estimated bandwidths[13] from the output co-sensitivity plots for each channel indicate that the fastest channel has a bandwidth of 8.5 rad/sec, due to the helicopter's aerodynamic geometry, followed by 4.6 rad/sec and 2.7 rad/sec. The bandwidths reflect the size of the moments of inertia from the smallest to the largest.

Figure 5.9 offers a wealth of information, since it also allows the designer to derive the smallest unstructured input/output multiplicative perturbation that could destabilize the system. Smaller peaks indicate increased tolerance to uncertainties. It can

[13] In terms of $\mathbf{T}_o$, the bandwidth is the highest frequency at which $|\mathbf{T}(j\omega)|$ crosses ≈ -3 dB from above.

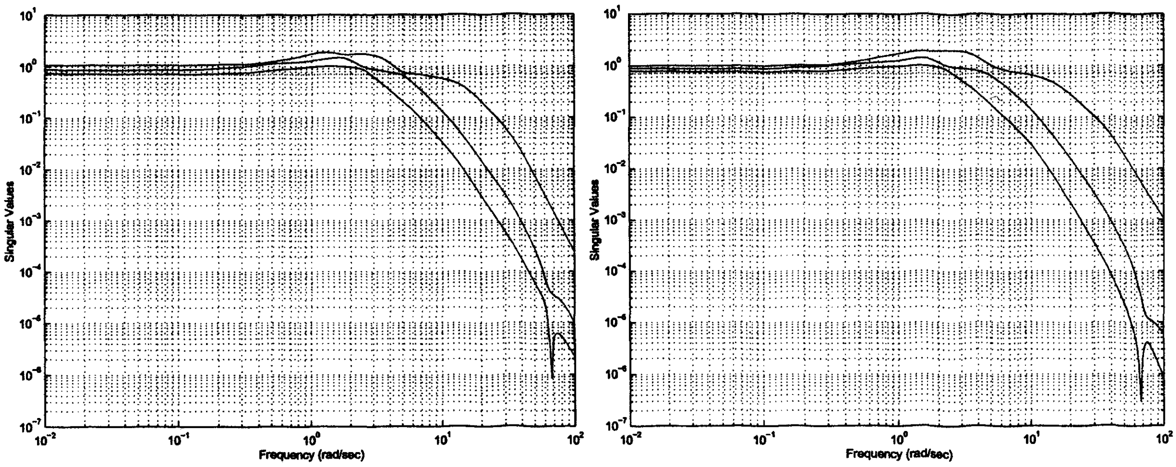

Figure 5.8: **a)** Input co-sensitivity $\mathbf{T}_i$ **b)** Output co-sensitivity $\mathbf{T}_o$ singular values

be seen that the system can satisfactorily tolerate multiplicative uncertainties up to 53 per cent in magnitude at the plant input, whereas at the plant output this is slightly less at 49 per cent. The main source of these uncertainties is unmodelled dynamics, where the rotor and its associated dynamics have dominating roles.

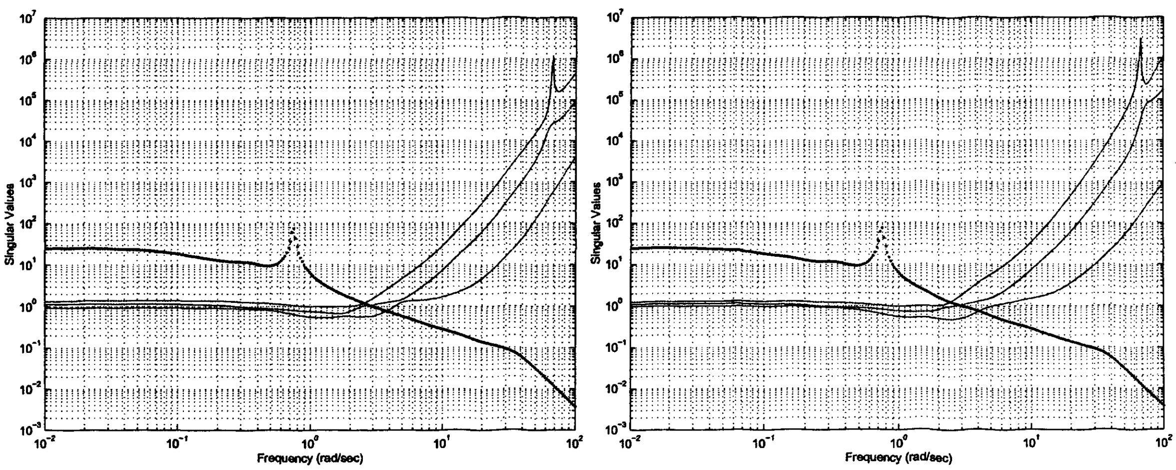

Figure 5.9: **a)** Inverse input co-sensitivity $\mathbf{T}_i$ **b)** Inverse output co-sensitivity $\mathbf{T}_o$ singular values vs. $\overline{\sigma}(\mathbf{G})$

Superimposed in Figure 5.9 subplots *a)* and *b)* is $\overline{\sigma}(\mathbf{G})$, depicted together with the *inverse* of co-sensitivities. It is apparent that at high frequencies, above 10 rad/sec (where the unmodelled dynamics is a significant source of uncertainty), an unstructured input/output multiplicative perturbation larger than the magnitude of the plant can be tolerated in all channels. The fastest channel, seemingly, exhibits more sensitivity to this type of uncertainty.

Activity of the actuators due to output disturbances, where two of the control channels are quite sensitive (due to large peaks around the cross-over region), is illustrated in 5.10 subplot a). This figure also provides information about the robustness of the closed loop to additive uncertainties, mathematically represented by (operator) $\mathbf{KS}_o$. Actuator activity is most present in the low frequency range and the system's bandwidth range 2 rad/sec to 5 rad/sec. In subplot b) of the same figure it can be observed that at frequencies above 20 rad/sec the closed loop system tolerates slightly larger unstructured additive uncertainties compared to the magnitude of the plant.

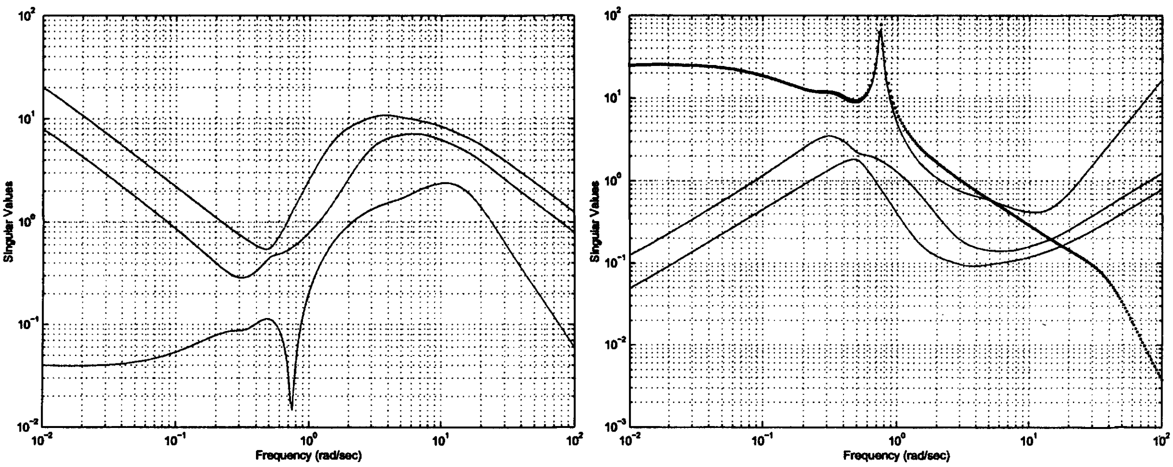

Figure 5.10: **a)** Actuator activity due to output disturbance **b)** Maximum allowable additive uncertainty vs. $\overline{\sigma}(\mathbf{G})$

Figure 5.11 depicts maximum singular value plots of the normalized *coprime* factors of the nominal plant- *continuous* line, reduced plant- *dashed* line, and shaped plant- *dotted*line. Consider a left *coprime* factorization of the shaped plant $\mathbf{G}_s = \widetilde{\mathbf{M}}_s^{-1}\widetilde{\mathbf{N}}_s$, it is evident that both transfer functions are bounded such that: $\overline{\sigma}(\bullet) \leq 1$.

Interpretation of these singular values requires consideration of the closed loop inequalities for robustness and performance (see Chapter 4 Theorem 4.3). In view of inequalities in Theorem 4.3 if we, crudely, associate $\widetilde{\mathbf{N}}_s$ with robustness properties of the plant, we can observe in subplot a) that augmenting the dynamics of the nominal plant with dynamic weighting functions has improved the robustness and insensitivity to sensor measurement noise at high frequencies by increasing the roll-off rate. A similar interpretation can be performed on $\widetilde{\mathbf{M}}_s$ by examining subplot b) in the same figure. By associating $\widetilde{\mathbf{M}}_s$ with low frequency performance specifications, it is evident that augmentation of the nominal plant (with weighting functions) has significantly improved performance characteristics such as disturbance rejection, tracking and input/output decoupling.

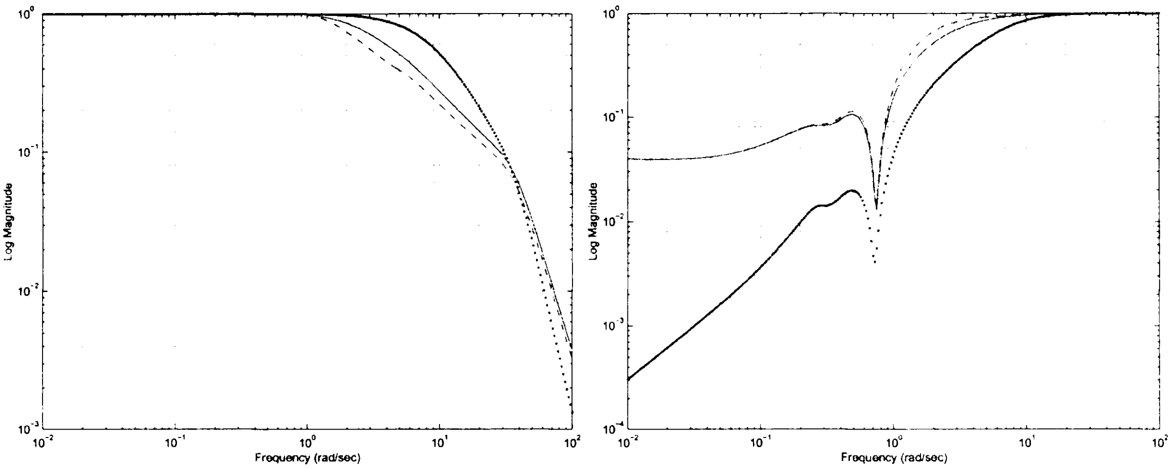

Figure 5.11: **a)** $\overline{\sigma}(\mathbf{N}_s)$ **b)** $\overline{\sigma}(\mathbf{M}_s)$ of shaped (dotted), nominal (continuous), reduced (dashed) plant

5.3.3 Diagonal weights: non-square nominal model- 1nsqDW

In this design case, we consider the scaled nominal plant **G**, with embedded time delays, accommodating more output variables $y = (\phi, \theta, r, p, q) \in \mathbb{C}^{5\times1}$ than control inputs $u = (\theta_{1c}, \theta_{1s}, \theta_{0tr}) \in \mathbb{C}^{3\times1}$. This is why we can expect to have independent and direct control over at most 3 independent linear combinations of the 5 output variables; this condition is dictated not only by *rank*(**G**) which is 3, but also by the ability of control axis actuators to effect directly only the corresponding axis behaviour. Although we have 5 output measurement variables we use for control only 3 of them; the Roll attitude (ϕ), Pitch attitude (θ) and Yaw rate (r) constitute the outputs to be controlled.

Remark 5.2 *Extra measurements result in a non-square plant which can still be accommodated in the* 1 *Dof* $\mathcal{H}_\infty$ *loop-shaping controller design procedure, however, without guarantees for zero steady-state error* ($e_{ss} = 0$) *in all channels.*

5.3.3.1 Selection of $\mathbf{W}_1$

For good tracking accuracy in the subset of measured outputs, and good disturbance rejection properties, the system must possesses high gain in the low frequency region. This was achieved by augmenting each input channel with a weighting transfer function having an undamped pole at the origin (of the complex plane). To reduce the roll-off rate through the frequency cross over region to an acceptable $20-25$ dB/dec around cross-over, appropriate zeros were added to every input channel. Although the presence of first order poles [14] at the origin is desirable from a performance stand point of view it has a detrimental impact on robustness properties. The phase lag of 90^o, introduced by the poles at the origin, was rectified by adjusting the gain in each channel. Appropriate proportional gains were embedded into the transfer functions (w_{11}, w_{22}, w_{33}) to increase robust stability, to decrease the phase-lag (at crossover) as well as to improve performance (by reducing the t_r of the transient time response).

The resulting diagonal pre-filter transfer function matrix $\mathbf{W}_1$ has a structure of a high gain band pass filter, with finite attenuation. Finite attenuation is a characteristic which adds to the reduction of the overshoot in the time domain response. The pre-filter is minimum phase, and has a **PI** structure:

$$\mathbf{W}_1 = \begin{bmatrix} \frac{1.87(s+2)}{s} & 0 & 0 \\ 0 & \frac{(s/0.3+1.5)}{s} & 0 \\ 0 & 0 & \frac{4.2(s/2+5)}{s} \end{bmatrix} \tag{5.4}$$

5.3.3.2 Selection of W_2

Roll-off rates of each output were found to be satisfactory, therefore the post-compensator (unlike for **1sqDW**) was kept constant, as an identity matrix, $W_2 = I_{5\times5}$. Hence, the pre-compensated shaped plant, denoted by $\mathbf{GW}_1$, was augmented with the diagonal post-compensator $W_2 = I_{5\times5}$. Figure 5.12 a) depicts the reduced order shaped plant and weighting function magnitudes as a function of frequency, whereas in b) one can see the singular values of the shaped plant $\mathbf{G}_s = W_2\mathbf{GW}_1$[15].

The structure of the post-filter allowed Pitch and Roll rates, q and p respectively, to be fed back but they were not to be controlled. [YP90] reported difficulty in controlling Pitch (θ) and Roll (ϕ) attitudes without information from their corresponding rates q and p. Later, we will empirically investigate the impact of feeding back Roll and Pitch rates on the design properties by investigating indicators for performance and robustness (characteristics). Comparison of the set of plots in Figure 5.12 with those in Figure 5.3 reveals that inclusion of extra measurements in the nominal plant has not contributed to modification of the low frequency (DC gain) characteristics of the nominal system. However, the effect of extra measurement can be observed in the mid

[14]In fact such a pole introduces phase lag in the whole frequency range considered, but we are particularly interested in the behaviour around the crossover region.

[15]Unlike $\mathbf{W}_1$, W_2 is a (constant) matrix, hence it is not bold font.

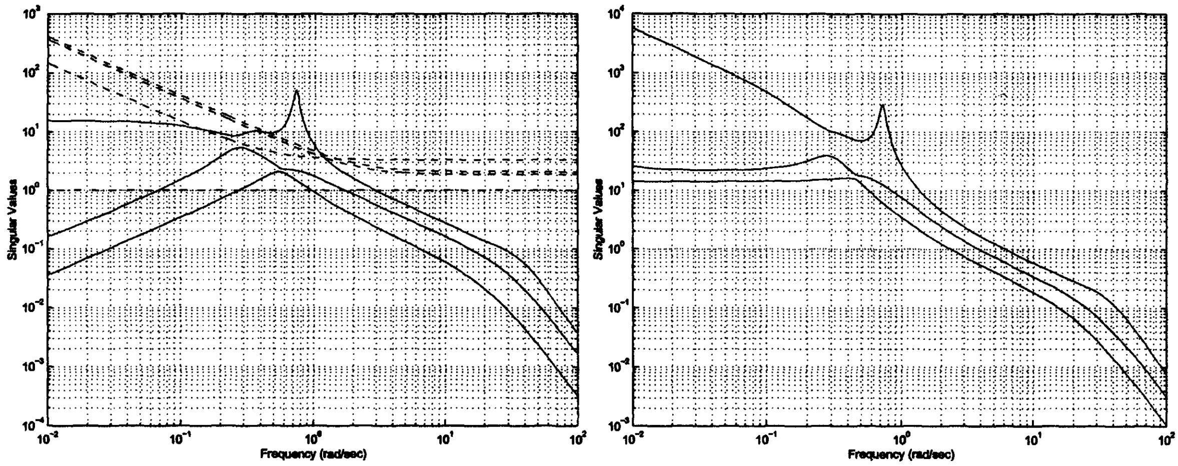

Figure 5.12: **a)** Nominal plant (*continuous*) and loop-shaping weights (*dashed*) **b)** Shaped plant

and (in particular) high frequency ranges. On the positive side, in the mid-frequency range, the crossover (ω_c) frequencies of all channels have increased slightly, hence resulting in (slightly) higher bandwidths in all channels; whereas in the high frequencies, on the negative side, extra measurements have significantly reduced the roll-off rates of two controlled outputs[16]. This may have adverse effects on the insensitivity of the system to measurement noise and/or system's robustness properties.

5.3.3.3 $\mathbf{K}_\infty$ Controller synthesis

After shaping the open loop frequency response to be compatible with the desired performance and robustness objectives a normalized *coprime* robustness optimization [GM89] was applied to $\mathbf{G}_s$ to synthesise a suboptimal (with 9 per cent scaling factor) controller $\mathbf{K}_\infty$ using the μ-Analysis and Synthesis Toolbox command $[\mathbf{K}_\infty, e_{max}] =$ ncfsyn$(\mathbf{G}_s, 1.09)$. The resulting controller had 20 states. When the maximum stability margin was $\epsilon_{max} = 0.40283$ the sub-optimal controller was synthesised for $\epsilon < \epsilon_{max}$. The achieved stability margin by $\mathbf{K}_\infty$ was $\epsilon = 0.3714$, and serves as an indicator of the level of compatibility of the achieved loop shapes with the design requirements. It also provides information that approximately 37 per cent uncertainty in the *coprime* factors of the shaped plant is allowed in the crossover frequency range. Figure 5.13 subplot a) illustrates the singular values of the synthesised controller $\mathbf{K}_\infty$.

Comparison with Figure 5.4 for **lsqDW** brings to evidence that $\mathbf{K}_\infty$ for control law

[16] It is reasonable to assume that those affected outputs are related to Pitch and Roll attitudes, since the extra measurements included were the rates of those attitudes.

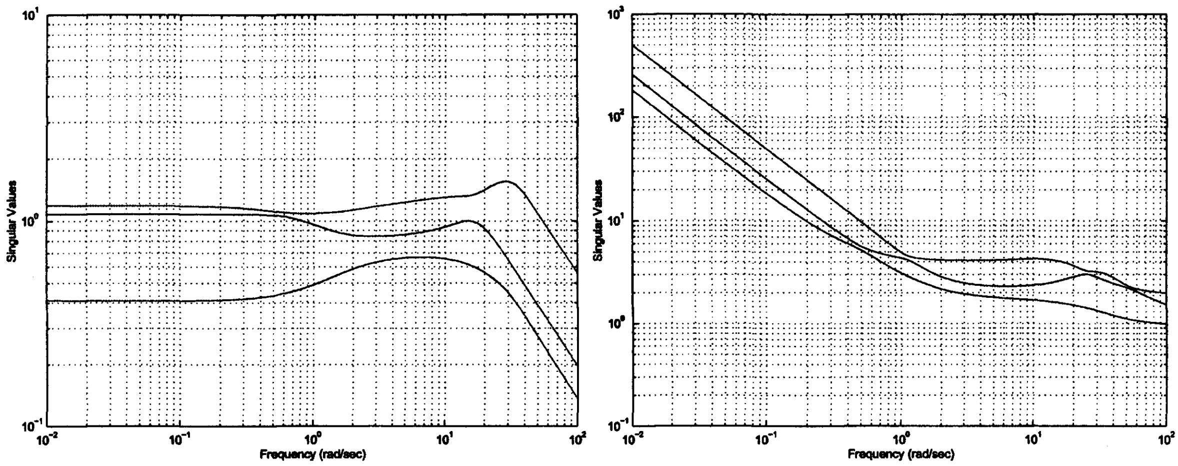

Figure 5.13: Singular values: **a)** Loop-shaping controller $\mathbf{K}_\infty$ **b)** Implemented controller $\mathbf{K}_{imp}$

lnsqDW provides higher gain at lower frequency, but does not modify the gain too much around the nominal plant crossover region.

We already know that the inclusion of $\mathbf{K}_\infty$ will have only limited effect on the designer specified loop shape when the stability margin is sufficiently high. The achieved stability margin was $\epsilon \gg 0.25$, and hence we shall anticipate that the distorting effect of the synthesized controller, denoted by $\mathbf{K}_\infty$, on the specified (desired) loop shape to be limited at low and high frequencies.

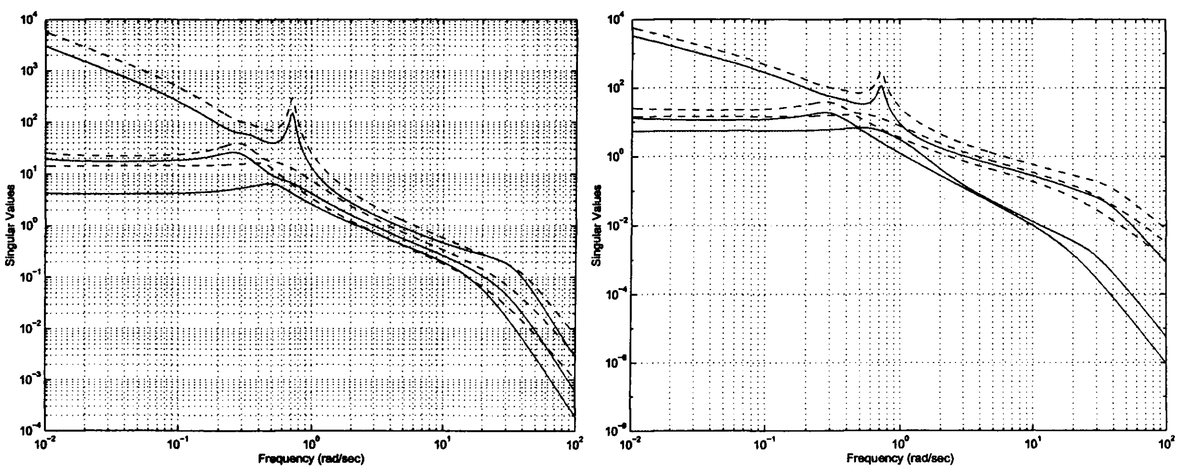

Figure 5.14: Shaped (*dashed*) vs. actual (*solid*) loop shapes: **a)** at the plant input $\mathbf{L}_i$ **b)** at the plant output $\mathbf{L}_o$

Shown in Figure 5.14 are the frequency responses of the actual loop shapes at the plant input, denoted by **KG**, and plant output, denoted by **GK**, where $\mathbf{K} = W_2\mathbf{K}_\infty\mathbf{W}_1$. It can be easily spotted that deterioration of the singular values at the plant input at low frequency is slightly higher than the change at high frequency; in particular, the minimum singular value $\underline{\sigma}(\mathbf{G}_s)$, which is thought to correspond to the slowest channel θ - Pitch attitude. However, the amount of change is limited. Inspection of the singular values of the actual loop shape at the plant output break point reveals that, $\sigma_2(\mathbf{L}_o)$ and $\sigma_3(\mathbf{L}_o)$ are most affected at high frequency. This mismatch is thought to be due to the absence of any dynamics in the weighting function at the plant output, i.e. the plant's row space $R(\mathbf{G}^*)$ is not modified by W_2. However, it was demonstrated through flight-test to be acceptable from a robustness point of view. This mismatch has also affected the crossover frequencies and will carry an impact on performance characteristics such as the speed of response, rise time and overshoot. It is of interest to note that inclusion of a dynamic post-filter shaping function in **1sqDW** has eliminated this off set. The controller synthesis law makes use of the secondary measurements (p, q) not present in the 1 Dof control law **(1sqDW)** reported in [PPTT02]. The structure of the 1 Dof controller architecture does not enable one to control and track 5 measurement outputs with only 3 control inputs. Hence, irrespective of the augmentation of the helicopter system with controller $\mathbf{K}_\infty$ with an attempt to enable $\mathbf{T}_{r \to y} = 1$, ensuring the $e_{ss} = 0$ will not be possible. Finally, to be implemented controller, $\mathbf{K}_{imp}$, resulted in 23 states with frequency response dynamics illustrated in Figure 5.13 subplot *b*). Comparison of Figure 5.13 with Figure 5.4 brings to evidence that $\mathbf{K}_{imp}$ for **1nsqDW** provides slightly more gain at low frequency region than $\mathbf{K}_{imp}$ of **1sqDW**, which is expected from the frequency dynamics (in the same range) of the loop-shaping controller $\mathbf{K}_\infty$ for **1nsqDW**. In the mid (crossover) frequency range **1nsqDW** $\mathbf{K}_{imp}$ controller gains are slightly lower than those of **1sqDW** controller, but ensure adequate and smooth transition through the crossover. Modification of the plant's (frequency) dynamics in the high frequency range is negligibly different than that provided by **1sqDW** controller. In conclusion, **1nsqDW** $\mathbf{K}_{imp}$ controller's main benefits lie in the low frequency and mid frequency regions.

5.3.4 Linear frequency domain analysis

5.3.4.1 Performance analysis

Inspection of some of the frequency domain indicators for performance, namely, the sensitivity functions $\mathbf{S}_i$ and $\mathbf{S}_o$ could serve as indicators for assessing the rate of disturbance attenuation at the plant input and output, reference tracking capabilities and input/output decoupling. As such $\mathbf{S}_o$ depicted in Figure 5.15 subplot *b*) reveals that although the disturbance rejection acting at the plant output is slightly better than disturbance rejection acting at the plant input, it is still not very satisfactory in channels corresponding to σ_1 and σ_2, which also correspond to channels with the lowest bandwidth. That is why reference signal tracking in those channels at low frequency may not be satisfactory[17]. It is important to point out that the singular values which are the largest and flat in the low frequency region correspond to the extra measurements, i.e rate outputs, which are not to be controlled and are not of concern in the analysis with performance objective.

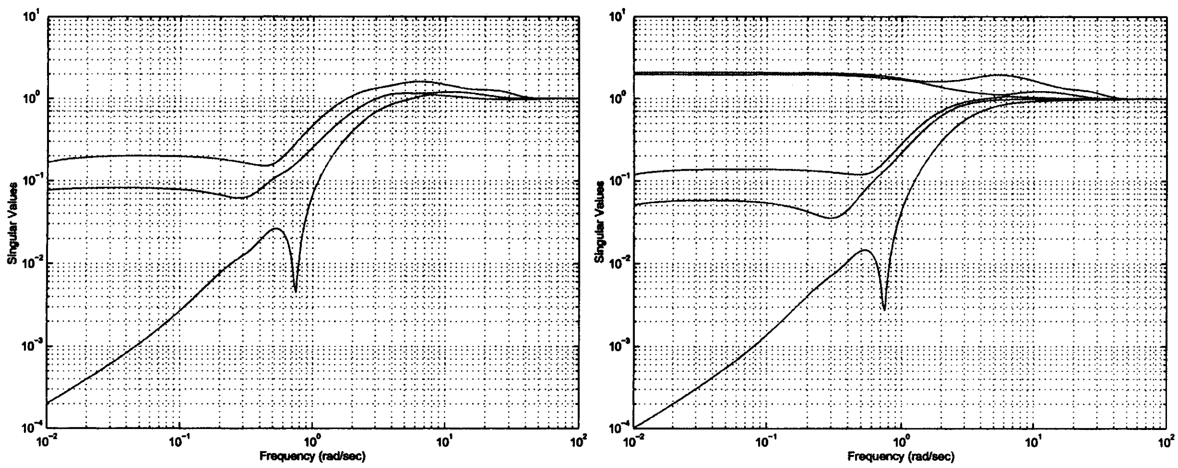

Figure 5.15: **a)** Input sensitivity $\mathbf{S}_i$ **b)** Output sensitivity $\mathbf{S}_o$ singular values

The size of $\overline{\sigma}(\mathbf{S}_i) = 1.61$ and $\overline{\sigma}(\mathbf{S}_o) = 2.0961$ provide also a measure, although sometimes conservative, of the smallest unstructured input and output inverse multiplicative uncertainty [SD91] which could destabilize the system. In this design case, at the plant input this has magnitude of $||\Delta_i||_\infty = \frac{1}{||\mathbf{S}_i||_\infty} = 0.6211$, and at the plant output $||\Delta_o||_\infty = \frac{1}{||\mathbf{S}_o||_\infty} = 0.4771$.

Gain and phase margins can be calculated on a loop basis using singular values but this will bring conservatism [YP90]. Both $\overline{\sigma}(\mathbf{S}_i)$ and $\overline{\sigma}(\mathbf{S}_o)$ frequency responses have peaks which are hard to remove partly due to the non-minimum phase of the plant and partly due to the condition dictated by the water-bed effect sensitivity formula [ZDG96] dictating that the integral of the natural logarithm of the sensitivity must remain zero in the frequency range considered. This implies that any attempt to remove the peaks will cause low frequency behaviour to deteriorate (and thus per-

[17] In helicopter control context high amplitude manoeuvres, such as Side step and Quick hop, usually have low frequency characteristics.

formance) which could destabilize the system.

Comparison with control law **1sqDW** brings to evidence that, **1nsqDW** controller augmented plant will be able to tolerate significantly more unstructured inverse multiplicative uncertainty than the plant augmented with **1sqDW** controller.

In Figure 5.16 one can see the frequency response of the closed loop system plant - augmented system- to disturbances acting at the plant input which, in closed loop transfer function terms, corresponds to $\|\mathbf{S}_o\mathbf{G}\|_\infty = 0.7479$.

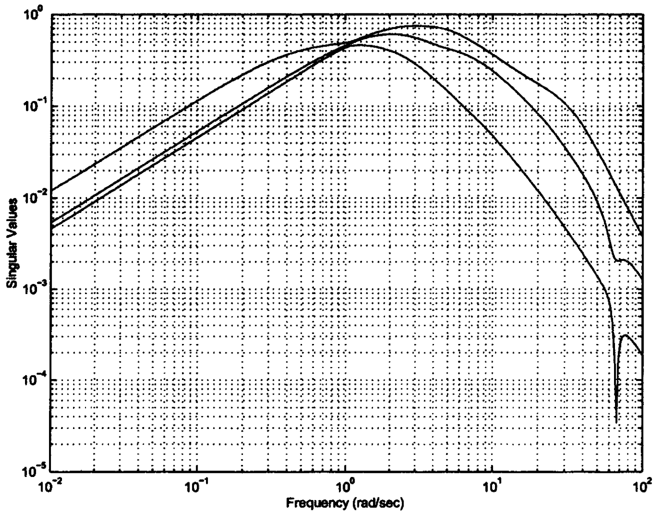

Figure 5.16: Singular values $\mathbf{S}_o\mathbf{G}$

It can be deduced that the control law ensures good attenuation of both low-frequency and high-frequency natured disturbances acting at the plant input, this is in comparison with **1sqDW**. The low-frequency attenuation is a result of the integral action introduced through the pre-filter weight- $\mathbf{W}_1$; the high-frequency attenuation comes because of the strictly proper nature of the shaped plant- $\mathbf{G}_s$.

While attenuation at the low and mid frequency ranges is seemingly better, in the high frequency range this is not the case. Better attenuation at high frequencies region observed in **1sqDW** came as a result of augmentation of $\mathbf{G}$ with the dynamic post weighting function $\mathbf{W}_2$. This ensured $\partial(\mathbf{G}_s)_{1sqDW} > \partial(\mathbf{G}_s)_{1nsqDW}$ and sharper attenuation (faster roll-off) at high frequencies; $\partial(\bullet)$ denotes the order of a plant.

5.3.4.2 Robustness analysis

By perusing Figure 5.17, a frequency plot of $\mathbf{T}_i$, it can be seen that roll-off at high frequency is relatively good which implies respectable robustness properties to multiplicative uncertainties, and satisfactory level of sensor noise attenuation. However, at the plant output (sensor level), roll-off at high frequency is not very good which translates to smaller tolerance to possible sensor noise. Note that robustness to uncertainties which can be modelled in multiplicative form is good.

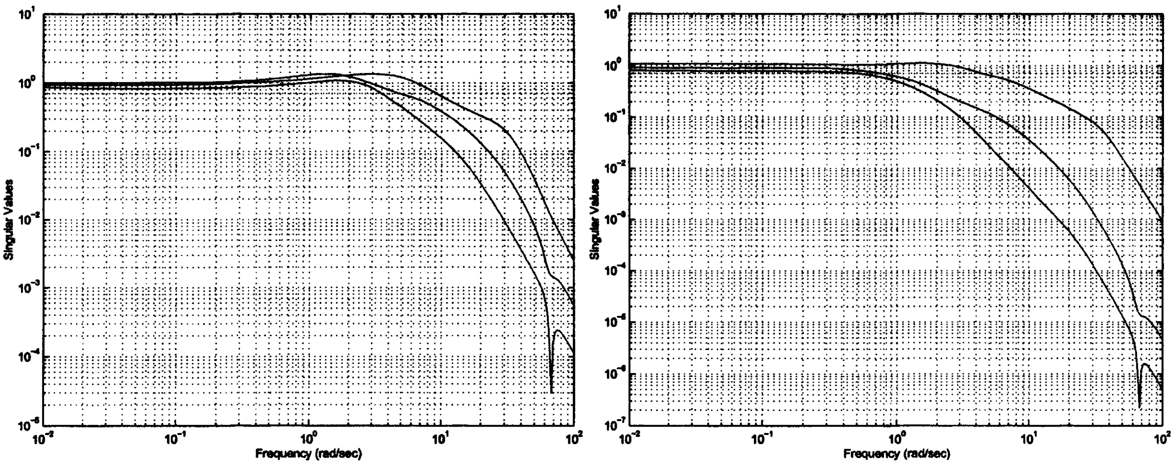

Figure 5.17: **a)** Input co-sensitivity $\mathbf{T}_i$ **b)** Output co-sensitivity $\mathbf{T}_o$ singular values

These judgements can be easily verified by inspecting Figure 5.17 where $||\mathbf{T}_i||_\infty = 1.3563$ and $||\mathbf{T}_o||_\infty = 1.1216$. These values, when compared with those derived from 5.8, point to better robustness (of the augmented system) to multiplicative type of uncertainty.

Figure 5.18 combines the Bode magnitude plots of $\overline{\sigma}(\mathbf{G})$ and inverse co-sensitivities. Subplot *a*) indicates that the augmented system can tolerate, at the plant input, multiplicative uncertainties up to 73 per cent, significantly larger than 1 Dof square plant augmented with diagonal weights. Whereas at the plant output, as depicted in subplot *b*), the system can maintain its stability even in the presence of output multiplicative uncertainties amounting to 89 per cent. This is by far more robust system compared to what **1sqDW** control law provides. In other words, the smallest unstructured multiplicative perturbation acting at plant input that could alter the system's stability is $||\Delta_i||_\infty = \frac{1}{||\mathbf{T}_i||_\infty} = 0.73$, whereas at the plant output this is $||\Delta_o||_\infty = \frac{1}{||\mathbf{T}_o||_\infty} = 0.89$. In the same Figure, one can establish comparison of the size of the tolerable (multiplicative) uncertainty at high frequencies in terms of the Bode magnitude of **G**. Slightly higher in magnitude multiplicative type of uncertainty can be tolerated at the plant output and in high frequencies.

Figure 5.19 *a*) shows the frequency response of the closed loop transfer function matrix, $\mathbf{KS}_o$, from output disturbances to plant input. Which gives a measure of the

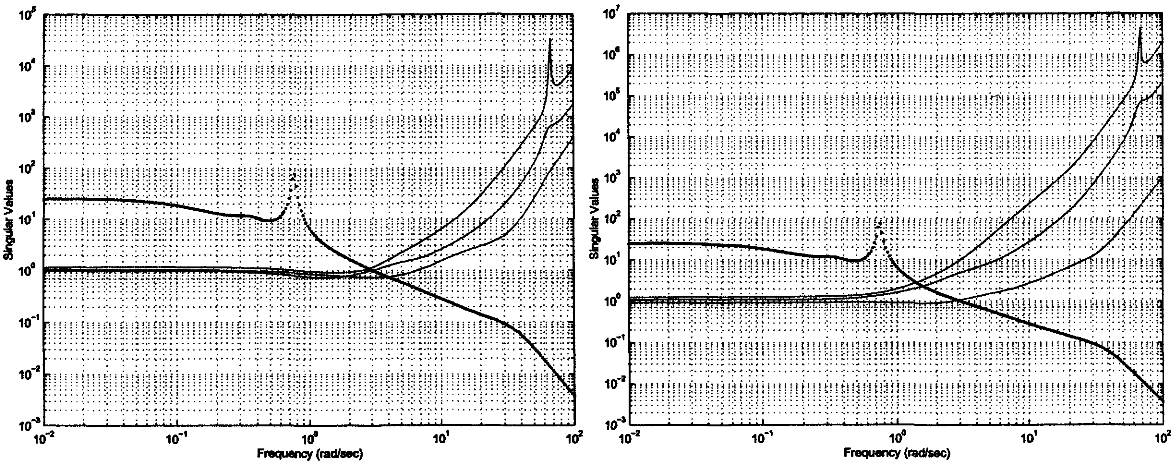

Figure 5.18: **a)** Inverse input co-sensitivity $\mathbf{T}_i$ **b)** Inverse output co-sensitivity $\mathbf{T}_o$ singular values vs. $\overline{\sigma}(\mathbf{G})$

actuator control activity in terms control signal amplitude; excessive actuator activity at low frequency is due to the control law's attempt to reduce the effect of ill conditioning in the plant.

Subplot *b)*, in the same figure, shows the allowable additive plant uncertainty as given by $(\mathbf{KS}_o)^{-1}$. For frequencies above 14 rad/sec the closed loop system tolerates a level of additive uncertainty much higher than the magnitude of the plant. Comparison with Figure 5.10 reveals that **1nsqDW** control law provides the closed loop system with higher robustness to additive type of uncertainty.

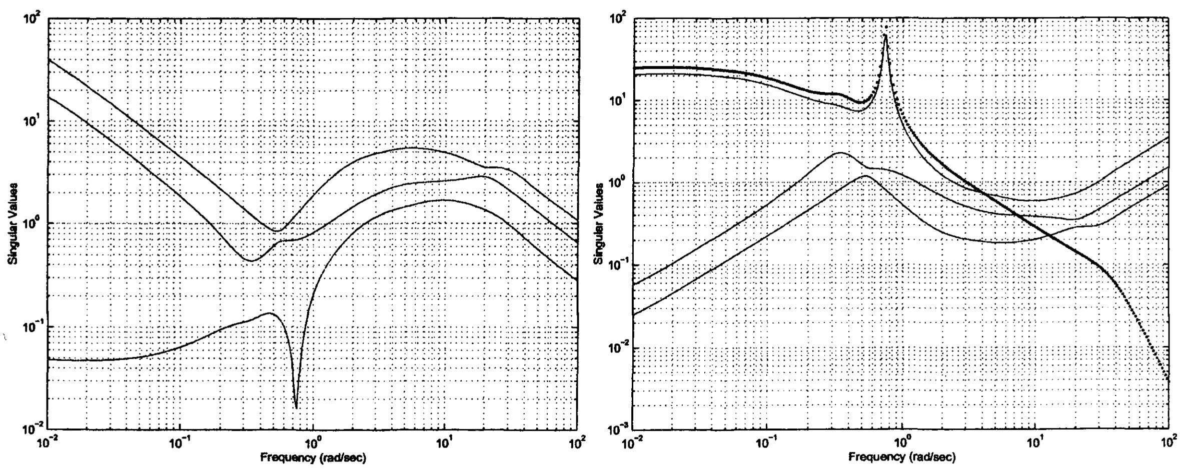

Figure 5.19: **a)** Actuator activity due output disturbance **b)** Maximum allowable additive uncertainty vs. $\overline{\sigma}(\mathbf{G})$

Shown in Figure 5.20 are the maximum singular values of the *coprime* factors of the nominal, reduced and shaped plants as a function of frequency. Interpretation of these graphs, as sources of valuable information for the augmented system's performance and robustness design properties, requires a careful consideration of inequalities (in Chapter 4 Theorem 4.3) approximating closed loop transfer functions with design variables in $\mathcal{H}_\infty$ loop-shaping design.

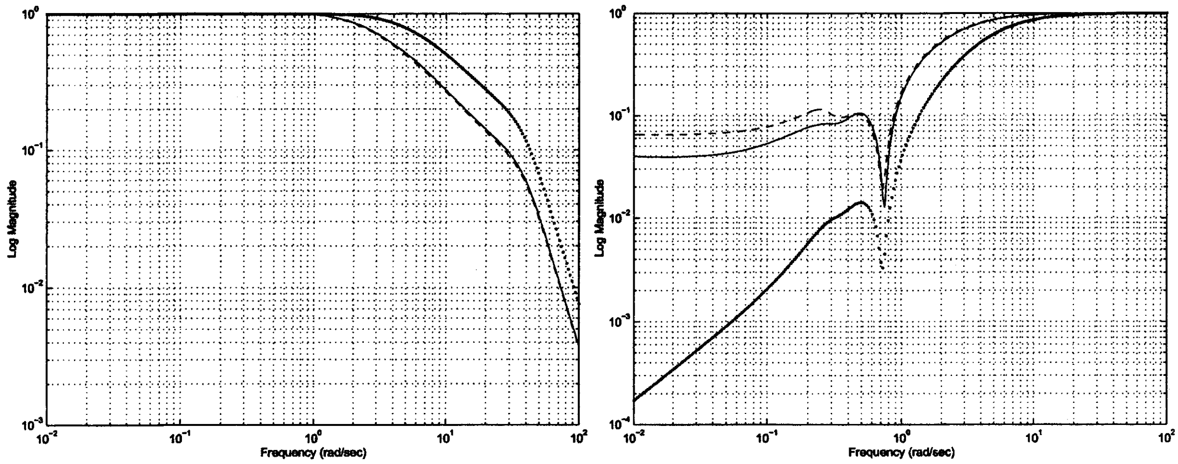

Figure 5.20: **a)** $\overline{\sigma}(\mathbf{N}_s)$ **b)** $\overline{\sigma}(\mathbf{M}_s)$ of shaped *(dotted)*, nominal *(continuous)*, reduced *(dashed)* plant

Several interesting issues can be addressed from a comparison of Figure 5.20 with Figure 5.11.

- Model reduction has more evident impact on the response characteristics of the square system.
- The designer can effectively consider shaping *coprime* factors of the nominal (or reduced) plant in the process of loop-shaping.

It is known that $\overline{\sigma}(\widetilde{\mathbf{N}}) \leq 1$ and $\overline{\sigma}(\widetilde{\mathbf{M}}) \leq 1$. The following presents a method of selecting $\mathbf{W}_1^{11}$ and $\mathbf{W}_2^{11}$ transfer functions.

1. Consider l.c.f of $\mathbf{G} = \widetilde{\mathbf{M}}^{-1}\widetilde{\mathbf{N}}$, we would like to attain a certain shape with $\sigma_1(\mathbf{G})$.
2. Plot the frequency response of $\overline{\sigma}(\widetilde{\mathbf{N}})$ and $\overline{\sigma}(\widetilde{\mathbf{M}})$ in the frequency range of interest.
3. At low frequency range $(0, \omega_l]$, $\omega_l < 2$ rad/sec, the frequency dynamics of $\overline{\sigma}(\mathbf{G})$ is entirely dictated by the dynamics of $\overline{\sigma}(\widetilde{\mathbf{M}})$. In this range $\overline{\sigma}(\widetilde{\mathbf{N}})$ acts as an all-pass filter, $\overline{\sigma}(\widetilde{\mathbf{N}}) = 1$, therefore attention can be devoted to shaping $\overline{\sigma}(\widetilde{\mathbf{M}})$ with a SISO weighting function $W_1^\star$, where $W_1^\star$ is a high-pass filter *bi-proper* and unit. This will effectively mean shaping of the frequency response of $\overline{\sigma}(\mathbf{G})$; denote

this shaping with $\Xi = W_1^{\star}\overline{\sigma}(\widetilde{\mathbf{M}})$. This step can be seen as shaping the sensitivity transfer function (in "*mixed*" sensitivity approach).

4. At high frequency range $[\omega_h, \infty)$, $\omega_l > 10$, $\overline{\sigma}(\widetilde{\mathbf{M}})$ acts as an all-pass filter, $\overline{\sigma}(\widetilde{\mathbf{M}}) = 1$, therefore one can consider shaping only $\overline{\sigma}(\widetilde{\mathbf{N}})$ in this frequency range with a SISO low-pass filter $W_2^{\star}$. With consideration of robustness properties this step can be thought of as shaping the co-sensitivity transfer function (in "*mixed*" sensitivity approach); define the shaped function with $\Upsilon = \overline{\sigma}(\widetilde{\mathbf{N}})W_2^{\star}$.

5. Ξ contains the low frequency dynamics, whereas Υ high frequency dynamics, of $\overline{\sigma}(\mathbf{G}_s)$, and $\overline{\sigma}(\mathbf{G}_s) = W_1^{\star}\overline{\sigma}(\widetilde{\mathbf{M}})\overline{\sigma}(\widetilde{\mathbf{N}})W_2^{\star}$. Therefore the dynamics of Ξ mostly will not affect the dynamics of Υ.

6. Transition through unity gain frequency range will be mostly affected by $W_1^{\star}$. The designer can modify $W_1^{\star}$ if the slope of $\overline{\sigma}(\mathbf{G}_s)$ is too steep.

7. Take the reciprocal of $W_1^{\star}$, this will be the element $\mathbf{W}_1^{11}$ of the weighting function matrix $\mathbf{W}_1$. Whereas, $W_2^{\star}$ transfer function will be the element W_2^{11} of $\mathbf{W}_2$.

8. Other elements of the pre and post weighting functions can be decided in the "*classical*" way. At this stage it is important to recall that bounds on the standard closed loop objectives are dependent either on $\overline{\sigma}(\widetilde{\mathbf{M}})$ ($\overline{\sigma}(\mathbf{M})$) or $\overline{\sigma}(\widetilde{\mathbf{N}})$ ($\overline{\sigma}(\mathbf{N})$), however, the shaping of other singular values of (normalized) *coprime* factors has importance from performance perspective.

5.3.5 Non-diagonal weights: Non-square nominal model- 1nsqNDW

The non-diagonal weight construction algorithm used herein, to facilitate the frequency shaping of the singular values of the system, is based on the one introduced in section 4.4.1.

Applications of non-diagonal weight construction algorithms reported in the literature [PG97], [PG02] and [Lan01] were applied to systems with equal number of inputs and outputs, i.e. square systems only. In view of the fact that square and non-square helicopter plants have different dimensions of the plant output space, the modified algorithm used herein allows post-filter weighting functions with higher dimensions (than pre-filter weighting functions) to be used in the construction of non-diagonal weighting functions for non-square plants $\mathbf{G}^{m \times n} \in \mathcal{RL}_\infty$. An alternative algorithm, presented as a matrix inequalities optimization problem in [Lan01], was designed to reduce significantly the onerous iterations made by the designer. However, due to time constraints imposed on the project the latter technique has not been implemented on the helicopter plant.

With the constructed diagonal weights (for control law **1nsqDW**) used in section 5.3.3 it was not possible to augment and increase only the minimum singular value of the shaped plant ($\underline{\sigma}(\mathbf{G}_s)$) without significantly affecting the shape of the other two singular values. Significant undesirable change in the loop shape was leading to a change in some performance criteria; for instance, the nominal tracking performance. This is why, to gain more authority in shaping $\sigma_i(\mathbf{G})$ motivated the very idea of using non-structured (full block) weights.

The non-diagonal weights could be constructed using directly the nominal scaled plant $\mathbf{G}$, or shaped with diagonal weights plant $\mathbf{G}_s$.

As non-diagonal weights are likely to be fully populated, i.e. full-block, the designer may not be able to decrease or increase the usage of one of the actuators in a straightforward and intuitive way [PG97] if $\mathbf{G}$ is used, hence, to maintain the transparency of loop-shaping, the shaped function $\mathbf{G}_s$ was preferred. Practice with weighting function design shows that it is always desirable to see if structured weights have met the requirements in the first place before taking the cumbersome task of semi-manual or LMI optimized non-diagonal weight design. This is mainly for two reasons: firstly, non-structured weights design is more time consuming and also computationally demanding, and secondly, the non-diagonal weights will inevitably bring about inflation in the number of states of the resulting controller, which may not be practical.

It must be born in mind that when constructing non-diagonal weights, the diagonalised weighted shaped plant $\mathbf{G}_s$, should be forced to achieve a high open loop bandwidth. In return, this will simplify the task to be accomplished by the non-diagonal weights.

5.3.5.1 Weighting function selection

The selection of weighting functions was made in view of the previously outlined objectives and with guidelines outlined in section 4.6.2. In this problem the frequency range $[\omega_l, \omega_h]$, was selected to be $[0.01, 100]$ rad/sec. This was the range where the continuous variations of the elements v_{jk}, ($j = 1, \ldots, m; k = 1, \ldots, n$) of $\mathbf{V}$ is to be ensured, and the fitting to each of those elements is to be performed. Some issues of concern with regards to the selection of this frequency range arose in the course of numerous design iterations in the construction, these are noted below:

◇ The selected frequency range must not be very large, as this will unnecessarily inflate the order of the fit to be performed on v_{jk}- the elements of $\mathbf{V}$. This will inevitably result in very high order of $\widehat{\mathbf{V}}$, and consequently of the non-diagonal weight[18].

◇ The designer must grid the frequency range of interest on the logarithmic scale to be sufficiently dense, preferably above 300 grid points. This will increase the preciseness of the fit and make the product. $\mathbf{V}^{*}\widehat{\mathbf{V}}$ close to identity. Too dense gridding will result in very high order of v_{jk}, and thus of $\mathbf{V}$ and the non-diagonal weight.

◇ The frequency range must include the target closed loop bandwidths and must not leave out necessary performance and robustness regions.

The selected frequency range ($[0.01, 100]$ rad/sec) was gridded with 300 grid points, and the shaped plant $\mathbf{G}_s$ was decided. Before decomposing $\mathbf{G}_s$ via *svd* and performing the fit on the elements v_{jk} of its right singular vector matrix, all integrators were factored out of $\mathbf{W}_1$. Figure 5.21 presents the singular values of the shaped plant augmented with a pre-filter without integrators.

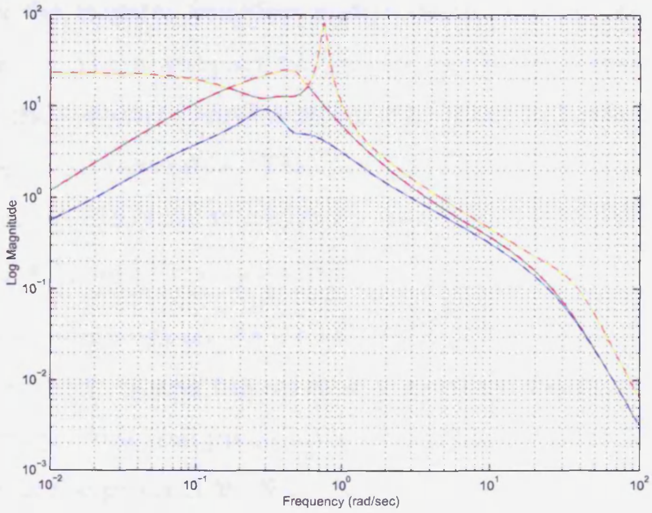

Figure 5.21: Plant augmented with integrators free pre-filter

[18]We are focusing on the construction of a non-diagonal pre-filter $\mathbf{W}_1$. Therefore, only the fitting of the elements of the right singular vectors of the transfer function matrix $\mathbf{V}$ will be considered.

The *co-spectral* factorization procedure in [Fra87] cannot accommodate integrators or near integrators. Therefore not only $\mathbf{W}_1$ should be free of integrators (or near integrators), but also the conditioning function Γ. Failure to comply with this requirement, leads to failure in computation of the non-diagonal weight with the co-spectral factorisation routine. $\mathbf{V}$ was extracted through *svd* of $\mathbf{G}_s$ and it was partitioned into elements $v_{j,k}$. Transfer functions of each element $v_{j,k}$ of $\mathbf{V}$ were fitted using command `optfitsys` [19]. Experience, on this complex problem, shows that fitting stable and minimum phase transfer functions in most cases results in rank deficiency even if the tolerance flag in the fit is set to be large ($0.5 <$ `tol` < 1). Therefore, no restrictions were imposed on the nature of the poles and zeros of the fitted transfer functions; the tolerance flag was set to `tol` $= 0.005$, no scaling was applied in the process of the fit.

Remark 5.3 *As accurate as possible fitting both in terms of phase and magnitude to each (SISO transfer function) element $v_{j,k}$ of $\mathbf{V}$ must be ensured. Failure to fit in one of the measures will impact on the co-spectral factorisation procedure, and will yield errors in the procedure, or generate non-diagonal weights with undesirable characteristics.*

After every fit the designer can reduce the order of each transfer function $\hat{v}_{j,k}$, or leave the reduction to be performed on the resulting right singular vectors transfer function matrix $\widehat{\mathbf{V}}$. The fit in this problem resulted in an unstable transfer function matrix $\widehat{\mathbf{V}}$ with 185 states, the distance quantified by $\|\mathbf{V} - \widehat{\mathbf{V}}\|_\infty = 0.00848$. Model reduction was performed on the transfer function matrix using Robust and Control Toolbox command `ohklmr`, as its counterpart `hankmr` in μ-Analysis and Synthesis toolbox can be used only if the system in hand is stable. The `sncfbal` resulted in the reduced system being close to undetectable. The command `ohklmr` was selected not only because it was applicable to unstable systems, but because it provided the smallest bound in terms of $\| \bullet \|_\infty$ and the ν-gap metric.

Finally, the reduced right singular vector matrix $\widehat{\mathbf{V}}_{red}$ had 75 states; three indicators were used as measures to assess the level of success of the fit. Superimposed frequency response (magnitude and phase) plots of the elements of $\mathbf{V}$ and $\widehat{\mathbf{V}}_{red}$ were examined. The value of the product $\mathbf{V} \cdot \widehat{\mathbf{V}}_{red}$ shown in Figure 5.22, along with $\overline{\sigma}(\widehat{\mathbf{V}}_{red} - \mathbf{V}) \ll 1$ which, in this case, was 0.00870. The smaller the value, the closer $\widehat{\mathbf{V}}_{red}$ will remain to $\mathbf{V}$, within, and outside the frequency range of interest $[\omega_l, \omega_h]$. Singular values

[19] This was coded in Matlab and created from μ-Analysis and Synthesis toolbox command `fitsys` to optimally fit a transfer function with the smallest order when given a tolerance.

of $\overline{\sigma}(\widehat{\mathbf{V}}_{red} - \mathbf{V})$ are depicted in Figure 5.23.

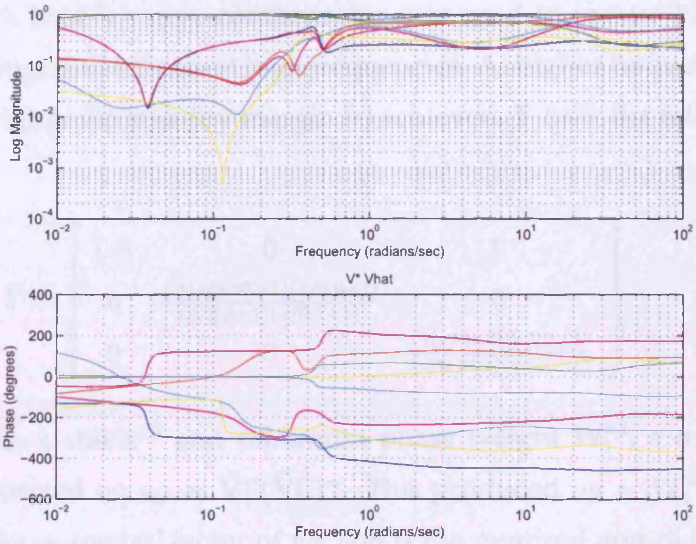

Figure 5.22: Frequency response of $(V \cdot \widehat{V}_{red})$

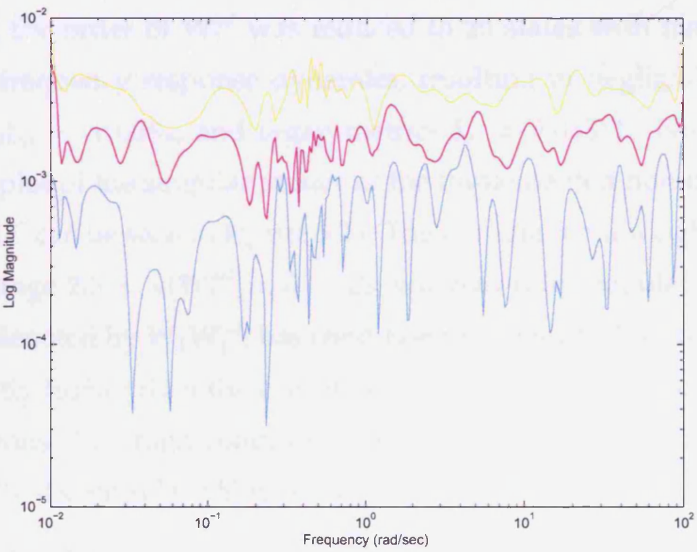

Figure 5.23: $\overline{\sigma}(V - \widehat{V}_{red})$

In highly accurate fit to $\mathbf{V}$, pre multiplying $\widehat{\mathbf{V}}$ with the *svd* of $\mathbf{G}_s$, $\mathbf{G}_s\widehat{\mathbf{V}} = U\Sigma\mathbf{V}^*\widehat{\mathbf{V}}$, and augmenting with Γ results in $\mathbf{G}_s\widehat{\mathbf{V}}\Gamma \simeq U\Sigma\Gamma$, $\sigma_i(\mathbf{G}\widehat{\mathbf{V}}\Gamma) \simeq \sigma_i|\gamma_i| = \Sigma_{G_s}^{desired}$.

Here $\Gamma \in \mathbb{R}^{3\times3}$, defined by the designer, is a diagonal transfer function matrix that reflects the desired conditioning, i.e. the dynamics, and the singular values of $\mathbf{W}_1^{nd}$, and each of its diagonal element ($\gamma_i, i = rank(\mathbf{G}_s)$) has direct impact on each singular value (σ_i) of the plant augmented with integrators free pre-filter.

Loop-shaping concepts carry through in the selection of transfer functions for the elements of Γ. A lead-lag type compensator was used to ensure high gain at low frequencies and high roll-off rate at high frequencies. At higher frequencies the higher the roll-off, the higher the stability margin (ϵ) achieved. Γ took the following form:

$$\Gamma = \begin{bmatrix} 0.8 & 0 & 0 \\ 0 & \frac{4.5(s/2.95+1)(s/0.6+1)}{(s/3.8+1)(s/0.1+1)} & 0 \\ 0 & 0 & \frac{17(s/2+1)(s/12+1)}{(s/0.2+1)(s/21+1)} \end{bmatrix}$$

In order to obtain a stable[20] and minimum phase weight $\mathbf{W}_1^{nd}$, a *co-spectral* factorization was performed on $vg = \widehat{\mathbf{V}}\Gamma(\widehat{\mathbf{V}}\Gamma)^{\sim}$. This produced $vg = \mathbf{W}_1^{nd}(\mathbf{W}_1^{nd})^{\sim}$, where $\mathbf{W}_1^{nd} \in \mathcal{RH}_\infty$ is the *co-spectral* factor of vg; and is the required non-diagonal pre-filter. $\mathbf{W}_1^{nd}$ accommodated 79 states. Since the states in $\mathbf{W}_1^{nd}$ directly influence the order of $\mathbf{K}_\infty$, to ensure that the $\mathcal{H}_\infty$ controller has a feasible number of states for practical implementation, the order of $\mathbf{W}_1^{nd}$ was reduced to 26 states with insignificant deterioration in the frequency response dynamics, resulting in negligible gap in terms of $\|\mathbf{W}_1^{nd} - \mathbf{W}_{1red}^{nd}\|_\infty = 0.0984$, and ν-gap metric- $\delta_\nu = 0.05311$. Now, $\sigma_i(\mathbf{G}_s\widehat{\mathbf{V}}\Gamma) \simeq \sigma_i(\mathbf{G}_s\mathbf{W}_1^{nd})$. The plot of the singular values of the implemented non-diagonal weight part $\sigma_i(\mathbf{W}_1^{nd})$ and Γ can be seen in Figure 5.24. The non-diagonal weight has condition number in the range $2.5 < \kappa(\mathbf{W}_1^{nd}(j\omega)) < 22$, whereas fully populated unstructured pre-filter $\mathbf{W}_1^{full}$, denoted by $\mathbf{W}_1\mathbf{W}_1^{nd}$, has condition number of $3.5 < \kappa(\mathbf{W}_1^{full}(j\omega)) < 24$ and is significantly higher than the condition numbers of the previous control law's weighting functions. The high condition number reflects on its property to modify more substantially the singular values of the shaped plant at low frequencies.

It is evident, and not surprising to see, that $\sigma_i(\mathbf{W}_1^{nd})$ are aligned with $\sigma_i(\Gamma)$, since $\mathbf{W}_1^{nd} \simeq (\widehat{\mathbf{V}}\Gamma)$. These two equalities analysed together are compatible with $\|\widehat{\mathbf{V}}\|_\infty \approx I$, and therefore it can be said that $\widehat{\mathbf{V}}$ also exhibits properties of a unitary matrix in the mid to high frequency ranges. Thus, its left/right multiplication with a transfer function matrix does not alter the final result: $\widehat{\mathbf{V}}\Gamma \simeq \mathbf{W}_1^{nd}$.

Figure 5.25 depicts the singular values (as a function of frequency) of the tentative non-diagonal weight -dashed- together with the (nominal) plant's singular values - continuous- shaped with the diagonal weight. Perusing the frequency response Bode magnitude plot of the non-diagonal weight, it is obvious that the dynamics of one

[20]The use of unstable weights in controller synthesis have been documented in [Mei95].

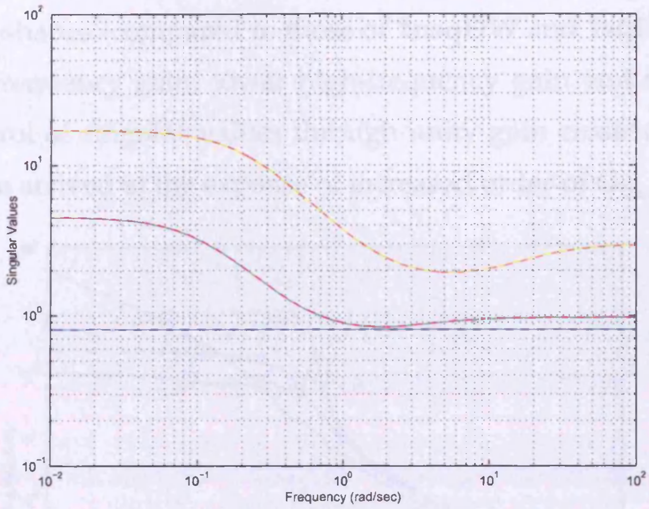

Figure 5.24: Non-diagonal weight and Γ

of the channels (of the plant) was aimed to be preserved throughout the frequency range; whereas the dynamics of the other two channels were augmented mainly in the low frequency range, preserved around the crossover and slightly altered in terms of roll-off at high frequency.

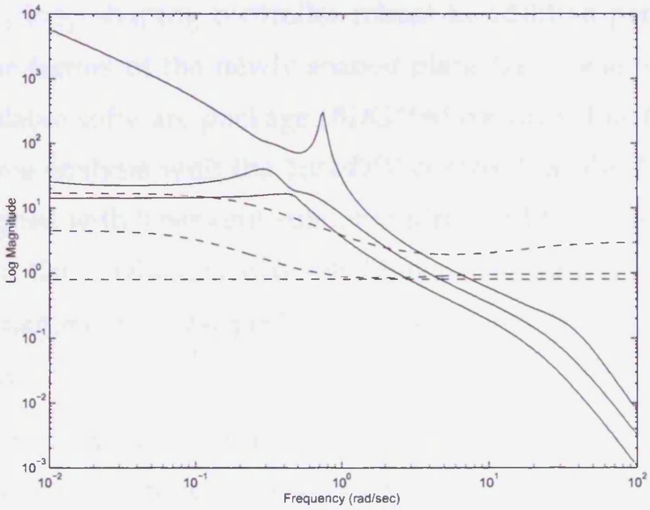

Figure 5.25: Diagonally weighted plant vs tentative non-diagonal weights

Integrators that had been factored out of $\mathbf{G}_s$ prior to the *svd* decomposition and fitting procedures were now put back into $\mathbf{W}_1$. Singular values of the newly shaped (weighted) plant, with diagonal and non-diagonal pre-compensator, has now acquired the following form $\mathbf{Gs}_{new} = W_2\mathbf{G}\mathbf{W}_1\mathbf{W}_1^{nd}$. Its frequency response Bode magnitude plot is illustrated in Figure 5.26. The transition rates of singular values through unity crossover were between 24-25 db/dec. As anticipated **1nsqNDW** control law lead to improved loop-shapes (compared to those of **1nsqDW** and **1sqDW** control laws): with higher low-frequency gain, lower high-frequency gain and tighter (and relatively easier) control of singular values through unity gain crossover. However, all these benefits were arrived at the expense of increased order of $\mathbf{Gs}_{new}$ with 43 states.

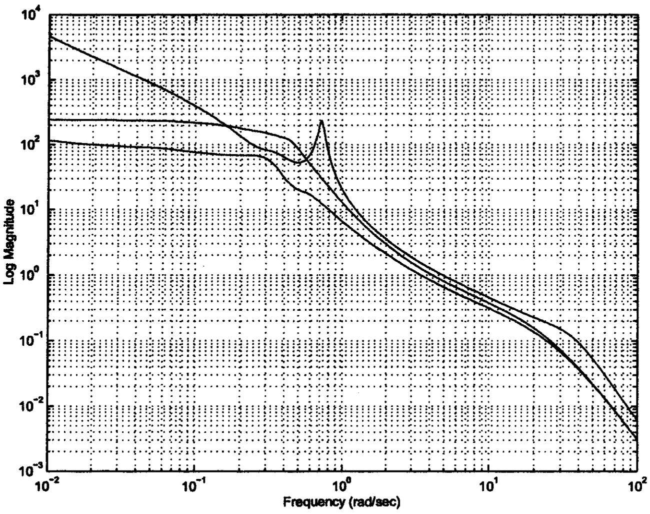

Figure 5.26: Shaped plant: with diagonal and non-diagonal loop-shaping pre-filters

A sub-optimal $\mathcal{H}_\infty$ loop-shaping controller robust to additive perturbations to the normalized *coprime* factors of the newly shaped plant $\mathbf{Gs}_{new}$ was synthesized using commercially available software package [BDG+98] command `ncfsyn`. In order to allow a comparative analysis with the **1nsqDW** control law, the **1nsqNDW** control law was also designed with 9 per cent suboptimality condition. The stability margin achieved was $\epsilon = 0.42097$, which is relatively higher than control law **1nsqDW**, with exactly the same diagonal pre and post compensators but lacking the non-diagonal weighting function.

The controller $\mathbf{K}_\infty$ initially had 43 states, but after an iterative reduction process using *Hankel* norm approximation they were successfully reduced to 20 states with negligible deterioration in the open loop gain and design properties. The closeness between original and reduced controllers was mathematically measured by ν-gap metric $\delta_\nu = 0.007065$ which, being very small ($\delta_\nu \ll 1$), serves as an indicator of closely matching frequency response properties of the closed loop of $\mathbf{K}_\infty$ and $\mathbf{K}_{\infty_{red}}$. The latter also suggests that the distance between both, if measured on the Riemann sphere would also be small [Vin00].

Singular values of $\mathbf{K}_\infty$ as a function of frequency can be seen in Figure 5.27.

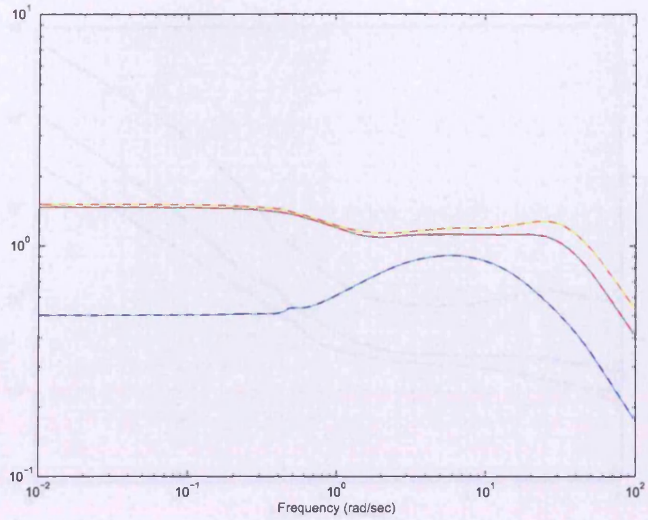

Figure 5.27: Loop shaping controller $\mathbf{K}_\infty$

The resulting controller to be implemented $\mathbf{K}_{imp}$ had 49 states, which is extremely high and practically infeasible for our helicopter plant. After optimal *Hankel* norm approximation its order was successfully reduced to 30 states, with corresponding $\delta_\nu = 0.161989$ as a measure to gauge the closeness of the frequency responses between the original and reduced controllers. The singular values of the original and reduced order- implemented controllers- $\mathbf{K}_{imp}$ are depicted in Figure 5.28. It is evident that the frequency response complies with the requirements for good performance ($\underline{\sigma}(\mathbf{K}_{imp}) \gg 1$), at some low frequency region. A careful look will also reveal that the requirement for good robustness and satisfactory sensor noise rejection, namely ($\overline{\sigma}(\mathbf{K}_{imp}) \leq 3$), has not been satisfied for all channels. $\sigma_{2,3}(\mathbf{K}_{imp}) \leq 3$ indicates good robustness properties in two of the (controlled) channels, whereas $\overline{\sigma}(\mathbf{K}_{imp}) > 3$ indicates high gain at the frequency region where the dynamics of the plant is not precisely captured through modelling. The high controller gain at high frequency region can be taken as a frequency domain explanation to the pilot's comments of unstable behaviour of the helicopter upon engaging the control law **1nsqNDW**- to this we shall return to later.

Actual loop-shapes (in terms of singular values) at the plant output (**GK**), plant input (**KG**) and desired loop shapes are all superimposed and reflected in Figure 5.29. Comparison with Figure 5.14 of control law **1nsqDW** indicates that the non-diagonal weight, as expected, has notably contributed to the reduction of mismatch between desired and actual loop-shapes at low frequency region and mid-frequency region, and increase in the bandwidths. Note particularly around the crossover region at the

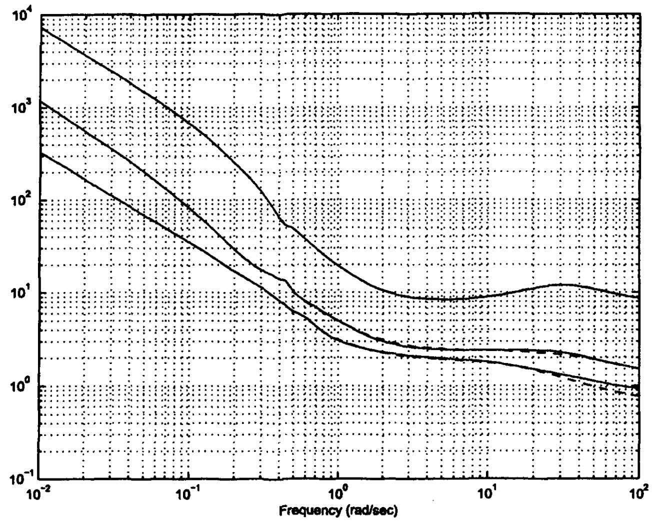

Figure 5.28: Implemented controller $\mathbf{K}_{imp}$: original (*continuous*) vs. reduced (*dashed*) order

plant input where the non-diagonal weight was applied. Additionally, when considered together with the other control laws' $\mathbf{L}_i$ and $\mathbf{L}_o$ vs. $\mathbf{G}_s$ characteristics it brings to evidence that unless dynamic (diagonal or non-diagonal) weighting is applied at the plant output the significant mismatch observed between desired and actual loop-shapes cannot be eliminated.

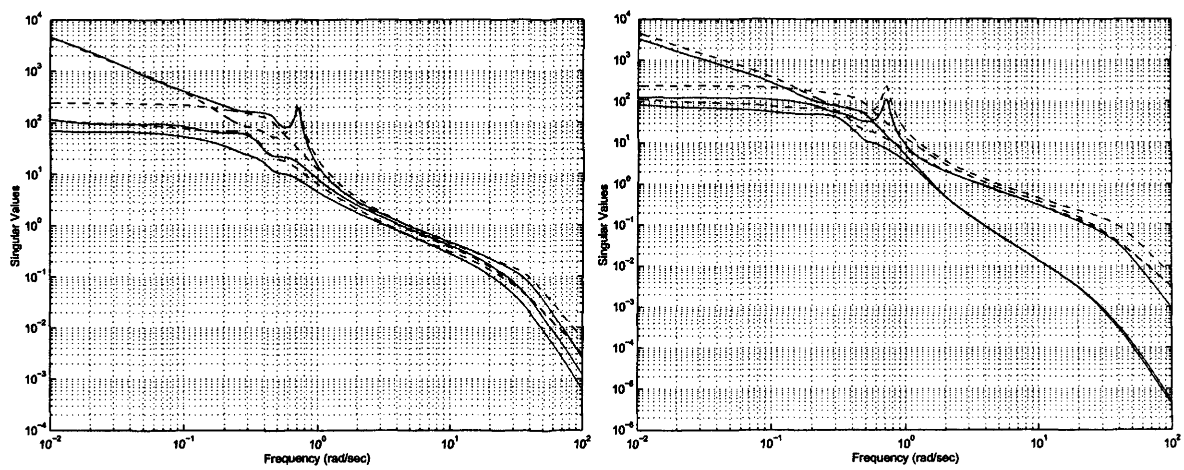

Figure 5.29: Shaped (*dashed*) vs. actual (*solid*) loop shapes: **a)** at the plant input $\mathbf{L}_i$ **b)** at the plant output $\mathbf{L}_o$- **1nsqNDW**

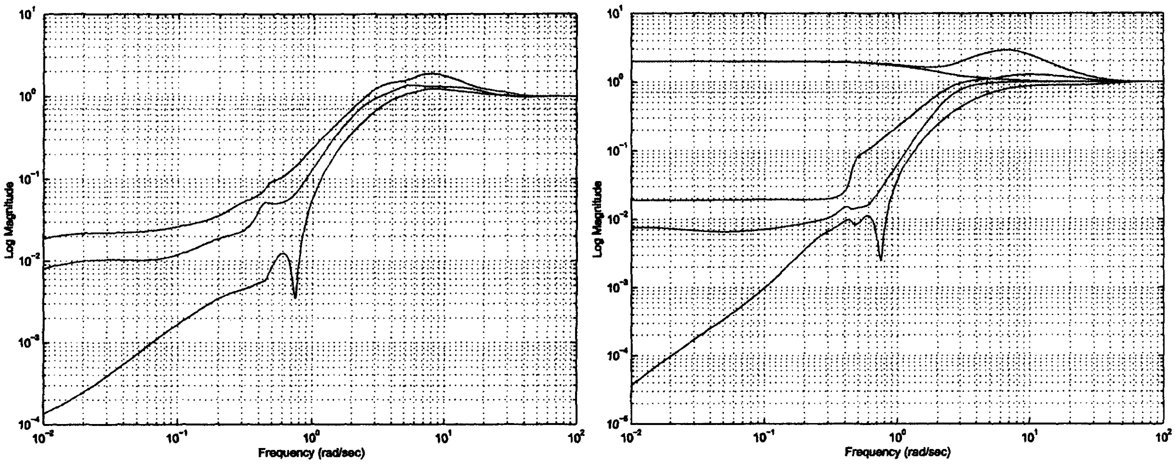

Figure 5.30: a) Input sensitivity $\mathbf{S}_i$ b) Output sensitivity $\mathbf{S}_o$

5.3.6 Linear frequency domain analysis

5.3.6.1 Performance analysis

Figure 5.30 shows the closed loop system's input $\mathbf{S}_i$ and output $\mathbf{S}_o$ sensitivity transfer functions frequency responses as indicators of nominal tracking performance and the ability to reject disturbances at plant inputs and outputs. We can observe that the disturbance rejection both at plant input and plant output has improved significantly. The improvement is much more notable for performance properties related with the plant input space, i.e. $\mathbf{R}(\mathbf{G}_s)$, where the gains and directions of inputs were effected by introduction of non-diagonal weighting function. A non-diagonal post-filter was not employed for several reasons: it was thought that the roll-off was sufficiently good; it would have inflated the order of the shaped plant and, consequently the controller. This, in the first place, would make construction of a practically feasible controller even more challenging, and above all, it would not facilitate a ground for objective comparative analysis with control law **1nsqDW** where the post-filter weighting function was kept constant.

These alternative design properties came at the expense of higher peaks of the sensitivity transfer functions with $||\mathbf{S}_i||_\infty = 1.8848$ and $||\mathbf{S}_o||_\infty = 2.8881$ indicating that the closed loop system is more vulnerable to unstructured inverse multiplicative perturbations at the plant output, which with size $||\Delta_o||_\infty = \frac{1}{\overline{\sigma}(\mathbf{S}_o)} = 0.3462$ may destabilize the system. At the plant input, the smallest possible perturbation of the same type that can destabilize the closed loop system would be with size $||\Delta_i||_\infty = \frac{1}{\overline{\sigma}(\mathbf{S}_i)} = 0.5306$.

An additional frequency domain measure for assessing the performance of a linear system is the closed loop transfer function $\mathbf{S}_o\mathbf{G}$, which illustrates the ability of the augmented (with control system law) helicopter to tolerate the effect of plant input disturbances on the outputs. Small values of $\overline{\sigma}(\mathbf{S}_o\mathbf{G})$ (in all channels) in Figure 5.31 reveal a notable improvement in the plant's ability to tolerate the effect of input disturbances on its outputs in comparison with Figure 5.16. The improvement is evident at low frequencies and is due to the integral action introduced by $\mathbf{W}_1$, whereas improvement in high frequencies is a result of the strictly proper nature of the plant. The order of $\mathbf{S}_o\mathbf{G}$, $\partial(\mathbf{S}_o\mathbf{G})$, is bigger than any other $\partial(\mathbf{S}_o\mathbf{G})$ in any of the presented control laws, and therefore it is expected that it will roll-off faster.

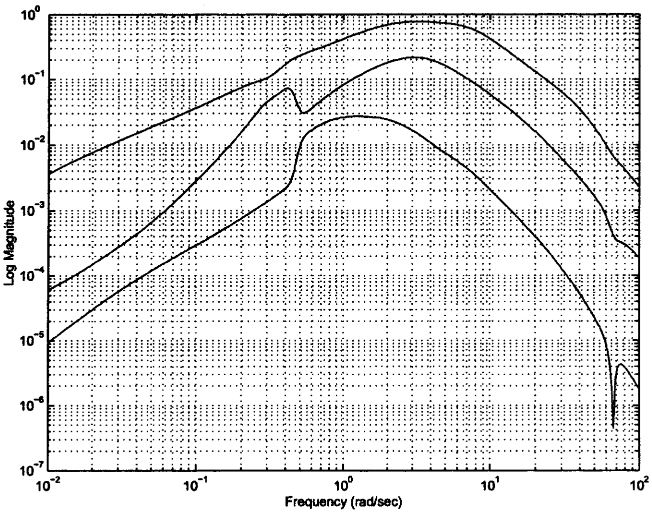

Figure 5.31: Singular values $\mathbf{S}_o\mathbf{G}$

5.3.6.2 Robustness analysis

In the process of any modelling, errors and omissions of not so well understood phenomena will inevitably occur. This is why, guarantees in robustness of stability become an indispensable characteristic of any control law, particularly those awaiting implementation.

Input ($\mathbf{T}_i$) and output ($\mathbf{T}_o$) complementary sensitivities' frequency responses Bode magnitudes are illustrated in Figure 5.32.

These provide information about the system's robustness to noise on the sensors and to uncertainties modelled as multiplicative perturbations at the plant input and plant output. The system seems most vulnerable to modelling errors in the frequency band 1 to 10 rad/sec and particularly at the plant input. Note $||\mathbf{T}_i||_\infty = 1.5755$ and $||\mathbf{T}_o||_\infty =$

1.3009, which are both acceptable [SP96].

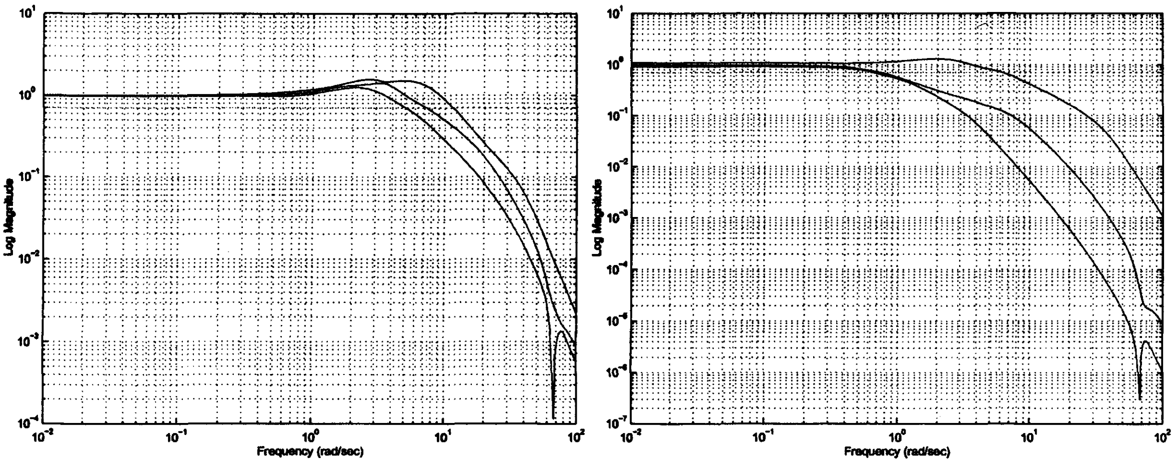

Figure 5.32: **a)** Input co-sensitivity $\mathbf{T}_i$ **b)** Output co-sensitivity $\mathbf{T}_o$

At the plant input the closed loop compensated system exhibits slightly better robustness at high frequencies compared to **1nsqDW** control law, however, the peak of $\|\mathbf{T}_i\|_\infty$ is slightly larger which affects the tolerable unstructured multiplicative uncertainty. At the plant output, the augmented system exhibits similar robustness properties to **1nsqDW** control law, but with slightly larger peak around the closed loop bandwidth which reduces the level of allowable output multiplicative uncertainty around the bandwidth.

Figure 5.33 provides information about the magnitude of maximum allowable unstructured input and output multiplicative uncertainties that can be tolerated by the augmented, with control law **1nsqNDW**, helicopter system. Straightforward algebraic manipulations give $\|\Delta_i\|_\infty \leq \frac{1}{\|T_i\|_\infty} = 0.6347$ as magnitude of the smallest unstructured multiplicative uncertainty at the plant input that can destabilize the system, whereas at the plant output this is slightly higher (higher robustness) $\|\Delta_o\|_\infty \leq \frac{1}{\|T_o\|_\infty} = 0.7687$. By scrutinising the plots one can also provide an alternative, simpler and visually perceivable interpretation of the constraints: any uncertainty in unstructured multiplicative uncertainty form, with magnitude below the lowest singular value ($\underline{\sigma}$) curve will be tolerated by virtue of robustness properties of the augmented plant. Whereas any uncertainty magnitude value above the $\underline{\sigma}$ curve will result in stability degradation. Both in subplot *a*) and subplot *b*) the Bode magnitude plot of $\overline{\sigma}(\mathbf{G})$ indicates that at high frequencies unstructured uncertainties larger than the magnitude of the plant can be tolerated. This tolerance is slightly better at the plant input; it is evident from the Figures that the higher the roll-off of the co-sensitivity the larger the area below the minimum singular value $\underline{\sigma}$, and hence increased robustness.

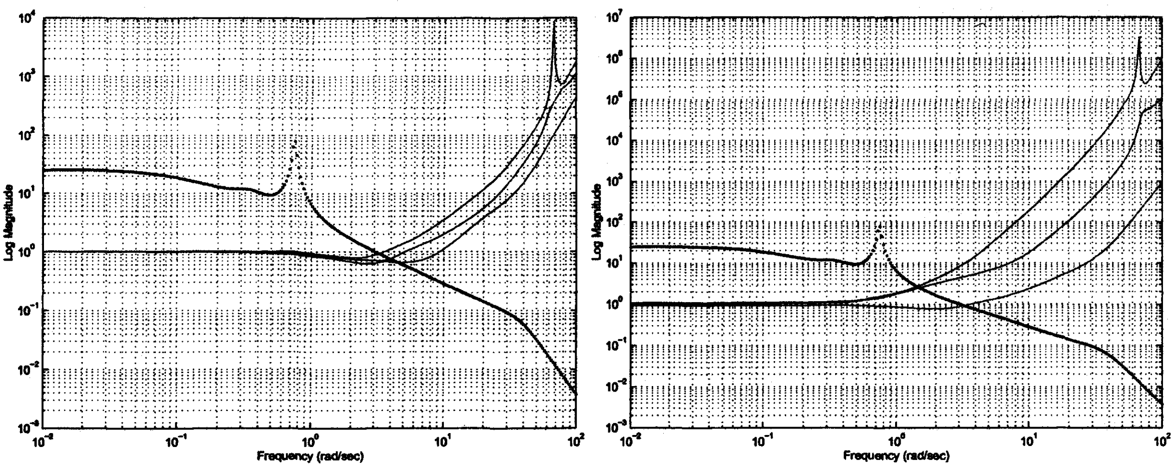

Figure 5.33: **a)** Inverse input co-sensitivity $\mathbf{T}_i$ vs. $\overline{\sigma}(\mathrm{G})$ **b)** Inverse output co-sensitivity $\mathbf{T}_o$ singular values vs. $\overline{\sigma}(\mathrm{G})$

To prevent actuators reaching their limits it is of particular interest to monitor the control signals for use of excessive control effort. One way, although conservative, is by frequency domain inspection of the actuator activity due to output disturbances; this can be performed by perusing subplot *a*) in Figure 5.34.

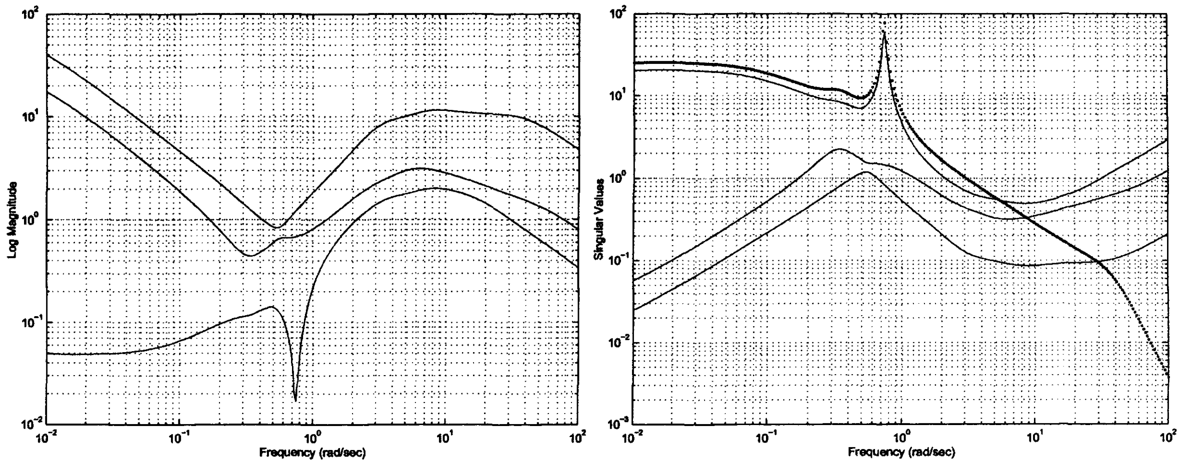

Figure 5.34: **a)** Actuator activity due output disturbance **b)** Maximum allowable additive uncertainty vs. $\overline{\sigma}(\mathrm{G})$

Subplot *b*) of the same Figure serves as a complementary indicator of the system's robustness, as it reveals information about the system's ability to tolerate unstructured uncertainty represented in additive form. While the system exhibits comparable levels of robustness to additive uncertainty at low and high frequencies when compared with control law **1nsqDW**, one of the channels' frequency responses indicates an excessive actuator activity within the bandwidth, and with a local magnitude peak of slightly above 10. As we shall see later, this coincides with the pilot comments of oscillatory divergent attitude and increased actuator activity given in the flight testing of control law **1nsqNDW** which was reported unstable. The yaw channel response has always been the fastest[21]; the structure of the non-diagonal weights were devised such that to attain the objective of increasing the gains and bandwidths in required channels (ϕ, θ), and decreasing in yaw. However, the nature of the final model reduction of the controller to be implemented, $\mathbf{K}_{imp}$, in an (unprecedented) effort to bring it to practically feasible control law is thought to have acted as a main contributing factor in modifying undesirably the structure of $\mathbf{K}_{imp}$. This, in the author's opinion, exacerbated the actuator gain in the yaw channel, and acted as destabilizing factor. It is important to emphasize that model reduction success indicators were within the acceptable limits.

Actuator activities will be further analysed in the time domain through simulated flight manoeuvres in the next chapter.

As mentioned in section 4.9 the order of controller to be accommodated and implemented on-board computer of the *Bell 205* was limited to 30 states. This imposed a hard constraint to meet with the awareness that reduction by 19 states, i.e. from 49 to 30 states, would inescapably deteriorate frequency and time domain characteristics of the controller. Recalling the equality that derives the order of the controller to be implemented ($\partial(\mathbf{K}_{imp})$) in the standard 1 Dof $\mathcal{H}_\infty$ loop-shaping controller architecture, but with non-diagonal weight objectives, we have:

$$\partial(\mathbf{K}_{imp}) = \partial(\mathbf{G}_{red}) + 2\partial(\mathbf{W}_1) + 2\partial(\mathbf{W}_1^{nd}) + 2\partial(W_2). \tag{5.5}$$

Given the order of the components within the $\mathbf{K}_{imp}$: $\partial(\mathbf{G}_{red}) = 14$, $\partial(\mathbf{W}_1) = 3$, $\partial W_2 = 0$, where *∂-indicates the order of a system*, one can easily arrive at inequality $\partial(\mathbf{W}_1^{nd}) \leq 5$ dictating the order of the *non-diagonal* weight.

Displayed in Figure 5.35 are frequency responses of the original, reduced, diagonally weighted and non-diagonally weighted plant's normalized left and right *coprime* factors. It becomes evident that the shaped plant has significantly improved singular value shapes of the *coprime* factors. In view of the high stability margin (ϵ) that $\mathbf{K}_\infty$ has guaranteed, one can interpret Figure 5.35 subplot a) and subplot b) together with

[21] It is natural to associate the singular value that gives the highest bandwidth with the fastest channel.

Theorem 4.3. After some very simple algebraic calculations on relevant closed loop transfer functions which are setting bounds on performance and robustness objectives, it can be deduced that $\overline{\sigma}(\mathbf{N}_s) \ll 1$ at high frequencies imparts good robustness and good sensor noise mitigation, whereas $\overline{\sigma}(\mathbf{M}_s) \ll 1$ at low frequencies indicates good performance: tracking, disturbance attenuation, input/output decoupling.

In conclusion, and with a certain degree of confidence, one can also say that $\mathbf{W}_1^{nd}$ had brought the anticipated effect on the singular values of the shaped plant, $\sigma_i(\mathbf{G}_s)$, and most closed loop objectives. Unfortunately this affect did not reflect on to the control law's flight-test performance and robustness characteristics. This can be explained by considering the amount of model reduction (of 53 states) performed on $\mathbf{W}_1^{nd}$- which is thought to have altered the "*desired*" structure of the non-diagonal weight although the distance in terms of infinity norm and ν gap-metric (δ_ν) did not indicate that. The distance measured in terms of the infinity norm and the δ_ν-gap metric may not always indicate accurately the degree of alteration in the dynamics of a given system (or parameter). In these cases point by point frequency analysis of the δ_ν-gap metric have to be conducted.

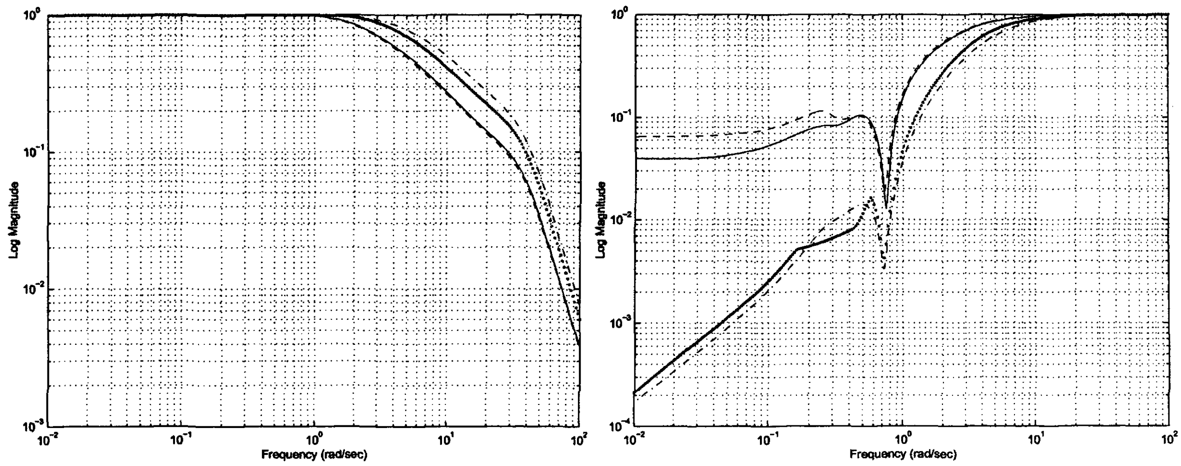

Figure 5.35: **a)** $\overline{\sigma}(\mathbf{N}_s)$ **b)** $\overline{\sigma}(\mathbf{M}_s)$ of shaped (*dotted*), nominal (*continuous*), reduced (*dashed*) plant

5.4 Two degree-of-freedom control law synthesis

Objectives in the multivariable helicopter control law design comprise of a blend of time domain performance and robustness specifications, which are best addressed in the frequency domain. A special controller architecture that facilitates an explicit inclusion of both of the main requirements (robustness and performance) of a controller synthesis, and also provides the designer with a choice to weight their impact in the design is the so called two degree-of-freedom controller.

In this control system architecture the designer can address disturbance rejection (along with robust stability) and time domain performance requirements in two separate stages. The objectives will be handled by two different controllers $\mathbf{K}_1$ and $\mathbf{K}_2$, which can be designed in one or two steps.

The feedback controller $\mathbf{K}_2$ is to meet disturbance rejection and robust stability specifications, whereas the pre-compensator $\mathbf{K}_1$ is to cater for the time domain (response) specifications of the closed loop.

Two degree-of-freedom controllers can be thought of as generalization of the one degree-of-freedom[22] controller architectures with the notion of robust stability carrying through from 1 Dof $\mathcal{H}_\infty$ loop-shaping to 2 Dof architecture. A prescribed level of robust stability is guaranteed via the normalized *coprime* factor robust stabilization procedure, while at the same time the closed loop transfer function from references to outputs (see Figure 4.9) is forced to approximate the transfer function matrix representing an ideal time response (model) $\mathbf{T}_{ref}$ characteristics. The two-degree-of-freedom architecture also has an estimator based structure [Wal96].

The design of 2 Dof control laws due to their aforementioned properties have received significant attention (particularly) in the aerospace control community with applications to both fixed wing aircraft [HG93], [PG02] and rotary-wing aircraft [PSW+99], [PPTT02], [PPT+05].

5.4.1 Design stage

The nature of the helicopter control system design problem brings demanding time response specifications, which with the existing 1 Dof structure are difficult to translate to the frequency domain.

Translating time domain requirements to frequency domain specifications on $\mathbf{L}_o$ via the loop shape $\mathbf{G}_s$ is a non-trivial task. To do this, engineers mostly rely on their engineering intuition which evolves with experience of using the loop-shaping concepts. There are several difficulties involved in acquiring a desired loop shape of $\mathbf{G}_s$: partic-

[22] The expression *degree of freedom's* meaning within control theory context is different from its name sake in physical/mechanical context.

ularly in MIMO systems, it is not very obvious as how individual transfer functions $\mathbf{L}_{o_{i,j}}$, $i = j$ affect for example $\mathbf{T}_{r \to y} = (I - \mathbf{L}_o)^{-1}\mathbf{L}_o$. That is why shaping $\mathbf{L}_{o_{i,j}}, i = j$ (for example) becomes a very challenging engineering task. The designer may not always be able to accurately and robustly shape the transfer function $\mathbf{T}_{r \to y}$ in the view of time domain design specifications embedded in $\mathbf{T}_{ref}$, this may be due to lack of transparency in the chain interactions from $\mathbf{G}_s$ to $\mathbf{T}_{r \to y}$. In summary: by shaping the nominal plant with pre/post filters we are trying to affect the closed loop transfer function $(I - \mathbf{L}_o)^{-1}\mathbf{L}_o$. These difficulties are independent of the positioning of the controller $\mathbf{K}_\infty$ in the feedback configuration.

5.4.2 Diagonal weights

The controller synthesis is making use of the non-square nominal model of the plant. The number of inputs, the number of outputs and their order of appearance in the system are the same as those (used) in the 1 Dof controller architecture (**1nsqDW**)- described earlier in the chapter.

5.4.2.1 Selection of $\mathbf{W}_1$

As a way of establishing a basis for comparative analysis with the 1 Dof control laws, **1nsqDW** and **1nsqNDW**, the diagonal weight ($\mathbf{W}_1$) selected in **1nsqDW** control law was used (see 5.4 in 5.3.3.1).

The weight is well conditioned ($1 < \kappa(\mathbf{W}_1(j\omega)) < 3$). Care must be taken when selecting the weights for ill-conditioned plants; ill-conditioned weights integrated with ill-conditioned plants may result in high condition numbers for some of the closed loop transfer functions and poor robustness properties at certain points of the loop which can lead to poor robust performance.

5.4.2.2 Selection of W_2

For compatibility with **1nsqDW** and **1nsqNDW** control laws, the post filter was chosen to be a constant diagonal matrix with unity gains in each channel, which effectively makes W_2 an all-pass filter:

$$W_2 = I_{5 \times 5}$$

Remark 5.4 *It was observed in numerous iterative designs that placing slightly more emphasis on Roll rate (p) and Pitch (q) rate added damping to the transient response of the corresponding attitude responses. This suggests (not surprisingly) that feeding back the rates acts as a "derivative" like control in the feedback interconnection.*

The nominal plant's and the (diagonal) weighting function frequency response Bode magnitudes are depicted in Figure 5.36 subplot *a*) and are identical to those used in **1nsqDW** and **1nsqNDW** control laws. Illustrated in subplot *b*) in the same Figure are the singular values of the (diagonally) shaped plant.

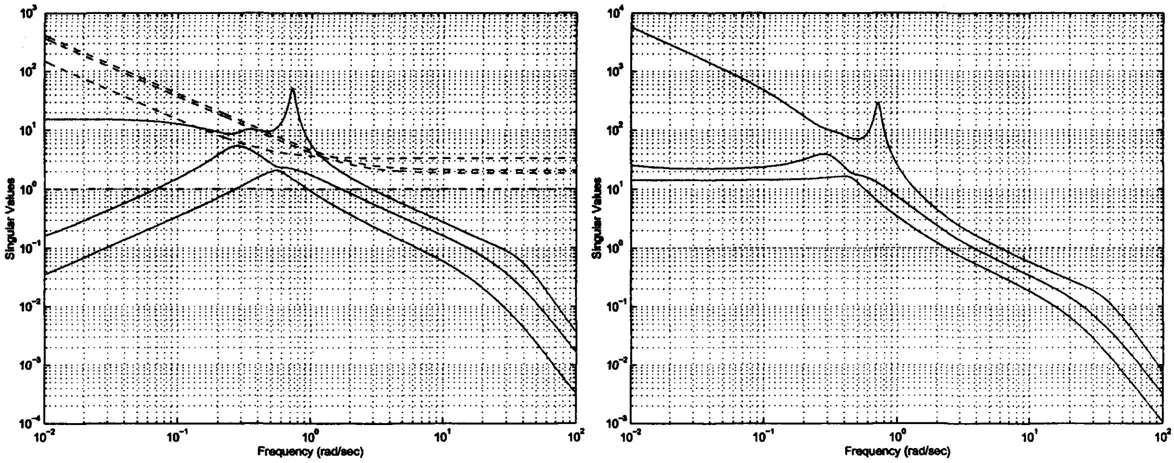

Figure 5.36: **a)** Nominal plant (*continuous*) and loop-shaping weights (*dashed*) **b)** Shaped plant

The objective of introducing 2 Dof controller architecture was to observe whether a controller synthesized with weights identical to these used in **1nsqDW** control law, but with incorporated time domain objectives, would exhibit any better nominal performance, particularly tracking, than **1nsqDW** control law.

5.4.2.3 K_∞ Controller synthesis

Before proceeding with the design steps distinctly unique to 2 Dof control law synthesis, a 1 Dof normalized *coprime* factor based robustly stabilizing suboptimal controller (with the same suboptimal scaling factor of 9 per cent) was synthesized using `ncfsyn` command from the commercially available package [BDG+98] of Matlab®. Performing this step will allow the designer to assess whether the shaped plant provides stability margin (ϵ) compatible with the low and high frequency design specifications. If the stability margin is not high new weighting functions have to be selected. A controller achieving low stability margin after the pure robust stabilization step of the 2 Dof architecture is very unlikely to attain performance objectives dictated by the $\mathbf{T}_{ref}$ reference transfer function model.

The achieved stability margin by $\mathbf{K}_{\infty}$ controller was $\epsilon = 0.3714$ which is immediately quite good, and equivalent to $\gamma = 2.6925$. This step is intermediate and in fact the design parameter should be identical in value to control law **1nsqDW**.

The selection of the target reference model $\mathbf{T}_{ref}$ which is to reflect the closed loop desired time domain response objectives in each of the controlled outputs of the closed loop system, comprises the next step before the controller synthesis procedure. This selection of the transfer functions (within the reference model transfer function matrix) is to be completed with consideration of handling qualities requirements outlined in ADS-33E [Ano00]. The model is required to be realistic- within the physical capabilities of the plant, i.e. it should not include very slow or very fast poles, or the resulting controller will produce excessive control signals, leading to poor robust stability and degraded performance. It is therefore possible that the selection may involve some iterations.

The desired closed loop reference model is preferred to accommodate low in order transfer functions, usually first or second order lags, and should also be selected so as to exhibit zero cross coupling. The latter, effectively translates to the requirement that (reference transfer function matrix) $\mathbf{T}_{ref}$ is diagonal. The bandwidth of every SISO transfer function on the diagonal of $\mathbf{T}_{ref}$ should be compatible with the aircraft bandwidth in the corresponding control output axis. Specifications outlined in ADS-33E documentation for different tasks and axes were not specifically tailored for *Bell 205* helicopter, but generally for helicopters, and more specifically for military helicopters. Therefore, time domain and short term response information on different task characteristics have been combined with past flight-control law design and test experience with *Bell 205* [WTS+99b], [PSW+99] and [SWP+01] to arrive at realistic frequency domain characteristics for each control axis.

The designer should note that translating time domain characteristics of each controlled channel into the frequency domain is an iterative process, and requires evaluation of the time domain characteristics (e.g: damping, speed of response, overshoot and steady-state error) of the chosen close-loop transfer function. If the chosen closed loop transfer function, characterising the dynamics of this axis, does not facilitate the desired time response of the system on this axis, then one of the following: ω_n, ζ or the order of the transfer function has to be adjusted.

Different rise time specifications of each controlled channel were addressed with second order lags with damping ratio (ζ) and, undamped natural frequency (ω_n); these are summarized in Table 5.4:

2nsqDW	ω_n (rad/sec)	ζ
Roll-(ϕ)	2.5	0.725
Pitch-(θ)	2.8	0.76
Yaw-(r)	1.95	0.75

Table 5.4: Reference model specification

Thus, the time response model took the form:

$$\mathbf{T}_{ref} = \begin{bmatrix} \frac{2.5^2}{s^2+2*0.725*2.5+2.5^2} & 0 & 0 \\ 0 & \frac{2.8^2}{s^2+2*0.76*2.8+2.8^2} & 0 \\ 0 & 0 & \frac{1.95^2}{s^2+2*0.75*1.95+1.95^2} \end{bmatrix} \tag{5.6}$$

After an iterative analysis of the closed loop time responses, the scalar model matching parameter ρ used to weight the relative importance of robust stability as compared to robust model matching, was selected to be $\rho = 1.45$. Increasing the value of the model matching parameter forces the closed loop response $r \rightarrow y$ to match the corresponding desired ($\mathbf{T}_{ref}$) model response characteristics, however at the expense of degraded robustness. A good value of ρ imparts a balance between both robustness and performance; it will act to minimize the error transients between the actual plant and the target reference model. In addition to these, in the 2 Dof configuration presented in [GL95] the scaling factor ρ weighs also robust disturbance rejection property.

Secondary[23] measurements (p and q) were not used in the robust model matching part, therefore they have been taken out of the synthesis by a scalar output selection matrix W_o:

$$W_o = \begin{bmatrix} 1 & 0 & 0 & 0 & 0 \\ 0 & 1 & 0 & 0 & 0 \\ 0 & 0 & 1 & 0 & 0 \end{bmatrix} \tag{5.7}$$

[23]Primary measurements are attitude angles.

The optimization problem was cast in a general framework as in [SP96] (pp.388 – 389) and the source code provided therein was used to synthesize an $\mathcal{H}_\infty$ controller in single step using `hinfsyn` command. The achieved was $\gamma_{opt} = 3.29$, however, our objective was to obtain a suboptimal control law which is why a "*one step*" second iteration utilizing γ_{opt} with boundaries of the optimization $\gamma_{min} = \gamma_{opt} * 1.09$ and $\gamma_{max} = \gamma_{opt} * 1.09$ was run to obtain the suboptimal controller achieving $\gamma_{subopt} = 3.5861$.

The resulting controller **K** had 26 states and was partitioned into two controllers, $\mathbf{K}_1$ and $\mathbf{K}_2$, which facilitated the construction of the test-bed system interconnection for performance and stability analysis. The feedforward controller $\mathbf{K}_1$ which affects only the performance, as it is nested in the forward loop, had 26 states; the feedback controller $\mathbf{K}_2$, which commands robust stability and was to be used in frequency domain robust stability analysis, also had 26 states. Effectively both controllers share the same state space. The order of the implemented controller $\mathbf{K}_{imp}$ was 29 and being within the maximum allowable states- 30, no model reduction was deemed necessary, hence the structure of the controller **K** was preserved.

In order to produce better model matching in the frequency ranges of interest, before constructing the final (to be implemented) controller, $\mathbf{K}_{imp}$, the feed-forward part $\mathbf{K}_1$ was scaled (with a factor) to take the form:

$$\mathbf{K}_1 = \mathbf{K}_1 \left[W_o((I - \mathbf{G}_s\mathbf{K}_2)^{-1}\mathbf{G}_s\mathbf{K}_1)^{-1}(0)\mathbf{T}_{ref}(0) \right] \tag{5.8}$$

Illustrated in Figure 5.37 is the frequency response magnitude plot of the resulting controller $\mathbf{K}_{imp}$.

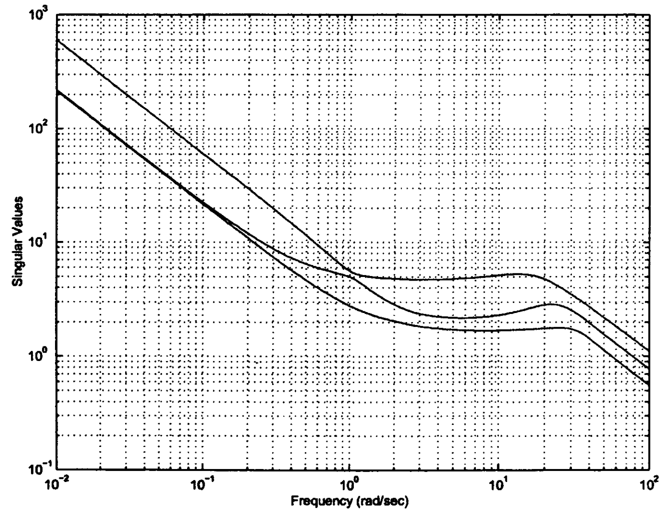

Figure 5.37: Singular values of $\mathbf{K}_{imp}$

It exhibits a slightly higher gain at low frequency $\underline{\sigma}(\mathbf{K}_{imp}) \gg 1$ in comparison to its counterpart in **1nsqDW** and complies with the performance requirements; it also has a much better roll-off at higher frequencies with $\overline{\sigma}(\mathbf{K}_{imp}) \leq 4$. However, a source of concern was the higher gain (exhibited by the maximum singular value) around the bandwidth and slightly above the bandwidth. The gain in the same frequency is larger than its counterpart $\mathbf{K}_{imp}$ of **1nsqDW**. This, up to 20 per cent, extra gain around the tentative bandwidth, is seen as primary cause of the control law **2nsqDW** to have been reported as unstable shortly after initial manoeuvre engagement during the qualitative in-flight assessments of the controller.

Figure 5.38 depicts, as a function of frequency, the Bode magnitude history of the desired and actual loops, at plant input (KG) and output (GK) respectively.

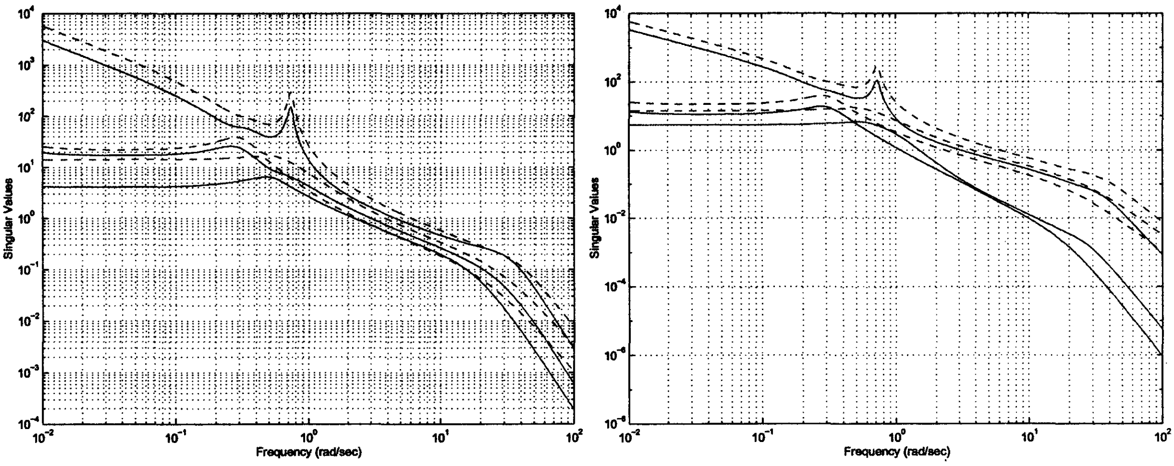

Figure 5.38: Shaped (*dashed*) vs. actual (*solid*) loop- shapes at: **a)** the plant input $\mathbf{L}_i$ **b)** the plant output $\mathbf{L}_o$ for **2nsqDW**

5.4.3 Linear frequency domain analysis

5.4.3.1 Performance analysis

Inspection of some of the closed loop performance characteristics in the frequency domain using output sensitivity ($\mathbf{S}_o$) and input sensitivity ($\mathbf{S}_i$) transfer functions in Figure 5.39 highlights the effect of the integral action in each channel at low frequencies. Comparisons with frequency performance indicators of control law **1nsqDW** shows that characteristics like: disturbance rejection, reference tracking and some transient response characteristics (as speed of the response) have improved slightly between 5 and 25 per cent, signifying the effect of including the feed-forward controller $\mathbf{K}_1$, i.e. the second degree-of-freedom. However, the 2 Dof control law falls short in matching frequency performance characteristics of non-diagonal weight control law **1nsqNDW**.

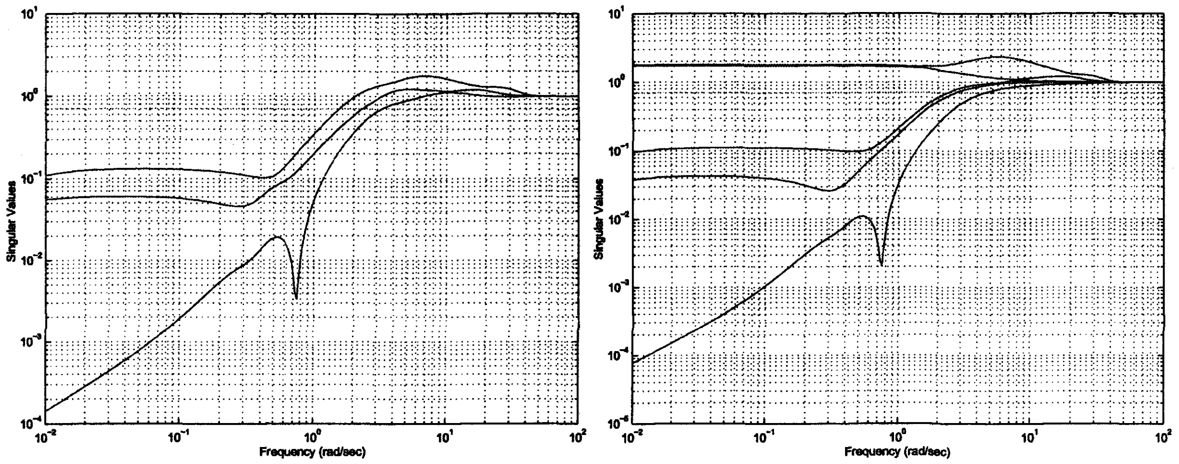

Figure 5.39: **a)** Input sensitivity $\mathbf{S}_i$ **b)** Output sensitivity $\mathbf{S}_o$ singular values

A comparative analysis of 1 Dof input/output sensitivities ($\mathbf{S}_{i,o}$) depicted in Figure 5.15 and 2 Dof input/output sensitivities ($\mathbf{S}_{i,o}$) illustrated in Figure 5.39 underlines two issues: firstly, that attenuation of both input disturbances effect on the plant input, and output disturbances effect on the plant output at low frequencies have improved in all directions in 2 Dof design; secondly, that bandwidths of all channels if measured in terms of sensitivity (**S**) have increased. However, rejecting of the disturbances at the input/output of the plant may still require significant control effort.

Further analysis of Figure 5.39 also brings to light that this improvement in performance characteristics (like tracking and disturbance rejection) comes at the cost of higher sensitivity peaks $||\mathbf{S}_i||_\infty = 1.7638$ and $||\mathbf{S}_o||_\infty = 2.3489$ in the bandwidth region, which point to decreased tolerance of the closed loop system to unstructured input/output inverse multiplicative uncertainties acting on the plant. The smallest unstructured inverse multiplicative uncertainty that can possibly destabilize the system at the plant input is with size $||\Delta_i||_\infty = 0.5670$, and at the plant output is with size $||\Delta_o||_\infty = 0.4257$.

Figure 5.40 readily reveals that attenuating the effect of input disturbances on the plant outputs has also improved and is satisfactory at all frequencies, but particularly at low frequencies and slightly better than that demonstrated by 1 Dof controller **1nsqDW**. This is due to an integral action effect carried to $\mathbf{K}_{imp} = \mathbf{K}$ from $\mathbf{W}_1$. Fast roll-off at high frequency is as a result of strictly proper nature of the shaped plant $\mathbf{G}_s$.

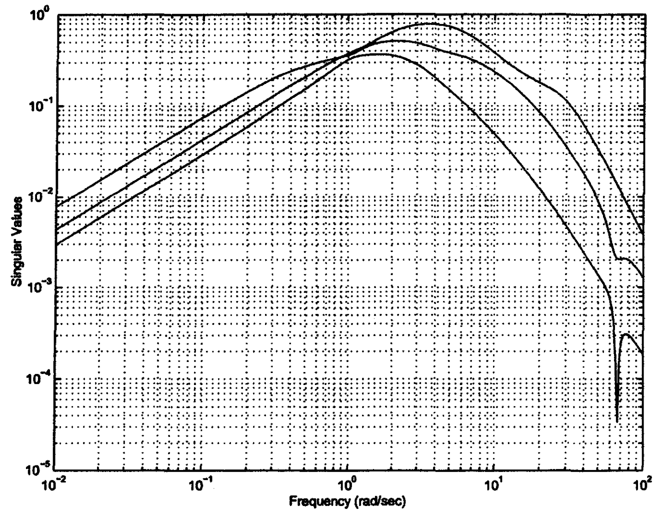

Figure 5.40: Singular values $\mathbf{S}_o\mathbf{G}$

5.4.3.2 Robustness analysis

Limited insight into the robustness properties (such as tolerance to high frequency measurement sensor noise, and tolerance to uncertainty modelled as a multiplicative perturbation) of the augmented closed loop system can be obtained by perusing Figure 5.41 and Figure 5.42; which illustrate frequency response dynamics of co-sensitivities ($\mathbf{T}_i$ and $\mathbf{T}_o$), and inverse co-sensitivities, respectively. Comparison with the same indicators of robustness of control law **1nsqDW**, in Figure 5.18, brings to evidence that **2nsqDW** controller can tolerate, at the plant input, unstructured multiplicative uncertainties up to 66 per cent, which is lower than **1nsqDW** control law. Whereas at the plant output, as shown in subplot *b*) of Figure 5.42, the system can maintain stability in the presence (of the same type of uncertainty) up to 90 per cent, which is slightly better than **1nsqDW**. Therefore the size of the smallest unstructured input (and output) multiplicative uncertainty destabilizing the plant will be 0.66 acting around $\omega = 4$ rad/sec (and 0.90 acting around $\omega = 2$ rad/sec). In Figure 5.42 one can also observe that in high frequencies the closed loop system offers a higher level of tolerance to unstructured multiplicative uncertainties at the plant input than at the plant output. This comes as a result of the presence of an open loop-shaping filter at the plant input.

Presented in Figure 5.43 subplot *a*) are singular values of $\mathbf{KS}_o$ which offers frequency response interpretation of the activity of actuators in the presence of perturbations at plant output. It can be seen that the augmented system exhibits extreme sensitivity

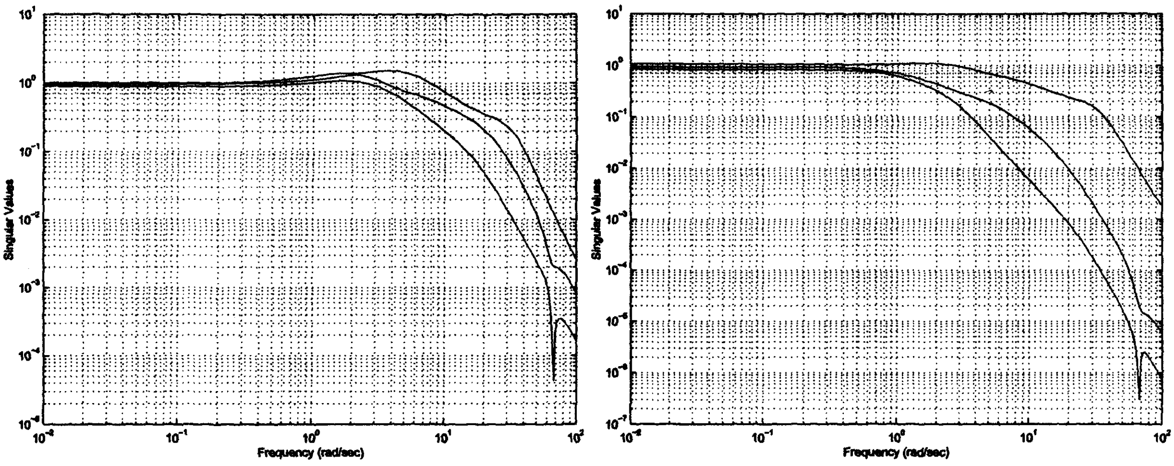

Figure 5.41: **a)** Input co-sensitivity $\mathbf{T}_i$ **b)** Output co-sensitivity $\mathbf{T}_o$ singular values

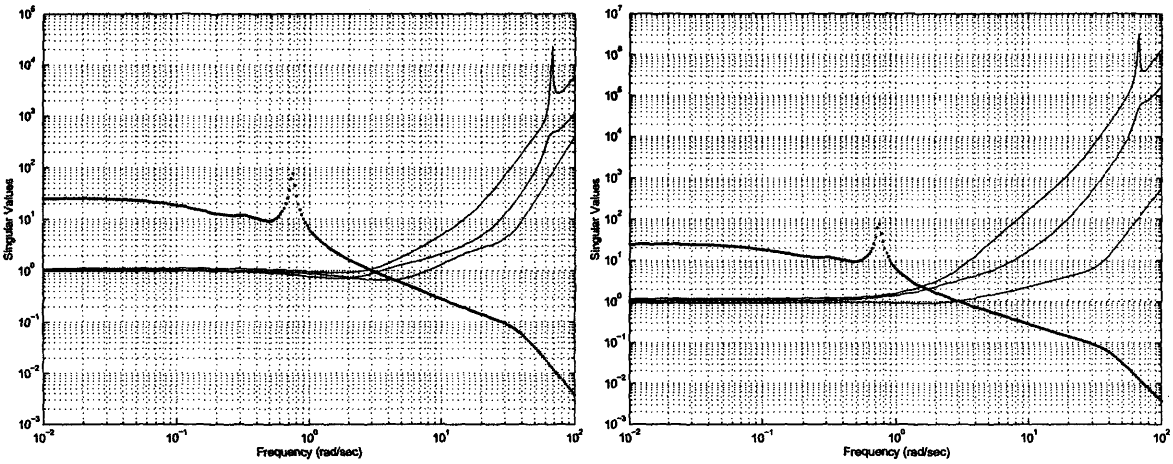

Figure 5.42: **a)** Inverse input co-sensitivity $\mathbf{T}_i$ vs. $\overline{\sigma}(\mathbf{G})$ **b)** Inverse output co-sensitivity $\mathbf{T}_o$ singular values vs. $\overline{\sigma}(\mathbf{G})$

at frequencies just above the fundamental (first) (anti-) resonant mode. In the same Figure subplot *b*) one can observe the robustness of the plant to additive uncertainties, i.e. allowable additive uncertainty before the system goes unstable. It can be seen that for high frequencies (above 18 rad/sec) the augmented system can tolerate additive uncertainty higher than the magnitude of the plant **G**. However, comparison with the same properties of **1nsqDW** control law in Figure 5.19 confirms that the system augmented with control law **2nsqDW** exhibits slightly higher sensitivity to additive uncertainty due to the increased actuator activity.

In conclusion, it can be asserted that the 2 Dof architecture has improved performance associated properties of the system through introduction of $\mathbf{K}_1$ and $\mathbf{T}_{ref}$, however, at the expense of degraded robustness qualities. This suggests that the scalar model

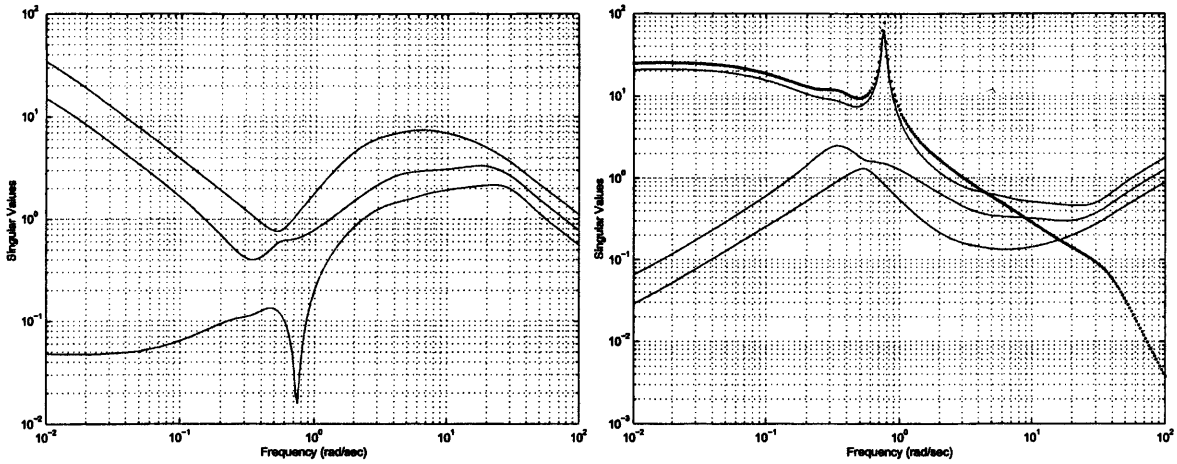

Figure 5.43: **a)** Actuator activity due output disturbance **b)** Maximum allowable additive uncertainty vs. $\bar{\sigma}(\mathbf{G})$

matching parameter $\rho = 1.45$ has to be decreased if certain robustness properties are desired to be improved at the expense of performance properties. A reasonable choice of ρ is usually slightly higher than 1.

5.4.4 Non-diagonal weights

Attempts to incorporate the non-diagonal weights obtained for 1 Dof (**1nsqNDW**) controller structure into the 2 Dof architecture **2nsqDW** prior to $\mathcal{H}_\infty$ optimization led to time consuming γ iterations with no significant improvement reported. Given the experience with non-diagonal weight design it will be safe to assume that this may not be feasible in systems with high orders or its benefits will not outweigh the time demanding computational complexities of the technique. Reference [PG02] presents an algorithm for incorporating non-diagonal weights into 2 Dof controller architecture using a fully optimized LMI algorithm, however, the algorithm has been demonstrated on a low order system.

5.5 Summary and comments

This chapter presented step by step designs of four control laws based on the normalized *coprime* factor $\mathcal{H}_\infty$ loop-shaping design procedure; all of the designed controllers were flight-tested as described later. Controllers utilize both diagonal and non-diagonal weights; the designs enabled a number of issues to be addressed in simulations and conclusions to be strengthened with real applications. The 2Dof $\mathcal{H}_\infty$ optimization problem setup ensured a guaranteed level of robust stability through normalized *coprime* factor robust stabilization; robust disturbance and robust reference tracking.

Stability robustness was assessed using frequency response singular values of some closed loop transfer functions which, although they introduced some degree of conservatism, served as handy and useful indicators of the limitations and capabilities of the control systems. The controller designs were not approved for flight testing if their linear and nonlinear time responses did not comply with specified design requirements described in terms of: rise time, per cent overshot M_p, settling time and steady-state error. Although inclusion of the linear and nonlinear time domain simulations, and flight test results associated with each design case, in this chapter, would have given a complete treatment of every control law, this would have significantly inflated the size of the chapter. Therefore, this has been purposefully avoided. Instead, simulation results will be presented in a separate chapter.

In the following chapter we will present evaluations of the control laws, synthesised in this current chapter, through extensive linear and nonlinear simulations performed in the time domain. These simulations will be complemented with flight-test (data) extracted responses, together with Quantitative and Qualitative evaluations of the flight-tested control laws. For the application of the algorithm to complex systems which are usually of high order (as the one described in this work) careful thought must be given before deciding to use non-diagonal weights.

Table 5.5 presents, for comparative purpose, a summary of important frequency domain quantities used in the the course of the controller design. For a complete picture of the comparison they have to be considered together with associated (closed loop) transfer functions frequency response Bode magnitudes; ∂- denotes the order of the controller. It would be useful to consider some additional measures (like μ, ν-gap metric, pointwise version of the stability margin) for assessing the robustness and performance characteristics of each control law in order to acquire a broader picture on the strengths and capabilities of each control law.

Comparison of frequency domain performance and robustness indicators between the **1nsqDW** controller and **1sqDW** controller confirms that *"squaring down"* the system by removing the rates p and q affects adversely the robustness characteristics (of the augmented plant) to various types of uncertainties due to reduction in stability

Control law	ϵ		$\partial(\mathbf{K}_\infty)$	$\|\mathbf{S}_i\|_\infty$	$\|\mathbf{S}_o\|_\infty$	$\|\mathbf{S}_o\mathbf{G}\|_\infty$	$\|\mathbf{T}_i\|_\infty$	$\|\mathbf{T}_o\|_\infty$
	ϵ_{max}	ϵ						
1sqDW	0.30	0.278	21	2.19	2.48	0.88	1.88	2.04
1nsqDW	0.403	0.371	20	1.62	2.1	0.75	1.36	1.21
1nsqNDW	0.457	0.42	20*	1.88	2.89	0.77	1.56	1.30
2nsqDW	0.403*	0.371*	26**	1.76	2.35	0.79	1.51	1.11

Table 5.5: Frequency response design characteristics of control laws: $*$- model reduced, $\star$- pure robust stabilization, $\star\star$- $\partial(\mathbf{K}_{1,2})$

margin (ϵ). However, all this is at the expense of significantly improved performance characteristics: faster response, smaller damping (p and q act like *derivative* control), smaller steady-state off-set, smaller overshoot.

Initial observations suggest that by *"squaring down"* the size we have traded robustness for performance. These observations may be problem dependent (and in particular, dependent on the variables removed), therefore, drawing out any rigorous conclusions about the effect of extra measurements based on this observation will be inconclusive. Further theoretical justification will be required so that the results can be brought to a level to stand scientific scrutiny. Tools like Relative Gain Array, structured singular value (μ) and ν-gap metric can be used for this purpose.

While every controller architecture is designed to bring along benefits, not all of those can be unveiled unless the method used for controller design is applied in practice. Therefore, the selection of the *"best"* possible controller architecture and weight structure requires considerable practical experience in controller design. This comprises, but is not limited to, the ability to select the right design indicators (frequency, time or both) for assessment, to interpret them accurately and to reflect the interpretation and analysis precisely on the values of variables used in the design.

Chapter 6

Simulations, Flight-tests and Analyses

This chapter presents the simulation results derived from implementing the previously designed controllers on both linearized and fully nonlinear flight dynamics representations of different helicopter configurations. These have been complemented with simulations extracted from flight-test data and their comparative analysis. Flight test data were gathered in a limited number of flight tests.

The flight control laws' response characteristics and handling qualities were assessed quantitatively by using ADS-33E standards and flight test data, and qualitatively based on in-flight pilot evaluations using Cooper-Harper [CH69] handling qualities rating scale on several hover/low speed flight-test multi-axis mission task element (MTE) manoeuvres such as: Quick-Hop also known as Quick-Step *QS*; Side-Step *SS*; Turn-to-Target *TtT*; Precision hover and, pirouette. ACAH response type characteristics were used for handling qualities assessment.

It has been accepted as a common rule in the rotorcraft community that accurate subjective assessment of flying qualities of any control law should involve the judgements of at least three pilots, preferably more and, in order to aid the design, HQRs should be plotted with mean, max and min assigned by all the pilots [Pad00]. A range of two or three pilot ratings would indicate to the control engineer a fault in experimental design. Our flight tests have been conducted with two pilots per sortie (one Safety Pilot who sits on the left hand side in the cockpit, and one Evaluation Pilot who sits on the right side in the cockpit), however only one of them, namely the evaluation pilot, was actively involved in flying qualities assessment of the control laws. The safety pilot could provide insight on the activity of the actuators since his control stick is directly linked to the actuators.

Appendix I, at the end of the thesis, provides a concise overview with the most frequently used definitions and parameters in quantitative and qualitative analysis of rotary-wing flight test results for those who are unfamiliar with the terminology.

6.1 Square plant - **1sqDW control law**

The first control law design- **1sqDW**- was performed and flight tested in June 2001 on the square (3×3- three inputs and three outputs) helicopter plant.

6.1.1 Desk-top simulations: Linear response time domain analysis

This subsection presents linear simulation results of the augmented system which, as a baseline, used the linearized 14 states (see section 5.2) model of the helicopter with built-in 75 ms time delays.

To facilitate a basis for a realistic comparative analysis between linear, nonlinear models and the real plant and to allow for realistic predictions on the real plant's dynamic response, amplitudes of the input demand signals for the Pitch and Roll channels were chosen to be 0.2 rad[1], whereas for the Yaw channel was chosen to be 0.2 rad/sec.

Figure 6.1 illustrates the response of the linearized system to a lateral cyclic step input demand of 0.2 rad to Roll axis. The transient response is crisp, fast, with rise time (t_r) of approximately 1.7 sec; with no overshoot (which indicates good stability margin), and high damping coefficient ($\zeta > 0.7$). The steady state error is within the acceptable design specifications ($e_{ss} \approx 2$ per cent).

Due to the asymmetric geometry of the rotorcraft, a pilot demand injected in any primary axis is likely to introduce some coupling in off-axes. Reduction or elimination of this cross-axis coupling is amongst the objectives of every control law design.

Illustrated in Figure 6.2 subplot *a*) and subplot *b*) are the off axes responses in Pitch axis and Yaw axis, respectively.

It can be easily noticed that the couplings are really too small to be of any concern. They are $\frac{\theta}{\phi} \approx 0.4$ per cent, and $\frac{r}{\phi} \approx 0.5$ per cent. The first result interpreted with coupling criteria [Ano00] for forward flight and hover indicate that *Level 1* (where

[1]Application of input demand with magnitude of 1 rad is common in theoretical case studies, however in the rotorcraft flight control context this is not realistic and, hence is of little practical value. It does, if possible, make it easier to draw out conclusions about the amount of cross-axis interaction, and other performance characteristics.

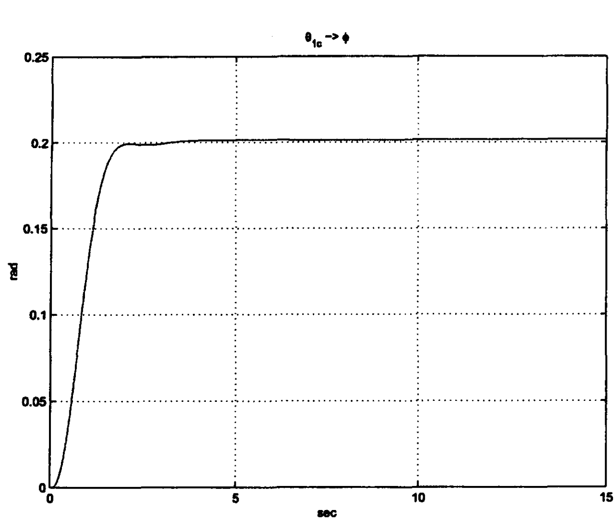

Figure 6.1: Linear response to lateral cyclic step demand of 0.2 rad

pilot compensation is not a factor for desired performance) flying qualities may be possible.

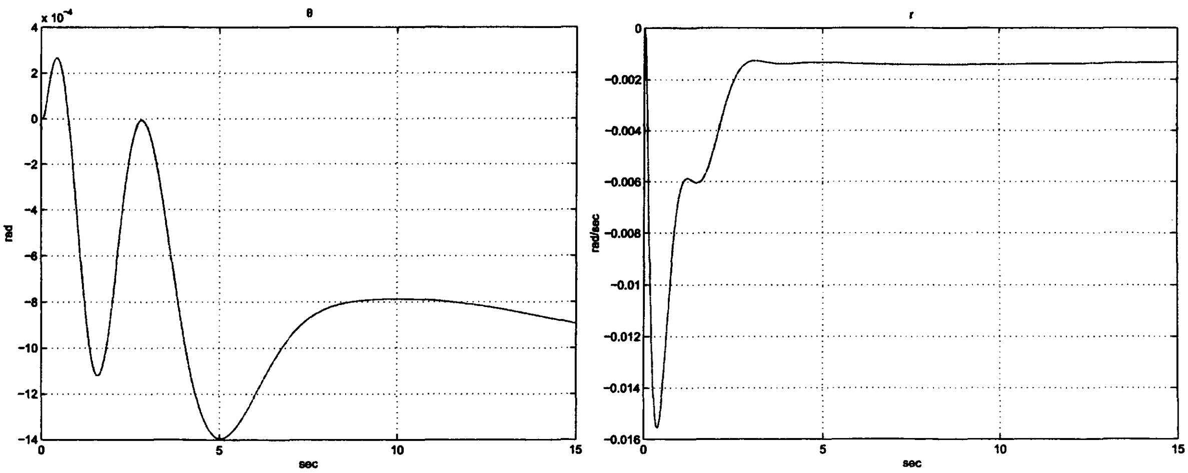

Figure 6.2: Couplings to lateral cyclic step demand of 0.2 rad **a)** θ **b)** r

Figure 6.3 shows the linear response of the system to a longitudinal cyclic step input demand of 0.2 rad in the Pitch channel. The transient response is with rise time (t_r) of approximately 2.4 sec, which is higher than the Roll axis response. This can be justified by the low bandwidth of the Pitch axis dynamics. Both of these characteristics, which restrict the flight manoeuvrability of the rotorcraft about Pitch axis, can be seen as a result of the greatest moment of inertia (I_{yy}) about the helicopter's yy principal axis. The low bandwidth also yields a response that exhibits slightly higher overshoot (3 per cent) compared to the Roll primary axis response; the response takes longer to settle, and with significantly larger (than Roll axis) steady-state error $e_{ss} \approx 9$

per cent. These performance indicators suggest that there is room for significant improvement in low frequency performance requirements by ensuring higher gain at low frequencies.

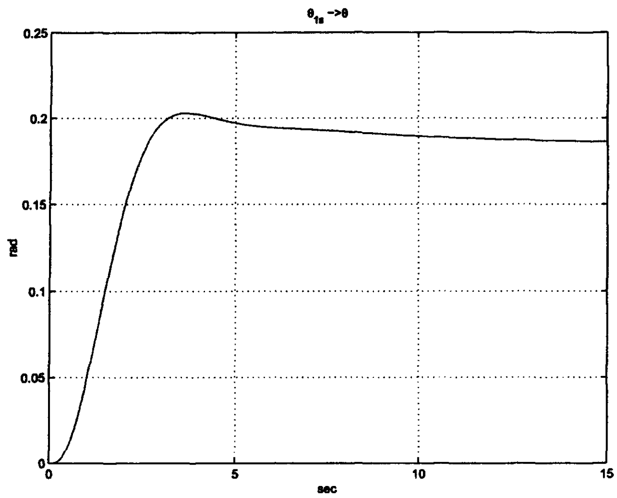

Figure 6.3: Linear response to longitudinal cyclic step demand of 0.2 rad

The cross-coupling depicted in Figure 6.4 between the primary controlled channel (Pitch) and the off-axis channels (Roll and Yaw) is approximately $\frac{\phi}{\theta} \approx 7.5$ per cent, and $\frac{r}{\theta} \approx 1.5$ per cent, respectively. The former suggests a considerable coupling between Pitch to Roll, nevertheless the value is still within an acceptable region for *Level 1* flying qualities range as required in ADS-33E coupling criteria for forward flight and hover.

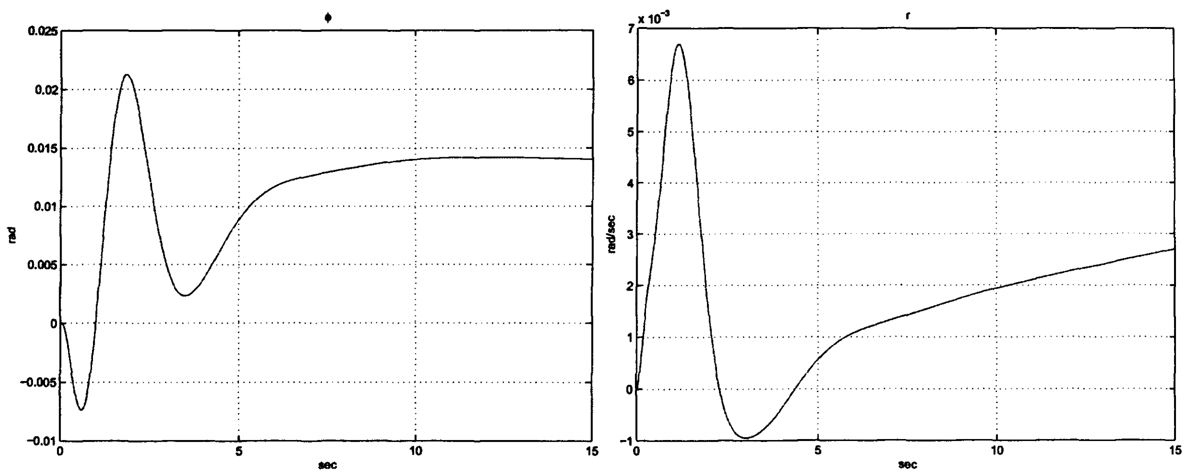

Figure 6.4: Couplings to longitudinal cyclic step demand of 0.2 rad **a)**ϕ **b)** r

Figure 6.5 depicts the linear response to a pedal step input demand of 0.2 rad/sec in the fastest and most difficult to maintain control channel, Yaw. Rise time (t_r) of the channel's response is slightly less than 1 sec, and the transient response shows negligible (0.5 per cent) overshoot, and steady-state error of $e_{ss} \approx 0.5$ per cent. The fast rise time can be justified with the existence of anti-torque tail rotor- which essentially acts as a source balancing the main rotor torque.

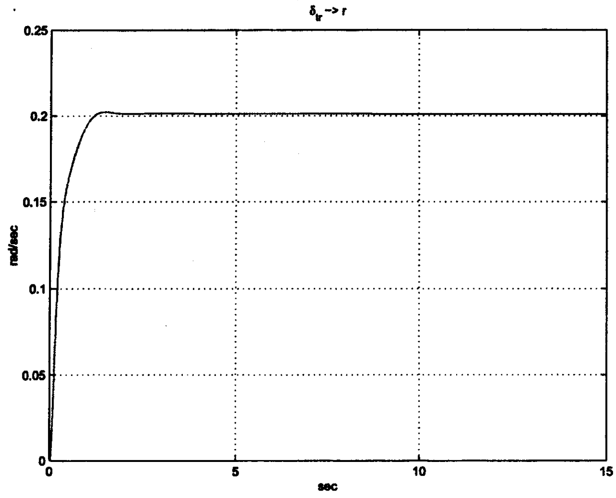

Figure 6.5: Linear response to pedal step demand of 0.2 rad/sec

Representative of the linear coupling of the Yaw response with the other axes attitudes can be seen in Figure 6.6 subplot *a*) for Yaw to Roll which is $\frac{\phi}{r} \approx 1$ per cent, and in subplot *b*) for Yaw to Pitch which is $\frac{\theta}{r} \approx 2.25$ per cent. ADS-33E coupling criteria do not apply to off axis responses initiated by demands to the Yaw axis.

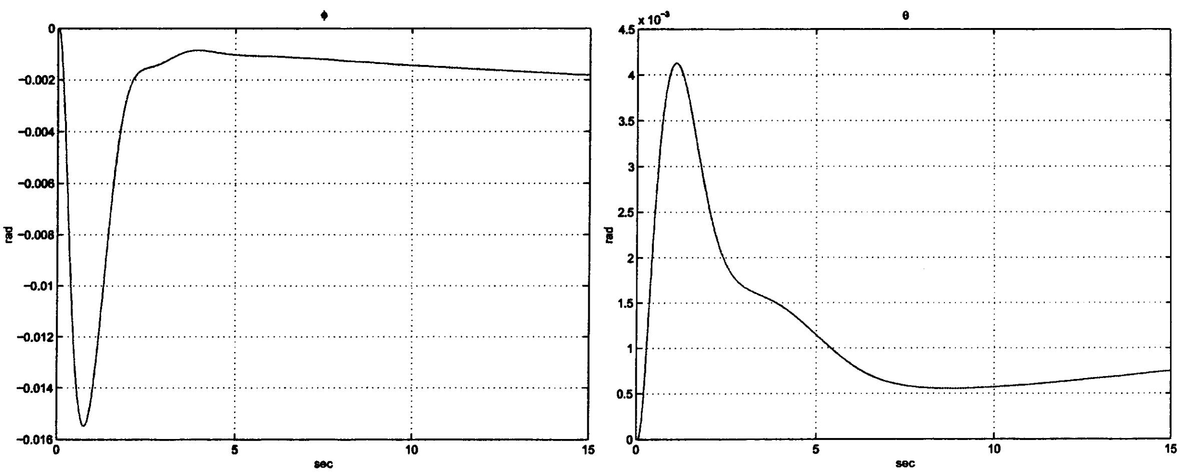

Figure 6.6: Coupling to pedal demand of 0.2 rad/sec **a)** ϕ **b)** θ

6.2 Flying and Handling Qualities assessment

This section presents an assessment of the flying and handling qualities of the control laws presented in this thesis. The assessment was conducted in view of the handling and flying qualities specifications set for rotorcraft in the [Ano00], which quantify the minimum acceptable parameters characterizing the rotary-wing aircraft dynamics and performance. Handling qualities were evaluated in two ways: quantitatively and qualitatively. Quantitative evaluation was based on a linear model transfer function which used ADS Handling Qualities Toolbox [How90], and on an analysis of frequency-domain transfer functions derived from pilot induced frequency control sweeps flight-test data. These transfer functions represent the gain and phase frequency responses of a helicopter's attitude to pilot's cyclic (or pedal) command.

While both approaches of evaluation are dependent on the task to be performed, and fundamentally based on specifications outlined in [Ano00], the second is conducted by the pilot and thus, in its assignment, factors like the environment of flight, pilot skill and experience are influential in evaluation.

All manoeuvres in our flight test were performed in the day time and combined with their describing characteristics, an ACAH response type was found the most appropriate in all the flight test series; in Yaw axis RCAH response type was applied. In ACAH response type (theoretically) a unit input given in lateral and longitudinal cyclic on Roll and Pitch channels will impart a unit change in Roll (ϕ) and Pitch (θ) attitudes, whereas a unit pilot input through pedal will result in a unit rate response.

6.2.1 Quantitative evaluation: Linearized model based evaluation

To demonstrate the potential of the 1 DoF $\mathcal{H}_\infty$ loop-shaping design approach, in this section, flight test data gathered during the testing of the controllers will be analyzed on two-parameter[2] (ω_{bw}, τ_p) handling qualities diagrams and the frequency domain.

The bandwidth and phase delay parameters for different mission task elements (MTE) classes for the Pitch, Roll and Yaw axes channels extracted from linear simulations can be seen in Figure 6.7, Figure 6.8 and Figure 6.9 respectively. The lower, vertical portions of each boundary indicate the minimum acceptable bandwidths for different

[2] Appendix A8 and A9 provide more information on handling qualities parameters ω_{bw}, τ_p; for more exhaustive treatment the reader is referred to [Ano00] and [Pad00].

MTE's. The upper, straight or curved portions of the boundaries indicate that the higher the bandwidth, the higher phase delay will be tolerated for a given MTE.

For example small amplitude Roll, Pitch and Yaw bandwidths are to be no less than 2 rad/sec if *Level 1* flying qualities are to be achieved.

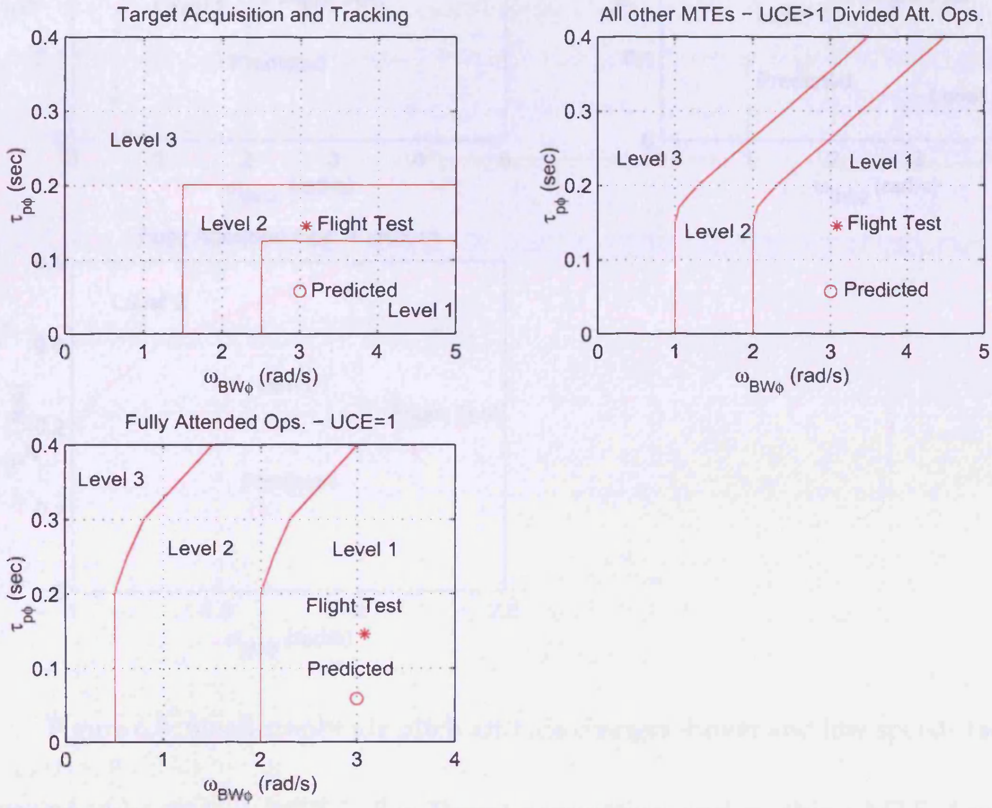

Figure 6.7: Small amplitude **roll** attitude changes -hover and low speed-**1sqDW**

Linear model based quantitative evaluation of the control law **1sqDW** for different MTE using ADS Toolbox [How90] predicts high bandwidths and small phase delays which indicates that *Level 1* flying qualities can be achieved for small amplitude changes about Roll axis.

Similar low phase delay characteristic is not the case for small amplitude changes about (naturally low bandwidth) Pitch axis, where for workload demanding MTEs (like Target acquisition and tracking, and UCE> 1) depicted in Figure 6.8 phase delay is higher and bandwidth lower. However, despite of the predicted (by linearized model) *Level 2* flying qualities, the flight test data indicate *Level 1* flying qualities in all three MTEs.

Illustrated in Figure 6.9 are handling qualities predicted for small amplitude heading changes in low speed region and hover. Note that for Yaw axis assessment is per-

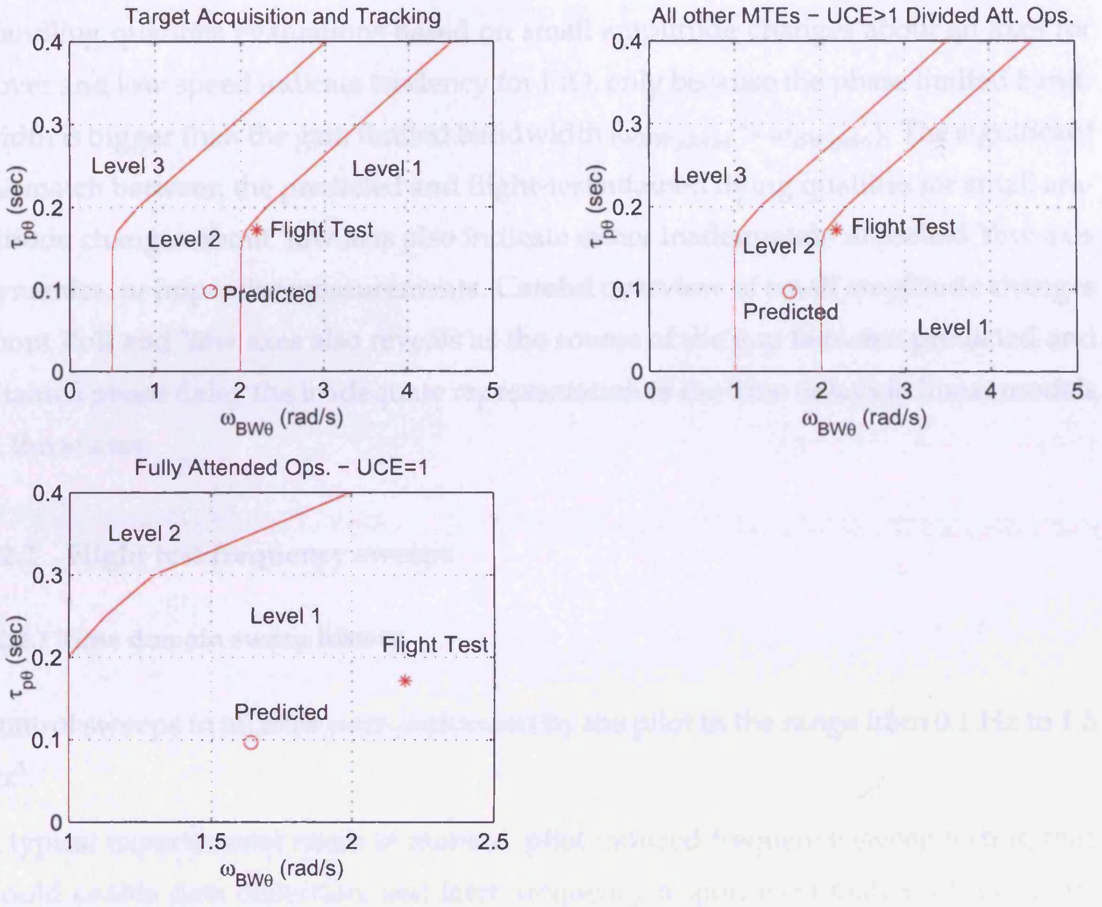

Figure 6.8: Small amplitude **pitch** attitude changes -hover and low speed- **1sqDW**

formed only on two MTEs. For Target acquisition and tracking MTE, *Level 2* flying quality is predicted as attainable; this is mainly due to the low bandwidth although the phase delay is the smallest among all axes. Flight test data analysis, however, indicate that *Level 1* flying qualities were possible for those specific MTEs.

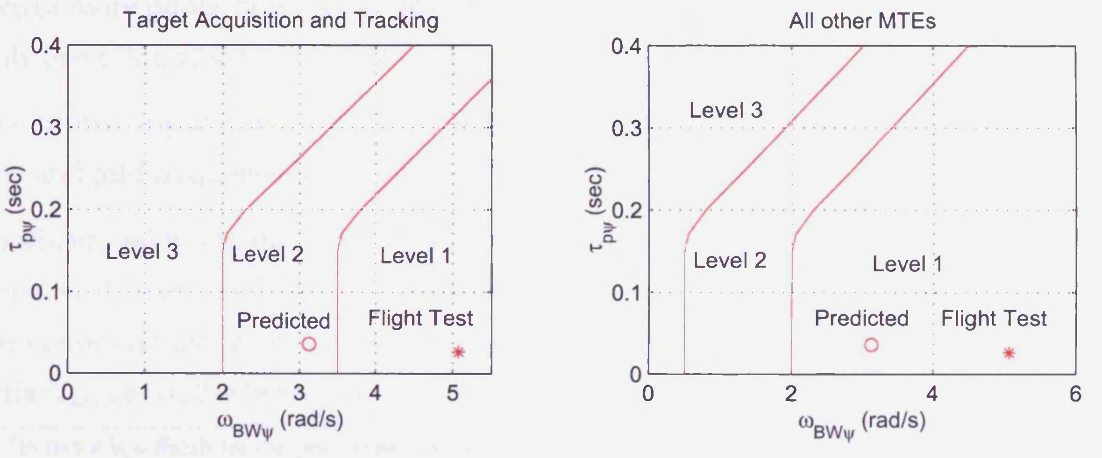

Figure 6.9: Small amplitude **heading** changes -hover and low speed-**1sqDW**

Handling qualities evaluations based on small amplitude changes about all axes for hover and low speed indicate tendency for PIO, only because the phase limited bandwidth is bigger than the gain limited bandwidth ($\omega_{BWphase} > \omega_{BWgain}$). The significant mismatch between the predicted and flight-test attained flying qualities for small amplitude changes about Yaw axis also indicate either inadequately modelled Yaw axis dynamics, or imprecise measurements. Careful overview of small amplitude changes about Roll and Yaw axes also reveals as the source of the gap between predicted and attained phase delay the inadequate representation of the time delays in linear models in those axes.

6.2.2 Flight test frequency sweeps

6.2.2.1 Time domain sweep history

Control sweeps in all axes were performed by the pilot in the range from 0.1 Hz to 1.5 Hz[3].

A typical experimental result of manual, pilot induced frequency sweep testing that would enable data collection, and later, frequency response estimation of the rotorcraft primary axes transfer functions, is shown in Figure 6.10 for lateral cyclic input, in Figure 6.11 for longitudinal cyclic input and in Figure 6.12 for pedal input. Every figure also depicts resultant actuator activity induced by the frequency sweep demands. In order to create a database capturing the rotorcraft's dynamic characteristic modes, input and response data were recorded for a period of about 70 sec; recordings up to 90 sec are common. It is advised that frequency sweeps are conducted by two or more pilots, however in this control law frequency sweeps were performed by only one pilot, albeit an experienced one.

The control input size should be as small as possible but still big enough to capture low and mid frequency bare-airframe dynamic responses.

As illustrated in Figure 6.10, the rotorcraft attitude in Roll (ϕ) follows the sweep manoeuver demand quite nicely even at high frequencies. This can be associated with the (aerodynamic) geometry of the rotorcraft which gives the smallest moment of inertia (I_{xx}) about the helicopter's xx principal axis. Depicted in the same figure, in the

[3] In fact it is difficult for the pilot to estimate accurately the frequency of the input above 1 Hz. Conducting frequency sweeps at high frequencies can have damaging effect on rotorcraft components, such as the fuselage or rotor mast, due to resonance frequencies.

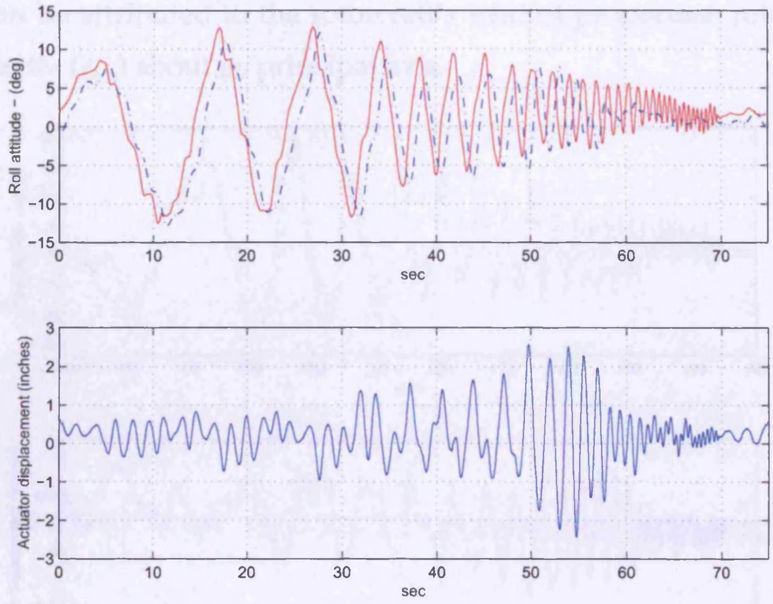

Figure 6.10: Roll axis frequency sweep: red-(demand), dash dot-(response), blue-(actuator displacement) for **1sqDW**

bottom subplot, the actuator activity is seen to be low for low frequency excitation, and high for high frequency excitation.

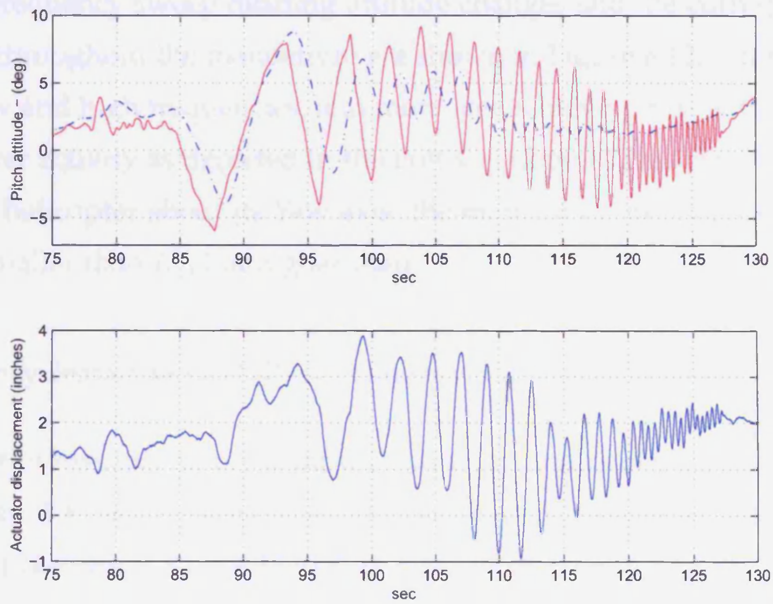

Figure 6.11: Pitch axis frequency sweep: red-(demand), dash dot-(response), blue-(actuator displacement) for **1sqDW**

The attitude response to Pitch axis cyclic input frequency control sweep in Figure 6.11 illustrates significant actuator activity and relatively poor attitude tracking characteristics. This can be attributed to the rotorcraft's inertial properties- rotorcraft's large moment of inertia (I_{yy}) about yy principal axis.

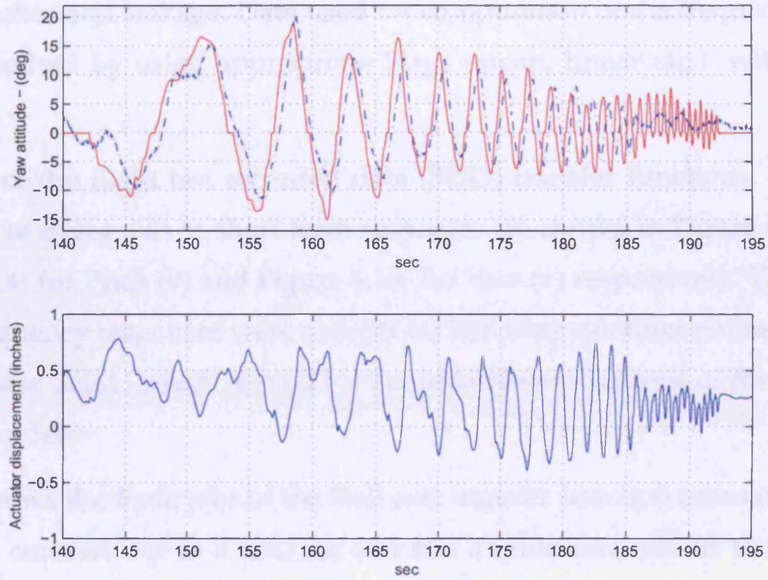

Figure 6.12: Yaw axis frequency sweep: red-(demand), dash dot-(response), blue-(actuator displacement) for **1sqDW**

Pedal input frequency sweep heading attitude changes and the corresponding actuator activity throughout the manoeuvre are shown in Figure 6.12. Attitude retention is good at low and high frequencies, and moreover achieving this with relatively low actuator power activity as depicted in the bottom subplot. This can be related to the agility of the helicopter about its Yaw axis- the moment of inertia about zz principal axis (I_{zz}) is smaller than I_{yy}, but higher than I_{xx}.

6.2.2.2 Frequency domain sweep history-Frequency response estimation

Transfer functions representing the input/output dynamics of each primary axis were estimated from the frequency sweeps' time history data using the `tfe` (transfer function estimate) command in the Matlab® Signal Processing Toolbox. Alternatively, one can use `vspect` from the μ-Analysis and Synthesis Toolbox.

In the use of `tfe` command the system input and system output were divided into 512 overlapping sections, each of which was linearly detrended, then windowed by the WINDOW parameter and then zero-padded to length 1024. Sampling frequency was 64 Hz.

To increase the quality of the frequency response in the frequency range[4] of interest overlapping windows were used, and a 1024 point *Hanning* window was selected to prevent side lobes and leakage. Data used for computation of the frequency response was also smoothed by using appropriate Flags (mean, linear etc.) within the `tfe` command.

Estimated from the flight test recorded data (SISO) transfer functions, representing the dynamics of every axis in short term response, are shown in Figure 6.13- for Roll (ϕ), Figure 6.14- for Pitch (θ) and Figure 6.15- for Yaw (r) respectively. These transfer functions' frequency responses were sources for handling qualities parameters (bandwidth and phase delay) which served for quantitative evaluations of the flight tested **1sqDW** control law.

Figure 6.13 shows the Bode plot of the Roll axis transfer function estimate, where the magnitude is constant up to 3 rad/sec and has a quite fast roll-off thereafter. The shape of the phase curve is steep around the phase limited bandwidth, but reduces its slope beyond the natural bandwidth frequency.

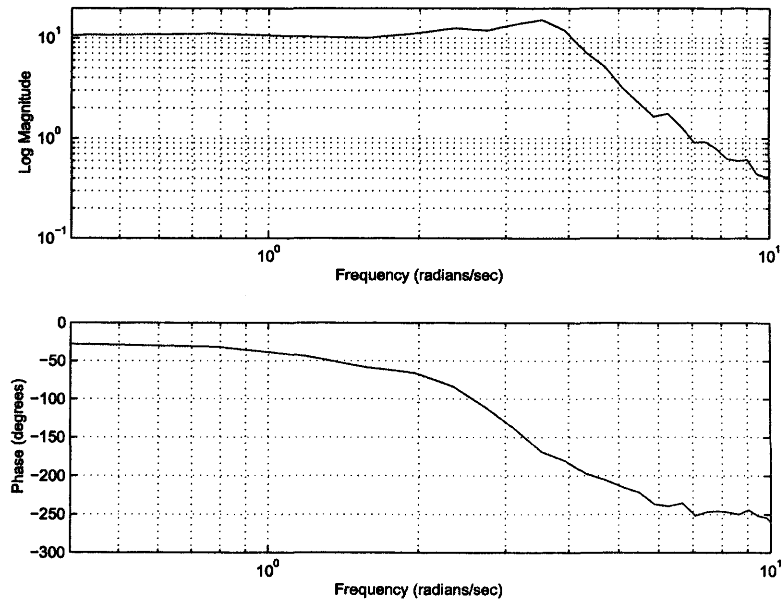

Figure 6.13: Roll axis frequency estimate for **1sqDW**

Flight test data derived transfer function's gain and phase characteristics of the Pitch axis rotorcraft dynamics are depicted in Figure 6.14. A closer look at the slope of the phase curve between ω_{180} and $2\omega_{180}$ implies slightly higher pilot workload in Pitch axis in comparison to the Roll axis.

[4]Sufficient data could be generated up to 10 rad/sec, this is how the upper limit was decided.

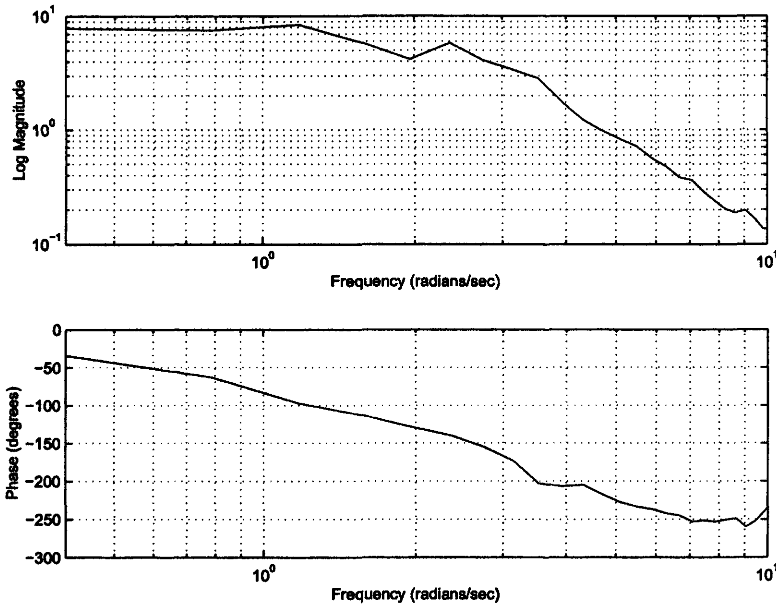

Figure 6.14: Pitch axis frequency estimate for **1sqDW**

Illustrated in Figure 6.15 is rotorcraft's estimated Yaw axis frequency response gain and phase characteristics.

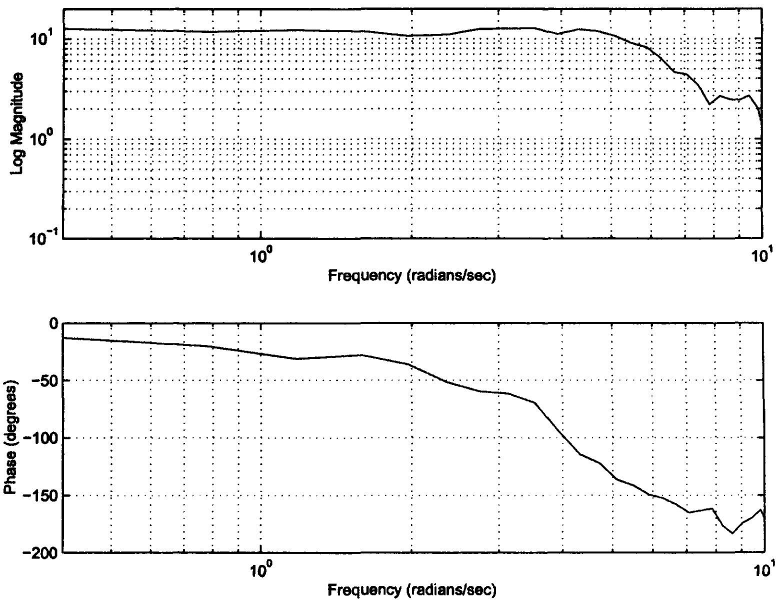

Figure 6.15: Yaw axis frequency estimate for **1sqDW**

The frequency response shows an almost constant magnitude curve up to 5 rad/sec and a fast decrease thereafter. Which implies that inputs will be subjected to constant amplification by a factor of 12 up to 5 rad/sec frequency. The shape of the phase curve up to 3 rad/sec indicates a very small phase delay, the slope increases in the range 3 rad/sec and 8 rad/sec, however in the range ω_{180} and $2\omega_{180}$ the phase is the lowest among all other axes. Which, in theory, suggests that piloting of manoeuvres significantly involving the Yaw axis can be expected to be the least demanding, and with quite fast responses (due to the high bandwidth).

The estimated linear response and the flight-test data derived phase limited bandwidth and phase delay handling qualities parameters for all axes for the hover flight condition are presented in Table 6.1.

Controller	$\omega_{B/W}$	τ_p	Handling Quality		PIO
1sqDW	rad/sec	sec	Target Acq. Track.	UCE = 1	
Pitch (θ)	1.64 (2.19)	0.096 (0.17)	2 (1)	1 (1)	Yes
Roll (ϕ)	2.99 (3.07)	0.06 (0.15)	1 (2)	1 (1)	Yes
Yaw	3.12 (5.07)	0.04 (0.03)	2 (1)	n/a	Yes

Table 6.1: Handling qualities for small amplitude attitude changes; Predicted, (Flight-Test Data derived)

Analyzing Table 6.1 indicates that the time delay which was integrated into the plant to enhance realism of the linear simulations and to increase robustness, was not sufficiently large for the Roll and Pitch axes.

It can be seen that, although the estimated values of the phase limited bandwidth for Pitch, Roll and Yaw are below the achieved ones, they seem to be very close and lie within the margin of error of the bandwidth method, except the Yaw axis which is significantly off the achieved value.

This is concerning, because it emphasizes that either the ADS-33 HQ Toolbox has not been updated- which is unlikely due to the relatively accurate predictions in the other two axes, or that the linearized model Yaw axis dynamics representation is poor.

A similar mismatch between predictions based on the linearized model and those achieved in practice exists in the phase delays and indicates that elements influencing the phase delay parameter are more prevalent in the Pitch and Yaw axis.

6.2.3 Qualitative evaluation

In July 2001, the controller was implemented on the *Bell 205* helicopter in a series of flight tests. Unfortunately, significant mechanical problems associated with the Yaw axis gyro[5], actuators and mechanical linkages hindered accurate acquisition of data in the initial phases of the flight tests. Results from the limited number of flight tests were promising, and to a greater extent confirmed the consistency between simulations and flight test results.

The evaluations based on pilot comments combined with ADS-33E specifications on each channel comprised qualitative assessment of the performed task; the flight control law design is required to achieve *Level 1* HQ.

6.2.3.1 Flight test evaluation of Mission Task Elements

Figure 6.16 shows the responses of the helicopter at hover to an input train of alternate step demand control pulses in Pitch axis in different time sequence ratio. It can be clearly seen that in the first two doublet inputs the rotorcraft exhibits good attitude tracking, however the rate response builds up too slowly and in the long run affects the attitude retention which results in unwanted oscillations.

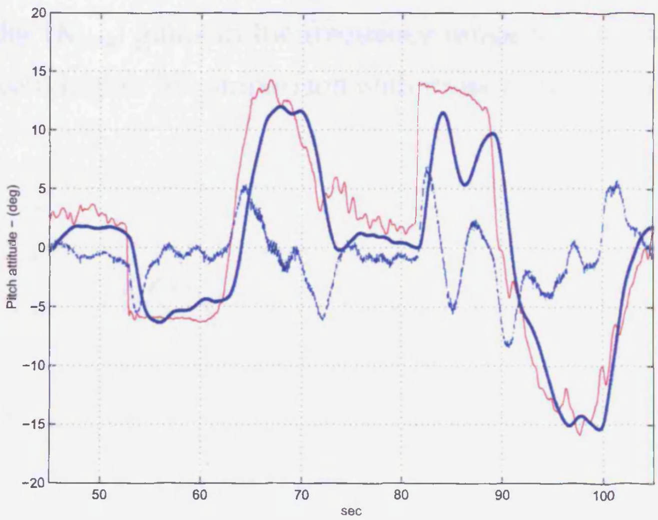

Figure 6.16: Pitch axis in-flight response: demand, solid (θ), dash dot (q) for **1sqDW**

In conclusion attitude retention is acceptable, but not at the level to satisfy the design objectives. Illustrated in Figure 6.17 is the pitch actuator's activity as a result of the demands shown in Figure 6.16. Excessive actuator activity is evident where the pilot had imposed a cone like type demand (in the interval 90 to 105 sec).

Figure 6.18 illustrates the ACAH response type in Roll to attempted doublet demands.

[5]Yaw gyro was found to provide inaccurate measurements, and was replaced with a laser gyro in time for testing of control law **1nsqDW**.

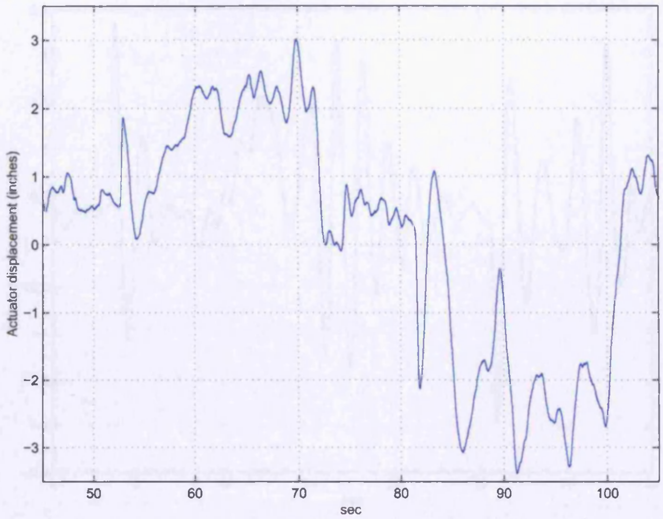

Figure 6.17: Pitch axis actuator (FDE) activity

The attitude response is underdamped, very oscillatory with significant steady-state error (e_{ss}) characteristics which were not predicted by the linear model. The pilot stressed the easily excited high frequency lateral oscillations. These can be related to very high controller ($\mathbf{K}_{imp}$) gains in the frequency range 6 to 15 rad/sec; these gains are up to 100 per cent higher in comparison with those of $\mathbf{K}_{imp}$ controller of **1nsqDW** control law.

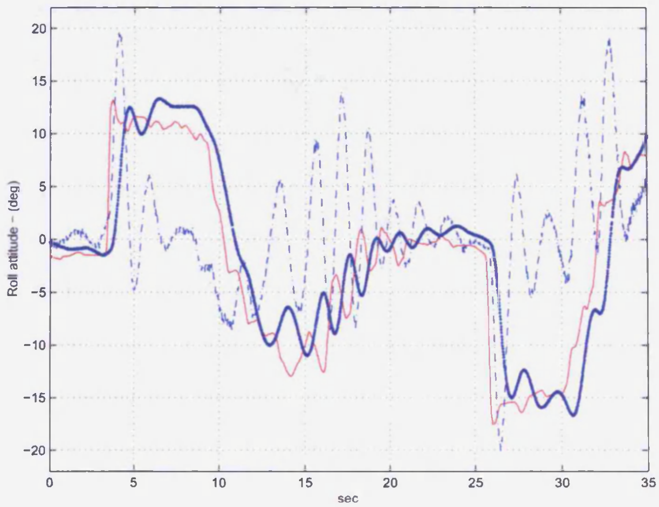

Figure 6.18: Roll axis in-flight response: demand; solid (ϕ); dash dot (p) for **1sqDW**

The response dynamics reflect onto the axes' actuator activity illustrated in Figure 6.19. It is likely that in manoeuvres heavily involving the Roll axis, e.g *Side Step*, this will adversely affect HQ properties ratings. Excessive and jittery actuator activity is evident where the pilot had imposed a cone like type demand.

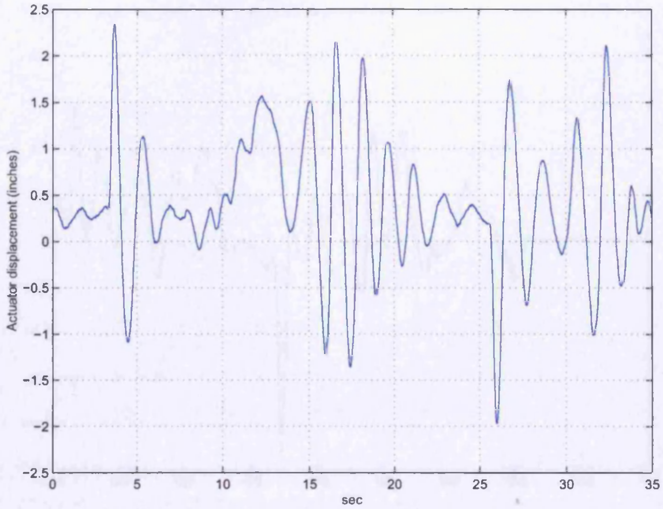

Figure 6.19: Roll axis actuator (FDA) activity

Shown in Figure 6.20 is the rotorcraft's response to two doublet step type demands of up to 20 deg in Yaw axis. Given the dynamic characteristics of the Yaw axis, the response is fast, with slight overshoot and oscillatory (i.e $\zeta < 0.7$ thus underdamped) behaviour which adversely affects the tracking of the demand. Control of this axis dynamics appeared to be the most challenging. This was due to the significant amount of parametric uncertainty.

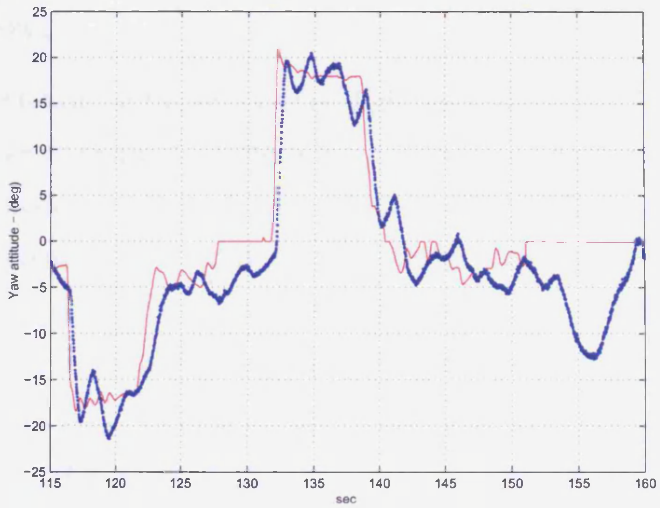

Figure 6.20: Yaw axis in-flight response: demand; response for **1sqDW**

Figure 6.21 shows the actuator activity in the Yaw channel. Although the manoeuvre is very demanding, the work load it imparts on the actuators appears to be the lowest among all the axes actuator dynamics.

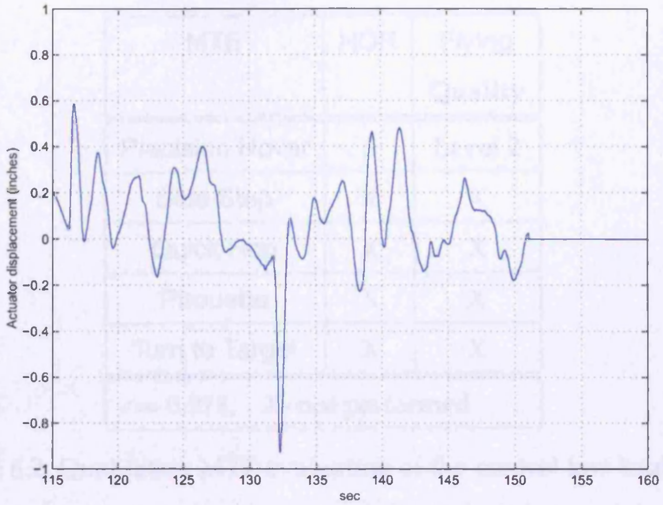

Figure 6.21: Yaw axis actuator (FDR) activity

6.2.3.2 Pilot Comments

Frequency sweeps and step inputs applied to every axis allows the pilot to evaluate the dynamic characteristics of the rotorcraft around every axis and its suitability of performing different MTEs. Once the rotary-wing aircraft (augmented with the control law) is subjected to frequency sweeps and step inputs and found adequate for HQ testing the pilot would proceed with testing of the control law for different manoeuvres of MTEs.

In view of the limitation on the number of flight tests and control law characteristics the pilot deemed as appropriate performing only one qualitative evaluations for one manoeuvre- the precision hover. This resulted in *HQR* of *5*, signifying moderate to objectionable deficiencies in aircraft characteristics, corresponding to *Level 2* flying qualities. The pilot has also reported considerable backing out of the loop to suppress PIO, and easily excited lateral axis high frequency oscillations.

Table 6.2 presents in a compact way the pilot's qualitative evaluations of the controller in view of the ADS-33E requirements.

6.3 Non-square plant: diagonal weights - **1nsqDW control law**

Inclusion of extra measurements (angular rates p and q) in the 1 Dof loop-shaping resulted in non-square helicopter system plant representation. The design presented in this section is for control law (**1nsqDW**) and was performed on a non-square ($5 \times$

MTE	HQR	Flying Quality
Precision Hover	5	Level 2
Side Step	X	X
Quick Hop	X	X
Pirouette	X	X
Turn to Target	X	X
$\epsilon = 0.278$, X- not performed		

Table 6.2: Qualitative MTE evaluation of the control law **1sqDW**

3) (rectangular) helicopter system plant in May and June 2003; the control law was evaluated in flight tests.

6.3.1 Desk-top simulations: Linear response time domain analysis

Figure 6.22 depicts the linear response of the helicopter to a step input demand of amplitude 0.2 rad in Roll axis. The response is overdamped with rise time of approximately 4 sec and steady-state error of 2 per cent.

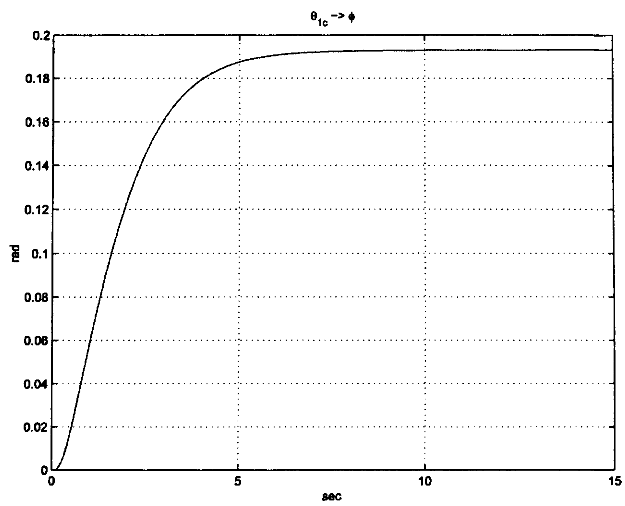

Figure 6.22: Linear response to lateral cyclic step demand of 0.2 rad

Examining Figure 6.23 reveals Roll to Yaw ($\frac{r}{\phi}$) coupling of 10 per cent, which is higher than coupling between Roll and Pitch ($\frac{\theta}{\phi}$) of approximately 3 per cent.

Shown in Figure 6.24 is the linear response to a step input demand of 0.2 rad in Pitch channel. The response is overdamped and the rise time of the channel's response, seen

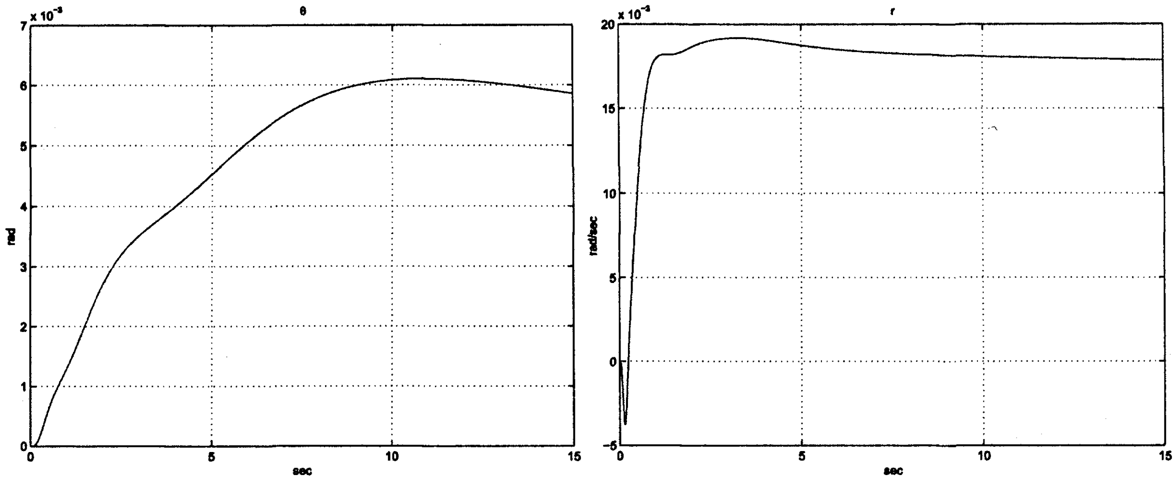

Figure 6.23: Coupling to lateral cyclic step demand of 0.2 rad

in the same Figure, is approximately 4 sec, which is quite high hence slow response.

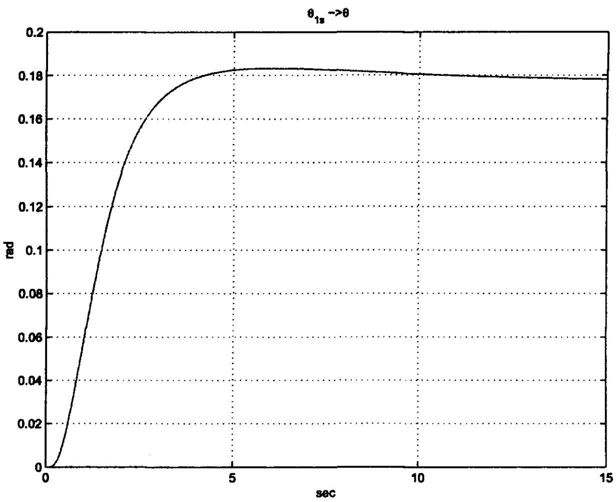

Figure 6.24: Linear response to longitudinal cyclic step demand of 0.2 rad

The cross coupling from Pitch to Roll ($\frac{\phi}{\theta} \approx 3$) per cent, and from Pitch to Yaw ($\frac{r}{\theta} \approx 5$) per cent, all illustrated in Figure 6.25.

Illustrated in Figure 6.26 is the linear system's response to 0.2 rad/sec amplitude step demand in Yaw channel. Due to the aerodynamic frame asymmetry and main rotor-tail rotor interaction this is expected to be the most challenging channel to control in the helicopter system. The response (as expected from the high bandwidth) is sharp, with rise time $t_r < 1$ sec, overshoot of about 10 per cent and $e_{ss} \approx 10$.

Analysis of Figure 6.27 indicates significant cross-axis coupling between Yaw and Roll ($\frac{\phi}{r}$) which manifests itself with about 19 per cent interaction; coupling from Yaw to

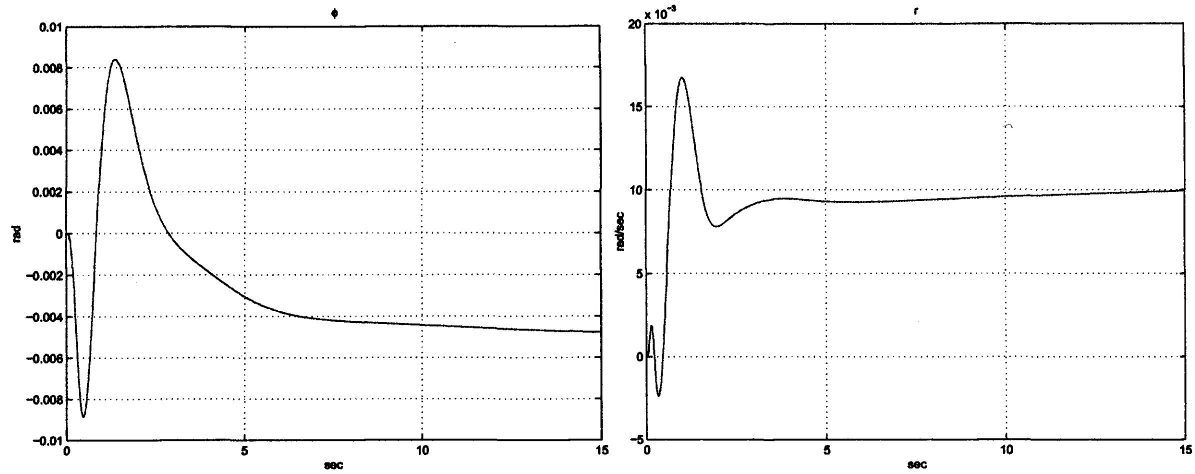

Figure 6.25: Coupling to longitudinal cyclic step demand of 0.2 rad a)θ b)ϕ

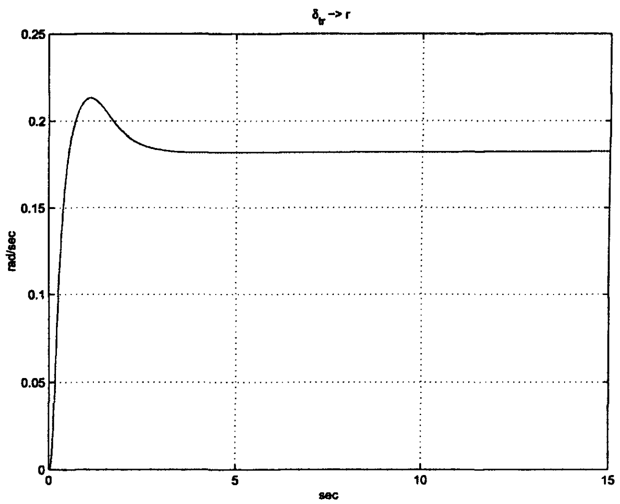

Figure 6.26: Linear response to pedal demand of 0.2 rad/sec

Pitch ($\frac{\theta}{r}$) is just 4 per cent. Although these are linear simulations, they confirm the difficulty posed in the control of the Yaw axis dynamics.

It is worth mentioning that in all the linear dynamic response simulations of the system, augmented with **lnsqDW** control law, the input demand was fixed to be 0.2 rad or (0.2 rad/sec) while, in fact, the greatest amplitude of in-flight demands[6] are as follows [Gub02]:

- Quick Hop: -10^o for acceleration and $+30^o$ for deceleration.
- Side Step: about 25^o on acceleration and up to $+35^o$ on deceleration.

[6] These demands have been used in the assessment of every control law, however, for consistency with in-flight demands, they will not be presented herein.

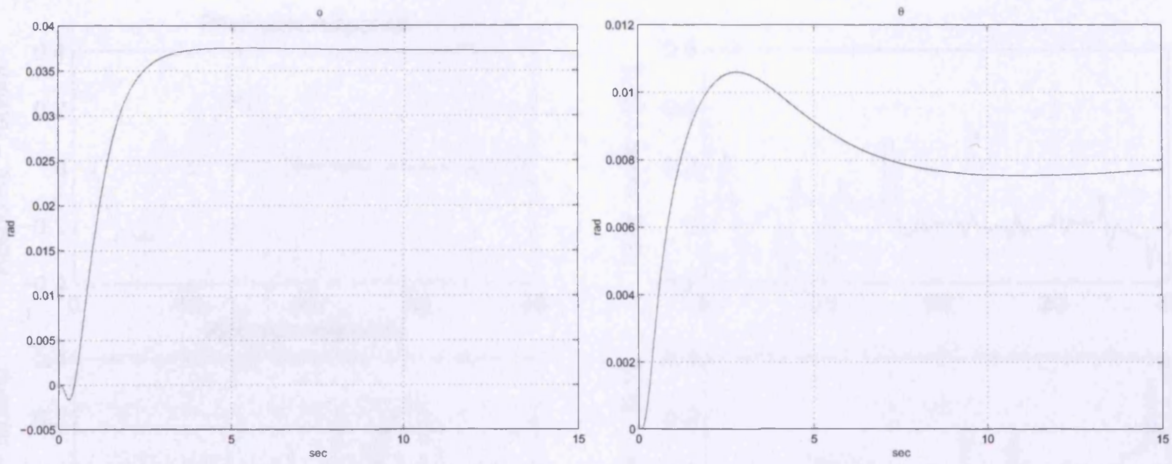

Figure 6.27: Coupling to pedal step demand of 0.2 rad/sec

- Turn to Target: the pilot should be demanding around $20 - 30$ deg/sec.

6.3.2 Desk-top simulations: Nonlinear response time domain analysis

Depicted in Figure 6.28 are nonlinear simulations of the helicopter's nonlinear model augmented with **1nsqDW** controller architecture (which utilized diagonal weights).

Subplots in the first column in the (3×2) matrix structured Figure 6.28 denote the demands, attitude and angular rate responses in Pitch, Roll and Yaw channels respectively, while subplots in the second column reflect the actuator activity in each channel during the performed tasks.

The way the subplots are structured in Figure 6.28 allows the designer to obtain an accurate picture about tracking, actuator activity and inter-axis coupling. The labels on the vertical axes in the subplots (:,2) should read as: Longitudinal cyclic [-1,1], where 1 is fully forward; Lateral cyclic [-1,1], where 1 is fully right; and Tail rotor collective [-1,1], where 1 is fully right.

Subplot (1,1) in the Figure 6.28 gives the response to -0.25 rad (nose down, forward flight) or equivalent of -14^o step ramp like doublet demand with duration of 4 sec in Pitch channel.

This demand pattern can be associated with the *Quick Hop* (*Quick Step*) manoeuvre. The response is rather slow and overdamped; the same tendency can be observed from linear simulations in Figure 6.24. Information about actuator activity, for this manoeuvre, can be extracted from subplot (1,2), which indicates low to acceptable moderate activity. The coupling from Pitch and Yaw ($\frac{r}{\theta}$) is slightly higher than in Pitch

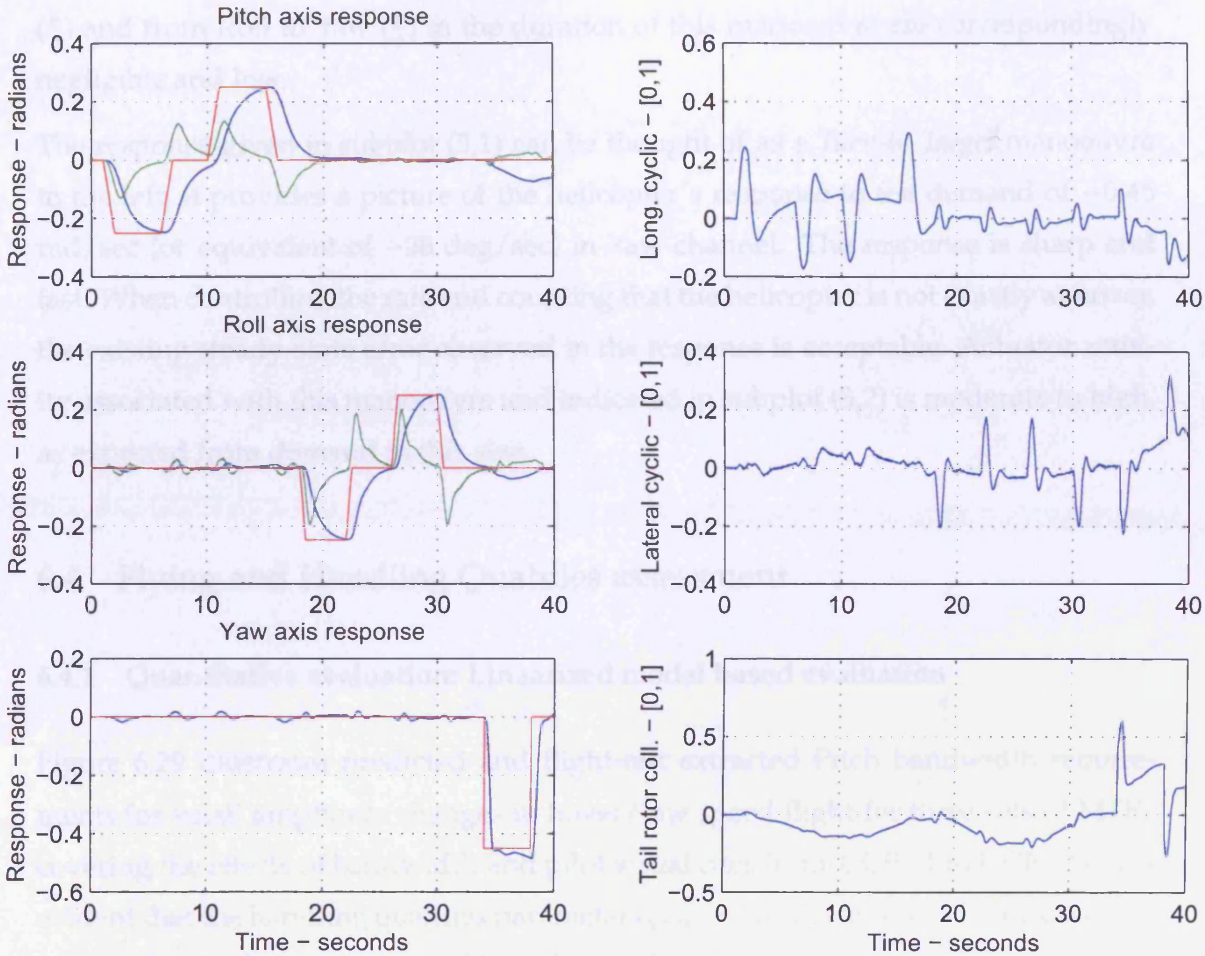

Figure 6.28: Left column- Nonlinear model: demand, rate, attitude responses; Right column: actuator activities for **1nsqDW**

to Roll ($\frac{\phi}{\theta}$), however, both of them are very small (< 3) per cent. These measurements are compatible with observations made from linear response simulations where the coupling was correspondingly 3 per cent and 5 per cent.

Subplot (2,1) illustrates in simulation a *Side Step* manoeuvre with demand of -0.25 rad (side flight to the right[7]) or equivalent of -14^o, in Roll channel with 3.5 sec duration. The response, as expected from linear simulation (in Figure 6.22) is smooth, overdamped and slow. However it is slightly faster than the Pitch channel, which can be justified with the aero-mechanical structure (primarily the value of principal moments of inertia- $I_{yy} > I_{zz} > I_{xx}$) of the *Bell 205*. This manoeuvre results in low actuator activity as depicted in subplot (2,2). Inter-axis couplings from Roll to Pitch

[7]Experience from Handling Qualities ratings of MTEs have shown that, due to the asymmetric aerodynamics structure, pilot ratings on Side Step manoeuvre to the left differ from those on the Side Step manoeuvre to the right. Tail rotor's positioning and its torque can be pointed as sources for this difference.

($\frac{\theta}{\phi}$) and from Roll to Yaw ($\frac{r}{\phi}$) in the duration of this manoeuvre are correspondingly negligible and low.

The response given in subplot (3,1) can be thought of as a *Turn-to-Target* manoeuvre to the left, it provides a picture of the helicopter's response to the demand of -0.45 rad/sec (or equivalent of -26 deg/sec) in Yaw channel. The response is sharp and fast. When controlling the rate and counting that the helicopter is not exactly at hover, the existing steady-state error observed in the response is acceptable. Actuator activity associated with this manoeuvre and indicated in subplot (3,2) is moderate to high, as expected from demand in this size.

6.4 Flying and Handling Qualities assessment

6.4.1 Quantitative evaluation: Linearized model based evaluation

Figure 6.29 illustrates predicted and flight-test extracted Pitch bandwidth requirements for small amplitude changes in hover/low speed flight for three sets of MTEs covering the effects of bandwidth and pilot visual cues from(UCE=1 to UCE>1). It is evident that the handling qualities parameters (ω_{bw}, τ_p) indicate *Level 1* flying qualities as a result of high bandwidth and low phase delay. Note the strong similarity between predicted (using the linearised model) and achieved (in flight-tests) bandwidth values. The slight difference between predicted and achieved phase delay values could be a result of insufficient representation of computational delays, or time delays originating from filters or actuators.

Shown in Figure 6.30 are Roll bandwidth requirements for small amplitude changes in hover/low speed and forward flight for demanding combat Target acquisition, and other MTEs- with more relaxed (ω_{bw}, τ_p) boundaries.

It is seen that according to the predicted handling qualities parameters of phase limited bandwidth and phase delay of the aircraft in small amplitude roll attitude changes *Level 1* flying qualities are satisfied not only in demanding Target Acquisition MTE, but also in Fully Attended Operations as well as in Divided Attention Operations (UCE> 1). Careful examination will also reveal that although bandwidths are predicted with significant accuracy, phase delay predictions are lagging significantly. This, firstly suggests that the slope of the phase curve between neutral frequency (ω_{180}) and ($2\omega_{180}$) is much steeper than that predicted by the linearized model, and

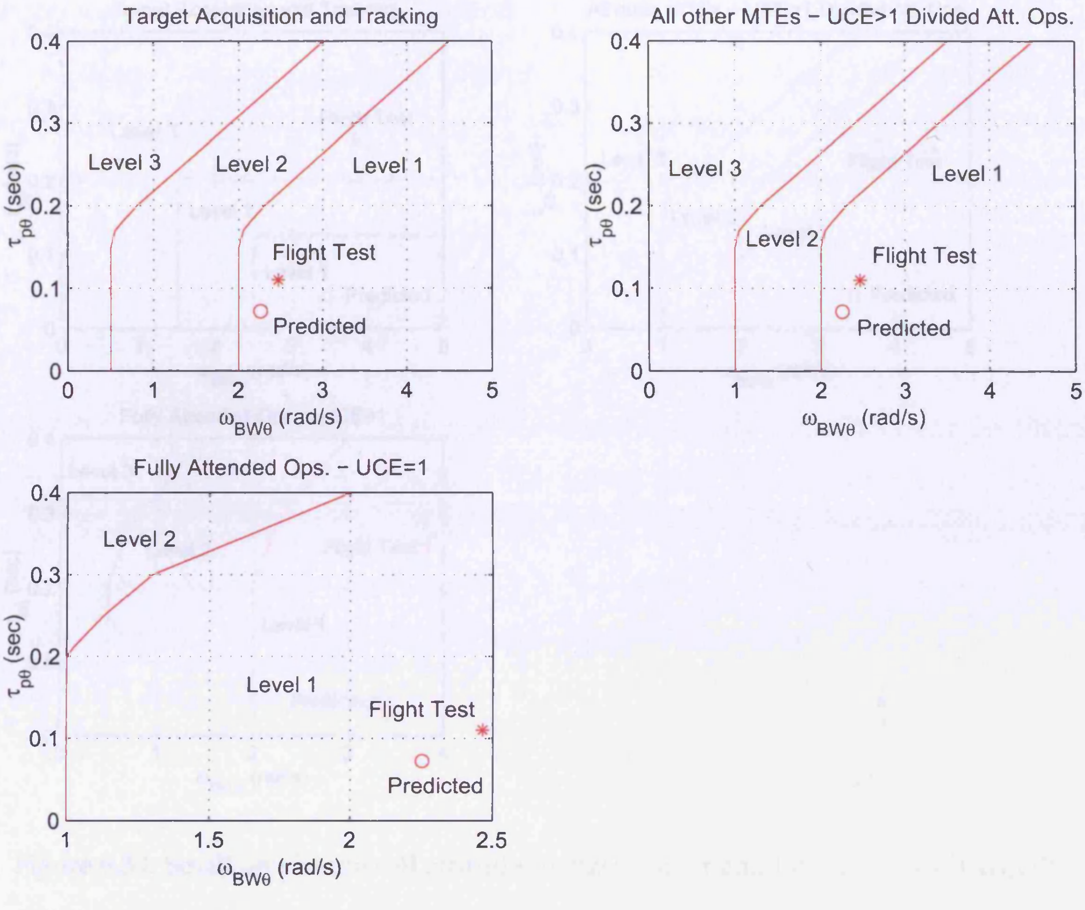

Figure 6.29: Small amplitude **pitch** attitude changes -hover and low speed- for **1nsqDW**

second, the time delays present in this axis are much higher than the integrated 75 msec in the linear model.

Illustrated in Figure 6.31 are the rotorcraft's Yaw bandwidth requirements for small amplitude changes in hover/low speed flight for only two MTEs together with predicted and flight-tested aircraft bandwidth and phase delay parameter values. Note the consistency between predicted and flight test derived phase delay parameters τ_p, indicating that the time delays (transport delay, rotor lag delay, filter lag delays) have been accurately represented. However, the significant difference in the bandwidth suggests that the linearized model might have lost those modes which significantly influence the heading dynamics[8]. It will be interesting to know what would have been the phase delay prediction, had the heading state been kept within the linearized model. The aircraft's bandwidth was predicted to achieve *Level 3* and *Level 2* in combat and other MTEs, but, what it achieved in reality was much higher than predicted- yielding *Level 1* flying qualities in performed and evaluated MTEs.

[8]In fact, in Chapter 5 section 5.2 $\psi_{heading}$ state was removed by truncation.

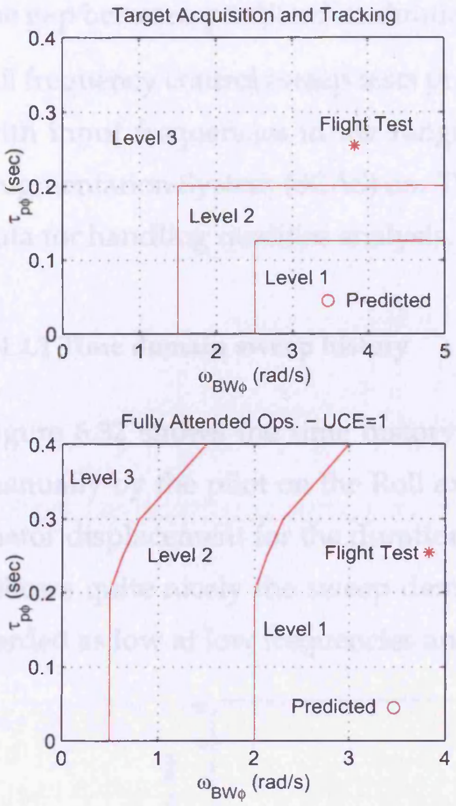

Figure 6.30: Small amplitude **roll** attitude changes -hover and low speed- for **1nsqDW**

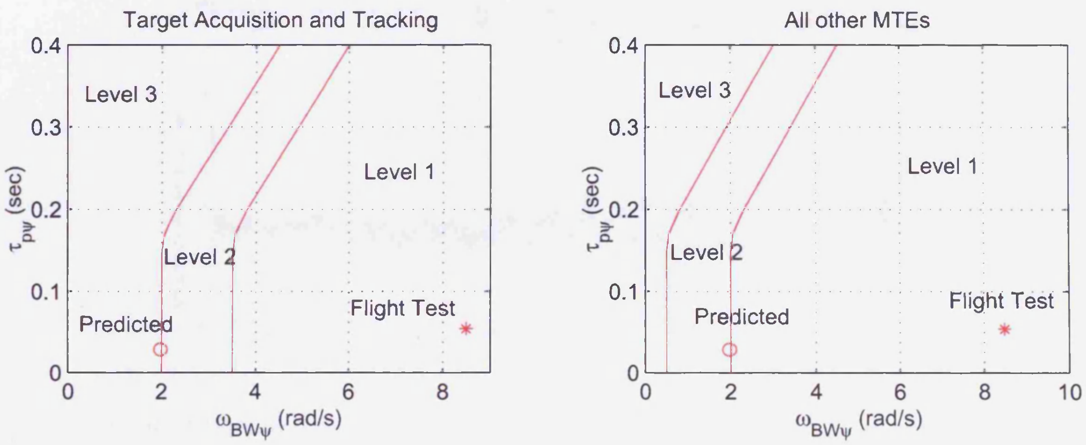

Figure 6.31: Small amplitude **heading** changes -hover and low speed- for **1nsqDW**

6.4.2 Flight test frequency sweeps

The flight-tests described in this section, and onwards, were performed on the *Bell 205* which had been equipped with a new inertial system[9] and improved engine performance. These elements significantly improved controller performance and reduced

[9] Laser gyroscopes on every principal control axis.

the gap between predicted in simulations and achieved in flight results.

All frequency control sweep tests presented for control law **1nsqDW** were conducted with input frequencies in the range 0.1 Hz and 1.5 Hz with Stability and Control Augmentation System (SCAS) on. This frequency range is sufficient for acquisition of data for handling qualities analysis.

6.4.2.1 Time domain sweep history

Figure 6.32 shows the time history of the frequency sweep manoeuvre performed manually by the pilot on the Roll axis; the same Figure also depicts lateral cyclic actuator displacement for the duration of this manoeuvre. It is evident that the aircraft follows quite nicely the sweep demands in Roll axis. Actuator control power is regarded as low at low frequencies and high at high frequencies.

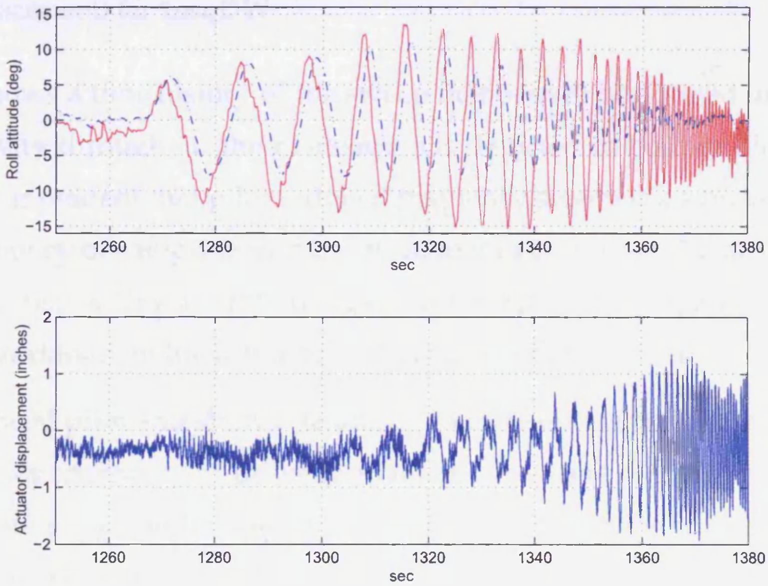

Figure 6.32: Roll axis frequency sweep: red-(demand), dash dot-(response), solid blue-(actuator displacement) for **1nsqDW**

Figure 6.33 illustrates longitudinal cyclic frequency sweep: Pitch angular attitude response to cockpit controller deflection together with longitudinal cyclic actuator activity. Attitude response tracking at low frequencies is good, however it degrades as the frequency of the sweep demand increases. This is mainly due to high inertia of the rotorcraft about its Pitch axis. Actuator workload increases as the frequency of the demand increases, but the magnitude of the actuator signal remains in the same magnitude band.

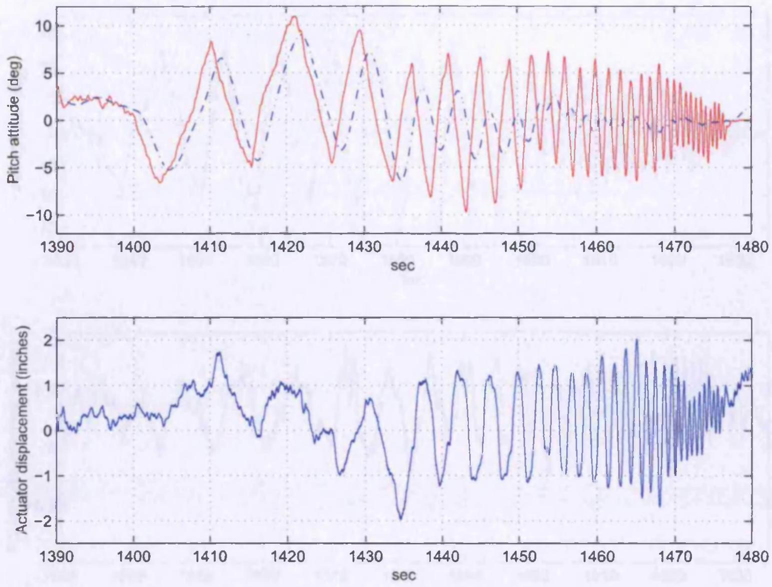

Figure 6.33: Pitch axis frequency sweep: red-(demand), dash dot-(response), solid blue-(actuator displacement) for **1nsqDW**

Figure 6.34 shows a time history of the sweep manoeuvre performed in the Yaw axis. Actuator activity throughout the manoeuvre is depicted in bottom plot of the same Figure 6.34. It is evident that pilot induced frequency sweep is a sinusoidal input signal with frequency of sampling varying from low to medium. The attitude response is very quick, crisp with good following of the sweep command; all yield to reduced activity and workload on the actuator (in Yaw axis) engaged in this manoeuvre.

An inexperienced pilot will show a tendency to increase the control input amplitude as the frequency increases, in order to maintain the same overall amplitude of the rotorcraft response. It can be seen from the frequency sweeps control tests- Figures (6.32 through 6.34)- that control inputs' amplitudes remained almost the same in the frequency range of the sweep tests, although the response amplitudes decreased in Figure 6.32 and Figure 6.33; an indication of professional piloting.

Remark 6.1 *At the end of frequency sweeps the Evaluation Pilot estimated moderate bandwidth (ω_{bw}), detected Longitudinal to Roll coupling and (surprisingly) marginal Lateral stability.*

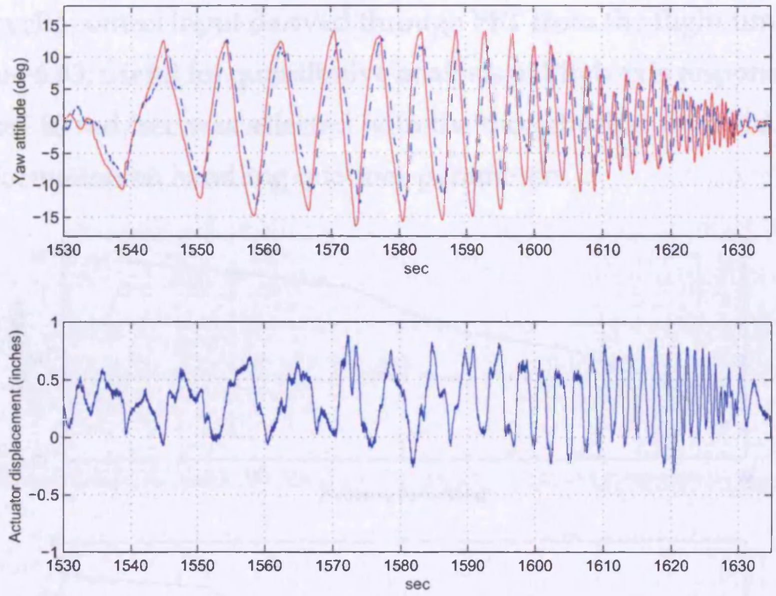

Figure 6.34: Yaw axis frequency sweep: red-(demand), dash dot-(response), solid blue-(actuator displacement) for **1sqDW**

6.4.2.2 Frequency domain sweep history-Frequency response estimation

This section compiles frequency domain responses extracted from frequency sweep manoeuvres which were performed in all principal- control- axes. Figure 6.35 shows the estimated Roll axis transfer function frequency response on the Bode diagram.

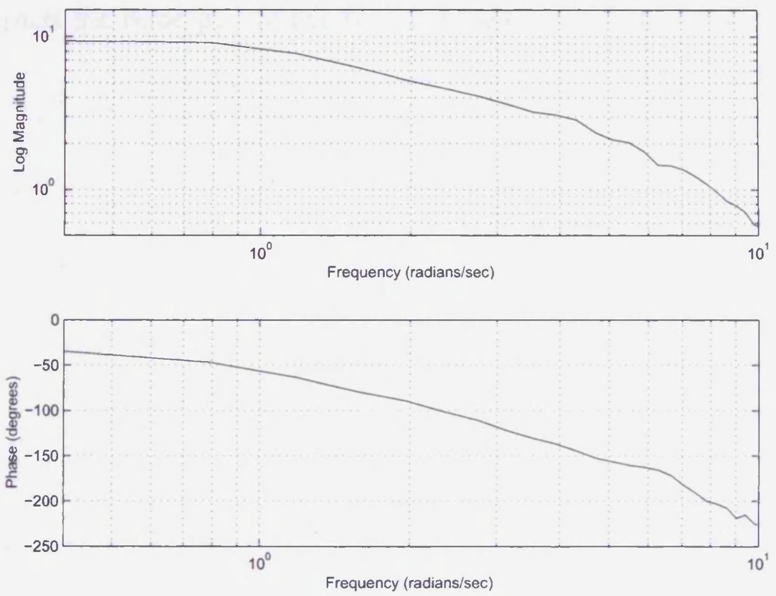

Figure 6.35: Roll axis frequency estimate

Figure 6.36 presents the frequency response plot of the rotorcraft's Pitch attitude to longitudinal cyclic control input derived through FFT from the flight time history depicted in Figure 6.33; useful for quantitative analysis of Pitch axis response. The range 0.4 rad/sec and 10 rad/sec was selected with the thought that it would be sufficient to provide information on handling qualities parameters.

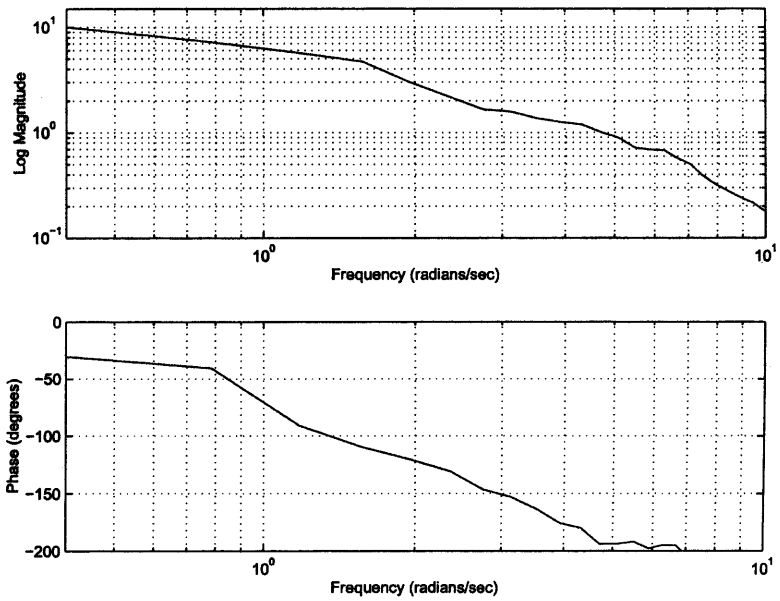

Figure 6.36: Pitch axis frequency estimate

Measurements of the bandwidth and the phase delay handling qualities parameters for short term, small amplitude Yaw axis response criteria can be obtained from Figure 6.37 which depicts the Bode plot of the Yaw axis frequency response dynamics.

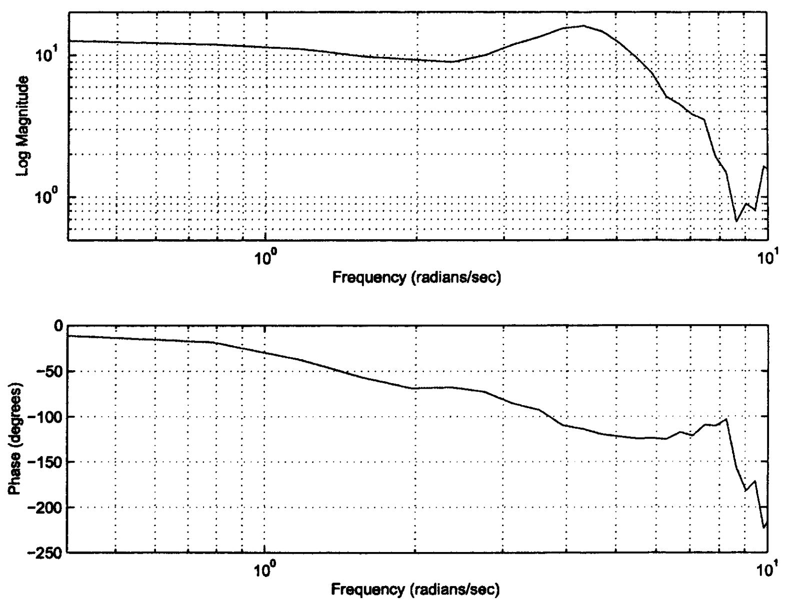

Figure 6.37: Yaw axis frequency estimate

Table 6.3 presents estimated and flight-test data derived bandwidth and phase delay values in all principal axes, for small amplitude changes at hover and low speed. Two types of responses were used: ACAH and RCAH. Bandwidth frequencies were derived according to the phase limited bandwidth definition. It is important to note that all axes phase limited bandwidths were greater than the gain limited bandwidths. It may, therefore, be that the rotorcraft may be PIO prone in manoeuvres requiring significant pilot workload, high precision manoeuvres or aggressive manoeuvres.

Controller	$\omega_{B/W}$	τ_p	Handling Quality	
1nsqDW	rad/sec	sec	Target Acq. and Track.	UCE = 1
Pitch-(θ)	2.25 (2.46)	0.07 (0.11)	1 (1)	1 (1)
Roll-(ϕ)	3.46 (3.83)	0.044 (0.25)	1 (3)	1 (1)
Yaw	1.97 (8.48)	0.029 (0.054)	3 (1)	2(1)

Table 6.3: Handling qualities for small amplitude attitude changes; Predicted, (Flight-Test Data derived)

Table 6.3 indicates good compatibility between predicted (based on the helicopter model linearized around hover flight), and results derived from flight-test control frequency sweeps bandwidths and phase delays. The exception is the Yaw axis predicted bandwidth and phase delay which are lower than achieved. The case was similar in control law **1sqDW**, where only the bandwidth was mismatching. The assumption that the Yaw axis dynamics is poorly represented in linearised model carries through. It is seen that achieved Handling Qualities, for short term small amplitude changes in all axes, match the predicted in all MTEs, except for Roll in Target tracking MTE.

6.4.3 Qualitative evaluation

6.4.3.1 Flight test evaluation of Mission Task Elements

While in hover with the helicopter trimmed, a series of doublets type demands with amplitude varying in the range $10^o - 15^o$, as illustrated in Figure 6.38, were applied through longitudinal cyclic on the Pitch axis. The response which can be thought of as *Quick Step* is slow but smooth, with good attitude retention; overshoot varying between 10 to 15 per cent and steady-state error (e_{ss}) in the range from 2 per cent up to 20 per cent[10].

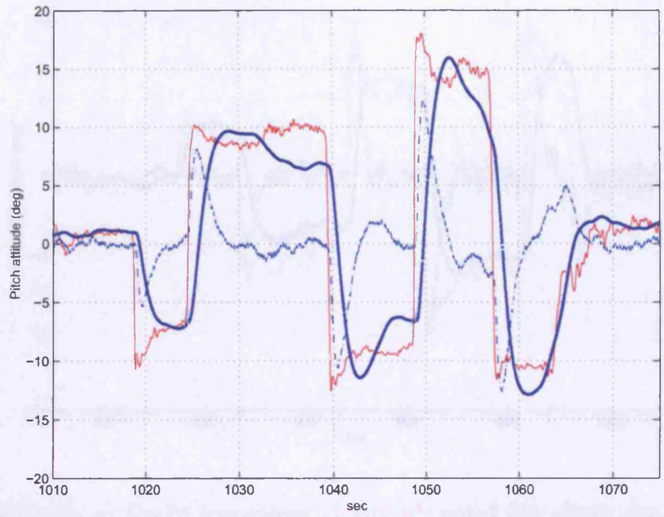

Figure 6.38: Pitch axis in-flight response: demand; solid (θ); dash dot (q) for **1sqDW**

Pitch actuator (FDE) displacement (in inches) as a function of time is illustrated in Figure 6.39. Activity can be described as moderate.

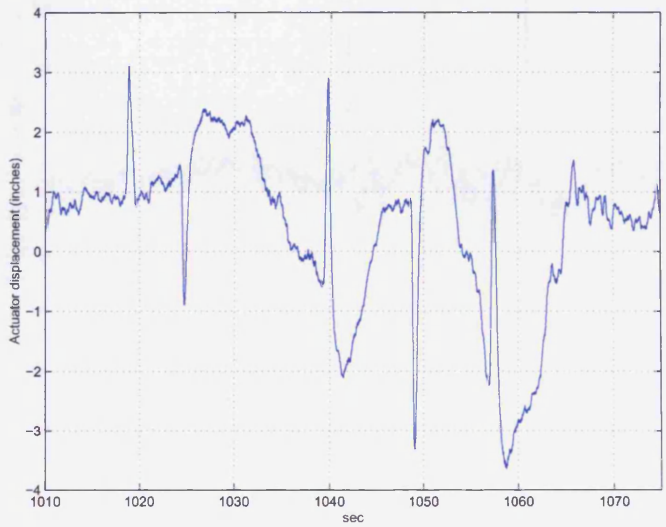

Figure 6.39: Pitch axis actuator (FDE) activity

The helicopter's response in Roll axis to a series of doublet type input demands with amplitude varying in the range $8^o - 15^o$ is depicted in Figure 6.40. It is evident that the tracking is crisp and smooth with relatively small (5 to 10 per cent) steady-state error (e_{ss}), and negligible overshoot in the first couple of demands.

[10]Pilots are not sensitive to small state errors, but more sensitive to quickness of the response and actuator activity.

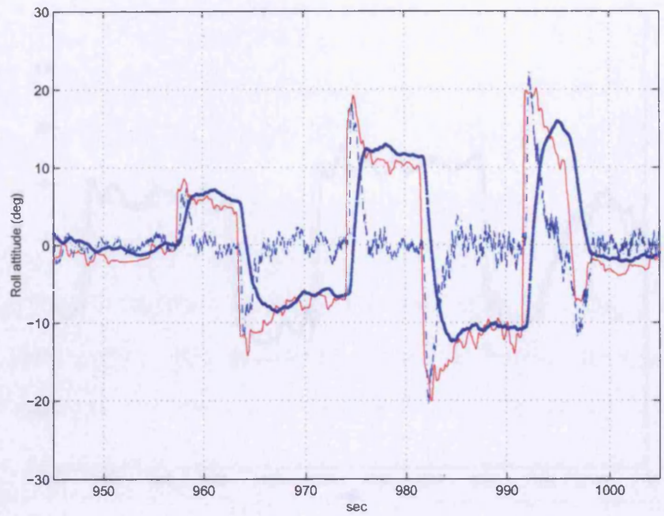

Figure 6.40: Roll axis in-flight response: demand; solid (ϕ); dash dot (p) for **1sqDW**

These satisfactory performance characteristics of the response eased the workload on the Roll axis FDA actuators- Figure 6.41.

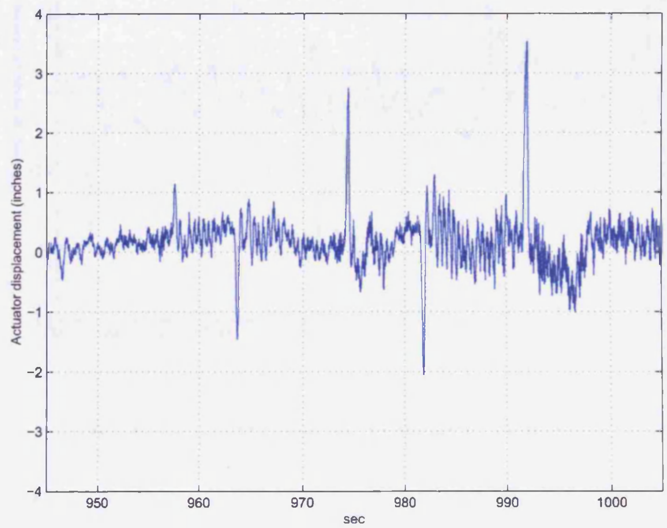

Figure 6.41: Roll axis actuator (FDA) activity

Figure 6.42 shows the *Bell 205* Yaw axis response to a series of pedal step pulse input demands around hover flight regime. The response, although oscillatory, is fast, slightly underdamped but with good tracking characteristics.

An account for the Yaw axis (FDR) actuator in inches throughout the manoeuvre is shown in Figure 6.43. The activity is low, as predicted by the nonlinear simulations, and is the lowest among other axes primary actuators.

In summary, the *Bell 205* has *Level 1* handling qualities for Target Acquisition and

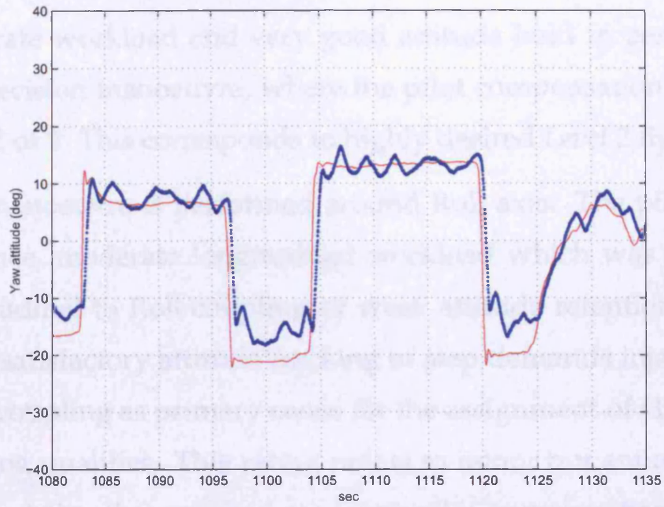

Figure 6.42: Yaw axis in-flight response: demand; response for **1nsqDW**

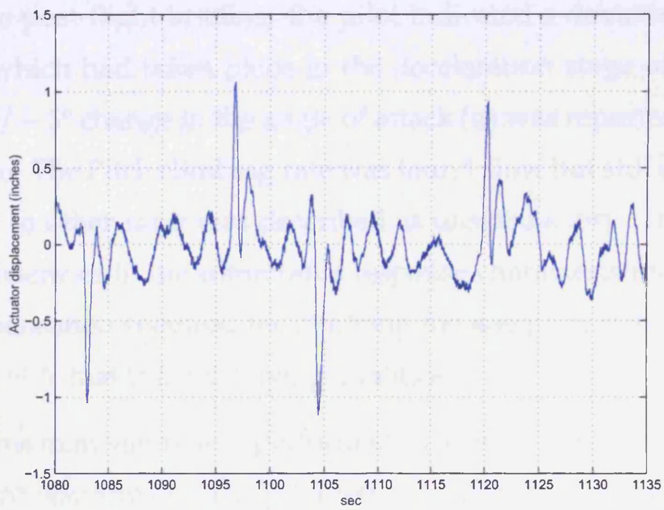

Figure 6.43: Yaw axis actuator (FDR) activity

Tracking, for Fully Attended Operations and Divided Attention Operations.

6.4.3.2 Pilot Comments

The following are in-flight comments and handling qualities evaluation of the augmented helicopter for several flight manoeuvres performed with the control law **1nsqDW**.

<u>**Hover**</u>: Desirable performance was noted with $+/-1^o$ excursions in the Roll channel-ϕ, and some deviation in heading ψ. Lateral directional oscillations have slightly reduced the ride quality and therefore the pilot assigned an HQR of 3 rating for this manoeuvre, which is *Level 1* desirable handling qualities requiring minimal pilot compensation.

Pirouette: Moderate workload and very good attitude hold in performing this demanding high-precision manoeuvre, where the pilot compensation was not a factor in achieving HQR of 2. This corresponds to highly desired *Level* 2 flying qualities.

Side step: This manoeuvre is performed around Roll axis. The pilot described desirable performance, moderate longitudinal workload which was said to be either because of longitudinal to Roll coupling or weak attitude retention. A look at Figure 6.40 deduces satisfactory attitude tracking of step demands injected in Roll axis, thus, leaving the coupling as primary cause for the assignment of HQR of 4, which is upper *Level* 2 flying qualities. This rating points to minor but annoying deficiencies in aircraft characteristics, that required moderate pilot compensation for attaining the desired performance.

Quick hop: In the post-flight briefing, the pilot indicated a deviation of $+/-10^o$ in *heading*- $\psi_{heading}$ which had taken place in the deceleration stage of the manoeuvre. An uncommon $+/-5^o$ change in the angle of attack (α) was reported in the course of the *QS* manoeuvre. The Pitch climbing rate was found slow but still satisfactory, however, its coupling to other rates was described as unsatisfactory. These moderate to objectionable deficiencies in the rotorcraft's response characteristics, and the considerable pilot compensation required for attaining the adequate performance resulted in award of HQR of 5, that is *Level* 2 flying qualities.

Turn to Target: This manoeuvre was performed two times, with 10 sec and 8 sec duration of engagement respectively. The pilot reported satisfactory attitude hold accompanied with tight lateral-directional oscillation in hover flight regime. These mildly unpleasant deficiencies in rotorcraft's response characteristics required minimal pilot compensation in attaining the desired performance. Therefore the pilot awarded HQR of 3 which corresponds to *Level 1* flying qualities.

The following Table 6.4 presents the qualitative evaluation of several manoeuvres for the rotorcraft augmented with control law **1nsqDW**. This evaluation was performed in view of the handling qualities requirements in ADS-33E for small amplitude changes in attitude about each of the principal axes.

The results presented in this section underline, once again, that controllers attaining *Level 1* flying qualities can indeed be synthesised providing that the appropriate response types are selected for the intended MTEs, and a high fidelity nonlinear dynamic model of the *Bell 205* is made available.

MTE	HQR	Flying Quality
Precision Hover	3	Level 1
Pirouette	2	Level 1
Turn to Target	3	Level 1
Side Step	4	Level 2
Quick Hop	5	Level 2
$\epsilon = 0.371$		

Table 6.4: Flight-test qualitative MTE evaluation of the control law **1nsqDW**

6.5 Non-square plant: Non-diagonal weights -**1nsqNDW control law**

This section presents results from desk-top computer simulations and in-flight evaluations of the control law **1nsqNDW**, which was evaluated in-flight in June 2003.

6.5.1 Desk-top simulations: Linear response time domain analysis

Figure 6.44 illustrates the linear response of the Roll channel to step input demand of 0.2 rad. The transient response is slow- with rise time $t_r \approx 4$ sec, well damped and without a notable steady-state error (e_{ss}), unlike the Roll response of **1nsqDW** control law.

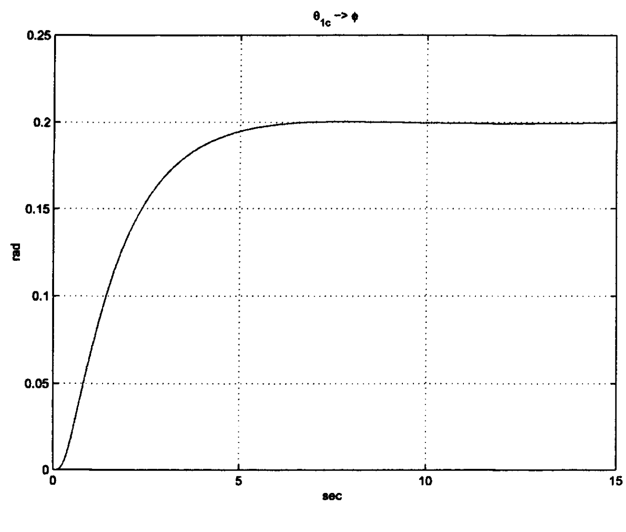

Figure 6.44: Linear response to lateral cyclic demand of 0.2 rad

The linear Roll attitude to Pitch attitude coupling ($\frac{\theta}{\phi}$) that can be derived from Figure

6.45 subplot a) is on average 1.5 per cent- which is smaller than its counterpart in 1 Dof diagonal weight controller **1nsqDW**. The Roll attitude to Yaw rate coupling depicted in Figure 6.45 subplot b) is approximately 4 per cent- slightly higher than what **1nsqDW** control law provided.

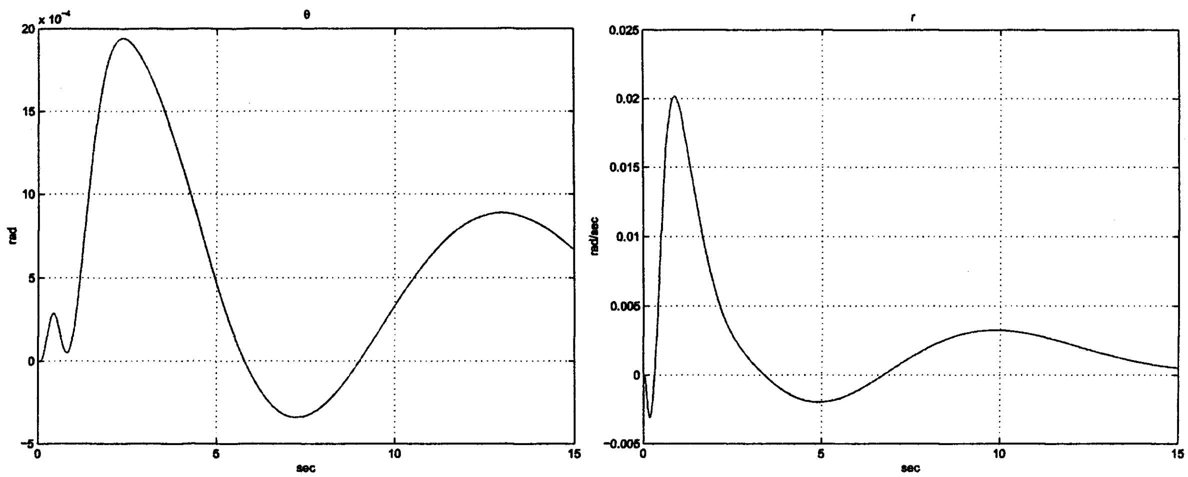

Figure 6.45: Coupling to lateral cyclic demand of 0.2 rad **a)** θ **b)** r

The Pitch axis attitude response to a step input demand with magnitude 0.2 rad is illustrated in 6.46. The response is slow, overdamped with steady-state error $e_{ss} \approx 2.5$ per cent, and the rise time is larger than expected- with value of 3.9 sec.

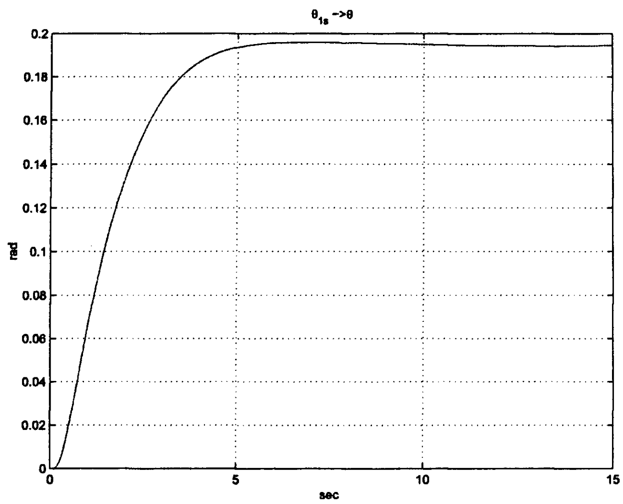

Figure 6.46: Linear response to longitudinal cyclic demand of 0.2 rad

Cross-couplings in Roll and Yaw channels to the demand of 0.2 rad in Pitch channel are illustrated in Figure 6.47 subplot a) ($\frac{\phi}{\theta} \approx 2.5$ percent) and b) respectively. It can be seen that control law **1nsqNDW** has reduced slightly the inter channel coupling when compared to **1nsqDW** control law cross coupling reduction characteristics.

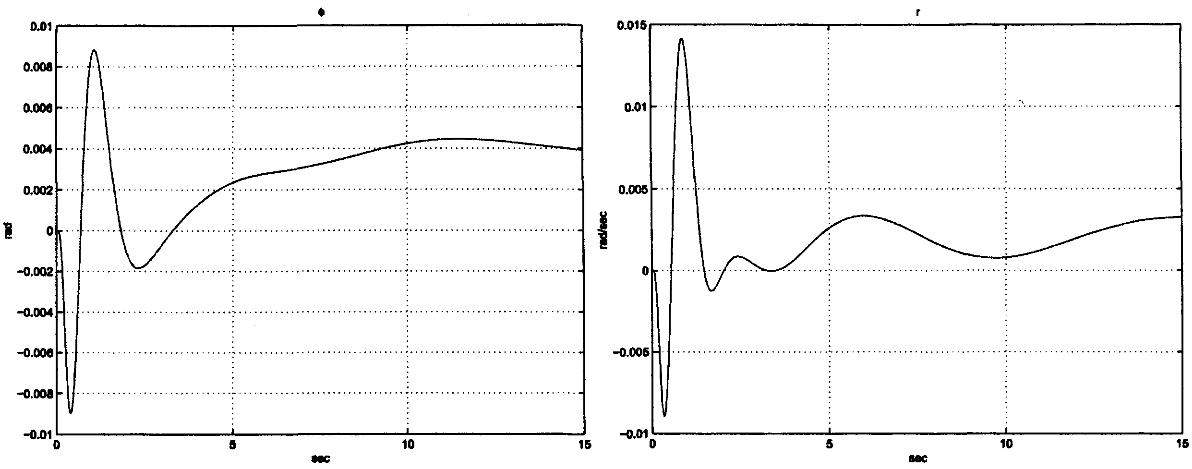

Figure 6.47: Coupling to longitudinal cyclic demand of 0.2 rad **a)**θ **b)**ϕ

The yaw channel time response history to a rate demand of 0.2 rad/sec is plotted in Figure 6.48. The response is very fast with rise time $t_r \approx 1$ sec and significant overshoot of about 20 per cent.

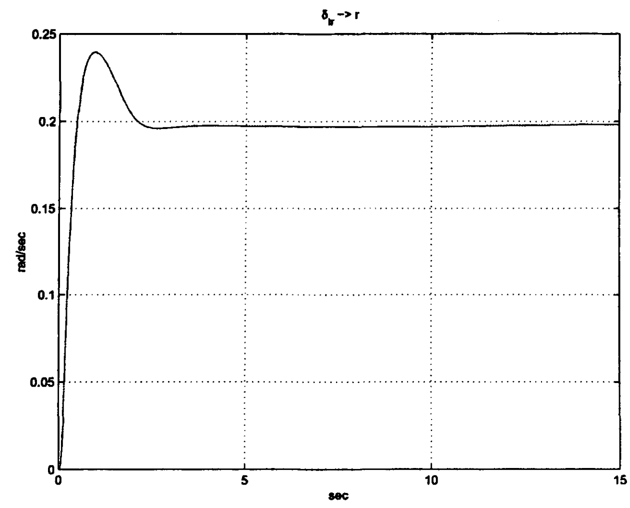

Figure 6.48: Linear response to pedal demand of 0.2 rad/sec

Coupling histories to the off axes are illustrated in Figure 6.49, where the coupling to Roll is significantly larger than the coupling to Pitch.

A careful observation of the linear time domain histories of all primary axis responses leads to the preliminary conclusion that in general the non-diagonal weights reduce the amount of inter channel cross-coupling and improve transient response characteristics. These linear simulations are only a guide and their validity will need to be confirmed with nonlinear simulations and flight-test results, which follows next.

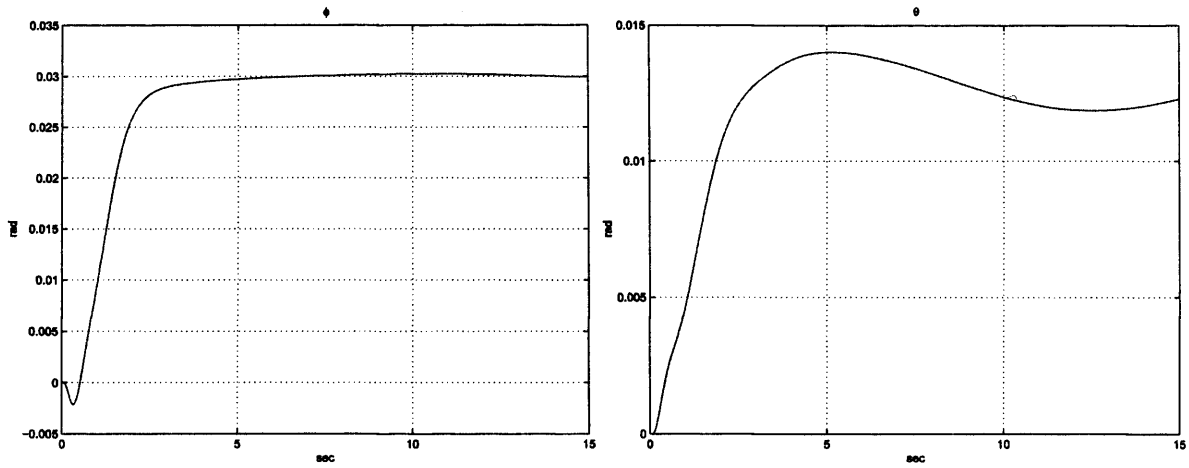

Figure 6.49: to pedal demand of 0.2 rad/sec **a)** ϕ **b)** θ

6.5.2 Desk-top simulations: Nonlinear response time domain analysis

Prior to flight testing, simulative step-like doublet type demands, emulating such manoeuvres as *Quick Hop*, *Side Step* and *Turn to Target* were performed correspondingly in Pitch, Roll and Yaw axes on the fully nonlinear (Simulink) model of the helicopter plant with the objective to assess the performance of the **1nsqNDW** control law. Demands were 0.25 rad in magnitude in Pitch and Roll channels, whereas in Yaw it was 0.45 rad/sec.

Unlike linear simulations, in order to assess for robust stability, variable actuator gains and time delays were represented in the model. The helicopter model robustness was assessed against 40 per cent gain variations at the plant input, and 75 ms time delay, again, at the plant input.

Subplots in the first column in a matrix structured Figure 6.50 present time histories of the helicopter's attitude response to doublet type demands with magnitude of 0.25 rad in Pitch and Roll channels, and 0.45 rad/sec in Yaw, in addition to the Pitch and Roll control axes rates; subplots in the second column show the actuator activity in each axis actuator during the simulatively performed tasks. The labels on the vertical axes in the subplots (:,2) should read as: Longitudinal cyclic [-1,1], where 1 is fully forward; Lateral cyclic [-1,1], where 1 is fully right; and Tail rotor collective [-1,1], where 1 is fully right.

The demand pattern with magnitude of -0.25 rad (nose down, and then up) or -14^o in Pitch axis depicted in subplot (1,1) of Figure 6.50 can also be considered as a simulation of *QH* manoeuvre. Comparison with its predecessor, pitch response of 1 Dof

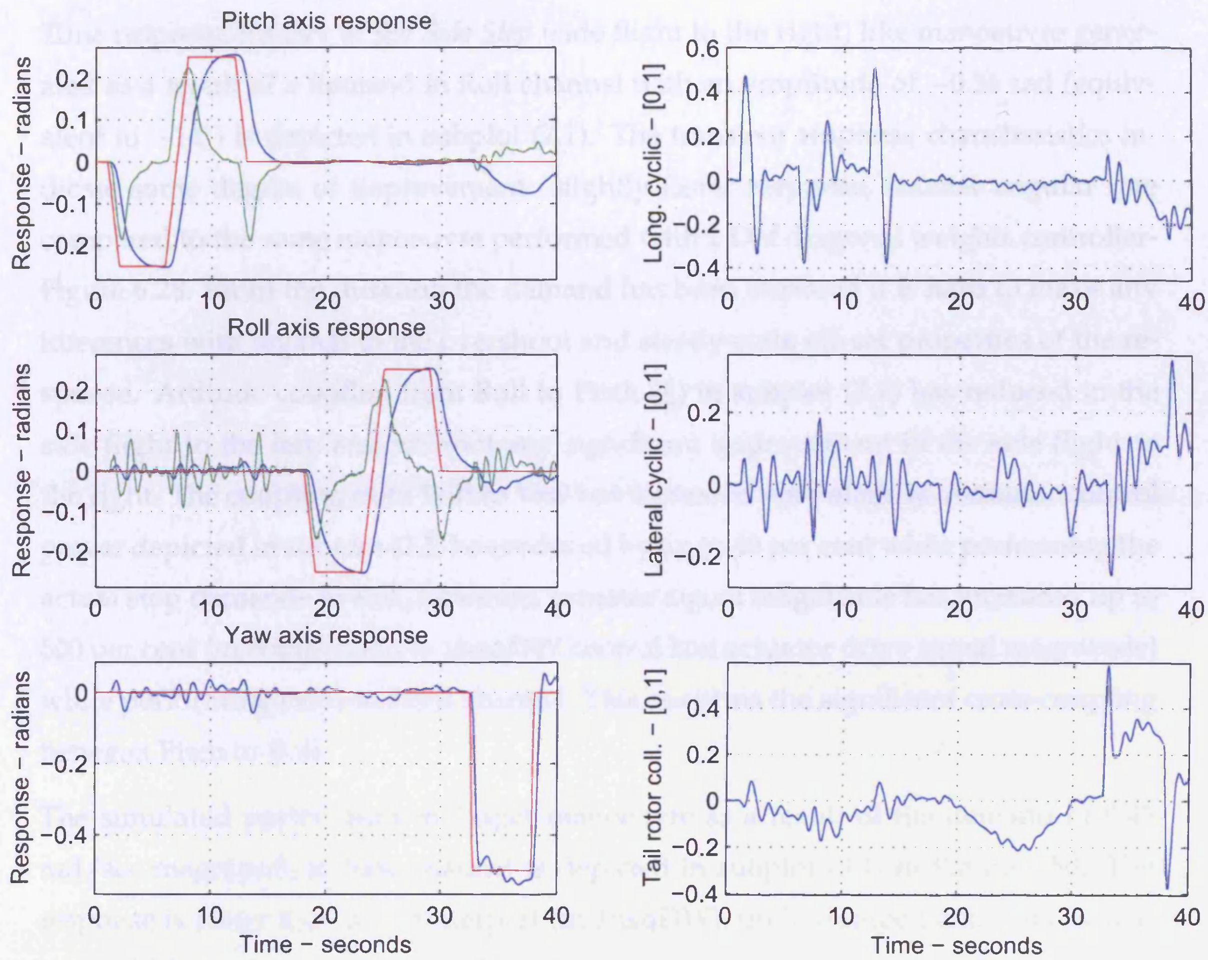

Figure 6.50: Left column- Nonlinear model: demand, rate, attitude responses; Right column: actuator activities for **1nsqNDW**

diagonal weight control law (**1nsqDW** in subplot (1,1) of Figure 6.28, shows that the non-diagonal weight has improved transient response characteristics. The most notable improvement is that the response is faster- with $t_r < 3$ sec, exhibits good tracking and results in negligible steady-state off-set. However, all these benefits come at the expense of increased activity in Pitch axis actuators as depicted in subplot (2,1). Pitch to Roll ($\frac{\phi}{\theta}$) and Pitch to Yaw ($\frac{r}{\theta}$) cross-couplings that can be seen in subplot (2,1) and subplot (3,1) respectively are slightly higher in comparison to 1 Dof control law (**1nsqDW**). Note in particular the Pitch rate to Roll rate couplings, which comes as a result of increased Pitch rate magnitude. Actuator magnitude illustrated in subplot (1,2) shows a 100 per cent increase in comparison to **1nsqDW** control law activity. Although still within the acceptable limits, the magnitude of the actuator signal may affect the feedback by the Safety Pilot- who has direct-drive cyclic feedback to the actuators.

Time response history of the *Side Step* (side flight to the right) like manoeuvre generated as a result of a demand in Roll channel with an amplitude of -0.25 rad (equivalent to -14^o) is depicted in subplot (2,1). The transient response characteristics indicate some degree of improvement: slightly faster response, smaller angular rate compared to the same manoeuvre performed with 1 Dof diagonal weights controller-Figure 6.28. From the duration the demand has been imposed it is hard to make any inferences with regards to the overshoot and steady-state off-set properties of the response. Attitude coupling from Roll to Pitch ($\frac{\theta}{\phi}$) in subplot (2,1) has reduced in the side flight to the left, and without any significant improvement in the side flight to the right. The coupling from Roll to Yaw has increased very slightly. Actuator control power depicted in subplot (2,2) has reduced by up to 40 per cent while performing the actual step demands in Roll, however, actuator signal magnitude has increased up to 500 per cent (in comparison to **1nsqDW** control law actuator drive signal magnitude) while performing steps in Pitch channel. This confirms the significant cross-coupling between Pitch to Roll.

The simulated partial Turn to Target manoeuvre as a result of the demand of 0.45 rad/sec magnitude in Yaw channel is depicted in subplot (3,1) in Figure 6.50. The response is faster than its counterpart (in **1nsqDW**), underdamped and thus oscillatory, which resulted in unacceptable tracking. The oscillatory nature of the response has significantly exacerbated the well-known Yaw to Pitch and Yaw to Roll coupling. However, this has not affected the actuator aggressiveness plotted in subplot (3,2). The magnitude of the drive signal has decreased up to 10 per cent at the instant of the demand in comparison to its corresponding in **1nsqDW**.

6.6 Flying and Handling Qualities assessment

Figures 6.51 through 6.53 present quantitative evaluations of the augmented (with **1nsqNDW** control law) linearized helicopter model for three categories of MTE: Target Tracking, Fully Attended Operations and Divided Attention Operations. Evaluation was performed using ADS handling qualities toolbox [How90]. Some of the boundaries for small amplitude Roll attitude changes were modified to comply with the most up to date ADS-33E requirements. The system augmented with control law **1nsqNDW**, for reasons explained in 6.6.2.1, was not fit for flight-testing -frequency sweeps, steps, manoeuvres- hence no flight data were recorded. Therefore, no qualitative handling qualities evaluations -based on data gathered from flight-tests- were performed.

6.6.1 Quantitative evaluation: Linearized model based evaluation

Shown in Figure 6.51 are predicted phase limited bandwidth and phase delay handling qualities parameters for several MTEs in small amplitude changes about Pitch axis in low speed flight regime.

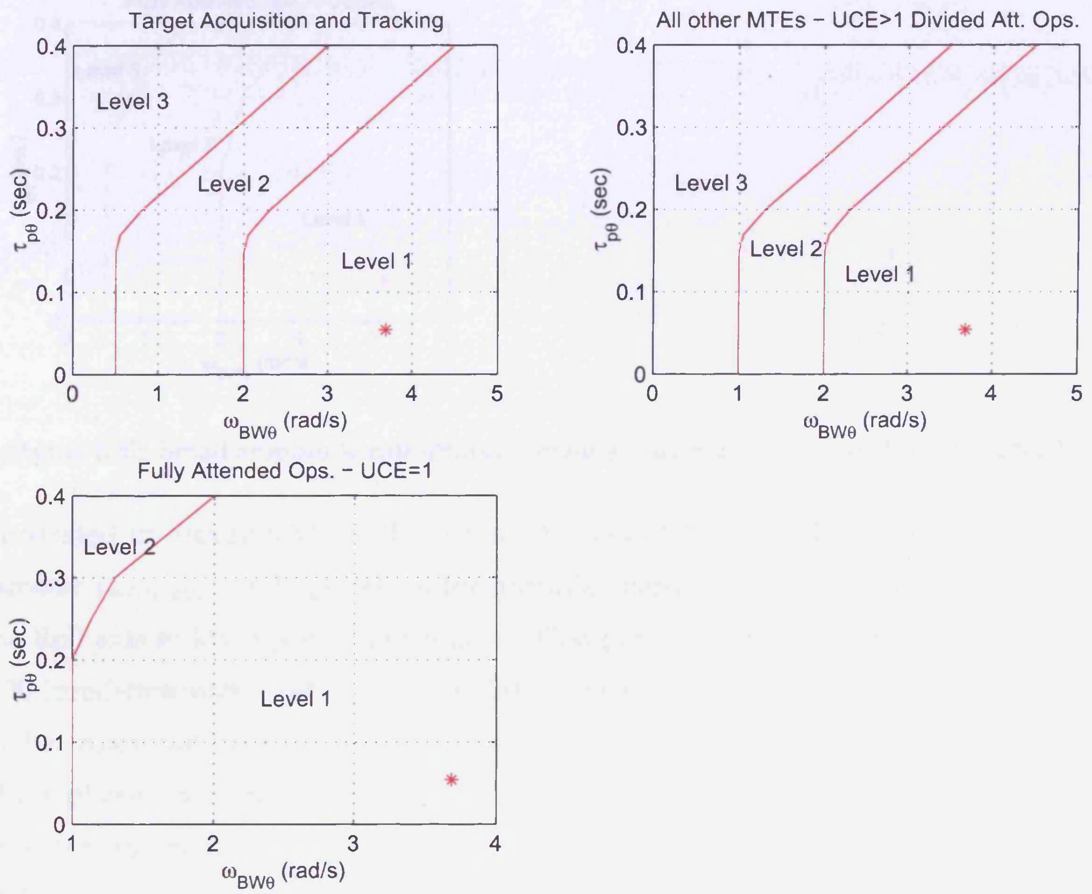

Figure 6.51: Small amplitude **pitch** attitude changes -hover and low speed- for **1nsqNDW**

Comparison with Figure 6.29 depicting the same measures attained by **1nsqDW** control law augmented linearized model, one can observe that the non-diagonal weight provided higher phase limited bandwidth and slightly lower phase delay. The latter, is suggesting a lower slope of the phase curve in the range ω_{180} and $2\omega_{180}$ and thus reduced pilot lead compensation and reduced workload in performing various manoeuvres as part of the MTEs. In all MTE scenarios about the Pitch axis the calculated handling qualities parameters indicate *Level 1* flying qualities.

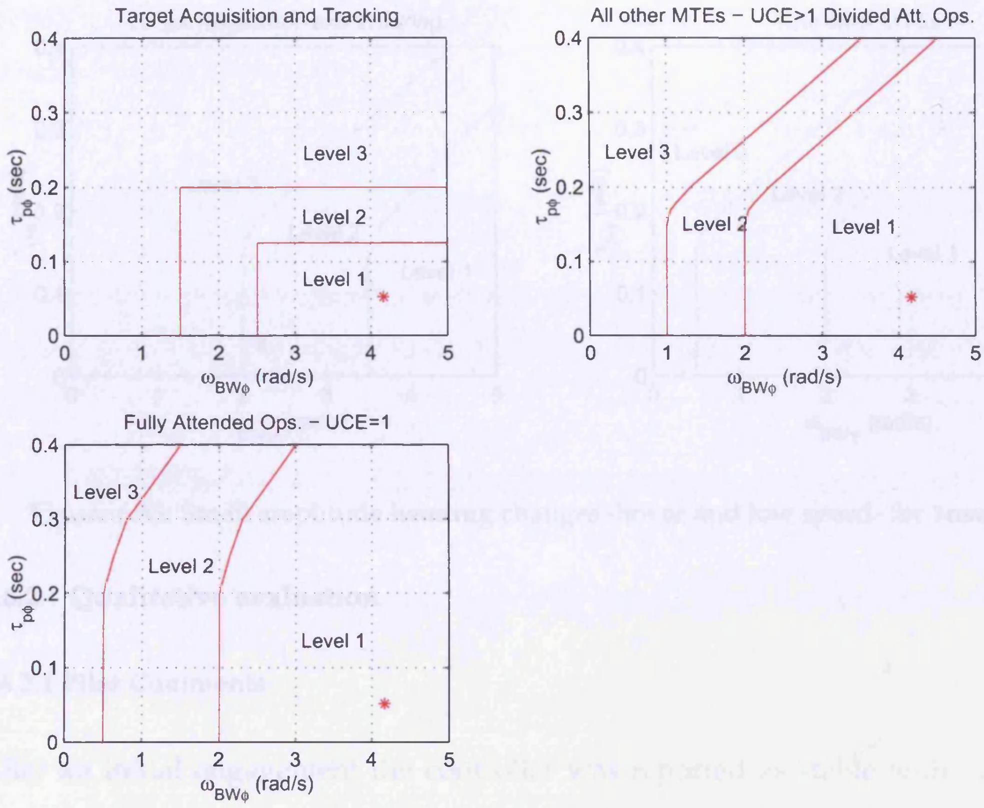

Figure 6.52: Small amplitude **roll** attitude changes -hover and low speed- for **1nsqNDW**

Illustrated in Figure 6.52 are the rotorcraft's calculated ADS handling qualities parameter ($\omega_{BWphase}$ and τ_p) values for attitude changes with small amplitude about the Roll axis in low speed flight regime. Comparison with its counterpart in Figure 6.30 (predicted with control law **1nsqDW**) reveals that **1nsqNDW** control law offers higher rotorcraft bandwidth (thus more control authority) and slightly lower slope of the phase curve in the region ω_{180} and $2\omega_{180}$. Translating the bandwidth on to the time domain characteristics of the roll attitude response and comparing subplot (1,2) of Figure 6.50 and subplot (1,2) of Figure 6.28 indicates slightly faster Roll attitude response with **1nsqNDW** in considered MTEs. Calculated HQ parameters indicate *Level 1* flying qualities in all MTE scenarios performed at hover or low speed and involve small amplitude attitude changes about the Roll axis.

Figure 6.53 depicts the calculated ADS handling qualities for the Yaw channel in the Target Acquisition/Tracking and all other MTEs. Comparison with **1nsqDW** in Figure 6.31 shows slightly higher bandwidth (thus more control power authority) and almost identical phase delay parameter values, which point to *Level 2* flying qualities in demanding Target Tracking MTE and *Level 1* in other MTE.

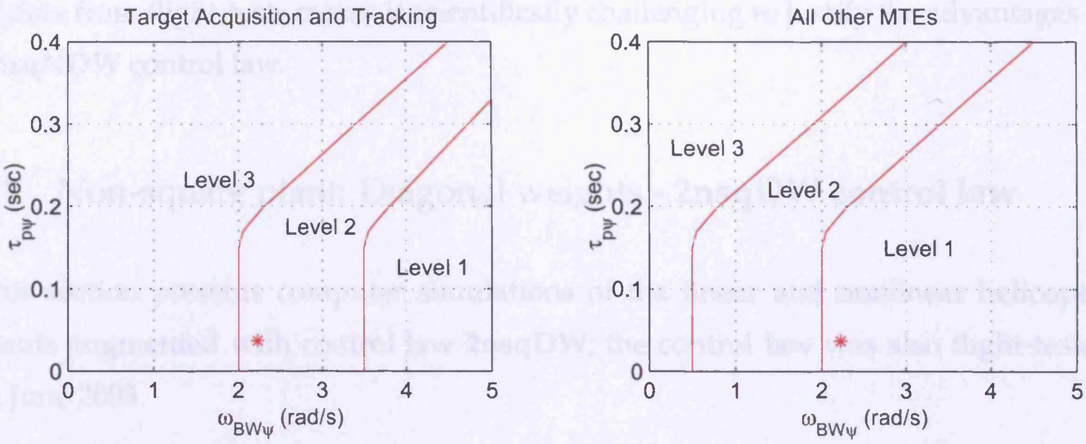

Figure 6.53: Small amplitude **heading** changes -hover and low speed- for **1nsqNDW**

6.6.2 Qualitative evaluation

6.6.2.1 Pilot Comments

After an initial engagement the controller was reported as stable with satisfactory attitude hold. However, further evaluations of the control law indicated that the rotorcraft was undamped (even after 10 sec) and the lateral axis exhibited slowly divergent oscillatory response. These characteristics prevented any steps and control sweeps evaluations on the aircraft while in-flight, hence qualitative handling qualities evaluations of any of the five Mission Task Elements were not possible.

Thus, the following Table 6.5 presents only the quantitative evaluations of each controller in view of the ADS-33E requirements for small amplitude changes in attitude about each of the principal axes at hover and low speed flight regimes.

Controller	$\omega_{B/W}$	τ_p	Handling Quality	
1nsqNDW	rad/sec	sec	Target Acquisition and Tracking	UCE = 1
Pitch (θ)	3.69	0.055	1	1
Roll (ϕ)	4.16	0.05	1	1
Yaw	2.22	0.03	2	n/a

Table 6.5: Handling qualities: Predicted

In conclusion, when compared with **1nsqDW** control law, it can be seen that control law **1nsqNDW**, in theory, offers higher bandwidths in all axes and almost similar phase delay handling quality parameters for the augmented system. However, lack of data from flight-tests makes it scientifically challenging to justify the advantages of **1nsqNDW** control law.

6.7 Non-square plant: Diagonal weights - **2nsqDW control law**

This section presents computer simulations of the linear and nonlinear helicopter plants augmented with control law **2nsqDW**; the control law was also flight-tested in June 2003.

6.7.1 Desk-top simulations: Linear response time domain analysis

Figure 6.54 shows the linear response of the closed loop of the Roll channel to a step demand of 0.2 rad. The response attempts to track an ideal model with rise time of $tr_{\phi ideal} = 1.3$ sec while the $tr_{\phi} = 3.1$ sec. The existing steady-state error is 2.5 per cent. The system response is stable, overdamped, and thus, without oscillations.

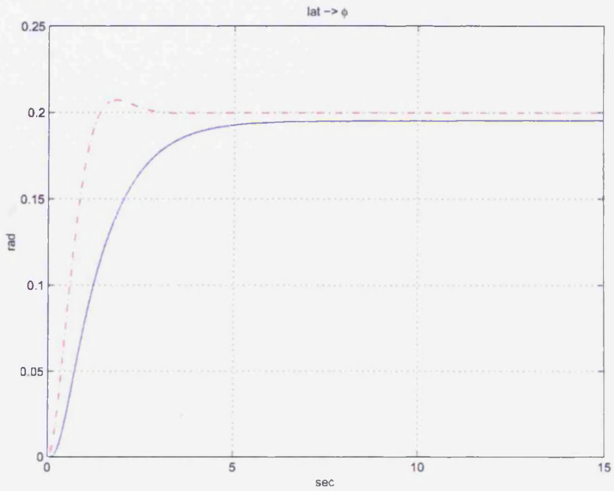

Figure 6.54: Linear responses to lateral cyclic demand of 0.2 rad: system response, ideal model

Figure 6.55 reveals information about the level of cross-axis couplings, which from Roll to Pitch is ($\frac{\theta}{\phi} \approx$) 1.25 per cent, and from the Roll attitude to Yaw rate response this is approximately 7 per cent.

The reference model response together with the plant's response to a 0.2 rad step demand in Pitch channel are depicted in Figure 6.56. Although the ideal rise time is $tr_{\theta ideal} = 1.3$ sec the plants linear attitude response rise time is $t_{r_\theta} = 3.2$ sec. Comparison with corresponding linear response characteristics of the plant augmented with

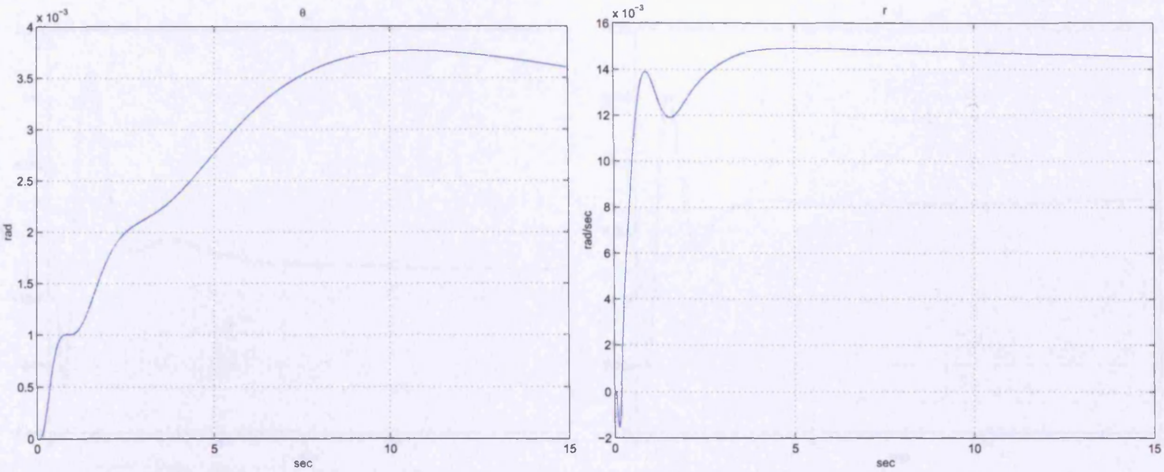

Figure 6.55: Coupling to lateral cyclic demand of 0.2 rad **a)** θ **b)** r

1nsqDW control law, it is easy to deduce that the rise time is smaller, hence faster transient response characteristics than observed with **1nsqDW** controller augmented system.

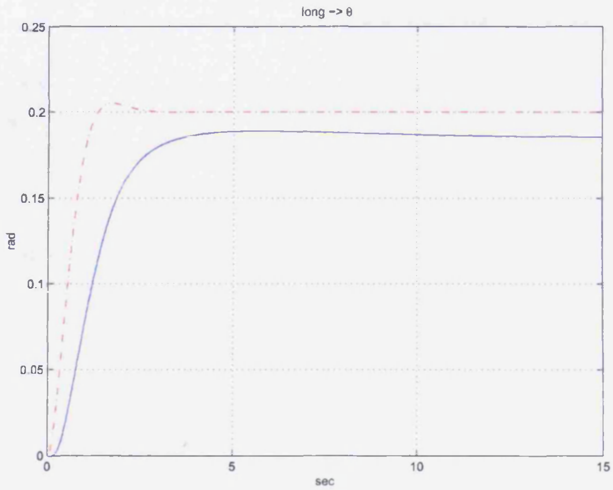

Figure 6.56: Linear response to longitudinal cyclic demand of 0.2 rad: system response, ideal model

The responses presented in Figure 6.57 provide a clear picture of the inter-axis coupling between primary axis and off-axis channels after an attitude demand of magnitude 0.2 rad in Pitch channel; Pitch to Roll coupling appears to be approximately 3.75 per cent.

The ideal transfer function model response together with the linearized plant closed loop transient response to a 0.2 rad/sec in magnitude step demand in Yaw channel are depicted in Figure 6.58. It is relatively easy to note the small rise time $tr_r = 1.9$ sec

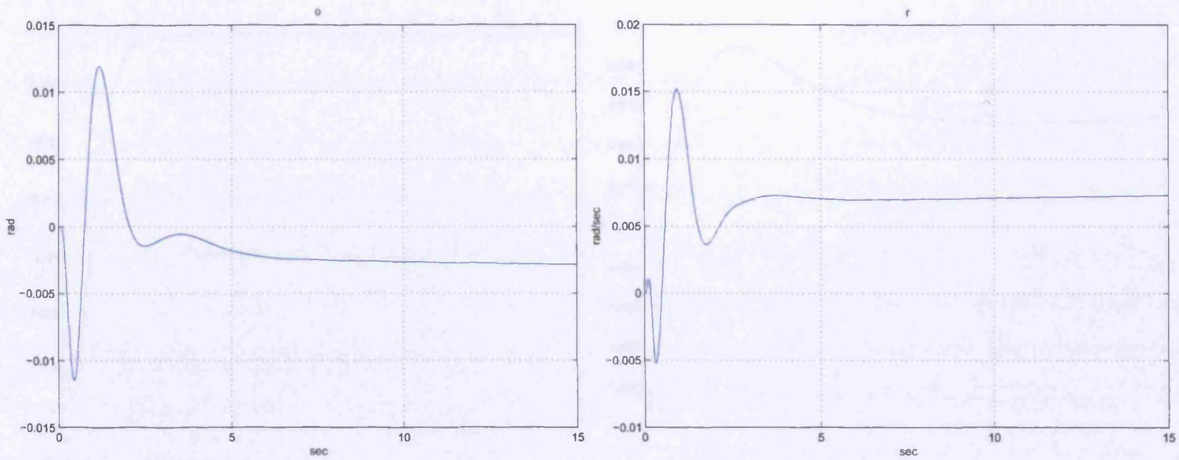

Figure 6.57: Coupling to longitudinal cyclic demand of 0.2 rad **a)** ϕ **b)**r

and the relatively high overshoot ($M_p \approx 10$ per cent).

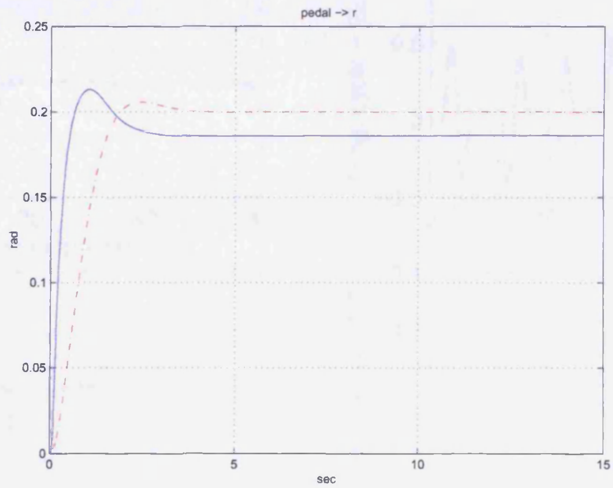

Figure 6.58: Linear response to pedal demand of 0.2 rad/sec: system response, ideal model

Cross-axis coupling is evident in Figure 6.59 and the coupling from Yaw to Roll with 14.7 per cent is the second highest level of cross coupling (amongst all control laws presented), whereas from the Yaw to Pitch is only 4.7 per cent.

Subplots in the first column in Figure 6.60 illustrate attitude demands, corresponding responses and associated angular rates whereas subplots in the second column show actuator aggressiveness for each simulative flight manoeuvre performed on the non-linear model. This is the set of nonlinear simulations for 2 Dof controller architecture with diagonal weights. The labels on the vertical axes in the subplots (:,2) should read as: Longitudinal cyclic [-1,1], where 1 is fully forward; Lateral cyclic [-1,1], where 1 is fully right; and Tail rotor collective [-1,1], where 1 is fully right.

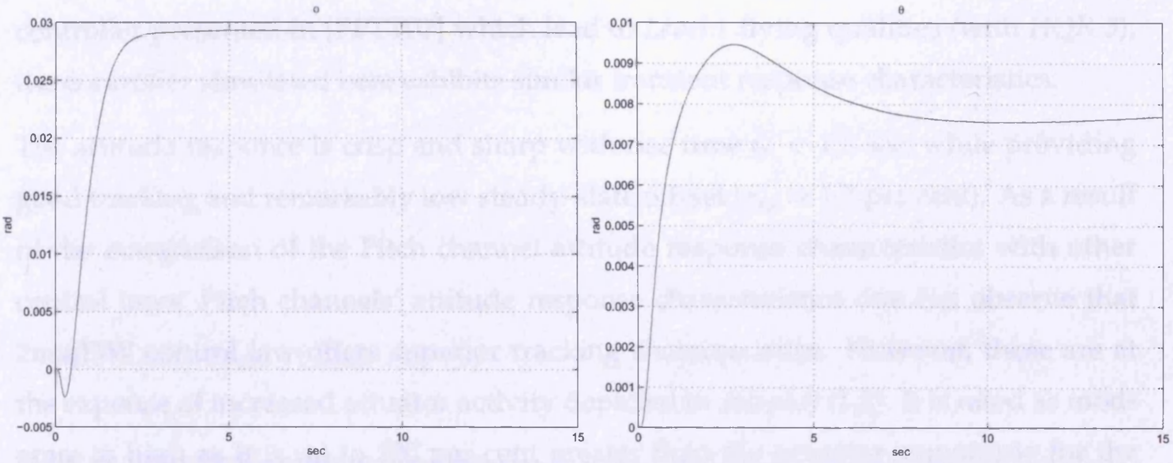

Figure 6.59: Coupling to pedal demand of 0.2 rad/sec a) ϕ b) θ

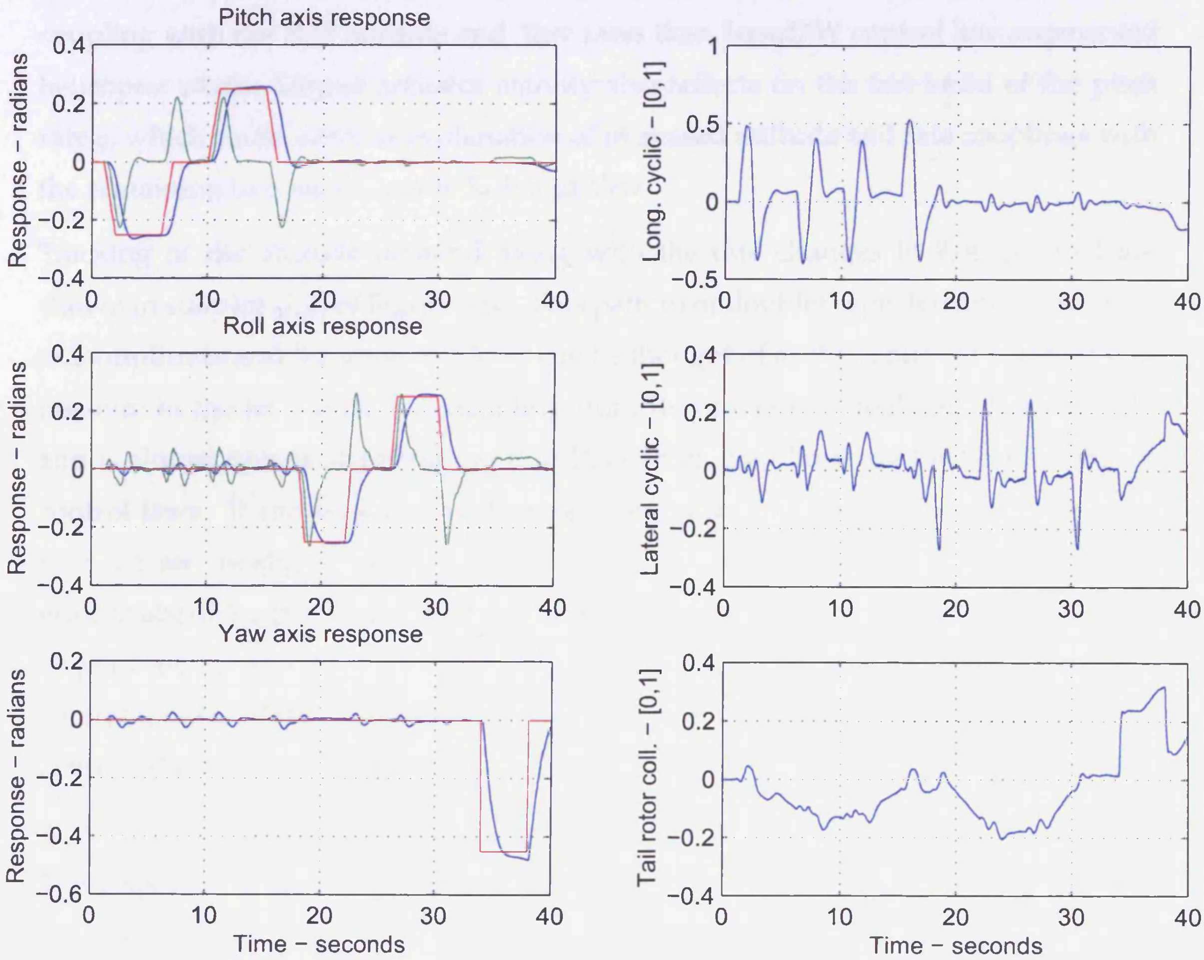

Figure 6.60: Nonlinear attitude responses, rates and actuator activities for **2nsqDW**

Subplot (1,1) provides with the picture of the nonlinear helicopter plant's closed loop response performance on replicated *Quick Hop* manoeuvre with duration of 4 sec. Comparing with the nonlinear simulations of the $\mathcal{H}_\infty$ "*mixed*"-sensitivity decoupled controller presented in [PPTT02] which lead to *Level 1* flying qualities (with *HQR* 3), the controller simulated here exhibits similar transient response characteristics.

The attitude response is crisp and sharp with rise time $t_r < 1.8$ sec, while providing good tracking and remarkably low steady-state off-set ($e_{ss} \approx 1.2$ per cent). As a result of the comparison of the Pitch channel attitude response characteristics with other control laws' Pitch channels' attitude response characteristics one can observe that **2nsqDW** control law offers superior tracking characteristics. However, these are at the expense of increased actuator activity depicted in subplot (1,2). It is rated as moderate to high as it is up to 200 per cent greater than the actuator magnitude for the same manoeuvre of the system plant when it was augmented with **1nsqDW** control law. The **2nsqDW** control law augmented system also shows slightly higher cross-coupling with the Roll attitude and Yaw rates than **1nsqDW** control law augmented helicopter plant. Higher actuator activity also reflects on the fast build of the pitch rate q, which could serve as explanation of increased attitude and rate couplings with the remaining two axes, namely Roll and Yaw.

Tracking of the altitude demand along with the rate changes in Roll channel are shown in subplot (2,1) of Figure 6.60. This pattern of doublet type demand with -0.25 rad amplitude and duration of 3.5 sec can be thought of as the replica of *Side Step* manoeuvre to the left. Inter-axis coupling from Roll to Yaw is negligible (very small), and is almost non-existent from Roll to Pitch; both couplings are the best among all control laws. It can be seen that transient response is fast and crisp with rise time $t_r \approx 1.8$ sec, negligible overshoot and excellent attitude tracking. The steady-state error is about 1.2 per cent. These characteristics come, again, at the expense of up to 60 per cent increased actuator signal magnitude with comparison to the smallest in control law **1nsqDW** for the same manoeuvre. Although the actuator aggressiveness is the highest among all control laws, except **1sqDW**, it can, nevertheless, be rated as low.

The response of the helicopter to a demand in the Yaw channel with amplitude of -0.45 rad/sec for 4 sec is shown in subplot (3,1) of Figure 6.60. This type of demand can be seen as partial *Turn to Target* manoeuvre to the left. The response is relatively fast with rise time of $t_r \approx 1.75$ sec but has slight overshoot; the absence of low pass noise filter contributes to the small (4 per cent) steady-state error, which is comparable to **1nsqDW** control law for the same manoeuvre. The dominant in all control laws coupling from Yaw to the other channels responses has been eliminated in **2nsqDW** control law. As the control input is the rate there is almost no attitude cross-coupling however, as expected, there is Yaw to Roll and Yaw to Pitch rate coupling. Actuator driving signal magnitude depicted in subplot (3,2) has decreased on average by up to 35 per cent in comparison to the same axis actuator's activity in other control laws while performing the same type of manoeuvre.

6.8 Flying and Handling Qualities assessment

This section presents qualitative and quantitative evaluation of the control law **2nsqDW**.

6.8.1 Quantitative Evaluation: Linearized model based evaluation

Handling qualities toolbox of [How90] will be used in the quantitative evaluation of the augmented (with **2nsqDW** control law) linearized helicopter model.

Figures 6.61 through 6.63 summarizes the predicted flying qualities in different axes for small amplitude changes in low speed flight conditions for three categories of MTE.

Bandwidth and phase delay handling quality parameters for small pitch attitude changes around hover flight regime are illustrated in Figure 6.61.

Comparison with Figures 6.29 and Figure 6.51 depicting the same parameters for the same axis attained, correspondingly, by **1nsqDW** and **1nsqNDW** control laws point out that **2nsqDW** attains the highest phase delay and the second highest bandwidth after **1nsqNDW** controller. This suggests that the slope of the phase curve between the natural bandwidth and twice the natural bandwidth is the largest which may impart the highest pilot workload in performing various MTEs in Pitch axis.

Predicted rotorcraft bandwidth and phase delay parameters indicate that *Level 1* flying qualities are possible in all three MTEs: Combat Tracking, Divided Attention Operations and Fully Attended Operations.

Shown in Figure 6.62 are calculated ADS33 handling qualities measures for various MTEs performed while in low speed and hover flight regime about the Roll axis. Comparison with Figures 6.30 (for **1nsqDW**) and Figure 6.52 (for **1nsqNDW**) reveals that the τ_p remained unchanged and that $\omega_{BW_{phase}}$ is the highest bandwidth of all control laws. This is, in theory, also confirmed by the fastest nonlinear closed loop

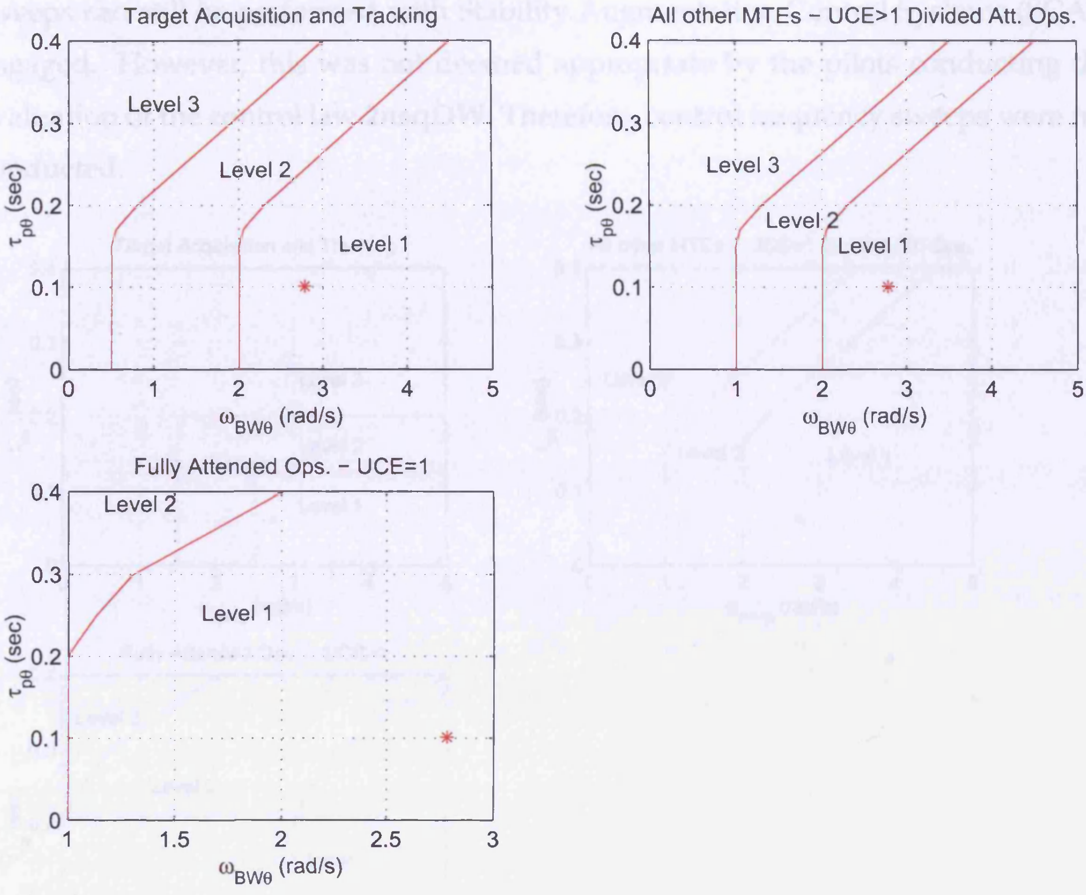

Figure 6.61: Small amplitude **pitch** attitude changes -hover and low speed for **2nsqDW**

Roll axis response to small doublet type demands illustrated in subplot (2,1) in Figure 6.50. The rotorcraft accommodating this control law is predicted to achieve *Level 1* flying qualities in all the three distinctive MTEs.

Figure 6.63 plots rotorcraft's Yaw axis bandwidth and phase delay parameters. Calculations were made for small amplitude attitude manoeuvres for only two MTEs. Cross-comparison with **1nsqDW** in Figure 6.31 and **1nsqNDW** in Figure 6.53 indicated that **2nsqDW** control law has significantly reduced aircraft bandwidth and increased phase delay characteristics which resulted in flying qualities of *Level 3* for the demanding Combat Tracking and *Level 2* for all other MTEs (UCE= 1 and UCE> 1). There is a mismatch between predicted results and nonlinear simulations.

6.8.2 Flight test frequency sweeps

In practice it is accepted that in the cases when open loop frequency sweeps are not possible due to poor natural stability characteristics of the rotorcraft, frequency sweeps can still be performed with Stability Augmentation Control Systems (SCAS) engaged. However, this was not deemed appropriate by the pilots conducting the evaluation of the control law **2nsqDW**. Therefore, control frequency sweeps were not conducted.

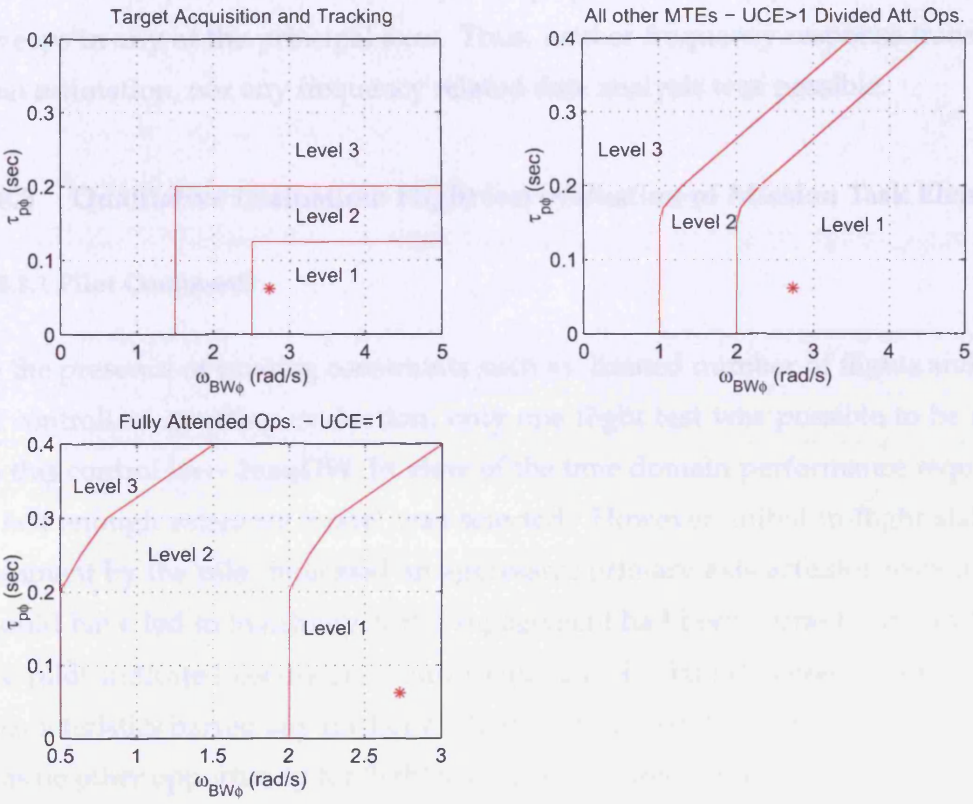

Figure 6.62: Small amplitude **roll** attitude changes -hover and low speed for **2nsqDW**

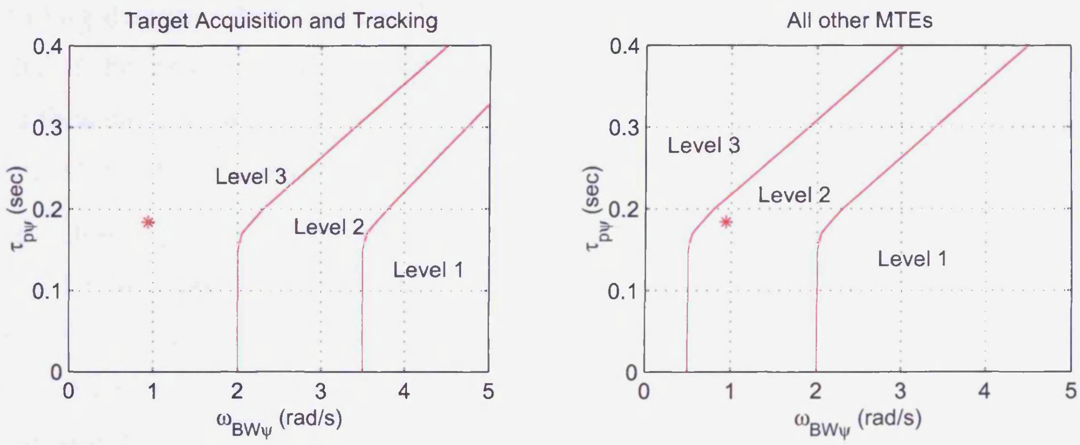

Figure 6.63: Small amplitude **heading** changes -hover and low speed for **2nsqDW**

6.8.2.1 Time domain sweep history, Frequency domain sweep history-Frequency response estimation

Instability of the helicopter as a result of small amplitude engagements conducted around hover prior to the frequency sweeps prevented any pilot-induced frequency sweeps in any of the principal axes. Thus, neither frequency response transfer function estimation, nor any frequency related data analysis was possible.

6.8.3 Qualitative Evaluation: Flight test evaluation of Mission Task Elements

6.8.3.1 Pilot Comments

In the presence of existing constraints such as: limited number of flights and number of controllers awaiting evaluation, only one flight test was possible to be allocated to this control law- **2nsqDW**. In view of the time domain performance requirements a fast enough reference model was selected. However, initial in-flight stability assessment by the pilot indicated an aggressive primary axis actuator response which would have led to instability, if the engagement had been carried out. Additionally the pilot indicated oscillatory (with frequency of 1 Hz) divergent response. These characteristics barred any further evaluation of this control law. Unfortunately, there was no other opportunity for flight testing of the same control law, which would have undoubtedly allowed pilots' comments to be reflected into a new 2 Dof controller design. This was a *"one go"*[11] control design which, in practice, hardly leads to objective fulfilling designs. Post-flight evaluations have pointed in the direction of the feasibility of the time domain reference model, which was found to be slightly too fast and thus stood as a potential source of the reported excessive actuator activity and, reduced stability robustness of the augmented plant.

The following Table 6.6 presents a summary of the quantitative evaluations of each controller in view of the ADS-33E requirements for several MTEs performed with small amplitude changes in attitude about each of the principal axes at hover and low speed flight regimes.

[11]The control law design did not benefit from any previously obtained in-flight pilot feedback on 2 Dof controller architecture, it was based on requirements documented in ADS-33 only.

Controller	$\omega_{B/W}$	τ_p	Handling Quality	
2nsqDW	rad/sec	sec	Target Acquisition and Tracking	UCE = 1
Pitch-(θ)	2.78	0.1	1	1
Roll-(ϕ)	2.73	0.06	1	1
Yaw	0.94	0.18	3	2

Table 6.6: Handling qualities: Predicted

6.9 Summary and Comments

This chapter has presented detailed studies and comparative analyses of linear and nonlinear simulations, together with flight-test based ADS 33 quantitative and qualitative handling qualities evaluations of various degrees of freedom, coupled $\mathcal{H}_\infty$ loop-shaping controllers which were applied to a practical design problem: the *Bell 205* multipurpose rotary-wing aircraft.

The study of the differences between predicted ADS33 handling qualities parameters (particularly phase delay τ_p) for small amplitude attitude changes in different MTEs and, flight-test achieved helicopter's bandwidth and phase delay indicate that removing the source of pure time delay from the model, namely the rotor, as the greatest source of error, accounts for the significant portion of the mismatch.

The flight-test results from the set of $\mathcal{H}_\infty$ loop-shaping controllers presented in this chapter, in [PPTT02] and in [PPT+05] have demonstrated that even if *"mixed rates"* p_{mix} and q_{mix} are not included in the synthesis of $\mathcal{H}_\infty$ loop-shaping controllers, controllers that deliver to the expectations of the pilots and facilitate *Level 1* flying qualities in-flight can be synthesised. This can be seen as attribute to the increased fidelity (made possible by the inclusion of high frequency dynamic characteristics) of the nonlinear model of the helicopter.

Flight tests have, once again, confirmed that the normalized *coprime* robust optimization theory is indeed robust, however, attaining desired handling qualities and retaining robustness of performance throughout an operating envelope does require a mathematical model which can accurately and adequately capture the dynamical behaviour of the plant, as well as appropriate selection of response types for different missions.

Chapter 7

Concluding remarks

Valuable insight into several control system design approaches in the context of $\mathcal{H}_\infty$ loop-shaping have been gained by utilizing different structured weighting functions. The limitations of (semi-manually constructed) non-diagonal weighting functions in applications to aeromechanically complex, nonlinear, multivariable, multipurpose helicopter have been discussed.

The main contributions of this thesis are now summarised and recommendations outlined for future research.

7.1 The main contributions

7.1.1 Flight control law design

- The work included in this thesis represents the most recent report of the research carried out using $\mathcal{H}_\infty$ loop-shaping procedure for the controller designs on the most up-to-date (12 Dof) *Bell 205* nonlinear helicopter model provided by *QinetiQ*, Bedford, UK, exclusively for this project only. The model builds on the previous models of the *Bell 205* with the inclusion of components characterising high frequency dynamics and integrating 3 more degrees-of-freedom.
- All the designs have been based on a longitudinally and laterally coupled nonlinear model of the helicopter.
- The thesis presents extensive cross-comparative analyses based on the linear and nonlinear simulations and data gathered during the flight-tests for the three 1 Dof and one 2 Dof (synthesised with one step optimization) $\mathcal{H}_\infty$ loop-shaping

controller architectures. The control laws utilized weights with both diagonal and non-diagonal structures.

- The techniques for constructing non-diagonal weighting functions reported in the literature [PG97], [Lan01] considered only square and low order ($\leq$ 8) systems. In order to accommodate commonly encountered non-square plants, the procedure of [PG97] has been extended by using some known properties of the unitary matrices, to allow for the design of non-diagonal weighting functions for non-square (rectangular) system plants.

- Extensive study of the design (synthesis and analysis) has been presented for the non-square 1 Dof $\mathcal{H}_\infty$ loop-shaping controller synthesised for the 14 state helicopter plant after shaping the singular values with a non-diagonal weighting function. To the best of the author's knowledge this comprises the first ever pilot flight-tested non-square controller with embedded non-diagonal weights. The challenges which arise in the course of the non-diagonal weight design for such a high order plant have been carefully addressed.

- The thesis reports on the first flight-tested coupled, non-square 1 Dof $\mathcal{H}_\infty$ loop-shaping control law that achieved *Level 1* flying qualities in the demanding and high precision- *Pirouette, Precision Hover* and *Turn to Target* manoeuvres.

- The flight-test of coupled control laws and the achievement of three ratings of *Level 1* flying qualities for demanding and high-precision manoeuvres, underline, once again, that controllers achieving *Level 1* flying qualities can, indeed, be synthesised providing that the appropriate response types are selected for the intended MTEs. A high fidelity nonlinear dynamic model of the *Bell 205* is made available and suitable weighting functions used.

- All the coupled 1 Dof and 2 Dof $\mathcal{H}_\infty$ loop-shaping controllers presented herein were implemented in the forward path as described in section 4.8, and not in the observer based form in the implementation stage. They employ only state feedback of selected state variables (namely attitudes and rates) and yet, delivered highly rated (by the pilots) in-flight performance characteristics. This is in contrast to many control laws implemented and flight-tested on this helicopter prior to 2001 [PSW+99], [SWP+01].

- None of the controller designs made use of the Pitch (q_{mix}) and Roll (p_{mix}) "*mixed*" angular rates p_{mix} and q_{mix}, instead, actual rate sensor signals for p and q were fed back in the designs.

- In the absence of some high frequency dynamic characteristics (such as dynamic inflow as a combination of uniform and first harmonic components) the coupled 1 and 2 Dof $\mathcal{H}_\infty$ loop-shaping control laws achieved HQR of 4 [PSW+99], [SWP+01] corresponding to *Level* 2 flying qualities. The incorporation of high frequency dynamic characteristics in the nonlinear helicopter model has closed significantly the gap between predicted helicopter responses and flight-test derived results. However, integration of several extra elements such as anti-aliasing filters, rate-limits, discretisation and truncation of the controller realisation to between six and eight decimal places [PPT+05] has also proved extremely effective towards fulfilment of this objective.

- The handling qualities toolbox [How90]- based on a previous version of ADS-33 standard- was updated to reflect the most-up-to-date ADS-33E [Ano00] standard properties. Quantitative handling qualities evaluations of the flight-tested control laws were then based on the updated version of the toolbox. This has increased the compatibility between predicted response flying qualities and pilot in-flight feedback.

7.1.2 Issues concerning the non-diagonal weight procedure

Tackling a problem of such a complex nature that incorporates a range of unwanted phenomena (non-square system plant, time delays, *RHP* poles and zeros, ill-conditioning at some frequencies- strong directionality) establishes a platform not only for evaluating a designer's skills and experience but also for the rigour of the technique under investigation. This helps to unveil the deficiencies of the technique and by this to set new research directions for the designer to explore.

In the light of the experience gained by the application of an algorithm to construct non-diagonal weights and diagonal weights, the following are some remarks and recommendations. These may prove useful in enhancing the effectiveness (in terms of robustness and performance) and reducing the complexity of the non-diagonal weight design optimization procedure within the context of the $\mathcal{H}_\infty$ loop-shaping technique.

- The conclusion at this point of time is that, in the context of $\mathcal{H}_\infty$ loop-shaping, the construction of non-diagonal weights provides the designer with more insight and authority to attain the desired singular values of the shaped plant $\mathbf{G}_s$. This is because non-diagonal weights can always provide improved singular value shapes when compared with diagonal weights in the context of 1 Dof and 2 Dof $\mathcal{H}_\infty$ loop-shaping. However, the procedure integrates a second pre-filter selection and thus, does not relieve the designer from the step of yet another weight selection. In fact, as the order of the plant increases, as a part of the algorithm, the designer faces an even more challenging task with the selection of an even more complex, diagonal weighting function Γ as a means to augment the singular values of $\mathbf{G}_s$. The designer still requires significant engineering hands-on experience and intuition in the course of the selection of the diagonal transfer function Γ, which essentially contains the dynamics of the non-diagonal weight. The resulting non-diagonal weight $\mathbf{W}_1^{nd}$, in return, through $\widehat{\mathbf{V}_s}$, contains the input dynamics of the shaped plant $\mathbf{G}_s$. Therefore, it is clear that, unlike classical diagonal weight selection, the non-diagonal weight's order will be always dependent on the nominal/shaped plant. An issue which can clearly exacerbate computational complexity of the procedure.

- When applied to high order plants (often encountered in real world applications), due to the high number of elements in $\mathbf{U}$ and $\mathbf{V}$, to which fittings in the frequency domain will need to be performed, the non-diagonal weight algorithm generates controllers of extremely high order. Considerable effort and time were spent on model reduction of appropriate elements such as $\mathbf{W}_1^{nd}$, $\widehat{\mathbf{V}_s}$, $\mathbf{K}_\infty$ and $\mathbf{K}_{imp}$ at various stages of the non-diagonal weight construction procedure. Both the number of states of the system plant and its dimensions lead to high order fittings of the right singular vector matrix transfer function.

- In the model reduction stages the designer, if possible, should retain the dynamics of the non-diagonal weight $\mathbf{W}_1^{nd}$ by preserving its structure obtained from the *co-spectral* factorization. Instead, s/he should try careful model reduction of $\widehat{\mathbf{V}_s}$, the robustly stabilizing loop-shaping controller $\mathbf{K}_\infty$, or the implemented controller $\mathbf{K}_{imp}$, or both, while using appropriate measures to gauge distance from the original model. Extensive model reduction of different controllers in the course of the design becomes inevitable. This requires significant experience on the side of the designer with the best use of the model reduction techniques for arriving at practically feasible controllers.

- The results presented herein also bring to evidence that complex controllers come with a significant (computational and labour) cost and do not always, and necessarily, perform better than more simpler ones when, for example, compared to those obtained by utilizing diagonal weighting functions in the loop-shaping.

- Analysis of both non-diagonal weight construction algorithms suggest that procedures (for controller synthesis) involving fitting in the frequency domain are bound to culminate in controllers with very high orders. Therefore an algorithm formulated in state-space form that has a state-space solution should be considered. This will significantly reduce (or eliminate) the number of iterations the designer has to perform in the frequency domain, and will allow the direct-"*one shot*" construction of non-diagonal weights. Additionally, this will also alleviate a problem which may arise when the system has repeated singular values, since then the continuity of left/right singular vectors may not be possible.

- The reader should note that only the non-diagonal pre-filter was constructed for the shaped plant; the construction of the non-diagonal post-filter was thought to be unnecessary. However, its construction would have inflated the order of the implementable controller to an extent that would render its application impossible. This underlines, once again, that the use of the non-diagonal weights requires careful consideration and unless certain issues in their selection are addressed, then the disadvantages of using non-diagonal weights on high order system plants will usually outweigh their advantages (when compared to diagonal weights).

7.1.3 Issues concerning the weighting of output variables through W_2

- In the 1 Dof controller architecture reducing the relative importance of the Roll rate (p) and Pitch rate (q) by simply scaling them with numerical values between 0.4-0.95 produced controllers with good performance characteristics but they were very fragile, i.e with good optimal nominal performance but very sensitive to changes of inputs of different magnitudes- poor robustness characteristics.

- It was observed that in the 1 Dof controller architecture, where both diagonal and non-diagonal pre-compensators were constructed, placing an emphasis on those elements in W_2 which affect p and q leads to shifting the poles to the right of the complex plane, thus tending to provide the response with additional damping.

- Preliminary studies were carried out on the effect of extra measurements- p and q on the performance and robustness characteristics of the design. These confirm that (while retaining the pre-filter $\mathbf{W}_1$) squaring down the system by removing the measured output rates p and q affects adversely the robustness characteristics of the augmented plant; an argument strengthened by reduced stability margin ϵ, and higher peaks in the frequency response magnitude of the co-sensitivity operator/s. However, this comes at the expense of improved performance characteristics: faster responses, smaller steady-state off-set and smaller overshoot. This is the classical trade-off between robustness and performance. The impact of squaring down the system plant on various properties of the controllers will be problem dependent (and more precisely, dependent on the variables removed). Therefore, drawing out more generalizing conclusions about the effect of extra measurements based on above (mentioned) observation will be inconclusive. Further theoretical justification will be required so that the results can be brought to a satisfactory level of scientific scrutiny.

- In the 2 Dof controller architecture, in stark contrast to what has been observed in the 1 Dof, a slight increase in the emphasis on the Roll (p) and Pitch (q) rate speeds up the associated channels' attitude responses. These observations are from empirical simulation studies and will therefore require further theoretical studies before drawing out conclusive statements.

7.2 Future Work

- Although singular value sensitivities (**S**, **T**, **KS** etc.) are known to be useful analytical operators (and tools) for describing the robustness of feedback properties of the closed loop under certain type of perturbations to the nominal plant, it was challenging and not always straightforward to interpret and then to translate the frequency response behaviour of those operators, particularly at high frequencies, onto anticipated time response characteristics or constraints of the system. Therefore, while these operators remain as valuable sources of information about the robustness characteristics of the augmented plant, future work may concentrate on complementary and rigorous tools, such as μ structured singular value bounds and a pointwise version of the stability margin (ρ). This could be utilized in the design of the control laws for assessing the robustness properties of the closed loop system against perturbations at various points.

- In the light of experience gained with the semi-automated non-diagonal weight construction for square and non-square multivariable system plants, an optimization algorithm which integrates and combines $\mathcal{H}_\infty$ loop-shaping synthesis (for robust stability) and μ structured singular value (for robust performance) will ensure synthesis of control laws with two distinguished characteristics: robustness and performance- desirable assets of every practically implementable control law.
- It is typical that a controller designed with this methodology will have an order comparable to that of the assigned plants. While properties guaranteeing closed loop stability, and performance are a "*must*" for a controller to be considered for implementation on a real system, feasibility of the controller in the implementation phase does strongly depend on its order. This underlines the order of the resulting controller as a constraint which may need to be integrated into the controller synthesis procedure.

Additionally, in the light of deficiencies such as:

- inability to accommodate diagonal weights or plants with integrators in the *co-/spectral factorization*, and
- inability to take into account explicitly the phase properties of the plant, and misalignment between controller output subspace $R(\mathbf{K}^*)$ and the plant input subspace $R(\mathbf{G})$,

future work may concentrate on integrating these in the foundations of an alternative state-space optimization algorithm that will produce non-diagonal weighting functions with minimum number of iterations. This may make use of the *spectral* factorization via *Hermitian* matrix pencils and thus facilitate the use of pre-filters that are not units. Also:

- Any good design method should offer ways of conveniently translating design specifications to design requirements on the controller synthesis problem.

- It would be useful to conduct rigorous studies on the fundamental question: how are a system's robustness and performance characteristics affected by the structure (square or rectangular) of the plant? This could perhaps be done by considering the angles between subspaces [BG73], [Mey00] of appropriate transfer functions.

- The application of the LPV/LMI approach to controller design for the complete flight envelope in one step (without the need to carry out spot designs followed by *ad hoc* gain scheduling) is a direction worth exploring.

- After the construction of the non-diagonal weight it will be beneficial to investigate the influence of non-diagonal elements (of the non-diagonal weight) on the shaping of the (nominal/shaped plant) singular values in an attempt to create a sparse weighting function which would retain the properties of its predecessor but will have its order reduced. This will ensure the synthesis of controllers with smaller order.

7.2.1 Limits of Performance

Control system design is dictated not only by design (performance and robustness) considerations but also inherent physical constraints that the system possesses. It is well known that constraints such as geometrical shape of the plant, *RHP* poles, non-minimum phase zeros, time delays (arising mostly due to the system's aero-mechanical structure and the environment it operates in) set stringent bounds on the achievable sensitivity **S** and complementary sensitivity **T** transfer functions in linear [Che98], [Che99], [Che00] and nonlinear [SBG97] MIMO systems. These constraints will inherently limit the level of achievable performance, independent of the control design method applied. Therefore it is desirable to recognise, *a-priori*, whether or not the desired level of performance is attainable and how different arrangements of measurements in the system are related to the best achievable level of performance with the system in hand. This will provide a clear indication on what and how plant properties may inherently conflict and thus undermine some or all performance objectives; this information can then be integrated in the $\mathcal{H}_\infty$ loop-shaping controller design procedure.

Appendix A

Appendix A

This appendix is primarily presented for completeness and thus is a compilation of some of the key terms, range of concepts, definitions and parameters that are part of the quantitative and qualitative assessment of any control law for a given task. For a more detailed and complete exposition on the technical and historical background of the contents, the reader can consult references such as: [Ano00], [Pad00] and [Pro95].

A.1 Flying Qualities

Stability of the rotorcraft and its safety in flight are an outcome of good flying qualities, which will also contribute to enhancement of performance. Since requirements for military rotorcraft are more performance oriented, and for civil rotary-wing aircrafts are more safety oriented, flying qualities can be seen as a synergy between internal to and external to the aircraft and pilot influencing factors. In [Key88] flying qualities were described as stability and performance characteristics (internal attributes-factors) of the rotorcraft, whereas Handling qualities were defined with the task and environment included (external influences). To evaluate an aircraft's suitability for a given role or mission task, flying qualities require a quality measurement scale. The most developed, and widely recognized quality assessment scale is due to *Cooper-Harper* [CH69]. Quality and success of the design are assessed according to this scale and can be measured in three *Levels*. Table A.1 represents *Cooper-Harper* handling qualities ratings scale, where *Level 1* flying qualities constitute the most desirable and required for most conventional helicopters rating; *Level 2* is rated as acceptable, adequate performance is attainable but the pilot may be subjected to significant workload; *Level 3* signifies major deficiencies in the control law characteristics and thus in rotorcraft flying qualities, it is therefore unacceptable, though the rotorcraft may be still controllable and flyable.

A.2 Handling Qualities Ratings-HQR

Each of the flying qualities *Levels* are further subdivided into three Handling qualities ratings. These are subjective ratings awarded by the pilots for a rotorcraft flying an MTEs (Mission Task Elements), and are based on a judgement of task performance achieved and work load exercised, all in accordance with the specifications embedded in the *Cooper-Harper* handling qualities scale [CH69] illustrated in Table A.1. Task performance, as flight-path accuracy, attitude retention and tracking performance, is measurable, whereas pilot work load is difficult to quantify. Therefore pilots usually resort to subjective qualifiers like: minimal, moderate, significant, extensive and maximum to describe the compensation required. Since pilots skill and experience is variable, and misinterpretation of HQRs and *Cooper-Harper* scale is common, the use of HQR is usually supported by pilot comments and after-flight task performance analysis. A blending of those two distinct assessors and accurate translation of the comments onto the controller design parameters requires significant designer experience.

A.3 Aeronautical Design Standard-ADS

Aeronautical Design Standard, described shortly as ADS33, evolved as a result of task performance requirements. On the contrary of Design Standard specifications for fixed wing aircrafts, ADS33 is not categorized according to aircraft size, or intended role of use of the rotorcraft, but only according to the required MTEs, therefore ADS33 holds a generic value. ADS33 quantify responsiveness and sensitivity and lay down quality boundaries on measurable parameters [Pad00].

A.4 Usable Cue Environment-UCE

Environment cues, as one of the influential factors on pilots' decision, are ranked on a Usable Cue Environment (UCE). The Usable Cue Environment measure is a result of

Aircraft characteristics	**Demands on the pilot in selected task or required operation**	**Pilot rating**
Excellent Highly desirable	Pilot compensation not a factor for desired performance	1
Good Negligible deficiencies	Pilot compensation not a factor for desired performance	2
Fair-some mildly unpleasant deficiencies	Minimal pilot compensation required for desired performance	3
Minor but annoying deficiencies	Desired performance requires moderate pilot compensation	4
Moderately objectionable deficiencies	Adequate performance requires considerable pilot compensation	5
Very objectionable but tolerable deficiencies	Adequate performance requires extensive pilot compensation	6
Major deficiencies	Adequate performance not attainable with maximum telerable compensation. Controllability not in question	7
Major deficiencies	Considerable pilot compensation is required for control	8
Major deficiencies	Intense pilot compensation is required for control	9
Major deficiencies	Control will be lost during some portion of required operation	10

Table A.1: *The Cooper-Harper handling qualities rating scale*

pilot's subjective rating of the quality of visual task cues. In dependence to the quality of the visual task cues, UCE is divided into three: UCE of 1 indicates normal daylight visual environment and very good visual cues to support the control of either attitude or velocity, or both, while UCE 3 indicates extremely poor (night visual environment), deficient visual cues where the pilot is restricted with the amount of corrections s/he can make to any of the controlled responses. The pilot combines the UCE information with the demanded task to be performed to decide on the type of response for the application.

A.5 Response Types

The response-type is associated with the character of the attitude response in the first few seconds (i.e. the transient characteristics of the response) after a pilot has applied a step control input through any of the control inceptors.

Different visual conditions (UCE) require different response-types to be applied in order to attain the same *Level 1* of flying qualities. This becomes more evident in Degraded Visual Environment (DVE), or nap-of-the-earth flight- (p.341) Figure 6.4 in [Pad00]. Therefore, UCE, MTE and the speed in (low/hover or forward) flight play key role in the selection of response-types. Some of the response types known are:

- AcC- Acceleration Command
- AC- Attitude Command
- RC- Rate Command
- TC- Turn Coordination (applies to yaw and pitch response)
- PH- Position Hold (applies to horizontal plane)
- ACAH- Attitude Command Attitude Hold (applies to roll and pitch)
- RCAH- Rate Command Attitude Hold (applies to yaw)
- RCDH- Rate Command Direction Hold (applies to yaw)
- RCHH- Rate Command Height Hold (applies to heave)

RC is the regarded as the simplest practical response-type applied in conventional helicopters. It must be noted that some response-types allow more gentle and sensitive corrections to be made during an assigned MTE, however, induces more pilot work load. For example, AC is easier to fly than RC, and TRC is easier to fly than ACAH which requires significant pilot attention. Highest performance can be achieved with AcC response-type through a direct force/moment inceptor but with significantly increased pilot work load.

Definition of the response-type alone is not sufficient in the tasks the pilot is likely to encounter, further characterization of the response-type in terms of amplitude (small, moderate and large) and frequency (short, medium and long term) is required. `ADS33` quantitative evaluations are made based on short term response.

A.6 Short-term response

Minimum requirements are established for control response-types and their characteristics. These requirements are categorized into terms of small, moderate, and large amplitude changes and are defined for comparison with the rotorcraft characteristics. This provides a quantitative assessment of the Levels of rotorcraft handling qualities based upon flying qualities parameters. The small amplitude response requirements include both short-term and mid-term responses; the short-term response refers to the rotorcraft characteristics in pilot tasks such as closed-loop, compensatory tracking; the mid-term response criteria is intended to ensure good flying qualities when less precise manoeuvering is required.

Short-term response has been focal point of handling qualities research both for fixed-wing and rotary-wing aircrafts and it is just one of the several criteria defined in ADS33. Short-term responses are characterized by the higher frequency ranges where the vehicle's dynamics is dominated by short period pitch mode and the roll subsidence mode.

A.7 Frequency response data- Frequency sweeps

Although frequency response data are more difficult to capture in-flight, and certainly more time consuming to analyze, they also provide an environment for conducting more robust analysis in comparison to properties of the time domain response criteria. Frequency response data will serve as a platform for determining key handling qualities parameters like bandwidth and phase delay. Frequency response plots are obtained through analysis of the data acquired in flight and in the course of the so called frequency sweep manoeuvre. The sweep manoeuvre is generated by the pilot manually applying at a primary control input a sine wave form with gradually increasing frequency. This excitation of aircraft on one of the control axis' continues for about a minute. Figure A.1 illustrates an example of frequency sweep manoeuvre applied to Yaw axis of *Bell 205* helicopter; presented are the pilot demand and helicopter response- in the top subplot, and related actuator activity- in the bottom subplot.

Fast Fourier Transform (FFT) is used to convert the time response data of sweep maneuver (performed in $[0, T]$) into the frequency domain complex function using the relation:

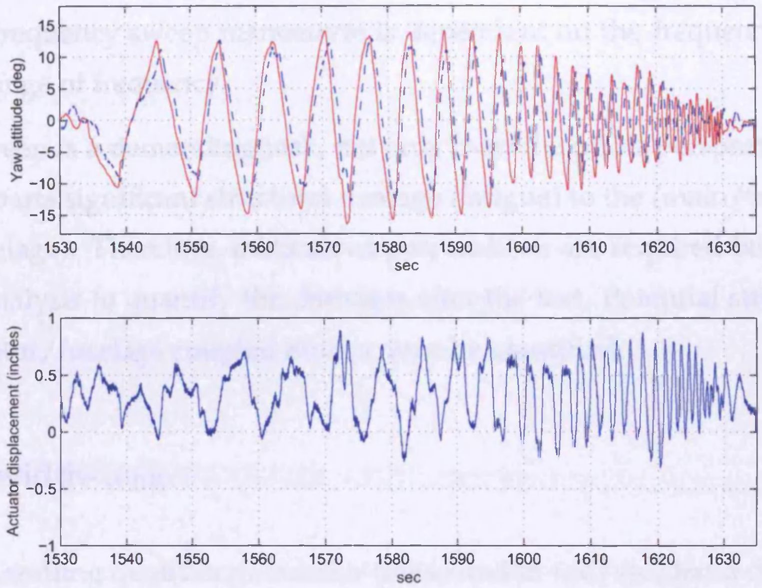

Figure A.1: Yaw axis sweep- top subplot: demand, response; bottom subplot: actuator displacement

$$y(\omega, T) = \int_0^T y(t)e^{-j\omega t}dt. \tag{A.1}$$

where $\omega = \frac{2\pi}{T}$ in rad/sec. The frequency response analysis assumes that the input-output relationship is approximately linear and, if there is any *"noise"*, it is random and uncorrelated with the primary response.

Frequency response amplitude and phase characteristics for a given rotary-wing aircraft can be obtained by exciting the rotorcraft around the natural frequencies. The data obtained provides characteristics to which low-order models can be fitted numerically. Thereafter natural frequency and damping can be estimated. The frequency range of the sweep maneuver need to include the phase characteristics of the response up to $2\omega_{180}$. This may not be known prior to the test, therefore some prior tests are necessary. Frequency sweep maneuver is carried out without any frequency augmentation, and thus, particularly in the low frequency range of the sweep, naturally, helicopters will be prone to divert from the trim conditions. To maintain the validity of the data, and free of contamination by excessive nonlinear characteristics, gathered during the sweeps, and the trim conditions, the pilot will apply uncorrelated corrected inputs superimposed on the sweep. This can be a very cumbersome task for sweeps conducted close to hover or for pitch axis sweeps at high speed. Providing that the rotorcraft is naturally stable the duration (which is usually between 50 sec to

100 sec) of a frequency sweep manoeuvre is dependant on the frequency range and the rate of change of frequency.

Frequency sweep is a demanding task, not only from the pilots perspective, but also because it imparts significant structural damage (fatigue) to the (main/tail) rotor and airframe (fuselage). Therefore, meticulous preparations are required before the test, and careful analysis to quantify the damages after the test. Potential structural resonances and rotor/fuselage coupled modes must be identified.

A.8 Bandwidth- ω_{BW}

This unique handling qualities parameter (measured in rad/sec) has a different definition than the control engineer's perception for the bandwidth. The only similarity that it bears with its name likewise is that, both of them are defined in the frequency domain. The bandwidth criteria in terms of ADS33 address small amplitude, short term handling qualities.

The definition of bandwidth stems from the crossover model [MK74]. When the pilot is operating like a pure gain system K_{pilot}, the neutral stability frequency is defined as ω_{180}. The 180^o phase is of paramount importance in ADS33, as it was from control theory perspective, because it represents a potential stability boundary for closed loop tracking control by the pilot. It is the frequency beyond which the rotorcraft will become unstable without any lead compensation, which will impart a significant pilot work load.

Two definitions of the bandwidth can be presented: the phase-limited and, the gain-limited bandwidth. Each of them deriving its name from the sources they have been obtained, correspondingly, the gain, or the phase frequency response of attitude to pilot's cyclic command.

Phase limited bandwidth- $\omega_{BW_{phase}}$

The phase limited bandwidth is defined purely on the phase plot of the frequency response, and is the frequency at which the phase is 135^o, that is, the attitude response lags behind the pilot's control input command by 135^o. In control terms, this is the frequency where the phase margin is 45^o with respect to the neutral frequency. From physical point of view low values of bandwidth, will result in slow, sluggish response (the response significantly lags behind the input command.)

Gain limited bandwidth- ω_{BWgain}

The gain limited bandwidth makes use of both the gain and phase characteristics of a frequency response; it is derived by the frequency at which the gain has increased by 6 db relative to the gain (at the frequency) when the phase was 180°. That is, the frequency where the gain margin is 6 dB with respect to the neutral stability frequency. Physical interpretation of 6 dB gain margin, translates to allowance for the pilot to increase his feedback gain by a factor of two before threatening stability.

It is important to emphasize that in ADS33 framework the bandwidth criteria apply to both rate and attitude response types, with an exception that for attitude response types (e.g. ACAH) only the phase limited bandwidth applies. Justification for not including the gain limited bandwidth is given in [HMA89], but generally speaking attitude command control systems allow the pilot to back-off and use a very low gain on attitude. ACAH response types should be avoided where the gain bandwidth is less than the phase limited bandwidth, especially where super-precision maneuvers (e.g. pirouette, hovering turn, transition to hover) are required.

It is known that for wide range of helicopters the phase limited bandwidth is equal to or less than the gain limited bandwidth ($\omega_{BWphase} \leq \omega_{BWgain}$). For Rate response types, our bandwidth will be selected as the smallest of the two frequencies.

A high phase limited bandwidth will allow the pilot to operate as a pure gain controller, accepting his own natural phase lags without threatening stability. The gain bandwidth limit protects against instability at high frequency, if the pilot decides to increase his gain or his level of aggressiveness. We would, naturally, like to have high gain limited bandwidth in response types where applicable, since a low value of gain margin is likely to lead to system which is PIO prone. In fact, if $\omega_{BWgain} < \omega_{BWphase}$ the rotorcraft may become PIO prone in super-precision maneuvers. This is so because, small changes in the pilot gain result in a rapid reduction in phase margin. [HMA89] describes PIO as insidious phenomenon depending on the piloting technique, pointing out that non-aggressive, smooth piloting may never come to encounter PIO whereas, a more aggressive piloting may encounter severe PIO.

A.9 Phase-delay

Phase delay τ_p (measured in sec) is another important frequency domain handling quality parameter measure used to represent the shape of the phase and is used together with the bandwidth in quantitative analysis of helicopter frequency response characteristics. Although this handling quality measure is independently computed, in the frequency domain, and beyond the bandwidth frequency, there is a unique relationship between the bandwidth frequency and the shape of the phase curve. The steeper the roll-off of the phase curve, the smaller the bandwidth, which affects adversely performing tasks requiring high precision and adaptation of control strategy to even small changes in frequency. Pilots are particularly sensitive to the slope of the phase at high frequency- beyond the bandwidth frequency, but still within the range of piloting, e.g. > 10 rad/sec. The shape of the phase is defined as:

$$\tau_p = \frac{\Delta\Phi_{2\omega_{180}}}{57.3 \times 2\omega_{180}} \qquad \text{(A.2)}$$

Where $\Delta\Phi_{2\omega_{180}}$ is the phase difference between the cross-over frequency ω_{180}, and $2\omega_{180}$. This frequency range is critical since the phase delay is related to the slope of the phase curve in this particular frequency range. The phase delay parameter serves information about system's effective dead time.

Large phase delays have several sources: filters, computational delays, actuators lags, but the most contributing of all is due to the rotor system. Delays resulted from the rotor system, for conventional helicopters, can vary in the range from 65 ms to 130 ms. It is also known that pure time delays, which impose bandwidth reduction, are more tolerable by teetering rotor helicopters.

The phase delay captures the dynamics of the helicopter beyond the bandwidth frequency. The pilot can still command the helicopter beyond the bandwidth frequency and neutral stability frequencies by introducing lead-compensation, which, in fact, increases the pilot's cross-over frequency. However, in the presence of very large phase lag the pilot's lead-compensation may become insufficient to prevent instabilities or PIOs since large values of τ_p indicate that the rotorcraft is very much prone to becoming unstable. Whereas small values of τ_p indicate that the pilot can increase the input frequency and still apply lead-compensation. Phase delay does not measure non-linear phase effects, such as rate limiting.

A.10 Cross-coupling

Pitch to roll (refers to roll response to longitudinal cyclic input) and roll to pitch (stemming from pitch response to lateral cyclic input) cross-coupling criteria adopted in ADS33 is based on a time domain formulation. It represents the ratio of the peak off-axis response to the desired on-axis response after approximately 4 sec following an abrupt step input. For example roll to pitch- $\frac{\theta_{pk}}{\phi}$, and pitch to roll- $\frac{\phi_{pk}}{\theta}$.

Flying Qualities	$\frac{\theta_{pk}}{\phi}$	$\frac{\phi_{pk}}{\theta}$
Level 1	≤ 0.25	
Level 2	≤ 0.6	
Level 3	> 0.6	

Table A.2: Roll-to-pitch and Pitch-to-roll coupling criteria for forward flight and hover

Table A.2 illustrates the coupling limits in ADS-33E for Roll to Pitch ($\frac{\theta_{pk}}{\phi}$) and Pitch to Roll ($\frac{\phi_{pk}}{\theta}$) for hover and low speed flight regime.

Bibliography

[A.91] Hyde R. A. *The Application of Robust control to VSTOL Aircraft*. PhD thesis, University of Cambridge, 1991.

[Abb01] S. Abbott. *Understanding Analysis*. Springer Verlag, New York Inc, 2001.

[ABDL03] J. C. Avila, B. Brogliato, A. Dzul, and R. Lozano. Nonlinear modelling and control of helicopters. *Automatica*, 39(9):1583–1596, 2003.

[Ano00] Anonymous. *Handling Qualities Requirements fo Military Rotorcraft, Aeronautical Design Standard ADS-33E*. United States Army ATCOM, St. Louis, MO, 2000.

[Ast00] K. J. Aström. Limitations on control system performance. *European Journal of Control*, 6(1):2–20, 2000.

[Aut02] L. Autonne. *Bull. Soc. Math. France*, 30:121–133, 1902.

[BB90] S. Boyd and V. Balakrishnam. A regularity result for the singular values of a transfer matrix and a quadratically convergent algorithm for computing its $\mathcal{L}_\infty$ norm. *Systems and Control Letters*, 15(1):1–7, 1990.

[BD92] A. Brambilla and L. D'Elia. Multivariable controller for distillation columns in the presence of strong directionality and model errors. *Industrial and Engineering Chemistry Research*, 31(2):536543, 1992.

[BDG+98] G. Balas, J. Doyle, K. Glover, A. Packard, and R. Smith. *μ-Analysis and Synthesis Toolbox*. The Mathworks, 1998.

[Bel73] E. Beltrami. Sulle funzioni bilineari. *Gionale di Mathematiche*, 11:98–106, 1873.

[BG73] A. Bjork and G. H. Golub. Numerical methods for computing angles between subspaces. *Mathematics of Computation*, 27(123):579–594, 1973.

[BMG94] S. W. Baillie, J. M. Morgan, and K. R. Goheen. Practical experiences in control systems design using the nrc bell 205 airborne simulator. *AGARD flight mechanics panel symposium on active control*, pages 27.1–27.12, January 1994.

[Bod45] H. W. Bode. *Network Analysis and Feedback Amplifier Design*. D. Van Nostrand, Princeton, 1945.

[BT94] U. Burnik and J. F. Tasiç. Fast singular value decomposition algorithms in image processing. *Proceedings of COST 229 Workshop on Adaptive Systems*, pages 185–189, 1994.

[CCM02] G. Chen, J. Chen, and R. Middleton. Optimal tracking performance for simo systems. *IEEE Transactions on Automatic Control*, 47(10):1770–1775, 2002.

[CG89] D. J. Clements and K. Glover. Spectral factorization via hermitian pencils. *Linear Algebra and its Applications*, pages 796–846, 1989.

[CH69] G. E. Cooper and R. P. Jr. Harper. The use of pilot ratings in the evaluation of aircraft handling qualities. *NASA TM D-5133*, 1969.

[Che98] J. Chen. Multivariable gain-phase and sensitivity integral relations and design trade-offs. *IEEE Transactions on Automatic Control*, 43:373–385, 1998.

[Che99] J. Chen. *Intrinsic performance limits of linear feedback control*. London: Springer Verlag, 1999.

[Che00] J. Chen. Logarithmic integrals, interpolation bounds, and performance limitations in mimo feedback systems. *IEEE Transcations on Automatic Control*, 45(6):1098–1115, 2000.

[Con90] J. B. Conway. *A Course in Functional Analysis*. Springer-Verlag, New York Inc., 1990.

[DFT92] J. Doyle, B. A. Francis, and A. Tannenbaum. *Feedback Control Theory*. Macmillan Publishing Company, Singapore, 1992.

[DGKF89] J. C. Doyle, K. Glover, P. P. Khargonekar, and B. A. Francis. State-space solutions to standard $\mathcal{H}_2$ and $\mathcal{H}_\infty$ control problems. *IEEE Transactions on Automatic Control*, 34(8):831–847, 1989.

[Doy78] J. C. Doyle. Guaranteed margins for lqg regulators. *IEEE Transactions on Automatic Control*, 23(4):756–757, 1978.

[Doy84a] J. Doyle. Advances in multivariable control. Workshop lecture notes, ONR-Honeywell, 1984.

[Doy84b] J. C. Doyle. Lecture notes in advances in multivariable control. Technical report, ONR/Honeywell workshop, Minneapolis, 1984.

[DS81] J. Doyle and G. Stein. Multivariable feedback design: Concepts for a classical/modern synthesis. *IEEE Transactions on Automatic Control*, 1:4–16, 1981.

[ES87] A. El-Sakhary. Some remarks on a geometric linear systems theory: A metric space approach. *In proceedings of* 10^{th} *IFAC Congress*, July 1987.

[EY36] C. Eckart and G. Young. The approximation of one matrix by another of lower rank. *Psychometrika*, 1:211–218, 1936.

[EY39] C. Eckart and G. Young. A principal axis transformation for non-hermitian matrices. *Bull. Amer. Math. Soc.*, 45:118–121, 1939.

[FL85] J. S. Freudenberg and D. Looze. Right half plane poles and zeros design trade-offs in feedback systems. *IEEE Transactions on Automatic Control*, AC-30(6):555–565, 1985.

[FL87] J. S. Feudenberg and D. P. Looze. *Frequency domain properties of scalar and multivariable feedback systems*, volume 104 of *Lecture Notes in Control and Information Science*. Springer-Verlag, Berlin, 1987.

[FPEN02] G. F. Franklin, J. D. Powell, and A. Emami-Naeini. *Feedback control of dynamic systems*. Prentice Hall, 2002.

[Fra87] B. A. Francis. *A Course in* $\mathcal{H}_\infty$ *Control Theory*. Springer Verlag, Berlin, 1987.

[Fre90] J. S. Freudenberg. Plant directionality, coupling and multivariable loop shaping. *International Journal of Control*, 51(2):365–390, 1990.

[GD88] K. Glover and J. C. Doyle. State-space formulae for all stabilizing controllers that satisfy an $\mathcal{H}_\infty$ norm bound and relations to risk sensitivity. *Systems and Control Letters*, 11:167–172, 1988.

[Geo88] T. Georgiou. On the computation of the gap metric. *Systems and Control Letters*, 11:253–257, 1988.

[Ger31] G. A. Gerschgorin. Uber die abgrenzung der eigenwerte einer matrix. *AH CCCP, Ser. Matem.*, 7:749–754, 1931.

[GGS00] G. Goodwin, S. Graebe, and M. Salgado. *Control System Design*. Prentice Hall, 2000.

[GK65] G. H. Golub and W. Kahan. Calculating the singular values and pseudo-inverse of a matrix. *SIAM Journal of Numerical Analysis*, 2:205–224, 1965.

[GL95] M. Green and D. J. N. Limebeer. *Linear Robust Control*. Prentice-Hall Inc., 1995.

[Glo84] K. Glover. All optimal hankel-norm approximations of linear multivariable systems and their -error bound. *International Journal of Control*, 39:1115–1193, 1984.

[Glo86] K. Glover. Robust stabilization of linear multivariable systems: Relations to approximation. *International Journal of Control*, 43:741–766, 1986.

[GLP89] W. L. Garrard, E. Low, and S. Prouty. Design of attitude and rate command systems for helicopters using eigenstructure assignment. *Journal of Guidance, Control and Dynamics*, 12(6), Nov-Dec 1989.

[GM89] K. Glover and D. McFarlane. Robust stabilization of normalized coprime factor plant descriptions with $\mathcal{H}_\infty$ -bounded uncertainty. *IEEE Transactions on Automatic Control*, 34(8):821–830, 1989.

[GNLC95] P. Gahinet, A. Nemirovski, A. J. Laub, and M. Chilali. *LMI control toolbox user's guide*. The MathWorks, Inc., 1995.

[GPGC] D. W. Gu, I. Postlethwaie, S. J. Goh, and P. Carter. An expert environment for robust control systems design. *Technical Report, Department of Engineering*.

[GR70] G. H. Golub and C. Reinsch. Singular value decomposition and least squares solutions. *Numerical Mathematics*, 14:403–420, 1970.

[Gri93] J. J. Gribble. Linear quadratic gaussian loop transfer recovery design for a helicopter in low speed flight. *Journal of Guidance, Control and Dynamics*, 16:754–761, 1993.

[GS90] T. Georgiou and M. Smith. Optimal robustness in the gap metric. *IEEE Transactions on Automatic Control*, 35:673–686, 1990.

[GSM90] K. Glover, J. Sefton, and D. C. McFarlane. A tutorial on loop shaping using $\mathcal{H}_\infty$ robust stabilization. *IFAC Congress, Tallin*, 1990.

[Gub02] A. W. Private Communication Gubbles, October 2002.

[GVL96] G. H. Golub and C. F. Van Loan. *Matrix Computations*. Johns Hopkins University Press, Series in the Mathematical Sciences, 1996.

[GW76] G. H. Golub and J. H. Wilkinson. Ill-conditioned eigensystems and the computation of the jordan canonical form. *SIAM Review*, 18:578–619, 1976.

[Hc01] S. Howell and A. McCallum Private communication, 2001.

[HG93] R. A. Hyde and K. Glover. The application of scheduled $\mathcal{H}_\infty$ controllers to a vstol aircraft. *IEEE Transactions on Automatic Control*, 38(7):1021–1039, 1993.

[HGT95] J. A. Ham, C. K. Gardner, and M. B. Tischler. Flight-testing and frequency-domain analysis for rotorcraft handling qualities. *Journal of the American Helicopter Society*, 25(6):28–38, 1995.

[HHL91] D. Hoyle, R. Hyde, and D. Limebeer. An $\mathcal{H}_\infty$ approach to two degree of freedom design. *Proceedings of the 30-th Conference on Decision and Control*, 1991.

[HJ85] R. Horn and C. Johnson. *Matrix Analysis*. Cambridge University Press, Cambridge, UK, 1985.

[HJBJ73] W. E. Hall Jr. and A. E. Bryson Jr. Inclusion of rotor dynamics in controller design for helicopters. *Journal of Aircraft*, 10(4), 1973.

[HJLVW79] R. D. Heffley, W. F. Jewell, J. M. Lehmann, and R. A. Van Winkle. A compilation and analysis of helicopter handling qualities data. *NASA-CR-3144 TR-1087-1*, 1979.

[HM81] Y. Hung and A. G. J. MacFarlane. *Multivariable Feedback: A Quasi-Classical Approach*. Lecture Notes in Control and Information Sciences 40, Springer-Verlag, 1981.

[HMA89] R. H. Hoh, D. G. Mitchell, and B. L. Aponso. Background information and user's guide for handling requirements for military rotorcraft. *US-AAVSCOM Technical Report 89-A-008*, 1989.

[HMS90] G. Hughes, M. A. Manness, and D. J. M. Smith. Eigenstructure assignment for handling qualities in helicopter flight control law design. *Seventeenth European Rotorcraft Forum, Glasgow, Scotland*, 1990.

[How90] J. Howitt. Matlab handling qualities toolbox. *DERA Internal Report*, 1990.

[HS89] J. W. Helton and A. Sideris. Frequency response algorithms for h optimization with time domain constraints. 34:427–434, 1989.

[HTPG04] G. Herrmann, M. C. Turner, I. Postlethwaite, and G. Guo. Practical implementation of a novel anti-windup scheme in a hdd-dual-stage servo-system. *IEEE Transactions on Mechatronics*, 9(3):580–592, 2004.

[Hyd95] R. A. Hyde. $\mathcal{H}_\infty$ *Aerospace Control Design*. Springer Verlag, London, 1995.

[IC94] J. S. Ingle and R. Celi. Effects of higher order dynamics on helicopter flight control law design. *The Journal of American Helicopter Society*, 39(3):12–23, 1994.

[IMS03] A. Isidori, L. Marconi, and A. Serrani. Robust nonlinear motion control of a helicopter. *IEEE Transactions on Automatic Control*, 48(3):413–426, 2003.

[Isi95] A. Isidori. *Nonlinear Control Systems*. Springer-Verlag, Berlin and Heidelberg GmbH Co. K, 1995.

[IU00] P. Iglesias and T. Urban. Loop shaping design for missle autopilots: Controller configurations and weighting filter selection. *Journal of Guidance Control and Dynamics*, 23(3):516–525, 2000.

[JKL97] Bongiorno J. J. Jr., F. Khorrami, and T. C. Lin. A wiener-hopf approach to trade-offs between stability margin and performance in two and three-degree-of-freedom multivariable control systems. *International Journal of Control*, 68(6):1337–1366, 1997.

[Kal60] R. E. Kalman. A new approach to linear filtering and prediction problems. *Journal of Basic Engineering*, 85:34–45, 1960.

[Key88] D. L. Key. A new handling qualities specification for us military rotorcraft. *Proceedings of International Conference, Helicopter Handling Qualities and Flight Control- RAeSoc*, 1988.

[KGP87] P. Khargonekar, T. Georgiou, and A. Pascoal. On the robust stabilizability of linear time-invariant plants with unstructured uncertainty. *IEEE Transactions on Automatic Control*, 32(3):201–207, 1987.

[Kha02] H. Khalil. *Nonlinear Systems*. Prentice Hall, third edition edition, January 2002.

[KL80] V. C Klema and A. J. Laub. The singular value decomposition: Its computation and some applications. *IEEE Transactions on Automatic Control*, 25:164–176, 1980.

[KS72] H. Kwakernaak and R. Sivan. *Linear Optimal Control Systems*. Wiley-Interscience, New York, 1972.

[Kwa83] H. Kwakernaak. Robustness optimization of linear feedback systems. *22nd IEEE Conference on Decision and Control, San Antonio, Texas, USA*, 1983.

[Kwa93] H. Kwakernaak. Robust control and $\mathcal{H}_\infty$ -optimization tutorial paper. *Automatica*, 29(123456789):255–273, 1993.

[Lan01] A. Lanzon. Simultaneous synthesis of weights and controllers in h-infinity loop-shaping. *40th IEEE Conference on Decision and Control*, 2001.

[LKP93] D. J. N. Limebeer, E. M. Kasenally, and J. D. Perkins. On the design of robust two-degree-of-freedom controllers. *Automatica*, 29(1):157–168, 1993.

[LWN03] T. T. Lee, F. Y. Wang, and R. B. Newell. Robust multivariable control of complex biological processes. *Journal of Process Control*, 14(1):1–17, 2003.

[Mac33] C. C. MacDuffee. *The Theory of Matrices*. Berlin: Springer, 1933.

[Mac82] A. G. J. MacFarlane. Gains, phases and angles in multivariable systems. *Proc. of Conference on Decision and Control*, 2:944–947, 1982.

[MB97] J. S. G. McVicar and R. Bradley. Efficient and robust algorithms for trim and stability analysis of advanced rotorcraft simulations. *The Aeronautical Journal*, 10:375–387, 1997.

[Mei95] G. Meinsma. Unstable and nonproper weights in $\mathcal{H}_\infty$ control. *Automatica*, 31(11):1655–1658, 1995.

[Mey00] C. Meyer. *Matrix Analysis and Applied Linear Algebra*. Society of Idustrial and Applied Mathematics Publications, 2000.

[MG90] D. C. McFarlane and K. Glover. *Robust Controller Design Using Normalised Coprime Factor Plant Descriptions*, volume 138. Lecture Notes in Control and Information Sciences, Springer Verlag, 1990.

[MG92] D. McFarlane and K. Glover. A loop shaping design procedure using $\mathcal{H}_\infty$ synthesis. *IEEE Transactions on Automatic Control*, 37(6):759–769, 1992.

[MGN88] D. McFarlane, K. Glover, and M. Noton. Robust stabilization of a flexible space-platform: An $\mathcal{H}_\infty$ coprime factorization approach. *Proceedings of IEE Control Conference*, 1988.

[MGS90] M. A. Manness, J. J. Gribble, and D. J. M. Smith. Multivariable methods for helicopter flight control law design: A review. *17th European Rotorcraft Forum, Glasgow*, 1990.

[MGV90] D. McFarlane, K. Glover, and M. Vidyasagar. Reduced-order controller design using coprime factor model reduction. *IEEE Transactions on Automatic Control*, 35(3):369–373, March 1990.

[MK74] D. T. McRuer and E. S. Krendel. Mathematical models of human pilot behaviour. *AGARDograph 188*, 1974.

[MSJ79] A. G. J. MacFarlane and D. F. A. Scott-Jones. Vector gain. *International Journal of Control*, 29(1):65–91, 1979.

[NS00] A. W. Naylor and G. R. Sell. *Linear Operator Theory in Engineering and Science*. Springer-Verlag, New York Inc., 2000.

[Nyq32] H. Nyquist. Regeneration theory. *Bell Systems Technology Journal*, 11:126–147, 1932.

[Oga02] K. Ogata. *Modern Control Engineering*. Prentice Hall Inc., New Jersey, 2002.

[Pad00] G. D. Padfield. *Helicopter Flight Dynamics: The Theory and Application of Flying Qualities and Simulation Modelling*. Blackwell Science Ltd, UK., 2000.

[Pap02] G Papageorgiou. Private communication, March 2002.

[PD93] A. Packard and J. C. Doyle. The complex structured singular value. *Automatica*, 29:71–109, 1993.

[PG97] G. Papageorgiou and K. Glover. A systematic procedure for designing non-diagonal weights to facilitate $\mathcal{H}_\infty$ loop shaping. *Proc. 36th Conference on Decision and Control*, 1997.

[PG99] G. Papageorgiou and K. Glover. $\mathcal{H}_\infty$ loop-shaping: Why is it a sensible procedure for designing robust flight controllers? *Proceedings of the AIAA Guidance, Navigation and Control Conference*, 99-4272/73, 1999.

[PG02] G. Papageorgiou and K. Glover. Two-degree-of-freedom control of an actively controlled wind-tunnel model. *Journal of Guidance, Control and Dynamics*, 25(3):510–516, May-June 2002.

[PGH97] G. Papageorgiou, K. Glover, and R. A. Hyde. *Robust Flight Control: A Design Challenge GARTEUR*, volume 224 of *Lecture Notes in Control and Information Sciences*. Springer-Verlag, 1997.

[Pie95] J. K. Pieper. Application of sliding mode control: Trc control of helicopter in hover. *Proceedings of the American Control Conference*, pages 1191–1195, 1995.

[PKS+99] I. Postlethwaite, I. K. Konstantopoulos, X. D. Sun, D . J. Walker, and A. G. Alford. Design, flight simulation and handling qualities evaluation of an lpv gain-scheduled helicopter flight control system. *European Control Conference*, 1999.

[PM79] I. Postlethwaite and A. G. J. MacFarlane. *A Complex Variable Approach to the Analysis of Linear Multivariable Feedback Systems*. Number 12 in Lecture Notes in Control and Information Sciences. Springer: Berlin, 1979.

[PP00] E. Prempain and I. Postlethwaite. A new two-degree-of-freedom gain scheduling method applied to the lynx mk7. *Procceding of Institute of Mechanical Engineers*, 214(I):299–311, 2000.

[PP01] E. Prempain and I. Postlethwaite. Feedforward control: a full information approach. *Automatica*, 37(1):17–28, 2001.

[PPT+02] I. Postlethwaite, E. Prempain, E. Turkoglu, M. C. Turner, A. W. Gubbels, and K. Ellis. Design and flight test of various $\mathcal{H}_\infty$ controllers for the bell 205 helicopter. *NATO Research and Technology Organisation Meeting Proceedings 95, Challenges in Dynamics, System Identification, Control and Handling Qualities for Land, Air, Sea and Space Vehicles, Berlin*, pages 28.1–28.12, 2002.

[PPT+05] I. Postlethwaite, E. Prempain, E. Turkoglu, M. C. Turner, K. Ellis, and A. W. Gubbels. Design and flight testing of various $\mathcal{H}_\infty$ controllers for the bell 205 helicopter. *Control Engineering Practice*, 13(3):383–398, 2005.

[PPTT02] I. Postlethwaite, E. Prempain, E. Turkoglu, and C. M. Turner. Various $\mathcal{H}_\infty$ controllers for the bell 205: Design and flight test. *15th IFAC Congress, Barcelona*, 2002.

[Pro95] R.W. Prouty. *Helicopter Performance, Stability and Control*. Krieger Publishing, Malabar, Florida, US., 1995.

[PSW+99] I. Postlethwaite, A. Smerlas, D. J. Walker, A. W. Gubbels, S. W. Baillie, M. E. Strange, and J. Howitt. $\mathcal{H}_\infty$ control of the NRC Bell 205 fly-by-wire helicopter. *Journal of the American Helicopter Society*, 44(4):276–284, 1999.

[PTG90] I. Postlethwaite, M-C. Tsai, and D-W. Gu. Weighting function selection in $\mathcal{H}_\infty$ design. *IFAC 11th Triennial World Congress*, pages 127–132, 1990.

[Red60] R. M. Redheffer. On a certain linear fractional transformation. *Journal of Mathematics and Physics*, 39:269–286, 1960.

[RR97] J. N. Rozak and A. Ray. Robust multivariable control of rotorcraft in forward flight. *Journal of the American Helicopter Society*, 45(5):149–160, April 1997.

[SA87] G. Stein and M. Athans. The lqg/ltr procedure for multivariable feedback design. *IEEE Transactions on Automatic Control*, 32(2):105–114, 1987.

[SAP90] C. Samblancatt, P. Apkarian, and R. J. Patton. Improvement of helicopter robustness and performance control law using eigenstructure techniques and $\mathcal{H}_\infty$ synthesis. *16th European Rotorcraft Forum*, 1990.

[SBG97] M. Seron, J. Braslavsky, and G. Goodwin. *Fundamental Limitations in Filtering and Control*. Springer Verlag, London, 1997.

[SD91] G. Stein and J. Doyle. Beyond singular values and loopshapes. *AIAA Journal of Guidance Dynamics and Control*, 14:5–16, 1991.

[SG90] J. A. Sefton and K. Glover. Pole/zero cancellations in the general $\mathcal{H}_\infty$ problem with the reference to a two block design. *Systems and Control Letters*, 14:295–306, 1990.

[SH98] M. E. Strange and J. Howitt. The configuring of helisim to represent the flight dynamics of the nrc bell 205 helicopter. *DERA internal report*, 1998.

[SL02] K. Skogestad, S.and Havre and T. Larsson. Control limitations for unstable plants. 15^{th} *Triennial World Congress, Barcelona, Spain*, 2002.

[SM34] S. Skogestad and M. Morari. Robust control of distillation columns. *123*, 123(123), 1234.

[SMD88] S. Skogestad, M. Morari, and J. Doyle. Robust control of ill-conditioned plants: high-purity distillation. *IEEE Transactions on Automatic Control*, 33(12):1092–1104, 1988.

[SP96] S. Skogestad and I. Postlethwaite. *Multivarible Feedback Control: Analysis and Design*. John Wiley, Chichester, 1996.

[Ste73] G. Stewart. *Introduction to Matrix Computations*. Academic Press-Computer Science and Applied Mathematics, 1973.

[Ste98] G. Stewart. *Matrix Algorithms: Volume 1*. Society of Industrial and Applied Mathematics: SIAM, 1998.

[SWP$^+$01] A. Smerlas, D. J. Walker, I. Postlethwaite, M. E. Strange, J. Howitt, and A. W. Gubbels. Evaluating $\mathcal{H}_\infty$ controllrs of nrc bell 205 fly-by-wire helicopter. *Control Engineering Practice*, 9(1):1–10, 2001.

[TCM$^+$99] M. B. Tishler, J. D. Colbourne, M. R. Morel, D. J. Biezad, K. K. Cheung, W. S. Levine, and V. Moldoveanu. A multidisciplinary flight control development environment and its application to a helicopter. *IEEE Control Systems Magazine*, 19(4):22–33, 1999.

[Tom87] M. S. Tombs. *Robust Control System Design with Application to High Performance Helicopters*. PhD thesis, University of Oxford, 1987.

[TP01] M. Trentini and J. K. Pieper. Mixed norm control of a helicopter. *Journal of Guidance, Control and Dynamics*, 24(3):555–565, 2001.

[TWA01] M. C. Turner, D. J. Walker, and A. G. Alford. Design and ground-based simulation of an $\mathcal{H}_\infty$ limited authority flight control system for the westlland lynx helicopter. *Aerospace Science and Technology*, 5:221–234, 2001.

[Vid84] M. Vidyasagar. The graph metric for unstable plants and robustness estimates for feedback stability. *IEEE Transactions on Automatic Control*, 29:403–417, 1984.

[Vid85] M. Vidyasagar. *Control System Synthesis: A Factorization Approach*. MIT Press, 1985.

[Vid88] M. Vidyasagar. Normalized coprime factorizations for non strictly proper systems. *IEEE Transactions on Automatic Control*, 33:300–301, 1988.

[Vid92] M. Vidyasagar. *Nonlinear Systems Analysis*. Prentice Hall, 1992.

[Vin00] G. Vinnicombe. *Uncertainty and Feedback: $\mathcal{H}_\infty$ Loop-shaping and the ν-gap Metric*. Imperial College Press, 2000.

[VJ84] M. Verma and E. Jonckheere. -compensation with mixed sensitivity as a broadband matching problem. *Systems and Control Letters*, 14:295–306, 1984.

[VK86] M. Vidyasagar and H. Kimura. Robust controllers for uncertain multivariable systems. *Automatica*, pages 85–94, 1986.

[Wae84] B. L. van der Waerden. *Geometry and Algebra in Ancient Civilization*. Springer Verlag, New York, 1984.

[Wal96] D. J. Walker. On the structure of a two-degree-of-freedom $\mathcal{H}_\infty$ loop-shaping controller. *International Journal of Control*, 63(6):1105–1127, 1996.

[WCG94] M. F. Weilenmann, U. Christen, and H. Geering. Robust helicopter position control at hover. *American Control Conference*, June 1994.

[WFM01] A. R. Woodyatt, J. S. Freudenberg, and R. H. Middleton. An integral constraint for single input two output feedback systems. *Automatica*, 37(11):1717–1726, 2001.

[WH90] S. J. Williams and R. Hyde. A comparison of different $\mathcal{H}_\infty$ methods in vstol flight control system design. *Proceedings of the American Control Conference*, pages 2508–2513, May 1990.

[Wie49] N. Wiener. *The Extrapolation, Interpolation, and Smoothing of Stationary Time Series with Engineering Applications*. Wiley, New York, 1949.

[WP96] D. J. Walker and I. Postlethwaite. Advanced helicopter flight control using two-degree-of-freedom $\mathcal{H}_\infty$ optimisation. *Journal of Guidance, Control and Dynamics*, 19(2):461–468, 1996.

[WTG00] D. J. Walker, M. C. Turner, and A. W. Gubbles. $\mathcal{H}_\infty$ control of helicopters-recent experiences with the bell 205. *Proceedings of 2000 American Control Conference*, pages 1–12, 2000.

[WTS+99a] D. J. Walker, M. C. Turner, A. J. Smerlas, M. Strange, and A. W. Gubbels. Robust control of the longitudinal and lateral dynamics of the bell 205. *Procedings of 1999 American Control Conference*, pages 2742–2746, 1999.

[WTS+99b] D.J. Walker, M.C. Turner, A. Smerlas, A. W. Gubbels, and M. E. Strange. Robust control of the longitudinal and lateral dynamics of the Bell 205 helicopter. *Proc. American Control Conference*, 4:2742–2726, 1999.

[YBJ85] D. C. Youla and J. J. Bongiorno Jr. A feedback theory of two-degree-of-freedom optimal wiener-hopf design. *IEEE Transactions on Automatic Control*, 30:652–665, July 1985.

[YBJ00] D. C. Youla and J. J. Bongiorno Jr. Wiener-hopf design of optimal decoupling one-degree-of-freedom controllers. *International Journal of Control*, 73(18):1657–1670, 2000.

[You88] N. Young. *An Introduction to Hilbert Space*. Cambridge University Press, 1988.

[YP90] A. Yue and I. Postlethwaite. Improvement of helicopter handling qualities using $\mathcal{H}_\infty$ optimisation. *IEE Proceedings-D Control Theory and Applications*, 137(2):115–129, 1990.

[YPP89] A. Yue, I. Postlethwaite, and G. Padfield. $\mathcal{H}_\infty$ design and the improvement of helicopter handling qualities. *Vertica*, 13(2):119–132, 1989.

[Zam63] G. Zames. Functional analysis applied to nonlinear feedback systems. *IEEE Transactions on Circuit Theory*, 10:392–404, 1963.

[Zam66a] G. Zames. On the input-output stability of time varying nonlinear feedback systems. part i: Conditions derived using concepts of loop gain, conicity, and positivity. *IEEE Transactions on Automatic Control*, 11(2):228–238, 1966.

[Zam66b] G. Zames. On the input-output stability of time-varying nonlinear feedback systems-part ii: Conditions involving circles in the frequency plane and sector nonlinearities. *IEEE Transactions on Automatic Control*, 11:228–238, 1966.

[Zam81] G. Zames. Feedback and optimal sensitivity : model reference tranformations, multiplicative seminorms, and approximate inverse. *IEEE Transactions on Automatic Control*, 26(2):301–320, 1981.

[ZDG96] K. Zhou, J. C. Doyle, and K. Glover. *Robust and Optimal Control*. Prentice Hall Inc., 1996.

[ZF83] G. Zames and B. Francis. Feedback, minimax sensitivity, and optimal robustness. *IEEE Transactions on Automatic Control*, 28(5):585–601, 1983.

[ZF90] Z. Zhang and J. Freudenberg. Loop transfer recovery for non-nimumum phase plants. *IEEE Transactions on Automatic Control*, 35(X):547–553, 1990.